



UNIVERSITY OF
LIVERPOOL

Positive Allosteric Modulators of the Strychnine
Sensitive Glycine Receptor
A New Concept in the Treatment of Chronic Pain

Thesis submitted in accordance with the requirements of the University of Liverpool
for the degree of Doctor of Philosophy by

Lee Taylor

Dec 2014

Declaration

This thesis is the result of my own work. The material contained in the thesis has not been presented, nor is currently being presented, either wholly or in part for any other degree or other qualification.

Lee Taylor

This research was carried out in the Department of Chemistry at the University of Liverpool.

Acknowledgements

First I wish to thank my supervisor Prof. Paul O'Neill for giving me the opportunity to study within his group and for his guidance and support throughout the last four years. I would also like to thank Dr Neil Berry, whose support, advice and patience has been invaluable to me throughout my studies.

Thanks must also go to all my collaborators, Dr Laiche Djouhri from the Department of Pharmacology at the University of Liverpool and Prof. McMahon from Kings College London, for carrying out the Chung lesion rat model of neuropathic pain. Miss Elinor Wilde from the Liverpool School of Tropical Medicine for carrying out pharmacokinetic studies, Prof. Laube of Tübingen University, Darmstadt for electrophysiology studies and ChemPartners, P.R. China for *in vitro* studies. Additionally, I would like to thank all the technical staff at The University of Liverpool for their analytical services and help, as well as to express my gratitude to the EPSRC for funding these studies.

Thanks must also go to all the members of the PON group both past and present, including David, Mike, Shirley, Nham, Paul, Kathryn and Matt, with whom I have shared many good times and have many treasured memories (of those nights I can remember).

Special thanks must go to Chandra. Not only are you the font of all chemistry knowledge, you are also one of the kindest and warm hearted people I have met. I am truly thankful to have you as my friend.

To Neil Kershaw, Emma Shore and Natalie Roberts, thank you for the lunches out, the banter and the elastic band fights. You made my time in the lab a joy and helped me through some real tough times. Huge thanks to Katie Alexander for all the tea breaks, foodie talk and belly laughs.

Finally my biggest thanks must go to my family. To my sister Hazel, you encouraged me to begin this journey and have supported me through the toughest of times, for that I will be eternally grateful. To my children, Christina-Rose and Jacob, you are without doubt my greatest achievement and I love you both more than I can express. Finally to my fiancée Lisa, without your constant love, support and understanding none of this would have been possible. Your strength and determination is a constant inspiration to me. You're not just my fiancée you're my best friend and I will love you always.

Dedication

This thesis is dedicated to the memory of my beloved parents

Audrey and Gerry

Thank you for everything

Abstract

Chronic pain is a global medical-health problem. It is estimated that approximately 20% of the adult population suffer from some form of chronic pain. Along with the physical and emotional burden that living with chronic pain brings to the individual, there is also a huge socio-economic cost implication currently estimated at more than €200 million per annum in Europe and at over \$150 million in the USA.

Unfortunately, because of a lack of efficacious treatments, chronic pain is poorly managed. Current therapies for chronic pain act upon well-established targets and have been shown not only to be inadequate for the majority of patients, with only 1 in 4 patients only finding up to 50% relief from their painful syndromes. There is, therefore, a continued need for novel analgesic drugs that act at novel therapeutic targets. With the elucidation of the role of $\alpha 1$ glycine receptor ($\alpha 1$ GlyR) plays in nociceptive pathways it has become an attractive target for novel analgesic compounds.

Previous work with the group has identified a series of potent bi-phenyl compounds targeting the $\alpha 1$ GlyR with EC_{50} values in the low nM range. However, these compounds suffered from poor physicochemical and pharmacokinetic properties.

Work in this thesis describes the rational design and synthesis of a library of compounds which selectively target the $\alpha 1$ GlyR with EC_{50} values in the sub nano-molar range. We have successfully progressed from hit to lead stage with improved efficacy and DMPK properties. The lead compound has shown excellent PK profiles, CNS penetration properties and no toxicity issues. We have obtained proof-of-concept for the lead compound in a rat model of neuropathic pain and are currently moving forward with lead optimisation.

Abbreviations

AcOH	Acetic acid
ADME	Absorption, Distribution, Metabolism, Excretion
ADR	Adverse drug reaction
Anal	Analysis
AUC	Area under the curve
BBB	Blood brain barrier
Bn	Benzyl
Cat	Catalytic
calcd	Calculated
CL/F	Clearance/Bioavailability
CL	Clearance
Cmax	Maximum concentration
ClogD	Calculated distribution coefficient
ClogP	Calculated partition coefficient
CNS	Central nervous system
d	Doublet
DCM	Dichloromethane
DMAP	4-(Dimethylamino)pyridine
DMF	Dimethylformamide
Dof	Dofetilide
EC ₅₀	Half maximal effective concentration
EtOAc	Ethyl acetate
Et ₂ O	Diethyl ether
EtOH	Ethanol
ES	Electrospray
g	Gram(s)
GABA _A R	Gamma aminobutyric acid (subtype A) receptor
GlyR	Glycine receptor
HD ₅₀	Hypnotic dose
Hep	Hepatocytes
hept	Heptet

HLM	Human liver microsomes
hr(s)	Hour(s)
HRMS	High resolution mass spectrometry
Hz	Hertz
IC ₅₀	Half maximal inhibitory concentration
ip	In progress
i-pr	Isopropyl
m	Multiplet
M ⁺ /M ⁻	Molecular ion
MDCK	Madin-Darby canine kidney
Me	Methyl
MeOH	Methanol
mg	Milligram(s)
mL	Millilitre(s)
Min(s)	Minute(s)
mM	Millimolar
mmol	Millimole
mp	Melting point
MPO	Multiparameter optimisation calculator
MRT	Mean residence time
MS	Mass spectrometry
ng	Nanogram(s)
NMR	Nuclear magnetic resonance
nM	Nanomolar
NT	Not tested
pKa	Negative logarithm of the acid dissociation constant
ppm	Parts per million
pM	Picomolar
QT	QT interval
RT	Room temperature
s	Singlet
t-Bu	Tert butyl
TDP	Torsade de Pointes
TFA	Trifluoroacetic acid

THF	Tetrahydrofuran
TLC	Thin layer chromatography
Tmax	Time to maximum concentration
TPSA	Topological surface area
$t_{1/2}$	Half life
Vd	Volume of distrobution
α	Alpha
B	Beta
γ	Gamma
Δ	Delta/Chemical shift

Content

Title Page		i
Declaration		ii
Acknowledgements		iii
Dedication		iv
Abstract		v
Abbreviations		vi
Chapter 1	General Introduction	1
Chapter 2	Targeting the α 1 Glycine Receptor	48
Chapter 3	Lead Generation	104
Chapter 4	Lead Optimisation	167
Chapter 5	Conclusions	202
Chapter 6	Experimental	214

Chapter I

General Introduction

Contents

1.0	Introduction	3
1.1	Pain	3
1.1.1	Nociceptive pain.....	4
1.1.2	Inflammatory pain.....	6
1.1.3	Neuropathic pain.....	7
1.1.4	Dysfunctional pain.....	8
1.2	Current Treatments	9
1.2.1	Paracetamol	9
1.2.2	Non-Steroidal Anti Inflammatory Drugs	10
1.3	Current Treatment for Neuropathic Pain	12
1.3.1	Tricyclic Antidepressants.....	12
1.3.2	Selective Serotonin Norepinephrine Reuptake Inhibitors.....	13
1.3.3	Anticonvulsants.....	14
1.3.4	Topical Treatments	15
1.3.5	Opioids	15
1.4	Potential drug targets.....	17
1.4.1	Na _v channels	17
1.4.2	Serotonin (5 HT)	19
1.4.3	Calcium channels.....	20
1.4.4	Vanilloid receptor (TRPV1).....	22
1.4.5	Potassium Channels	23
1.4.6	Nerve growth factor	24
1.4.7	Glycine Receptor	25
1.4.8	Gamma-Aminobutyric acid receptor	29
1.5	Propofol	30
1.6	Blood brain barrier	34
1.7	Aims	37
1.8	References.....	38

1 Introduction

1.1 Pain

The perception of pain is not uniform throughout the population, and the term “pain” can mean very different things to different people. Pain has been described as “an unpleasant multidimensional sensory and emotional experience that is linked to potential or actual tissue damage”¹. Acute pain is the pain we feel when we cut ourselves, touch a hotplate, break a bone etc.; this is an evolutionary alarm system that tells us of potential or actual damage to our body. If we are unfortunate enough to suffer an insult or injury the acute pain will persist as a warning to allow the injured area to heal. Once the body is healed the pain will subside and we can go about our lives as normal. Acute pain is therefore, an adaptive protective response in order to prevent injury or to allow damaged tissues to heal. What if the pain persists beyond the period of healing? What if the pain spreads to other parts of the body? This pain is termed chronic; it is maladaptive, that is to say, it is no longer a protective supportive process, but is a dysfunctional process thought to be a consequence of abnormalities within the somatosensory system^{2,3}. Chronic pain may result from damage to the nervous system itself (neuropathic pain) this could be as a result of viral infections such as, herpes, HIV, or as the results of tumours, cancer or even through surgical procedures and therapeutic interventions^{4,5}. In many chronic pain syndromes such as, fibromyalgia, irritable bowel syndrome and osteoarthritis the aetiology is not so discernible^{6,7,8}. One thing that is clear however is the devastating and debilitating effects chronic pain has upon sufferers.

1 in 5 adults in Europe suffer from chronic pain, this equates to ~8 million people in the UK alone⁹. In the US it is thought that 100 million adults, more than the total number affected by cancer, diabetes and heart disease, are afflicted with some form of chronic pain¹⁰.

Evidence indicates that chronic pain conditions can severely impact on quality of life with up to 50% of sufferers struggling with daily tasks such as, household chores, exercise, walking or driving⁹. Unsurprisingly anxiety disorders and depression are also associated with chronic pain; a review by Bair, Robinson, Katon, & Kroenke, found the prevalence of major depression in chronic pain sufferers was as high as 85%¹¹.

Unfortunately, because of a lack of efficacious treatments chronic pain is poorly managed. Current therapies for chronic pain act upon well-established targets and have been shown not only to be inadequate for the majority of patients, with only 1 in 4 patients only finding up to 50% relief from their painful syndromes, but they also have a high side effect burden and abuse potential^{12,13}. Crucially current medications used to treat chronic pain are symptomatic only, they are not curative or disease modifying, therefore, there exists an urgent unmet need for effective novel analgesic drugs with reduced side effects, abuse liability and tolerance issues which can target chronic pain states¹².

Pain can be described as four major states: Nociceptive, inflammatory, neuropathic and dysfunctional as described below.

1.1.1 Nociceptive pain

Nociceptive pain can be thought of as our alarm system, an early warning sign of contact with noxious stimuli¹⁴. The receptors which detect such noxious stimuli are termed nociceptors, which are highly specialised, high threshold sensory receptors found within the peripheral nervous system¹⁵. Nociceptors transduce noxious stimuli into an action potential from receptors or ion channels which are sensitive to thermal, chemical or mechanical stimuli¹⁶. The impulses travel along both the large calibre rapidly conducting myelinated A δ fibres, and the slower conducting unmyelinated C-fibre nociceptors. The input is conducted along the ascending pathway (Figure 1.1) to the spinal cord via the dorsal root ganglion (DRG) and then on to the higher regions of the central cortex where the sensation of pain is experienced^{16,17}.

The cortex activates descending pain control pathways which releases a variety of chemical mediators including, norepinephrine (NE), serotonin (5-HT), gamma-aminobutyric acid (GABA) and peptides such as endorphins and enkephalins, (Figure 1.2). These mediators activate a complicated cascade of interactions that inhibit the excitatory activity. The result is the formation of a pain-processing loop, activated by nociceptive input, ultimately inhibited by a descending antinociceptive output¹⁸.

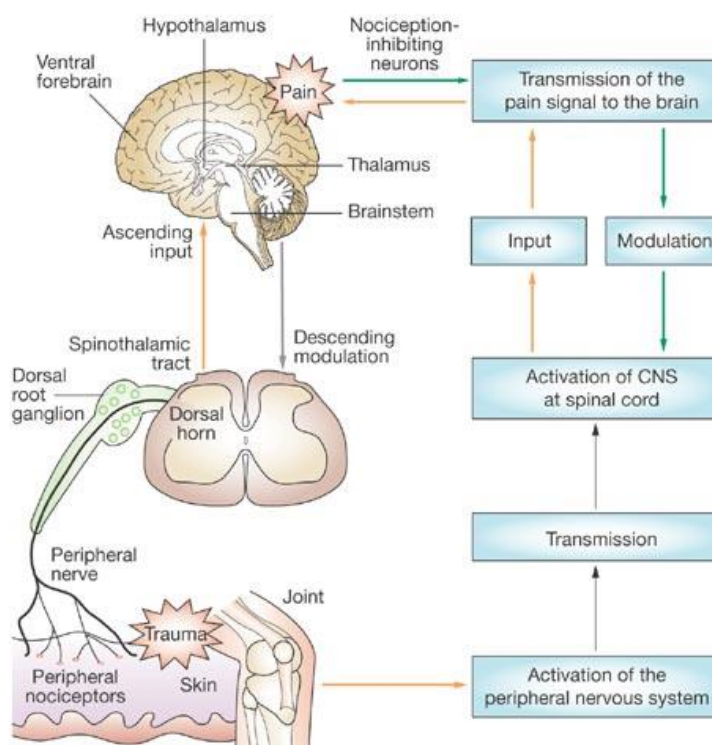


Figure 1.1¹⁹. The nociceptive pain pathway. Detection of noxious stimuli by nociceptors generates signals which travel to the dorsal horn of the spinal cord. The signals are transduced along the ascending pain pathway to the sensory cortex of the brain. The cortex releases a variety of chemical mediators to inhibit excitatory activity creating a pain processing loop.

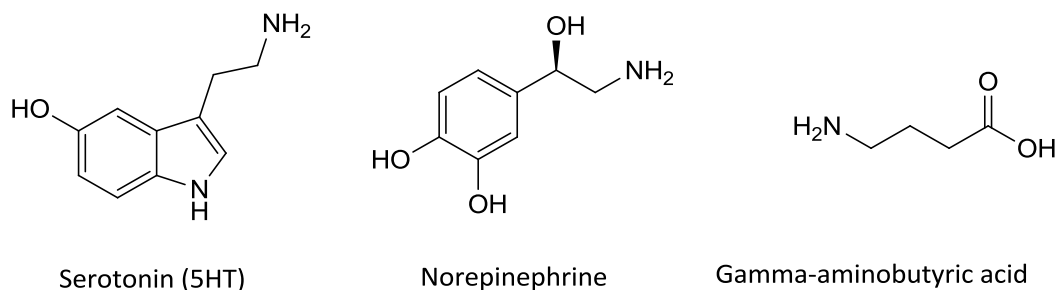


Figure 1.2. Serotonin, norepinephrine and gamma-aminobutyric acid.

Nociception is an adaptive protective process. It helps prevent injury by generating a reflex withdrawal response from a stimulus that could cause tissue damage. It also elicits a sensation so unpleasant it results in complicated behavioural strategies that help prevent future contact with such stimuli²⁰. Under normal circumstances nociceptive pain is not a clinical problem and should only be suppressed under the context of clinical procedures that involve noxious stimuli and result in tissue damage such as surgery.

In the rare autosomal condition Congenital Insensitivity to Pain with Anhidrosis (CIPA) loss of function of the nociceptive system is a problem. CIPA arises as a result gene alterations which encode for the Na_v1.7 voltage gated sodium channel. Na_v1.7 plays a crucial role in the production and propagation of action potentials and individuals who suffer from CIPA have an inability to feel pain. This typically leads to problems of mutilation, multiple scars, osteomyelitis, bone fractures, joint deformities, amputations, and early death^{21,22}.

Although powerful analgesics are used clinically to reduce pain, a careful balance must be maintained between the need of the individual to be pain free and comfortable and our requirement for the nociceptive system to warn us of impending tissue damage or severe trauma. It is, therefore, imperative that the nociceptive system is not so suppressed by analgesia that its protective role is lost²³.

1.1.2 Inflammatory pain

Inflammatory pain is another form of an adaptive protective response of the nociceptive system. As a result of particularly powerful noxious input nociceptors are exposed to a host of inflammatory mediators including prostaglandins (PGE₂), nerve growth factor (NGF) and bradykinin (B₂). These compounds act upon tyrosine kinase receptors and G-protein coupled receptors expressed at the terminals of the nociceptors²⁴. Activation of these receptors begins an intracellular phosphorylation cascade resulting in the lowering of the threshold of activation leading to an increase in excitability, an increase in sensitivity, and also, a decrease in inhibition of

the nociceptive system²⁵. Activation of peripheral receptors also modulates the release of neuropeptides such as substance P and cholecystinin, which mediate further activation of inflammatory pathways²⁶. Allodynia (elicitation of pain from an innocuous stimulus) and hyperalgesia (increased sensation of pain brought about by noxious stimuli) are both hallmarks of inflammatory pain. Allodynia and hyperalgesia can be thought of as protective, adaptive processes i.e. they help to prevent movement of an injured joint or broken limb during the healing process. In the majority of cases the peripheral sensitisation state is transient and as the injured tissue heals over time the system will return to baseline levels which require high intensity stimuli to innervate the nociceptive system once again²⁰. If the symptoms of allodynia and hyperalgesia persist beyond healing, however, they can be thought of as maladaptive. Maladaptive plasticity of normal physiological mechanisms can lead to chronic pain²⁷.

1.1.3 Neuropathic pain

Neuropathic pain is defined as “pain caused by a lesion or disease of the somatosensory system”²⁸. The main characteristic of neuropathic pain is that the input of noxious stimuli is no longer required to generate pain. When exposed to inflammatory mediators after insult or injury the nociceptive system can undergo significant change or plasticity. These changes occur most readily in nociceptors that have been sensitised during the inflammation process²³. Axons whose membrane potential has been significantly altered by the plasticity changes can become sufficiently hyperexcitable as to generate spontaneous action potentials²⁹. This increase in activity of the nociceptors in the dorsal horn of the spinal cord is termed central sensitisation³⁰. Synapses at the spinal cord level are subject to modulation by ligand gated ion channels such as, N-methyl-D-aspartate receptor (NMDAR), α -amino-3-hydroxy-5-methyl-4-isoxazolepropionic acid receptor (AMPA) and metabotropic receptors. The synapses are also modulated by several growth factors including brain-derived neurotrophic factor (BDNF) and nerve growth factor (NGF).

This gives rise to a complex phosphorylation cascade which ultimately leads to plasticity changes of the synapse at the spinal cord level³¹. It is possible for almost any pathological process known to create damage or dysfunction of neural tissue to be considered as potential causes for neuropathic pain (Table 1.1)³².

Table 1.1. Potential causes of neuropathic pain³².

Polyneuropathy
Diabetes
Alcoholism
Human immunodeficiency virus
Hypothyroidism
Renal failure
Chemotherapy (vincristine, cisplatin, paclitaxel, and metronidazole)
Anti-HIV drugs
B-12 and folate deficiencies
Fluoroquinolones (peripheral neuropathy)
Small-fiber neuropathy
Mononeuropathy
Entrapment syndromes
Traumatic injury
Tumour
Compressive lesions
Neuropathic low back pain
Inflammatory
Postherpetic neuralgia
Trigeminal neuralgia
Phantom limb pain

1.1.4 Dysfunctional pain

Dysfunctional pain can be described as maladaptive low threshold pain in the absence of noxious stimuli, inflammation or neural damage³³. Dysfunctional pain manifests itself in a number of painful syndromes including Fibromyalgia (FM), irritable bowel syndrome (IBS) and intestinal cystitis (IC). Disequilibrium between excitation and inhibition in the central nervous system (CNS) gives rise to spontaneous amplification of the nociceptive signals³⁴. This gives rise to a change in sensory processing which has been detected by functional imaging³⁵.

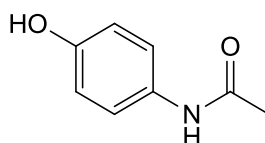
Having briefly defined the various states of pain there now follows a brief review of the current treatments for these types of pain.

1.2 Current Treatments

The cornerstone of treatment for acute nociceptive (adaptive) pain and inflammatory pain are analgesics such as paracetamol (acetaminophen, Figure 1.3) and non-steroidal anti-inflammatory drugs (NSAIDs).

1.2.1 Paracetamol

Paracetamol has both analgesic and anti-pyretic activity and although its mechanism of action is still to be fully elucidated it is thought to act via both peripheral and central pathways³⁶.



Paracetamol

Figure 1.3. Paracetamol

Although paracetamol is globally one of the most widely prescribed analgesics for mild to moderate pain, in high doses paracetamol is acutely hepatotoxic. Studies have shown paracetamol overdose is the highest cause of acute liver failure in Great Britain, Europe and the USA³⁷. Paracetamol is extensively metabolised in the liver by various cytochrome P450 enzymes including, CYP2E1 and 1A2. Small quantities of the drug are N-hydroxylated to form N-acetyl-*p*-benzoquinone imine (NAPQI, Figure 1.4), which under normal circumstances conjugates with glutathione and is excreted via the kidneys³⁶.

Upon ingestion of large amounts of paracetamol glutathione becomes depleted NAPQI reacts with hepatic proteins which, in severe cases, can lead to liver necrosis and death³⁸.

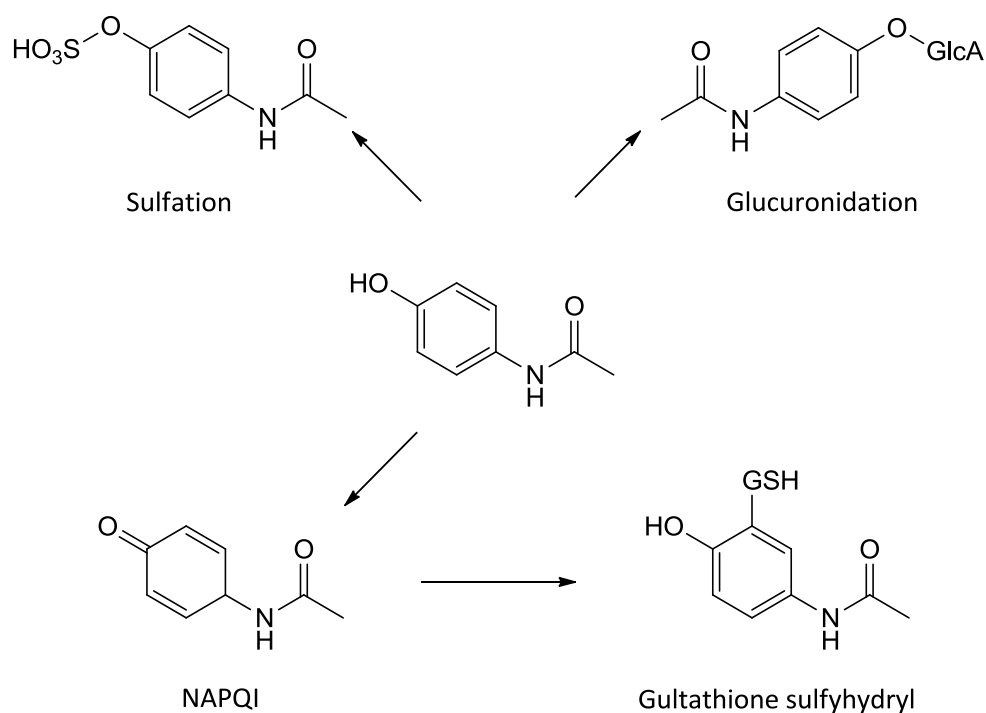


Figure 1.4. Paracetamol metabolic pathway

1.2.2 Non-Steroidal Anti Inflammatory Drugs (NSAIDs)

NSAIDs such as ibuprofen, naproxen, aspirin and diclofenac (Figure 1.6) are commonly used in the treatment of acute and inflammatory pain. NSAIDs are inhibitors of the pro-inflammatory enzymes cyclooxygenase 1&2 (COX, prostaglandin H₂ synthase), which are involved in the conversion of arachidonic acid to inflammatory mediators such as prostaglandins, prostacyclin and thromboxanes³⁹(Figure 1.5).

Following tissue injury or insult the release of pro-inflammatory mediators contributes to peripheral sensitisation and hyperalgesia, blockade of COX enzymes prevents prostaglandin production and relieves the symptoms of hyperalgesia.

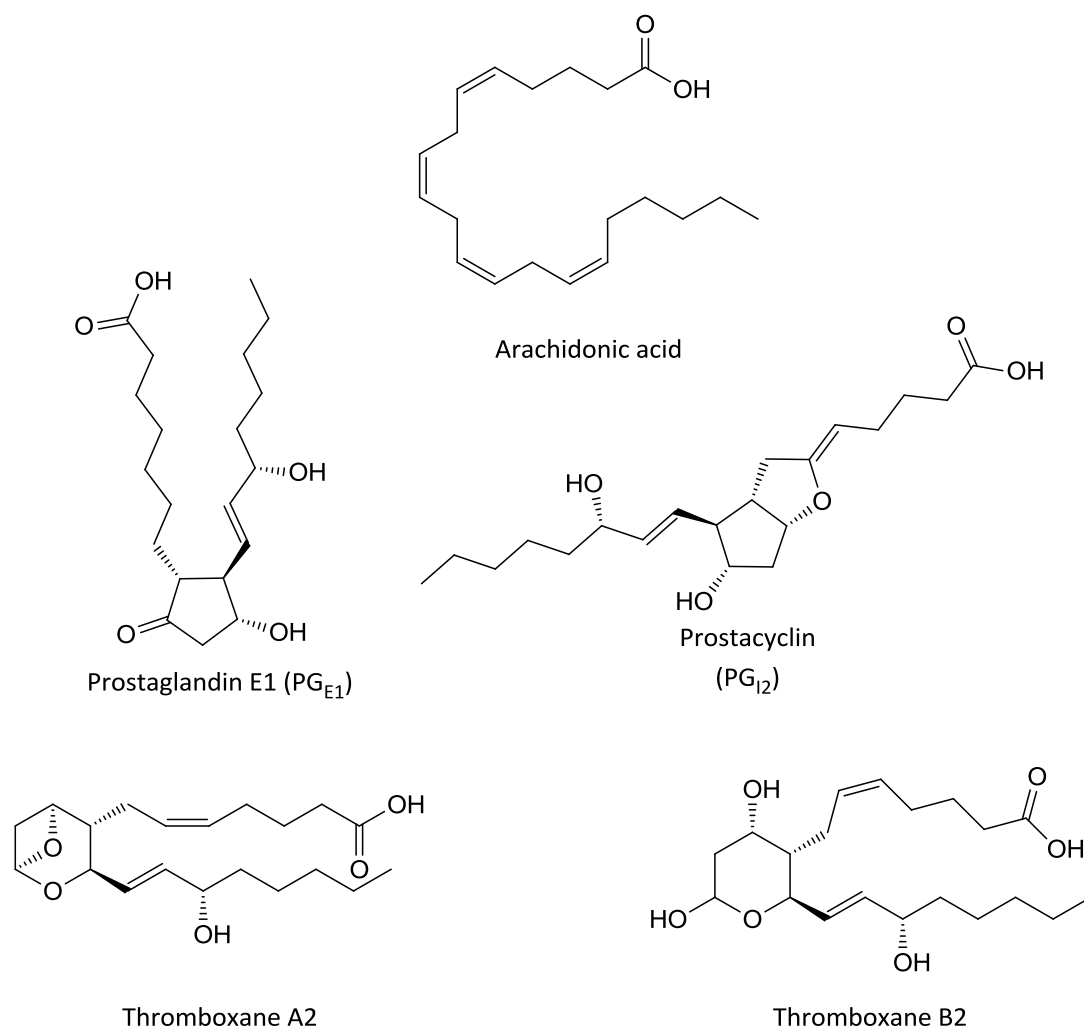


Figure 1.5. Pro-inflammatory mediators; prostaglandins, prostacyclin and thromboxanes, contribute to peripheral sensitisation.

As a consequence of their mechanism of action NSAIDs have a ceiling effect upon their analgesic efficacy and as such, this limits their use in cases of severe pain⁴⁰. Chronic NSAID use has been linked to gastrointestinal (GI) adverse effects such as abdominal pain, heartburn, nausea, vomiting, or dyspepsia⁴¹. Approximately 50% of NSAID users develop gastric erosion and up to 30% of those receiving long term NSAID therapy will develop peptic ulcers⁴².

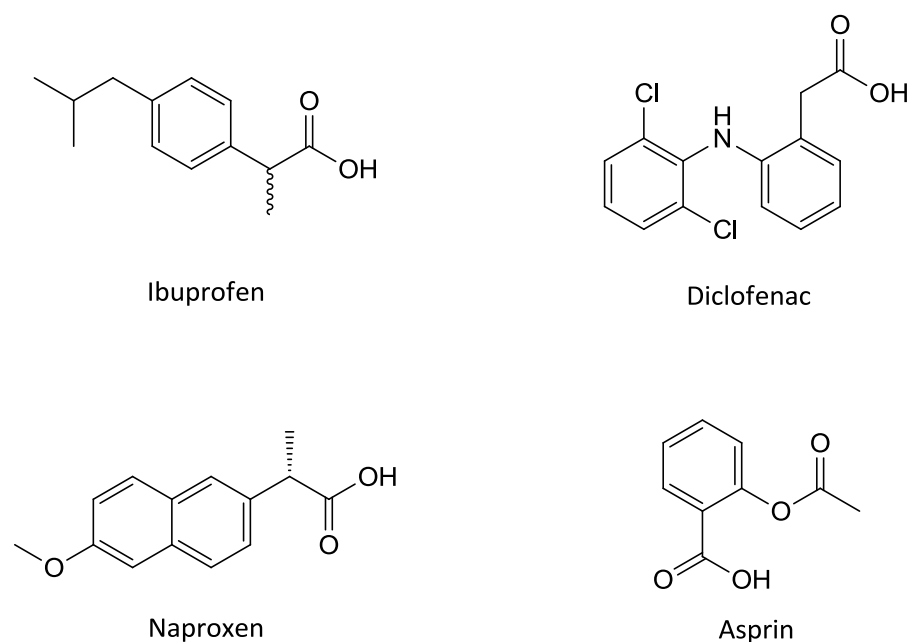


Figure 1.6. NSAIDs used to treat inflammatory pain.

1.3 Current Treatment for Neuropathic Pain

The current treatment strategy for neuropathic pain begins with a thorough assessment and diagnosis, and then progresses in a stepwise manner through the various treatment options available.

1.3.1 Tricyclic Antidepressants

One of the first line of treatments available for neuropathic pain are tricyclic antidepressants (TCAs) such as nortriptyline and desipramine⁴³ (Figure 1.7). TCAs have been shown to be effective in randomised clinical trials (RTC) for several different forms of neuropathic pain⁴⁴. The exact mechanisms involved in antinociception for TCAs have not yet been fully elucidated.

The main mechanism of action of antidepressants is thought to involve blockade of the sodium channel $\text{Na}_v1.7$ and also enhancement of descending inhibitory pathways by increasing the levels of noradrenaline and serotonin (5-HT) at both supraspinal and spinal levels⁴⁵.

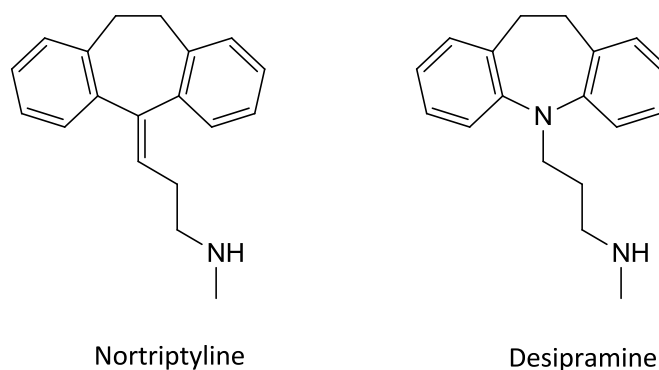


Figure 1.7. Tricyclic antidepressants nortriptyline and desipramine.

Depression is a common comorbidity in individuals suffering with neuropathic pain, but the analgesic effect of TCAs has been established in those who are classed as nondepressed^{44,46}. Adverse effects of TCAs are common and include dry mouth, urinary retention, orthostatic hypotension and sedation⁴⁷. TCAs have also been linked with an increased risk of myocardial infarction and current guidelines recommend caution in prescribing TCAs to individuals with cardiac disease^{48,49}.

1.3.2 Selective Serotonin Norepinephrine Reuptake Inhibitors

Selective serotonin norepinephrine reuptake inhibitors (SSNRI) duloxetine and venlafaxine, are also used as first line treatments for neuropathic pain⁴³. Duloxetine has shown effectiveness in peripheral neuropathic pain particularly against diabetic peripheral neuropathy (DPN), but its effectiveness at treating other forms of neuropathic pain have not yet been tested^{50,51}. Venlafaxine has also shown efficacy against DPN and various other painful polyneuropathies⁵².

Whilst the most common adverse effect of both duloxetine and venlafaxine (Figure 1.8) is nausea, venlafaxine has also been shown to have cardiac conduction abnormalities in a number of individuals and is advised in patients with pre-existing cardiac problems^{53,54}. When treatment with venlafaxine is discontinued withdrawal should be tapered as withdrawal syndrome has been indicated³².

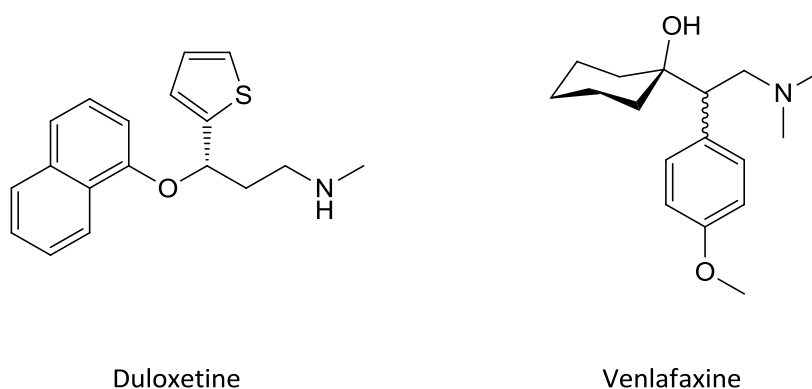
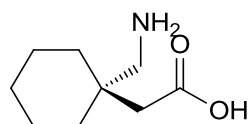


Figure 1.8. Selective serotonin norepinephrine reuptake inhibitors (SSNRI) duloxetine and venlafaxine.

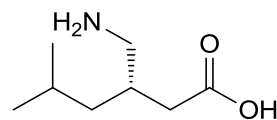
1.3.3 Anticonvulsants

The anticonvulsant drugs gabapentin and pregabalin (Figure 1.9) are also prescribed as first line medications to combat neuropathic pain. Both of these compounds have been shown to target the $\alpha 2\text{-}\delta$ subunit of voltage-gated calcium channels of activated neurons, thereby, reducing the release of inflammatory mediators glutamate, norepinephrine, and substance P⁵⁵. The pharmacokinetics of gabapentin are nonlinear, therefore, it has a complex dosing regimen when compared with other drugs in its class. As a consequence of this it can take much longer (up to two weeks) before the analgesic activity takes effect⁵⁶. Gabapentin also displays several dose limiting side effects such as dizziness, drowsiness, sedation and peripheral oedema and both drugs require careful monitoring in patients with renal impairments⁵⁷.

Pregabalin has shown efficacy against post herpetic neuralgia (PHN) and DPN in three RCTs and efficacy for neuropathic pain in a separate trial⁵⁸⁻⁶¹. Pregabalin has a similar side effect profile as gabapentin but due to linear pharmacokinetics the analgesic effects are achieved much quicker⁵⁹.



Gabapentin

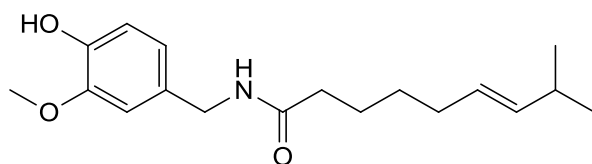


Pregabalin

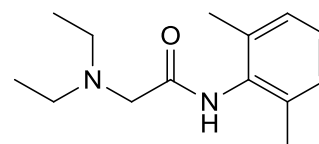
Figure 1.9. Anticonvulsant drugs gabapentin and pregabalin.

1.3.4 Topical Treatments

Other first line treatment options include topical medications such as lidocaine patches and capsaicin patches (Figure 1.10) which have both shown localised efficacy against some forms neuropathic pain^{62,63}.



Capsaicin



Lidocaine

Figure 1.10. Capsaicin and lidocaine.

1.3.5 Opioids

Opioid analgesics such as morphine, methadone, oxycodone, levorphanol and tramadol (Figure 1.11) are generally considered to be the second line treatment option for neuropathic pain.

Three primary opioid receptor subtypes μ , δ and κ have been identified which have clearly established roles in analgesia. These receptors are found in higher regions of the CNS, and once innervated they have roles in descending inhibitory pathways. This is where the antinociceptive properties of opioids are thought to stem from^{64,65}. Opioids have demonstrated efficacy against neuropathic pain, PHN, DPN and phantom limb pain. In head to head trials against TCAs and gabapentin, opioids have shown a higher rate of long term adverse events, with the most common reported events being nausea, constipation and sedation. Studies have shown the prevalence of opioid misuse among patients suffering with neuropathic pain can be as high as 25%⁶⁶. Because of the adverse effects and the risk of misuse outlined above, opioids are reserved for individuals who have either failed to respond to, or who cannot tolerate first line medications⁶⁷.

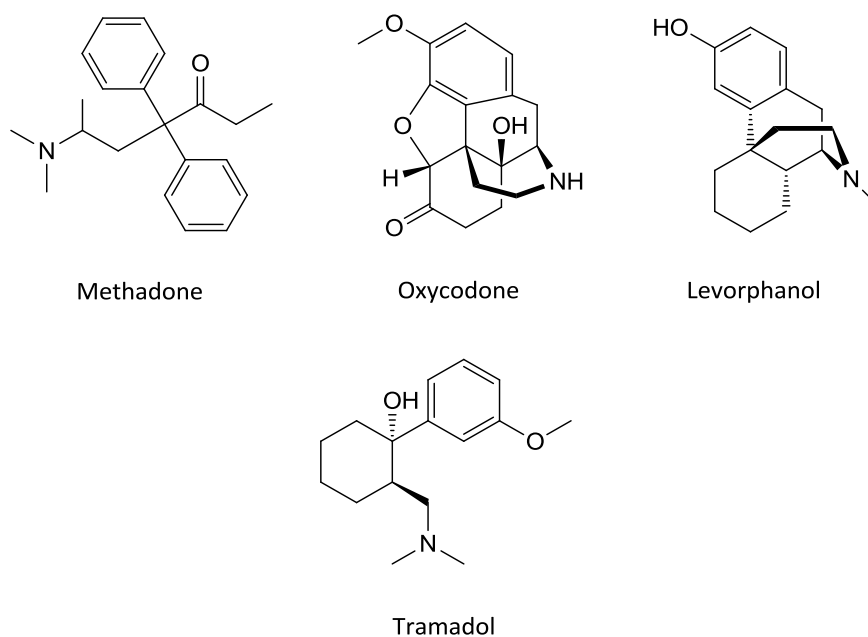


Figure 1.11. Opioid analgesics.

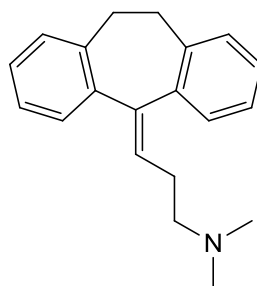
Having discussed some of the current therapies for pain management there follows an overview of some of the major drug targets within both the peripheral nociceptive system and central nervous system.

1.4 Potential drug targets

1.4.1 Na_v channels

Voltage gated sodium channels (Na_v) are responsible for the generation and propagation of action potentials in response to membrane depolarization. Na_v channels are heteromultimers of α -subunits, which form the pore, and smaller auxiliary β -subunits. The α -subunit is arranged into four domains each consisting of six transmembrane segments that are connected by linkers. The β -subunits are type I membrane proteins, each with a single transmembrane unit and a larger extracellular domain⁶⁸. Nine genes encode for the Na_v 1.1- Na_v 1.9 channels (SCN1A–5A, SCN8A–11A), of which only Na_v1.7, Na_v1.8 and Na_v1.9 are expressed in peripheral neurons⁶⁸. Studies have indicated that alterations in the properties of Nav1.7 can profoundly impact pain sensitivity. Based on these results, it is thought that Nav1.7 is likely to play an important role in neuropathic pain syndromes^{69,70}.

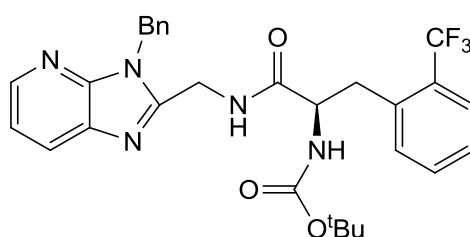
There are many current medications used for the treatment of neuropathic pain which possess sodium channel blocking properties. These include tricyclic antidepressants, amitriptyline (Figure 1.12), nortriptyline (Figure 1.7) and local anaesthetic lidocaine (Figure 1.10) has activity at sodium channels also. However, some of the sodium channel blockers that are currently available (e.g. tricyclic antidepressants) are associated with cardio-toxicity and adverse CNS effects, which, in part can be explained by their lack of selectivity for sodium channel isoforms^{71,72}.



Amitriptyline

Figure 1.12. Tricyclic antidepressant amitriptyline.

Recently several novel, benzodiazepine based, selective inhibitors of Na_v1.7 have been developed, several of which have shown a complete inhibition of spontaneous neuronal firing in the rat model of spinal nerve ligation (SNL). Although these compounds were highly efficacious they suffered from low oral exposure, high clearance rates. In an effort to combat the poor pharmacokinetic (PK) properties of the benzodiazepine compounds researchers developed a series of imidazopyridine-based sodium channel blockers (Figure 1.13) which showed improved PK and good efficacy in the SNL model⁷³.

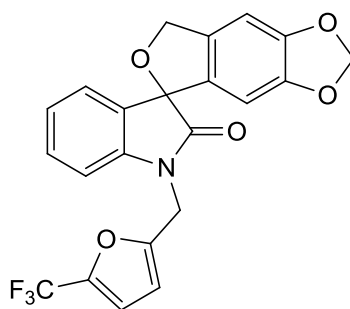


Imidazopyridine

Figure 1.13. Imidazopyridine based Na_v1.7 channel blocker.

XEN402 (Figure 1.14) is also a selective Na_v1.7 channel blocker and is currently in phase II clinical trials. In phase I trials XEN402, a spiro-indole derivative, was found to be well tolerated and showed no significant safety issues.

Currently phase II trials have only been conducted with a small cohort of patients and for short dosing periods (2 days). Although results from the trial showed reduced pain induction times and reduced overall pain experienced, further studies with larger patient numbers over an increased time frame, are required to give more accurate results of the analgesic properties of XEN402.



XEN402

Figure 1.14. Spiro-indole Na_v1.7 channel blocker.

1.4.2 Serotonin (5 HT)

5HT (fig. 1.1) has a direct effect on the activation and sensitisation of nociceptive neurons and is released from platelets in the periphery as a result of tissue damage or insult. 5-HT has been shown to bind to 7 distinct receptors (5-HT₁₋₇) which can be further subdivided into 14 separate subtypes (5-HT_{1AF}, 5-HT_{2A-C}, 5-HT₃, 5-HT₄, 5-HT_{5A}, 5-HT₆, 5-HT₇). So far 5HT has been the target for several pharmacological treatments for depression, anxiety and obsessive compulsive disorder⁷⁴. It is known that 5HT plays a modulatory role in the analgesic effects of several compounds (TCAs and duloxetine, Figure 1.8). The complex nature of the mechanisms controlling 5-HT function and the contradicting nature of clinical trial results combine to make the design of an analgesic targeting the 5HT without severe side effects very challenging.

To date the only successful analgesics known to target the 5HT system are the triptan (Figure 1.15) family which have success in treating migraines⁷⁵. 5HT has functional roles in both ascending and descending nociceptive pathways, but the exact role has yet to be elucidated⁴⁴.

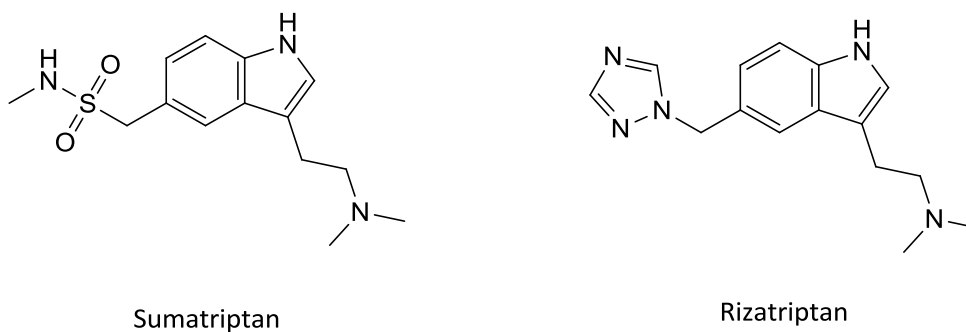


Figure 1.15. 5HT agonists, sumatriptan and rizatriptan have both had success treating migraine headaches.

1.4.3 Calcium channels

Voltage-gated calcium channels (Ca_v) are the primary sources for depolarisation-induced calcium entry into neurons. Ca_v regulate intracellular processes such as gene expression and neurotransmission. The calcium channel family can be broadly split into two subgroups based upon their voltage dependence of activation. The high voltage-activated channels, which can be further subdivided into the L,N,P,Q and R subtypes⁷⁶. The different ca_v isoforms show a diverse range of specific functions and have a distinct distribution throughout the cellular and subcellular levels. The N-type, P-type and Q-type channels are expressed on presynaptic nerve terminals where they modulate neurotransmitter release. The L-type channel is found in muscle and heart where they support excitation-contraction coupling⁷⁷. The diverse nature of the functional roles of the HVA calcium channels poses a challenge when designing a therapeutic agent with low risk of side effects.

Recently a number of inhibitors of N-type calcium channels inhibitors have been developed, aminopiperidine-sulfonamide⁷⁸, pyrazolpiperazines⁷⁹, TROX-1⁸⁰ and cilnidipine⁸¹ (Figure 1.16) which have all shown efficacy in various models of pain.

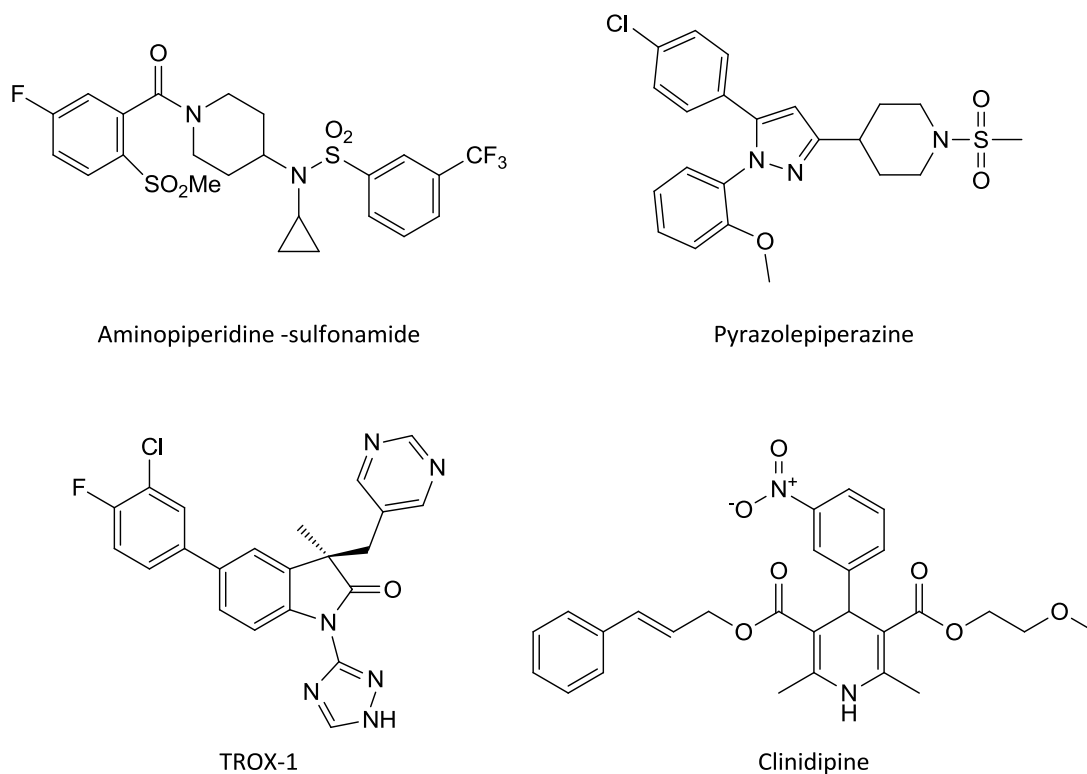
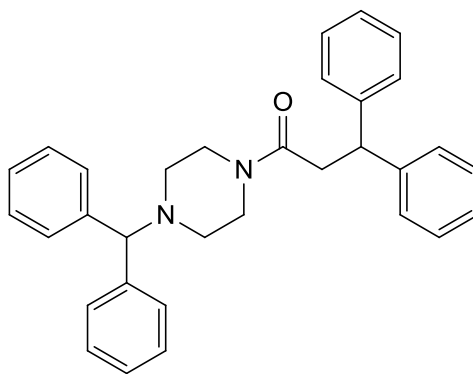


Figure 1.16. N-type calcium channels inhibitors.

A series of piperazine based compounds have been synthesised which, not only, display a high level of inhibition at inactivated calcium channels but also have a strong analgesic effect. Currently one of these compounds, Z160 (Figure 1.17), is in phase II clinical trials⁸².



Z160

Figure 1.17. Piperazine based calcium channel blocker, Z160.

The $\text{Ca}_v\alpha2\delta1$ has been found to be an important accessory subunit for HVA channels. It promotes the movement of HVA $\alpha1$ subunits to the plasma membrane. There is evidence that $\text{Ca}_v\alpha2\delta1$ is up regulated in neuropathic pain states and that this up regulation is linked to tactile allodynia. The $\text{Ca}_v\alpha2\delta1$ subunit is the primary target for gabapentinoids such as pregabalin and gabapentin (Figure 1.9). This target was confirmed by studies in transgenic knockout (KO) mice with a point mutation (R217A) in the $\text{Ca}_v\alpha2\delta1$ subunit. This rendered the KO mouse insensitive to the analgesic effects pregabalin.

Low voltage-activated T-type channels are activated by weak depolarisation and are transient. They are expressed in a diverse range of cell types and are involved in the control of repetitive firing and the shaping of action potentials. T-type channels contribute to neuronal signalling via multiple cellular mechanisms and pharmacological intervention of any of these may give rise to analgesia⁸³.

1.4.4 Vanilloid receptor (TRPV1)

The vanilloid receptor type 1 (TRPV1) is a ligand-gated nonselective cation channel and a member of the transient receptor potential (TRP) family of ion channels.

There are around 28 TRP channels discovered so far, 7 of which are known to detect hot or warm temperatures (TRPV1 - TRPV4, TRPM2, TRPM4, and TRPM5) and 2 which sense cold (TRPA1, TRPM8). All of the TRP channels share a topology that consists of 6 transmembrane domains (TM1-TM6) with the pore residing between TM5 and TM6. The C terminus is associated with the temperature sensing portion of the protein⁸⁴. TRPV1 channels are activated by a wide range of both exogenous and endogenous stimuli, including heat (>43°C) capsaicin (the active ingredient in chillies) (fig. 1.5) and low pH (<pH5)⁸⁵. The ion channel is activated upon detection of noxious stimuli which allows the influx of cations including Na⁺ and Ca²⁺. TRPV1 plays an important role in nociceptive pathways and can be modulated by inflammatory mediators including prostaglandins and bradykinin. TRPV1 receptors are found in both the peripheral central nervous systems localised on dorsal root ganglion neurons⁸⁶.

Capsaicin patches are used to treat localised neuropathic pain and typically include low concentrations of the active ingredient, containing between 1% and 8%. Although capsaicin, when applied to the skin, causes localised pain repeated applications causes a desensitisation of the nociceptor C fibres producing an analgesic effect⁸⁴. This desensitising effect is thought to be caused by the destruction of terminal axons and the dysfunction of localised nociceptors⁸⁷. New capsaicinoid therapies are in development such as the high-concentration 10% and 20% liquid capsaicin

1.4.5 Potassium Channels

Potassium (K⁺) channels are the most populous, diverse and widely distributed of all ion channels in the neurons. In humans their expression is governed by approximately 78 genes and further diversity is accomplished through the assembly various K⁺ channel subunits⁸⁸. K⁺ channels modulate an extremely rapid transmembrane K⁺ efflux which can not only influence the threshold of action potentials but can also modulate their frequency⁸⁹.

Several of the voltage-gated K⁺ channels (K_v) have a role in nociceptive pathways including K_v 9.1 and K_v2.1 which are down regulated in neuropathic pain models and K_v1.1 and K_v1.2 which may act together to reduce mechanical allodynia. It has long been known that G protein-coupled inwardly rectifying K⁺ (GiRK) channels play a role in pain signalling and also contribute to the analgesic effect of opioids. With the multitude of K⁺ channels distributed throughout the nervous system and the varying roles they play in pain pathways, there are many potential therapeutic targets to explore. Many of the K⁺ channels, however, are expressed in the brain and various excitable tissues. The challenge will be to selectively target K⁺ that are expressed in sensory neurons to avoid a host of adverse effects⁸³.

1.4.6 Nerve growth factor

Nerve growth factor NGF is a target derived neurotrophin secreted from cells of sympathetic and sensory neurons, and is involved in the growth, signalling, and survival of said neurons. The primary role of NGF in the developing system is one of neuronal survival, but in adults this role shifts to a more protective role by mediating pain from noxious stimuli. NGF signalling in these nociceptor neurons is mediated through two different receptors, the 75 kDa neurotrophin receptor (p75^{NTR}) and the tropomyosin-related kinase A (TrkA) receptor⁹⁰. Levels of NGF are known to be elevated in a variety of neuropathic pain states, including rheumatoid arthritis, spondyloarthritis, and endometriosis. Evidence has shown that NGF is important in the potentiation and mediation of pain and this has led to the development of NGF antagonists as potential analgesic agents. Several compounds have been developed to target NGF, the most successful being the humanised antibody IgG2 tanezumab, which has entered phase III clinical trials for the treatment of osteoarthritis. Whilst the initial results of the trials looked very encouraging several patients who took part in the trials have suffered from worsening of osteoarthritis probably due to over use of the joints. This has led the FDA to put a hold on the clinical trials for tanezumab⁹¹.

1.4.7 Glycine Receptor

Fast inhibitory neurotransmission in the spinal cord, caudal brain and brain stem are mediated by glycinergic synapses. Glycine receptors (GlyRs) are prominent in postsynaptic membranes, where they mediate a variety of motor and sensory functions including vision, audition and suppression of the nociceptive signals⁹². Activation of GlyRs, either by presynaptically released glycine or by an extracellularly applied agonist, facilitates the opening of the anion-selective pore. This allows an influx of Cl⁻ ions into the cell which results in a hyperpolarization of the postsynaptic membrane resulting in a stabilisation of the resting potential of the cell and, therefore, an inhibition of neuronal firing⁹³.

It is of interest to note, however, that during embryonic development GlyRs are not inhibitory but are in fact excitatory. This effect is due to a more positive equilibrium potential in embryonic neurons. Subsequently activation of the GlyR results in an efflux of Cl⁻ ions and a depolarisation of the membrane, which allows the activation of voltage gated Ca²⁺ channels. The rise in Ca²⁺ levels appears to be instrumental in the formation of the synapse as blockade of the Ca²⁺ channel disrupts localisation of the GlyRs at the nerve terminals. The Cl⁻ equilibrium potential shifts to a negative hyperpolarising value after birth^{94,95}.

GlyRs are members of the group I ligand-gated ion channel (LGIC) family, which also includes the anionic γ -amino-butyric acid (GABA_A and GABA_C) receptors and the cationic nicotinic acetylcholine (nACh) and serotonin (5HT) receptors. GlyRs have a pentameric arrangement of transmembrane domains which are arranged symmetrically around a central pore⁹⁶. To date five genes encoding for GlyR subunits have been cloned from mammalian tissue *Glr1-4* code for α subunits ($\alpha 1$ – $\alpha 4$) and a single *Glr5* codes for the β subunit. The α subunits share a high sequence identity of ~ 80% whilst the β subunit shows significant sequence differences compared with the α subunits of less than 50% identity⁹⁷.

Each GlyR subunit contains an N-terminal extracellular domain (ECD) which contains the agonist binding site, four transmembrane segments (TM1-TM4), a large intracellular loop between TM3 and TM4 which houses the phosphorylation sites and also the binding motifs for intracellular proteins. TM2 is amphiphilic and forms the anionic permeable pore⁹⁸. In adult mammalian CNS most GlyRs are heteropentameric and are composed of α 1 and β subunits whose stoichiometry is thought to be $2(\alpha 1)/3\beta$ ⁹⁹.

Many GlyRs are colocalised with the submembrane scaffold protein gephyrin, which interacts with intracellular components such as tubulin and proteins implicated in membrane protein transport⁹⁵.

GlyRs are modulated by a wide range of endogenous ligands including cations, Zn^{2+} and Ni, and the cannabinoid anandamide (Figure 1.18). Although to date no drugs have been developed to primarily target the GlyR a number of pharmaceutical agents are known to modulate the receptor including, alcohols (ethanol and trichloroethanol), tropines (tropisetron), and general anaesthetics (propofol and iosflurane) (Figure 1.18)^{100,101}.

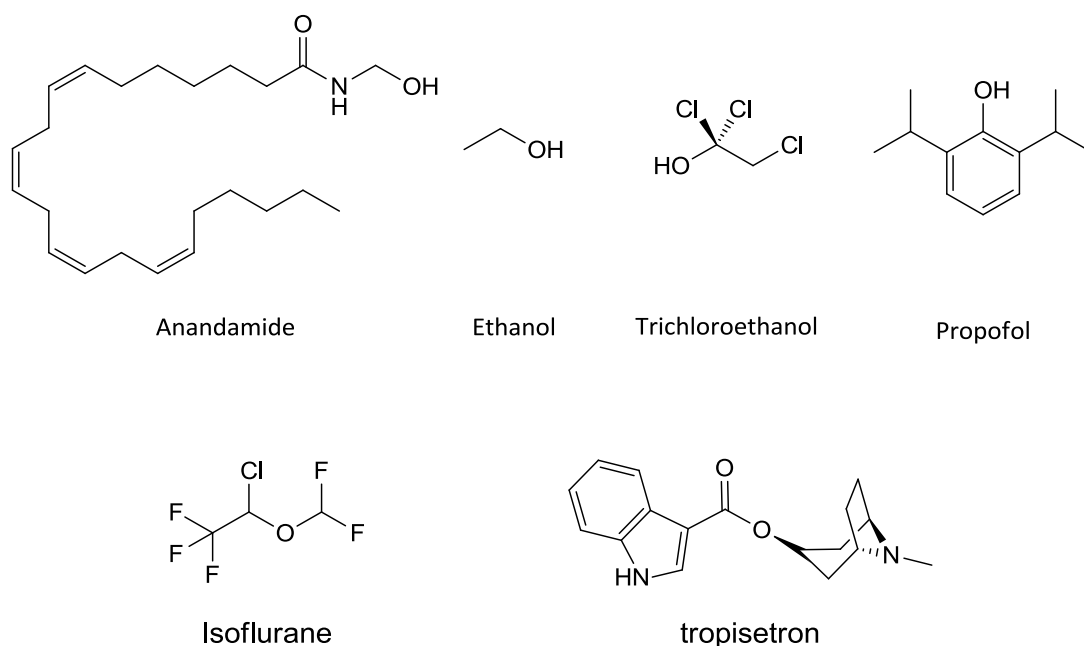


Figure 1.18. Modulators of the GlyR.

The binding site of propofol has been studied *in vivo* in transgenic and knock-in murine models. Zn^{2+} and tropines are thought to bind at or in close proximity to the extra cellular agonist binding site whilst the hydrophobic modulators, cannabinoids, anaesthetics and ethanol are thought to bind at the transmembrane domain whereas channel blockers such strychnine are thought to bind close to the intracellular domain (Figure 1.19) ^{102-104, 107}.

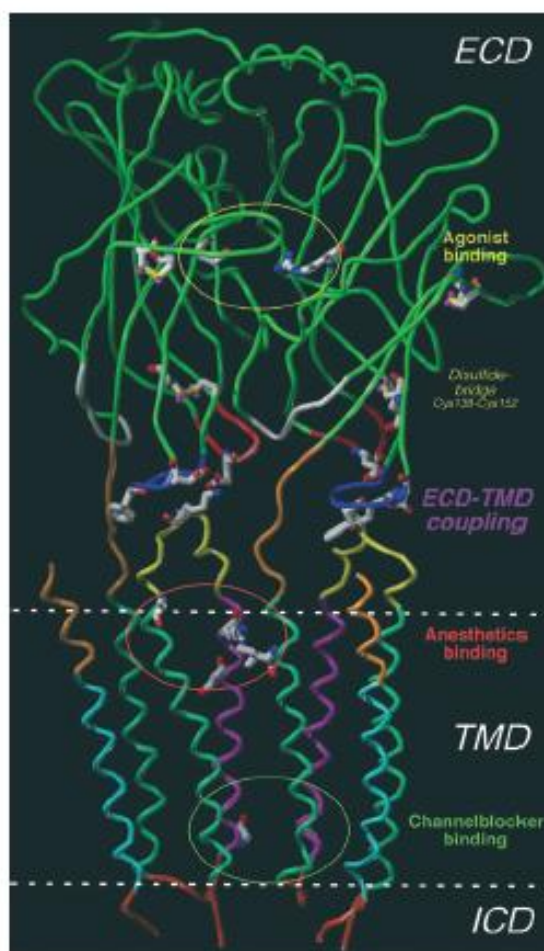
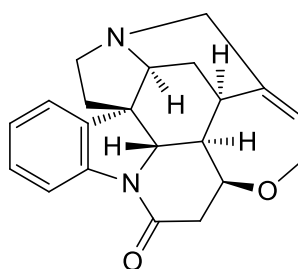


Figure 1.18. Ribbon model of the glycine receptor showing binding sites for propofol (anaesthetic binding) and strychnine (channel blocker binding). ECD - Extra cellular domain. TMD - Transmembrane domain. ICD – Intracellular domain (Taken from ref ¹⁰⁷).

Immunocytochemistry has revealed that the $\alpha 1$ and $\alpha 3$ GlyRs are distinctly expressed in the superficial layers of the spinal cord, specifically laminae I and II of the dorsal horn (the primary site of synaptic integration in the nociceptive pathway)¹⁰⁵.

From here a network of glycinergic interneurons regulates the transduction of pain signals to higher regions of the brain. Inflammatory pain originates from the disinhibition of dorsal horn neurons. Activation of prostaglandin E (EP2 subtype) receptors, via PGE₂ release, leads to phosphorylation and subsequent inhibition of GlyRs specifically the $\alpha 3$ subtype. In addition *Gla3* knock out studies have abolished dorsal horn glycinergic inhibition in the presence of PGE₂ in spinal cord slice preparations and PGE₂ mediated sensitisation in the animal model. It has also been shown that intrathecal injections of the GlyR antagonist strychnine (a convulsive indole alkaloid which is a powerful antagonist of GlyRs, (Figure 1.20) can elicit exaggerated nociceptive responses. It is, therefore, postulated that compounds which enhance glycinergic responses within the dorsal horn could have therapeutic potential as analgesic agents¹⁰⁵.



Strychnine

Figure 1.20. Indole alkaloid strychnine.

1.4.8 Gamma-Aminobutyric acid receptor

As with GlyRs, GABA receptors (GABARs) also inhibit fast inhibitory synaptic transmission throughout the brain and CNS. GABA_A and GABA_B are the two major isoforms of the receptor. The GABA_B receptor is a G protein coupled receptor and is found on both pre and post synaptic terminals. Activation of GABA_B receptors modulates a second messenger phosphorylation cascade which produces a variety of responses including modulation of calcium and potassium channels¹⁰⁶.

GABA_A receptors are members of the LGIC superfamily and as such are structurally related to GlyRs. To date 19 subunits of GABARs have been cloned, this underlies the diverse nature and complex pharmacology of these receptors¹⁰⁷.

GABA_A receptors are the primary site of action for many therapeutic agents including anxiolytics (alprazolam and ocinaplon, Figure 1.21), hypnotics (zolpidem and indiplon, Figure 1.21) and anaesthetics (propofol, Figure 1.19 and thiopental, Figure 1.21)¹⁰⁸. Many of the compounds that target the GABA_A receptors are associated with a range of unwanted side effects, tolerance and withdrawal issues. Although not a target for analgesia, it is important to understand the side effect burden which stems from potentiating the GABA_A¹⁰⁹.

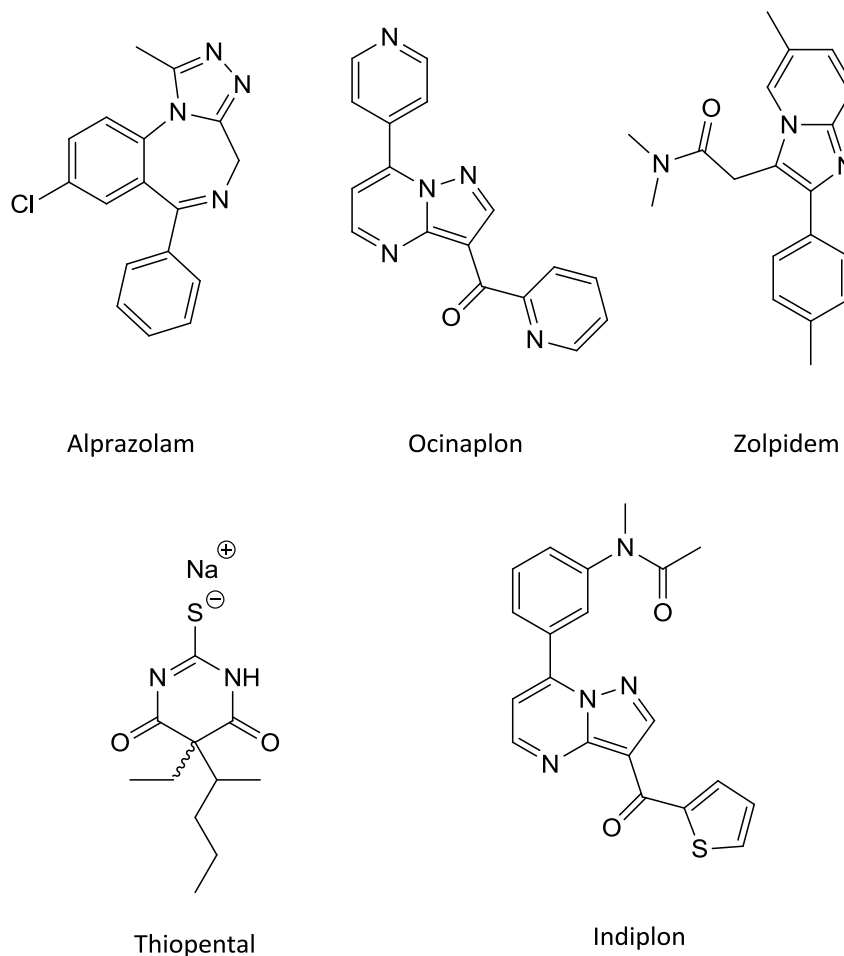


Figure 1.19. Modulators of the GABA_A receptor.

1.5 Propofol

The introduction of general anaesthetics in the mid-19th century revolutionised surgical procedures. What were once considered painful dangerous and often unsuccessful procedures have now become much safer, less painful and have much more predictable outcomes. For over a century anaesthesia was achieved using volatile gaseous anaesthetics such as, ether, nitrous oxide and chloroform (Figure 1.20).

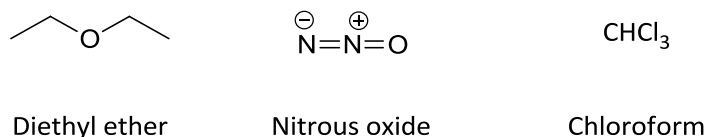


Figure 1.20. Early volatile gaseous anaesthetics

More recently intravenous anaesthetics have become the most popular method of inducing and maintain anaesthesia¹¹⁰. 2, 6-diisopropylphenol (propofol, Diprivan, Figure 1.18) is a fast acting sedative agent which was first introduced clinically in 1985¹¹¹. Since its approval for the induction and maintenance of general anaesthesia by the food and drug administration (FDA) in 1989, propofol has become the most widely used intravenous general anaesthetic agent in the world¹¹².

Propofol is a highly lipophilic alkyl phenol and as such has a low solubility in water and was originally prepared as 1% solution in Cremophor EL (CrEL). CrEL is a heterogeneous non-ionic surfactant which is produced by the reaction of castor oil with ethylene oxide. CrEL has been deemed as an unsuitable solvent in America, therefore, propofol is now prepared as an oil in water emulsion with 1% propofol, 10% soybean oil, 2.25% glycerol, and 1.2% egg lecithin^{110,113}.

Propofol is renowned for a rapid onset of sedation, approximately 40 seconds after administration; this is due to a rapid equilibration between plasma and highly perfused brain tissues. With the peak effect occurring within 1-2 minutes and duration of effect between 4-8 minutes (following a single intravenous dose of 1.5-2.5 mg/kg), propofol has a rapid emergence from sedation with little nausea or vomiting¹¹⁴.

In an effort to overcome the innate solubility issues seen with propofol, several water soluble alternatives have been synthesised. Propofol phosphate, propofol ethyl dioxy phosphate and fospropofol (Aquavan[®], Lusedra) are all phosphate prodrugs of propofol (Figure 1.23). Collectively they all rely upon enzymatic

cleavage of the phosphate moiety to release the parent drug and consequently they all have a markedly slower onset of sedation than the parent compound.

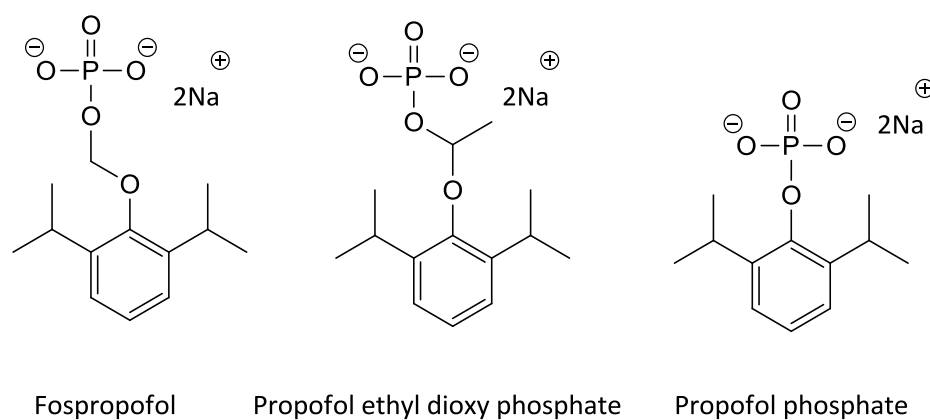


Figure 1.23. Phosphate prodrugs of propofol.

A major drawback to both propofol ethyl dioxy phosphate and fospropofol is that they liberate toxic compounds upon metabolism. Propofol ethyl dioxy phosphate liberates acetaldehyde, which has been linked to gastrointestinal tract cancer, whereas, fospropofol releases formaldehyde which is further metabolised to formate (Figure 1.24). Whilst formaldehyde is a naturally occurring metabolite from many cellular processes, elevated levels are thought to alter homeostasis within cells and may also play a role in enzyme induction, metabolic switching and cell proliferation¹¹⁵. The rapid conversion of formaldehyde to formate is mediated by aldehyde dehydrogenase in the liver and in erythrocytes and formate is further metabolised by 10-formyltetrahydrofolate dehydrogenase and tetrahydrofolate. On the basis of this the liberation of formaldehyde is not thought to be toxic in patients with normal levels of tetrahydrofolate^{116,117}.

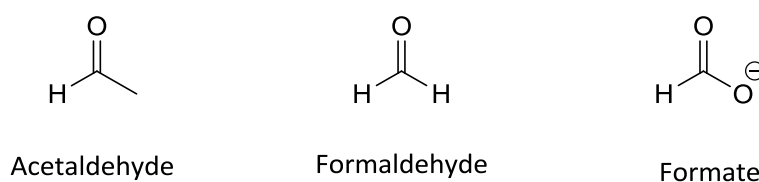


Figure 1.24. By-products of phosphate prodrug metabolism

The most common adverse effect associated with propofol use is pain at the injection site (occurring in 80-90% of patients). Although this is often attributed to propofol's lipid formulation, studies have shown that propofol can activate the TRPA1 receptor which is co-associated with TRVP1 receptors in 30% of nociceptive neurons. As a consequence the local anaesthetic lidocaine is generally administered prior to propofol use^{114,118}.

Studies have shown propofol exerts its sedatory effects by modulating the inhibitory function of the GABA_A receptor, specifically by decreasing cerebral metabolism in the hippocampus, parietal, frontal and occipital lobes. This involves areas of sensory, motor and limbic systems^{119,120}. Clinical relevant concentrations of propofol can markedly increase GABA induced Cl⁻ current and a report published in 2003 showed that a point mutation in the β3 subunit of the GABA_A receptor could eliminate propofol activity^{121,122}.

Propofol is also known to be a positive allosteric modulator of the strychnine sensitive glycine receptor¹²³. With the role the GlyRs play in nociceptive pathways it is thought that the binding of propofol to GlyRs and the subsequent increase in Cl⁻ could contribute to analgesia¹²⁴. Reports have shown that sub-hypnotic doses of propofol (0.25mg/Kg) can reduce laser induced pain in human volunteers and intravenous administration of 0.25mg/Kg followed by 25µg/Kg/min can significantly reduce pain intensity^{125,126}.

The short duration of action of propofol is due to a rapid redistribution and metabolism, primarily by the liver, into a range of inactive metabolites. The major route of metabolism for propofol is glucuronidation of the parent compound at the phenolic hydroxyl site (50-60% of the overall dose). The remaining is metabolised via ring hydroxylation to give the 4- hydroxyl propofol which is further subject to glucuronidation and sulfation. Glucuronidation is catalysed by uridine diphosphate-glucuronosyltransferases (UGT) such as UGT1A9, whereas sulfation is catalysed by sulfotransferases (SULTs). Oxidative metabolism of propofol is mediated via a range of cytochrome P450 enzymes (CYP450) including, CYP2C9 (removes around 50%), CYP2A6, 2C8, 2C18, 2C19, and 1A2 (Figure 1.25)^{127,128}.

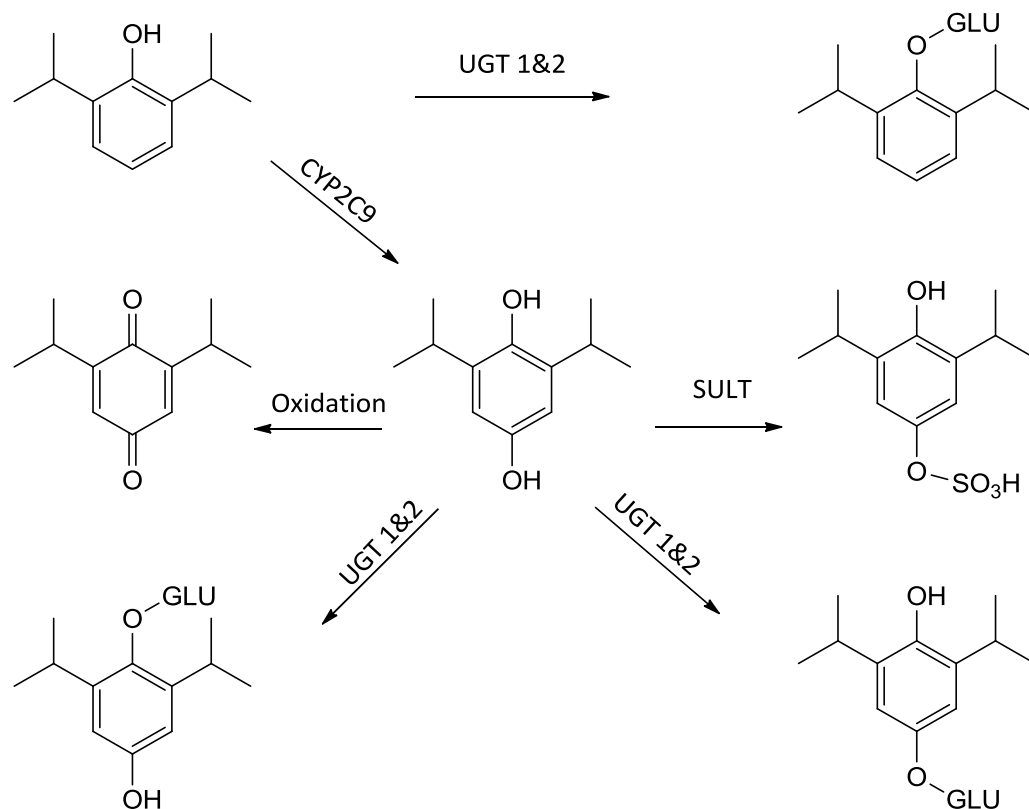


Figure 1.25. The metabolic pathway of propofol in humans. UGT— uridine diphosphateglucuronosyltransferase, SULT — sulfotransferases, CYP — cytochrome P450 isozymes, GLU — glucuronide.

Propofol modulates receptors within the CNS, but in order for propofol to access the CNS it must first cross the blood brain barrier.

1.6 Blood brain barrier

As propofol is a small lipophilic molecule it can freely diffuse through the barrier. For novel neurotherapeutics, however, the blood brain barrier has become somewhat of a bottle neck of drug development¹²⁹.

Figures indicate that less than 11% of novel pharmaceutical entering clinical development actually made it into the marketplace. The probability of CNS drug entering the marketplace, however, is considerably lower at around 7%.

Figures show that the average development timescale for drugs targeting cardiovascular or gastrointestinal indications is between 6-7.5 years, whereas on average the development of CNS indicated drugs took 12.6 years¹³⁰.

The attrition rate for CNS drug development is higher than average for several reasons; the complexity of the CNS, the lack of a mechanistic understanding for many of the CNS disorders and the inclination toward CNS mediated side effects such as dizziness and nausea¹³¹. Perhaps the biggest hurdle for many novel pharmaceutical agents is the penetration of the blood brain barrier (BBB), approximately 98% of small-molecule (~100 Da molecular mass or less) compounds and 100% of large-molecule (>750 Da) compounds never reaches the marketplace because of their inability to cross the BBB¹²⁹.

The BBB acts as a physical barrier between the CNS and the periphery. Consisting of tightly fenestrated endothelial cells, which line a network of capillaries which form the microvessels of the brain, the BBB is the largest interface for blood-brain exchange. The surface area of the vessels of the BBB are, on average, between 150-200 cm²g⁻¹ which for the average human adult gives between 12-18 m² of tissue for exchange within the brain¹³². The tight intracellular junctions of the endothelial cells regulate the exposure of the brain to xenobiotics and also minimises paracellular transport^{133,134} (Figure 1.26). Small gaseous molecules such as O₂ and CO₂ have the ability to freely diffuse across lipid membranes and this is also the route taken by small lipophilic drug molecules such as barbiturates and propofol¹³⁵. Astrocytes and pericytes also aid in the compartmentalisation of the CSF. Astrocytes are glial cells which interact closely with endothelial cells and have an essential role in maintenance of cerebral blood flow enzymatic systems and polar transporters. The tight junctions which make up the unique phenotype of the BBB are determined by the interaction of astrocytes and the cerebral endothelial cells. Pericytes are associated with the stabilisation of small vessels and angiogenesis. They are separated from the cerebral endothelial cells by the basal lamina¹³².

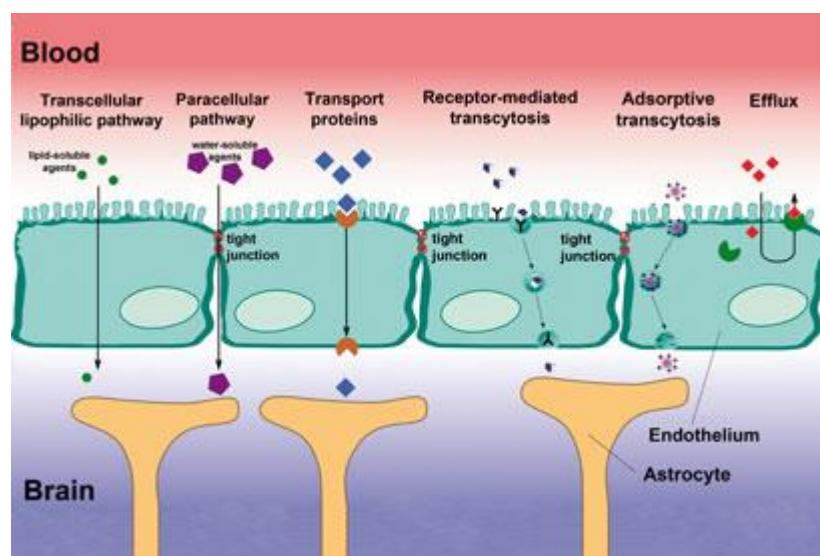


Figure 1.26. Blood brain barrier and transport mechanisms¹³⁶.

The BBB serves several functional roles. It supplies essential nutrients to the brain and mediates the efflux of waste some waste products. It controls the ionic composition of interstitial fluid (ISF) and cerebrospinal fluid (CSF) which provides a stable environment for neural functioning and synaptic signalling. This is important for preventing fluctuations of ion levels, especially after exercise or a meal. The BBB also helps to keep the pools of neurotransmitters that act peripherally and centrally separate, thus, preventing 'crosstalk' between similar agents used in both systems. The protein compositions of plasma and CSF are very different, the levels of protein in CSF is much lower than that of the plasma. The BBB also prevents macromolecules such as albumin, pro-thrombin and plasminogen from entering the CSF where they would cause severe pathological damage^{135,137}.

The high prevalence of active transporters, both uptake and efflux, combined with high concentrations of metabolising enzymes and low rates of passive diffusion present a complex biological barrier to the design of pharmaceutical agents targeting diseases of the CNS.

1.7 Aims

This thesis addresses the longstanding urgent, unmet medical need of chronic pain. Recent surveys have found that chronic pain affects up to 20% of adults in Europe and the USA⁹. One key issue is the fact that the symptomatic medication currently available is effective only in about 40% of chronic pain sufferers and even these patients struggle to maintain the balance between adequate pain relief and their ability to cope with substantial drug-induced adverse effects¹³⁸. This creates a vicious cycle of insufficient analgesia and unbearable side effects ultimately leading to discontinuation of treatment. A greater understanding of the underlying mechanisms of chronic pain has revealed the key role the glycine receptor (GlyR) plays in nociceptive pathways⁹⁷.

The aims of this research were to synthesise a series of novel analgesic compounds, based around a propofol core, with favourable DMPK and toxicity profiles which selectively target the $\alpha 1$ subtype of the GlyR. Selected compounds will be investigated in the Chung Lesion model of neuropathic pain to assess their analgesic activities.

1.8 References

1. Wachter-Shikora, N.L. Pain Theories and Their Relevance to the Pediatric Population. *Issues in Comprehensive Pediatric Nursing* **5**, 321-326 (1981).
2. Brower, V. New paths to pain relief. *Nature Biotechnology* **18**, 387-391 (2000).
3. Woolf, C.J. Pain: moving from symptom control toward mechanism-specific pharmacologic management. *Annals Of Internal Medicine* **140**, 441-451 (2004).
4. Fallon, M.T. Neuropathic pain in cancer. *British Journal of Anaesthesia : BJA* **111**, 105-111 (2013).
5. Gilron, I. & Max, M.B. Combination pharmacotherapy for neuropathic pain: current evidence and future directions. *Expert Review of Neurotherapeutics* **5**, 823-830 (2005).
6. Clauw, D.J. Fibromyalgia: an overview. *American Journal of Medicine* **122**, S3-S13 (2009).
7. van Tilburg, M.A., Zaki, E.A., Venkatesan, T. & Boles, R.G. Irritable bowel syndrome may be associated with maternal inheritance and mitochondrial DNA control region sequence variants. *Digestive Diseases & Sciences* **59**, 1392-1397 (2014).
8. Das, S.K. & Farooqi, A. Osteoarthritis. *Best Practice & Research Clinical Rheumatology* **22**, 657-675 (2008).
9. Breivik, H., Collett, B., Ventafridda, V., Cohen, R. & Gallacher, D. Survey of chronic pain in Europe: Prevalence, impact on daily life, and treatment. *European Journal of Pain* **10**, 287-333 (2006).
10. Steglitz, J., Buscemi, J. & Ferguson, M.J. The future of pain research, education, and treatment: a summary of the IOM report "Relieving pain in America: a blueprint for transforming prevention, care, education, and research". *Translational Behavioral Medicine* **2**, 6-8 (2012).
11. Bair, M.J., Robinson, R.L., Katon, W. & Kroenke, K. Depression and pain comorbidity: a literature review. *Archives of Internal Medicine* **163**, 2433-2445 (2003).
12. Backonja, M. & Woolf, C.J. Future directions in neuropathic pain therapy: closing the translational loop. *The Oncologist* **15**, 24-29 (2010).
13. Woolf, C.J. Overcoming obstacles to developing new analgesics. *Nature Medicine* **16**, 1241-1247 (2010).
14. Woolf, C.J. & Ma, Q. Nociceptors Noxious Stimulus Detectors. *Neuron* **55**, 353-364 (2007).
15. Greenspan, J.D. Nociceptors and the peripheral nervous system's role in pain. *Journal of Hand Therapy* **10**, 78-85 (1997).
16. Kandel, E.R., Schwartz, J.H. & Jessell, T.M. *Principles of Neural Science*, (McGraw-Hill, Health Professions Division, 2000).
17. Xie, Y.-f., Huo, Fu-quan, Tang, Jing-shi. Cerebral cortex modulation of pain. *Acta Pharmacologica Sinica* **30**, 31-41 (2009).

18. Millan, M.J. The induction of pain: an integrative review. *Progress in Neurobiology* **57**, 1-164 (1999).
19. Bingham, B., Ajit, S.K., Blake, D.R. & Samad, T.A. The molecular basis of pain and its clinical implications in rheumatology. *Nature Clinical Practice. Rheumatology* **5**, 28-37 (2009).
20. Latremoliere, A. & Woolf, C.J. Central Sensitization: A Generator of Pain Hypersensitivity by Central Neural Plasticity. *The Journal of Pain* **10**, 895-926 (2009).
21. Raouf, R., Quick, K. & Wood, J.N. Pain as a channelopathy. *Journal of Clinical Investigation* **120**, 3745-3752 (2010).
22. Zlotnik, A., Gruenbaum, S.E., Rozet, I., Zhumadilov, A. & Shapira, Y. Risk of aspiration during anesthesia in patients with congenital insensitivity to pain with anhidrosis: case reports and review of the literature. *Journal of Anesthesia* **24**, 778-782 (2010).
23. Woolf, C.J. What is this thing called pain? *Journal of Clinical Investigation* **120**, 3742-3742-3744 (2010).
24. Huang, J., Zhang, X. & McNaughton, P.A. Inflammatory pain: the cellular basis of heat hyperalgesia. *Current Neuropharmacology* **4**, 197-206 (2006).
25. Julius, D. & Basbaum, A.I. Molecular mechanisms of nociception. *Nature* **413**, 203-210 (2001).
26. Babos, M.B., Grady, B., Wisnoff, W. & McGhee, C. Pathophysiology of pain. *Disease-a-Month* **59**, 330-358 (2013).
27. Dubin, A.E. & Patapoutian, A. Nociceptors: the sensors of the pain pathway. *The Journal Of Clinical Investigation* **120**, 3760-3772 (2010).
28. Jensen, T.S. Baron, R. Haanpää, M. Kalso, E. Loeser, J. D. Rice, A. S. Treede, R. D. A new definition of neuropathic pain. *Pain* **152**, 2204-2205 (2011).
29. Hoffmann, T., Sauer, S.K., Horch, R.E. & Reeh, P.W. Sensory transduction in peripheral nerve axons elicits ectopic action potentials. *The Journal of Neuroscience : The Official Journal of the Society for Neuroscience* **28**, 6281-6284 (2008).
30. Pezet, S. Pezet, S. Marchand, F. D'Mello, R. Grist, J. Clark, A. K. Malcangio, M. Dickenson, A. H. Williams, J. McMahan, S. B. Phosphatidylinositol 3-kinase is a key mediator of central sensitization in painful inflammatory conditions. *The Journal of Neuroscience : The Official Journal of the Society for Neuroscience* **28**, 4261-4270 (2008).
31. Namaka, M. Gramlich, C. R. Ruhlen, D. Melanson, M. Sutton, I. Major, J. A treatment algorithm for neuropathic pain. *Clinical therapeutics* **26**, 951-979 (2004).
32. Jay, G.W. & Barkin, R.L. Neuropathic pain: etiology, pathophysiology, mechanisms, and evaluations. *Disease-a-Month* **60**, 6-47 (2014).
33. Micheletti, L., Radici, G. & Lynch, P.J. Provoked vestibulodynia: Inflammatory, neuropathic or dysfunctional pain? A neurobiological perspective. *Journal of Obstetrics & Gynaecology* **34**, 285-288 (2014).

34. Staud, R., Craggs, J.G., Perlstein, W.M., Robinson, M.E. & Price, D.D. Brain activity associated with slow temporal summation of C-fiber evoked pain in fibromyalgia patients and healthy controls. *European Journal of Pain* **12**, 1078-1089 (2008).
35. Staud, R. & Rodriguez, M.E. Mechanisms of disease: pain in fibromyalgia syndrome. *Nature Clinical Practice. Rheumatology* **2**, 90-98 (2006).
36. Pergolizzi, J.V., Jr., Raffa, R.B., Tallarida, R., Taylor, R. & Labhsetwar, S.A. Continuous multimechanistic postoperative analgesia: a rationale for transitioning from intravenous acetaminophen and opioids to oral formulations. *Pain Practice* **12**, 159-173 (2012).
37. Ostapowicz, G., Fontana, R. J.Schiødt, F. V., *et al.* Results of a prospective study of acute liver failure at 17 tertiary care centers in the United States. *Annals of Internal Medicine* **137**, 947-954 (2002).
38. Ward, B. & Alexander-Williams, J.M. Paracetamol revisited: A review of the pharmacokinetics and pharmacodynamics. *Acute Pain* **2**, 139-149 (1999).
39. Vane, J.R., Bakhle, Y.S. & Botting, R.M. Cyclooxygenases 1 and 2. *Annual Review of Pharmacology* **38**, 97-120 (1998).
40. Williams, M., Kowaluk, E.A. & Arneric, S.P. Emerging molecular approaches to pain therapy. *Journal of Medicinal Chemistry* **42**, 1481-1500 (1999).
41. Naesdall, J. & Brown, K. NSAID-associated adverse effects and acid control aids to prevent them - A review of current treatment options. *Drug Safety* **29**, 119-132 (2006).
42. Laine, L. Nonsteroidal anti-inflammatory drug gastropathy. *Gastrointestinal Endoscopy Clinics of North America* **6**, 489-504 (1996).
43. Dworkin, R.H. Alec B. O'Connor, and Christopher D. Wells. Recommendations for the pharmacological management of neuropathic pain: an overview and literature update. *Mayo Clinic Proceedings* **85**, S3-S14 (2010).
44. Bannister, K., Bee, L. & Dickenson, A. Preclinical and early clinical investigations related to monoaminergic pain modulation. *Neurotherapeutics* **6**, 703-712 (2009).
45. Ferjan, I. & Lipnik-Štangelj, M. Chronic pain treatment: the influence of tricyclic antidepressants on serotonin release and uptake in mast cells. *Mediators of Inflammation* **2013**, 340473 (2013).
46. Max, M.B. Culnane, M. Schafer, S. C. Gracely, R. H. Walther, D. J. Smoller, B. Dubner, R. Amitriptyline relieves diabetic neuropathy pain in patients with normal or depressed mood. *Neurology* **37**, 589-596 (1987).
47. Max, M.B. Lynch, S. A. Muir, J. Shoaf, S. E. Smoller, B. Dubner, R.. Effects of desipramine, amitriptyline, and fluoxetine on pain in diabetic neuropathy. *New England Journal of Medicine* **326**, 1250-1256 (1992).
48. Cohen, H.W., Gibson, G. & Alderman, M.H. Excess risk of myocardial infarction in patients treated with antidepressant medications: association with use of tricyclic agents. *American Journal of Medicine* **108**, 2-8 (2000).

49. Haanpää, M. Attal, N. Backonja, M., *et al.* NeuPSIG guidelines on neuropathic pain assessment. *Pain* **152**, 14-27 (2011).
50. Raskin, J. Pritchett, Y. L. Wang, F. D'Souza, D. N. Waninger, A. L. Iyengar, S. Wernicke, J. F. . A double-blind, randomized multicenter trial comparing duloxetine with placebo in the management of diabetic peripheral neuropathic pain. *Pain Medicine* **6**, 346-356 (2005).
51. Goldstein, D.J., Lu, Y., Detke, M.J., Lee, T.C. & Iyengar, S. Duloxetine vs. placebo in patients with painful diabetic neuropathy. *Pain* **116**, 109-118 (2005).
52. Sindrup, S.H., Bach, F.W., Madsen, C., Gram, L.F. & Jensen, T.S. Venlafaxine versus imipramine in painful polyneuropathy: a randomized, controlled trial. *Neurology* **60**, 1284-1289 (2003).
53. Dunner, D.L., Wohlreich, M.M., Mallinckrodt, C.H., Watkin, J.G. & Fava, M. Clinical consequences of initial duloxetine dosing strategies: Comparison of 30 and 60 mg QD starting doses. *Current Therapeutic Research* **66**, 522-540 (2005).
54. Rowbotham, M.C., Goli, V., Kunz, N.R. & Lei, D. Venlafaxine extended release in the treatment of painful diabetic neuropathy: a double-blind, placebo-controlled study. *Pain* **110**, 697-706 (2004).
55. Taylor, C.P. Mechanisms of analgesia by gabapentin and pregabalin--calcium channel alpha2-delta [Cavalpha2-delta] ligands. *Pain* **142**, 13-16 (2009).
56. Chen, C., Han, C.H., Sweeney, M. & Cowles, V.E. Pharmacokinetics, efficacy, and tolerability of a once-daily gastroretentive dosage form of gabapentin for the treatment of postherpetic neuralgia. *Journal of Pharmaceutical Sciences* **102**, 1155-1164 (2013).
57. Kaufman, K.R., Parikh, A., Chan, L., Bridgeman, M. & Shah, M. Myoclonus in renal failure: Two cases of gabapentin toxicity. *Epilepsy & Behavior Case Reports* **2**, 8-10 (2014).
58. Van Seventer, R., Feister, H. A. Young, J. P., Jr. Stoker, M. Versavel, M. Rigaudy, L. Efficacy and tolerability of twice-daily pregabalin for treating pain and related sleep interference in postherpetic neuralgia: a 13-week, randomized trial. *Current Medical Research & Opinion* **22**, 375-384 (2006).
59. Dworkin, R.H., Corbin, A. E. Young, J. P., Jr. Sharma, U. LaMoreaux, L. Bockbrader, H. Garofalo, E. A. Poole, R. M. Pregabalin for the treatment of postherpetic neuralgia: a randomized, placebo-controlled trial. *Neurology* **60**, 1274-1283 (2003).
60. Siddall, P.J., Cousins, M. J. Otte, A. Griesing, T. Chambers, R. Murphy, T. K. Pregabalin in central neuropathic pain associated with spinal cord injury: a placebo-controlled trial. *Neurology* **67**, 1792-1800 (2006).
61. Galvez, R., Cherry, D.A., Jacquot, F. & Versavel, M. Pregabalin Reduces Pain and Improves Sleep and Mood Disturbances in Patients with Postherpetic Neuralgia: Results of a Randomized, Placebo-Controlled Clinical Trial. *Anesthesiology Abstracts of Scientific Papers Annual Meeting*, A-970 (2003).

62. Devers, A. & Galer, B.S. Topical lidocaine patch relieves a variety of neuropathic pain conditions: an open-label study. *The Clinical Journal of Pain* **16**, 205-208 (2000).
63. Paice, J.A. , Ferrans, C. E. Lashley, F. R. Shott, S. Vizgirda, V. Pitrak, D. Topical capsaicin in the management of HIV-associated peripheral neuropathy. *Journal of Pain and Symptom Management* **19**, 45-52 (2000).
64. Kalyuzhny, A.E., Arvidsson, U., Wu, W. & Wessendorf, M.W. mu-Opioid and delta-opioid receptors are expressed in brainstem antinociceptive circuits: studies using immunocytochemistry and retrograde tract-tracing. *The Journal of Neuroscience : The Official Journal of the Society for Neuroscience* **16**, 6490-6503 (1996).
65. Mansour, A., Fox, C.A., Burke, S., Akil, H. & Watson, S.J. Immunohistochemical localization of the cloned mu opioid receptor in the rat CNS. *Journal of chemical neuroanatomy* **8**, 283-305 (1995).
66. Ambriz-Tututi, M., Rocha-González, H.I., Cruz, S.L. & Granados-Soto, V. Melatonin: A hormone that modulates pain. *Life Sciences* **84**, 489-498 (2009).
67. Dworkin, R.H., O'Connor, A. B. Backonja, M. *et al.* Pharmacologic management of neuropathic pain: evidence-based recommendations. *Pain* **132**, 237-251 (2007).
68. Dib-Hajj, S.D., Binshtok, A. M. Cummins, T. R. Jarvis, M. F. Samad, T. Zimmermann, K. Voltage-gated sodium channels in pain states: role in pathophysiology and targets for treatment. *Brain Research Reviews* **60**, 65-83 (2009).
69. Khaliq, Z.M., Gouwens, N.W. & Raman, I.M. The contribution of resurgent sodium current to high-frequency firing in Purkinje neurons: an experimental and modeling study. *The Journal of Neuroscience : The Official Journal of the Society for Neuroscience* **23**, 4899-4912 (2003).
70. Raman, I.M. & Bean, B.P. Resurgent sodium current and action potential formation in dissociated cerebellar Purkinje neurons. *The Journal of Neuroscience : The Official Journal of the Society for Neuroscience* **17**, 4517-4526 (1997).
71. Walia, K.S., Khan, E.A., Ko, D.H., Raza, S.S. & Khan, Y.N. Side Effects of Antiepileptics— A Review. *Pain Practice* **4**, 194-203 (2004).
72. Fava, M., Mulroy, R., Alpert, J., Nierenberg, A.A. & Rosenbaum, J.F. Emergence of adverse events following discontinuation of treatment with extended-release venlafaxine. *American Journal of Psychiatry* **154**, 1760-1762 (1997).
73. London, C., Hoyt, Scott B. Parsons, William H. *et al.* Imidazopyridines: A novel class of hNav1.7 channel blockers. *Bioorganic & Medicinal Chemistry Letters* **18**, 1696-1701 (2008).

74. Andrews, N. & O'Neill, M.F. It might be a big family but the pain remains—last chance saloon for selective 5-HT receptor ligands? *Current Opinion in Pharmacology* **11**, 39-44 (2011).
75. Colpaert, F.C. 5-HT(1A) receptor activation: new molecular and neuroadaptive mechanisms of pain relief. *Current Opinion in Investigational Drugs* **7**, 40-47 (2006).
76. Catterall, W.A., Striessnig, J., Snutch, T.P. & Perez-Reyes, E. International Union of Pharmacology. XL. Compendium of voltage-gated ion channels: Calcium channels. *Pharmacological reviews* **55**, 579-581 (2003).
77. Kisilevsky, A.E., Mulligan, Sean J. Altier, Christophe., *et al.* D1 receptors physically interact with N-type calcium channels to regulate channel distribution and dendritic calcium entry. *Neuron* **58**, 557-570 (2008).
78. Shao, P.P., Ye, Feng Chakravarty, Prasun K., *et al.* Aminopiperidine Sulfonamide Cav2.2 Channel Inhibitors for the Treatment of Chronic Pain. *Journal of Medicinal Chemistry* **55**, 9847-9855 (2012).
79. Subasinghe, N.L. Wall, Mark J. Winters, Michael P., *et al.* A novel series of pyrazolylpiperidine N-type calcium channel blockers. *Bioorganic & Medicinal Chemistry Letters* **22**, 4080-4083 (2012).
80. Abbadie, C. McManus, O. B. Sun, S. Y., *et al.* Analgesic effects of a substituted N-triazole oxindole (TROX-1), a state-dependent, voltage-gated calcium channel 2 blocker. *The Journal of Pharmacology and Experimental Therapeutics* **334**, 545-555 (2010).
81. Koganei, H., Shoji, M. & Iwata, S. Suppression of formalin-induced nociception by cilnidipine, a voltage-dependent calcium channel blocker. *Biological & Pharmaceutical Bulletin* **32**, 1695-1700 (2009).
82. *Calcium-Permeable Ion Channels in Pain Signaling*, (2014).
83. Waxman, S.G. & Zamponi, G.W. Regulating excitability of peripheral afferents: emerging ion channel targets. *Nature Neuroscience* **17**, 153-163 (2014).
84. Knotkova, H., Pappagallo, M. & Szallasi, A. Capsaicin (TRPV1 Agonist) therapy for pain relief: farewell or revival? *The Clinical Journal of Pain* **24**, 142-154 (2008).
85. Cui, M., Honore, P. Zhong, C., *et al.* TRPV1 receptors in the CNS play a key role in broad-spectrum analgesia of TRPV1 antagonists. *The Journal of Neuroscience : The Official Journal of the Society for Neuroscience* **26**, 9385-9393 (2006).
86. O'Neill, J. Brock, C. Olesen, A. E. Andresen, T. Nilsson, M. Dickenson, A. H. Unravelling the mystery of capsaicin: a tool to understand and treat pain. *Pharmacological reviews* **64**, 939-971 (2012).
87. Alawi, K. & Keeble, J. The paradoxical role of the transient receptor potential vanilloid 1 receptor in inflammation. *Pharmacology & Therapeutics* **125**, 181-195 (2010).

88. Maljevic, S. & Lerche, H. Potassium channels: a review of broadening therapeutic possibilities for neurological diseases. *J Neurology* **260**, 2201-2211 (2013).
89. Tsantoulas, C. & McMahon, S.B. Opening paths to novel analgesics: the role of potassium channels in chronic pain. *Trends in Neurosciences* **37**, 146-158 (2014).
90. Watson, J.J., Allen, S.J. & Dawbarn, D. Targeting nerve growth factor in pain: what is the therapeutic potential? *BioDrugs* **22**, 349-359 (2008).
91. Kumar, V. & Mahal, B.A. NGF - the TrkA to successful pain treatment. *Journal of Pain Research* **5**, 279-287 (2012).
92. Legendre, P. The glycinergic inhibitory synapse. *Cellular and Molecular Life Sciences* **58**, 760-793 (2001).
93. Laube, B., Maksay, G., Schemm, R. & Betz, H. Modulation of glycine receptor function: a novel approach for therapeutic intervention at inhibitory synapses? *Trends in Pharmacological Sciences* **23**, 519-527 (2002).
94. Reichling, D.B., Kyrozis, A., Wang, J. & MacDermott, A.B. Mechanisms of GABA and glycine depolarization-induced calcium transients in rat dorsal horn neurons. *The Journal of Physiology* **476**, 411-421 (1994).
95. Kirsch, J. & Betz, H. Glycine-receptor activation is required for receptor clustering in spinal neurons. *Nature* **392**, 717-720 (1998).
96. Nys, M., Kesters, D. & Ulens, C. Structural insights into Cys-loop receptor function and ligand recognition. *Biochemical Pharmacology* **86**, 1042-1053 (2013).
97. Lynch, J.W. Molecular structure and function of the glycine receptor chloride channel. *Physiological Reviews* **84**, 1051-1095 (2004).
98. Oertel, J., Villmann, C., Kettenmann, H., Kirchhoff, F. & Becker, C.M. A novel glycine receptor beta subunit splice variant predicts an unorthodox transmembrane topology. Assembly into heteromeric receptor complexes. *The Journal of Biological Chemistry* **282**, 2798-2807 (2007).
99. Yang, Z., Taran, E., Webb, T.I. & Lynch, J.W. Stoichiometry and subunit arrangement of $\alpha 1\beta$ glycine receptors as determined by atomic force microscopy. *Biochemistry* **51**, 5229-5231 (2012).
100. Yevenes, G.E. & Zeilhofer, H.U. Allosteric modulation of glycine receptors. *British Journal of Pharmacology* **164**, 224-236 (2011).
101. Maksay, G., Nemes, P. & B r , T. Synthesis of Tropeines and Allosteric Modulation of Ionotropic Glycine Receptors. *Journal of Medicinal Chemistry* **47**, 6384-6391 (2004).
102. Miller, P.S., Da Silva, H.M. & Smart, T.G. Molecular basis for zinc potentiation at strychnine-sensitive glycine receptors. *The Journal of Biological Chemistry* **280**, 37877-37884 (2005).
103. Maksay, G., Laube, B., Schemm, R., Grudzinska, J., Drwal, M., Betz, H. Different binding modes of tropeines mediating inhibition and potentiation of $\alpha 1$ glycine receptors. *Journal of Neurochemistry* **109**, 1725-1732 (2009).
104. Hirzel, K., M ller, U., Latal, A., T. H lsmann, S., Grudzinska, J., Seeliger, M., W. Betz, H., Laube, B. Hyperekplexia phenotype of glycine receptor $\alpha 1$

- subunit mutant mice identifies Zn(2+) as an essential endogenous modulator of glycinergic neurotransmission. *Neuron* **52**, 679-690 (2006).
105. Harvey, R.J., Depner, Ulrike B. Wässle, Heinz, *et al.* GlyR alpha3: an essential target for spinal PGE2-mediated inflammatory pain sensitization. *Science (New York, N.Y.)* **304**, 884-887 (2004).
 106. Lagrange, A.H. & Grier, M.D. Chapter 22 - GABAergic Neurotransmission. in *Primer on the Autonomic Nervous System (Third Edition)* (eds. Robertson, D., Biaggioni, I., Burnstock, G., Low, P.A. & Paton, J.F.R.) 109-111 (Academic Press, San Diego, 2012).
 107. Betz, H., Laube, B. Glycine receptors: recent insights into their structural organization and functional diversity. *Journal of Neurochemistry* **97**, 1600-1610 (2006).
 108. Möhler, H. GABA(A) receptor diversity and pharmacology. *Cell and Tissue Research* **326**, 505-516 (2006).
 109. Rowlett, J.K., Platt, D.M., Lelas, S., Atack, J.R. & Dawson, G.R. Different GABAA receptor subtypes mediate the anxiolytic, abuse-related, and motor effects of benzodiazepine-like drugs in primates. *Proceedings of the National Academy of Sciences of the United States of America* **102**, 915-920 (2005).
 110. Trapani, G., Altomare, C., Liso, G., Sanna, E. & Biggio, G. Propofol in anesthesia. Mechanism of action, structure-activity relationships, and drug delivery. *Current Medicinal Chemistry* **7**, 249-271 (2000).
 111. Pecaro, B.C. & Houting, T. Diprivan (ICI 35868, 2, 6, di-isopropylphenol), a new intravenous anesthetic. *Oral Surgery, Oral Medicine, Oral Pathology* **60**, 586-588 (1985).
 112. Yip, G.M., Chen, Z. W. Edge, C. J., *et al.* A propofol binding site on mammalian GABAA receptors identified by photolabeling. *Nature Chemical Biology* **9**, 715 (2013).
 113. Gelderblom, H., Verweij, J., Nooter, K. & Sparreboom, A. Cremophor EL: the drawbacks and advantages of vehicle selection for drug formulation. *European Journal of Cancer* **37**, 1590-1598 (2001).
 114. Ellett, M.L. Review of propofol and auxiliary medications used for sedation. *Gastroenterology Nursing* **33**, 284-295 (2010).
 115. Heck, H.D., Casanova, M. & Starr, T.B. Formaldehyde toxicity - new understanding. *Critical Reviews in Toxicology* **20**, 397-426 (1990).
 116. Fechner, J., Ihmsen, H., Jeleazcov, C. & Schüttler, J. Fospropofol disodium, a water-soluble prodrug of the intravenous anesthetic propofol (2,6-diisopropylphenol). *Expert Opinion on Investigational Drugs* **18**, 1565-1571 (2009).
 117. Welliver, M. & Rugari, S.M. New drug, fospropofol disodium: a propofol prodrug. *AANA journal* **77**, 301-308 (2009).
 118. Matta, J.A., Cornett, P. M. Miyares, R. L. Abe, K. Sahibzada, N. Ahern, G. P. General anesthetics activate a nociceptive ion channel to enhance pain and inflammation. *Proceedings of the National Academy of Sciences of the United States of America (PNAS)* **105**, 8784-8789 (2008).

119. Kikuchi, T., Wang, Y., Sato, K. & Okumura, F. In vivo effects of propofol on acetylcholine release from the frontal cortex, hippocampus and striatum studied by intracerebral microdialysis in freely moving rats. *British Journal of Anaesthesia : BJA* **80**, 644-648 (1998).
120. Sanna, E., Motzo, C. Usala, M. Serra, M. Dazzi, L. Maciocco, E. Trapani, G. Latrofa, A. Liso, G. Biggio, G.. Characterization of the electrophysiological and pharmacological effects of 4-iodo-2,6-diisopropylphenol, a propofol analogue devoid of sedative-anaesthetic properties. *British Journal of Pharmacology* **126**, 1444-1454 (1999).
121. Belelli, D., Pistis, M., Peters, J.A. & Lambert, J.J. The interaction of general anaesthetics and neurosteroids with GABAA and glycine receptors. *Neurochemistry International* **34**, 447-452 (1999).
122. Jurd, R., Arras, M. Lambert, S., *et al.* General anesthetic actions in vivo strongly attenuated by a point mutation in the GABA(A) receptor β 3 subunit. *The FASEB journal : Official Publication of the Federation of American Societies for Experimental Biology* **17**, 250-252 (2003).
123. Hales, T.G. & Lambert, J.J. The actions of propofol on inhibitory amino-acid receptors of bovine adrenomedullary chromaffin cells and rodent central neurons. *British Journal of Pharmacology* **104**, 619-628 (1991).
124. Dong, X.P., Xu, T.L. The actions of propofol on gamma-aminobutyric acid-A and glycine receptors in acutely dissociated spinal dorsal horn neurons of the rat. *Anesthesia and Analgesia* **95**, 907-914 (2002).
125. Anker-Møller, E., Spangsberg, N. Arendt-Nielsen, L. Schultz, P. Kristensen, M. S. Bjerring, P.,. Subhypnotic doses of thiopentone and propofol cause analgesia to experimentally induced acute pain. *British Journal of Anaesthesia* **66**, 185-188 (1991).
126. Zacny, J.P., Coalson, D. W. Young, C. J. Klapfta, J. M. Lichtor, J. L. Rupani, G. Thapar, P. Apfelbaum, J. L. Propofol at conscious sedation doses produces mild analgesia to cold pressor-induced pain in healthy volunteers. *Journal of Clinical Anesthesia* **8**, 469-474 (1996).
127. Lin, A.L., Shangari, N., Chan, T.S., Ramirez, D. & O'Brien, P.J. Herbal monoterpene alcohols inhibit propofol metabolism and prolong anesthesia time. *Life Sciences* **79**, 21-29 (2006).
128. Helfenbein, J., Lartigue, C. Noirault, E. Azim, E. Legailiard, J. Galmier, M. J. Madelmont, J. C. Isotopic Effect Study of Propofol Deuteration on the Metabolism, Activity, and Toxicity of the Anesthetic. *Journal of Medicinal Chemistry* **45**, 5806-5808 (2002).
129. Pardridge, W. The blood-brain barrier: Bottleneck in brain drug development. *Neurotherapeutics* **2**, 3-14 (2005).
130. Pangalos, M.N., Schechter, L.E. & Hurko, O. Drug development for CNS disorders: strategies for balancing risk and reducing attrition. *Nature Reviews. Drug Discovery* **6**, 521-U513 (2007).

131. Reichel, A. Addressing Central Nervous System (CNS) Penetration in Drug Discovery: Basics and Implications of the Evolving New Concept. *Chemistry & Biodiversity* **6**, 2030-2049 (2009).
132. Abbott, N.J., Rönnbäck, L. & Hansson, E. Astrocyte-endothelial interactions at the blood-brain barrier. *Nature Reviews. Neuroscience* **7**, 41-53 (2006).
133. Abbott, N.J. Astrocyte-endothelial interactions and blood-brain barrier permeability. *Journal of Anatomy* **200**, 629-638 (2002).
134. Persidsky, Y., Ramirez, S.H., Haorah, J. & Kanmogne, G.D. Blood-brain barrier: structural components and function under physiologic and pathologic conditions. *Journal of NeuroImmune Pharmacology* **1**, 223-236 (2006).
135. Abbott, N.J. Blood–brain barrier structure and function and the challenges for CNS drug delivery. *Journal of Inherited Metabolic Disease* **36**, 437-449 (2013).

136. <http://www.rsc.org/chemistryworld/Issues/2011/June/BreakingThroughTheBarrier.asp>

137. Bernacki, J., Dobrowolska, A., Nierwińska, K. & Małecki, A. Physiology and pharmacological role of the blood-brain barrier. *Pharmacological Reports* **60**, 600-622 (2008).
138. van Hecke, O., Torrance, N. & Smith, B.H. Chronic pain epidemiology and its clinical relevance. *British Journal of Anaesthesia* **111**, 13-18 (2013).

Chapter II

Targeting the α 1 Glycine Receptor

Contents

2.0	Introduction	50
2.1	Biological Testing.....	51
2.2	Substituted Phenols.....	52
2.2.1	Halogenated Propofol Derivitives	54
2.2.2	In vivo results of compound 8.....	56
2.3	Substituted bi-phenyl series.....	62
2.3.1	The Craig plot	63
2.3.2	Biological results of the bi-phenyl series	65
2.4	Results and discussion.....	68
2.4.1	Toxicological screening	73
2.4.2	hERG testing.....	74
2.4.3	The Ames test.....	75
2.4.4	Cytotoxicity	76
2.4.5	Metabolism and adverse drug reactions	76
2.5	Heterocycles and Solubilising groups.....	79
2.6	Synthesis.....	81
2.6.1	Suzuki Coupling	81
2.6.2	Bi-Phenyl Amide Synthesis.....	83
2.6.3	Heterocycle synthesis	84
2.7	Biological Data	86
2.8	Multiparameter Optimisation	89
2.8.1	MPO Review	89
2.8.2	MPO evaluation of heterocyclic compounds.....	94
2.9	Summary.....	97
2.10	References.....	99

2 Introduction (previous work)

The glycine receptor (GlyR) is known to play an important role in the modulation of pain signals at the dorsal root ganglion (DRG) level via the inhibition of neuronal firing¹. The $\alpha 1$ and $\alpha 3$ isoforms of the GlyR are found in high concentration within the laminae I and II of the dorsal horn and as such are of particular interest as targets for novel analgesic drugs².

Whilst studies have shown that propofol exerts its anaesthetic action by modulation of the GABA_A receptor (EC_{50} 3.9 μ M)³, it has also been shown to be a positive allosteric modulator of GlyRs (EC_{50} 4.8 μ M). Several studies have suggested that modulation of the GlyR may be responsible for propofol's analgesic properties⁴⁻⁷. Sedation, drowsiness and mental impairment are all unwanted side effects linked to therapeutic compounds which target the GABA_A receptor⁸. In order to alleviate this potential side effect it is, therefore, a priority that prospective analgesic compounds selectively target the GlyR and do not modulate the GABA_A.

Initial studies within the group focused on optimising the phenolic core of propofol at the $\alpha 1$ GlyR in an effort to increase potency which, provided that high μ M activity at the GABA_AR could be at least be maintained, would decrease the risk of activation of the GABA_AR resulting in unwanted off-target effects. A series of substituted analogues were synthesised which explored both the steric (additional substituents on the ring) and electronic (addition of halogens to modulate electron richness/deficiency around the ring) effects of a variety of moieties around the phenolic core of propofol. These compounds were tested for efficacy against the $\alpha 1$ GlyR (Table 2.1).

2.1 Biological Testing (previous work cont)

The *in vitro* activities of the phenolic analogues were evaluated using electrophysiology whole-cell voltage-clamp techniques. The voltage recordings were made from human embryonic kidney cells (HEK 293 cells) which were transfected with cDNA to express recombinant $\alpha 1\beta$ glycine receptors upon the cell surface. Figure 2.1 shows representative current traces for the determination of the EC_{50} value for 4-chloropropofol. The top trace shows the effect of a maximal glycine concentration (1000 μM), whilst the second trace shows a submaximal glycine concentration (10 μM). Each subsequent trace shows the effect of 10 μM glycine with increasing concentrations of 4-chloropropofol (1-100 nM). The chart in Figure 2.1 shows the potentiation of the chloride ion current in response to 10 μM glycine and the varying concentrations of 4-chloropropofol. The EC_{50} value is determined at 50% of the maximal potentiation of chloride ion response.

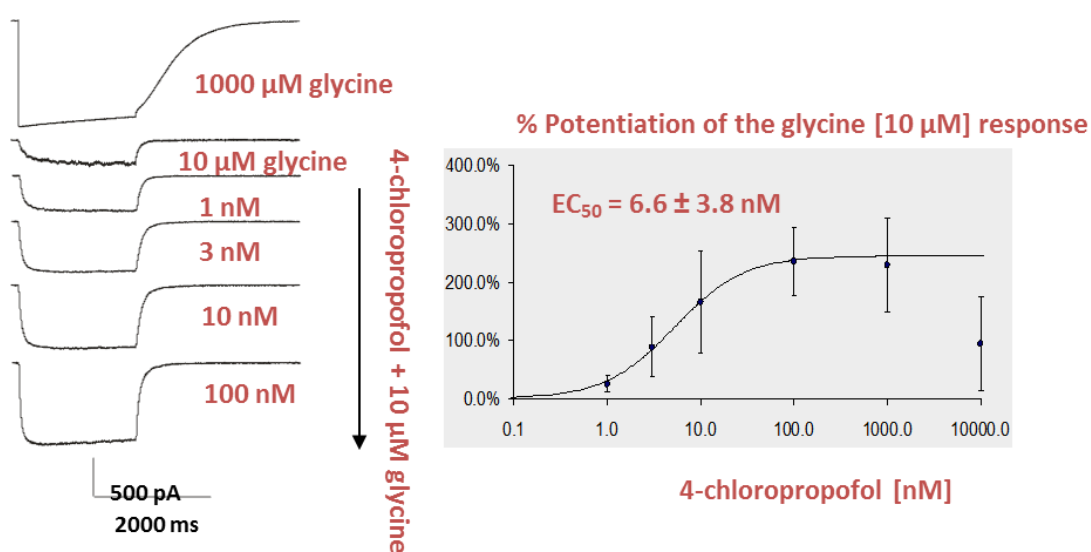


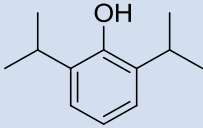
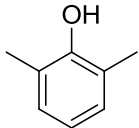
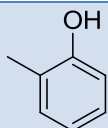
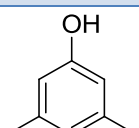
Figure 2.1. Representative trace showing the determination of EC_{50} values for positive allosteric modulators of the $\alpha 1$ glycine receptor.

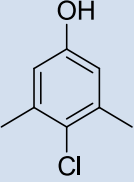
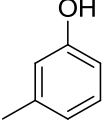
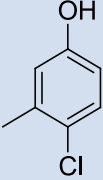
Due to the time consuming nature of developing a stable cell line and the large amounts of cells required, only a small selection of compounds synthesised were tested. Exact EC_{50} values were not determined for any compounds whose preliminary results showed no activity at $1\mu\text{M}$. All *in vitro* electrophysiology testing was carried out at the University of Tübingen under the supervision of Prof. Bodo Laube.

2.2 Substituted Phenols (previous work cont)

Table 2.1 contains several commercially available phenols with alkyl and chloro substituents at various positions around the phenyl ring. Compounds **2** and **4** were significantly less potent than propofol at the $\alpha 1\text{GlyR}$ with EC_{50} values in the high μM region. Both the *ortho* and *meta* monomethyl substituted analogues (compounds **3** and **6**) showed increased potency, with respect to the dimethyl analogues, but neither analogue was as potent as the parent drug. Interestingly when the 3-methyl and 3,5-dimethyl analogues were chlorinated at the 4-position both EC_{50} values were reduced dramatically to the low μM region (compounds **5** and **7**)³.

Table 2.1. Commercially available phenols tested for efficacy against the $\alpha 1$ GlyR.

Compound	Structure	EC_{50} (μM)
1		4.8 ± 1.2
2		226 ± 104
3		70 ± 19
4		254 ± 139

5		13 ± 4
6		59 ± 19
7		8 ± 5

An additional potential advantage of substitution at the 4-position of the phenyl ring is the blockade of a major route of phenol metabolism. Propofol itself is subject to extensive cytochrome P450 (CYP 450) mediated metabolism and rapid elimination. The major route of propofol metabolism is via glucuronidation of the parent drug, which consumes ~50-60% of the total dose.

Propofol also undergoes CYP 450 mediated ring hydroxylation at the 4-position via CYP2C9 and CYP2B6 which allows for further glucuronidation and sulfation of the hydroxylated metabolite. Substitution of propofol at the 4 position will block the CYP 450 mediated ring hydroxylation, slowing the metabolic clearance of the compound and in turn increasing the half-life of the drug (Figure 2.2)^{9,10}.

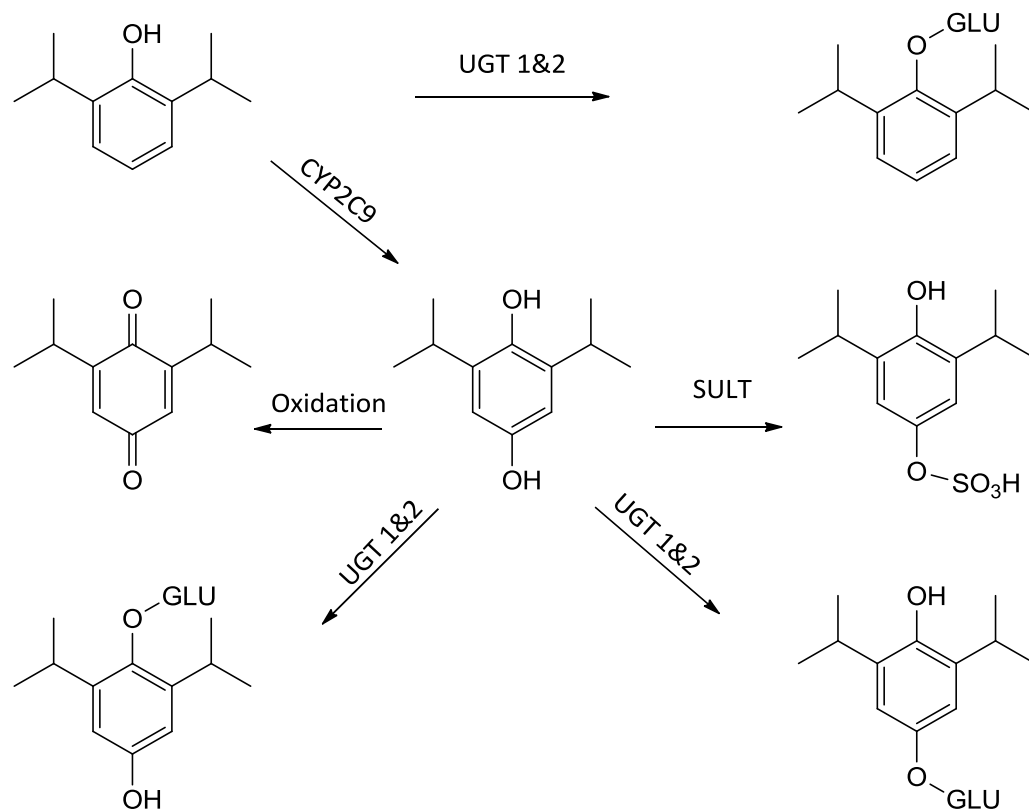
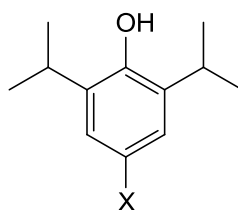


Figure 2.2. The metabolic pathway of propofol in humans. UGT— uridine diphosphate glucuronosyltransferase, SULT — sulfotransferases, CYP — cytochrome P450 isozyms, GLU — glucuronide.

2.2.1 Halogenated Propofol Derivatives (previous work cont)

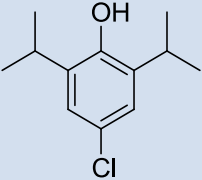
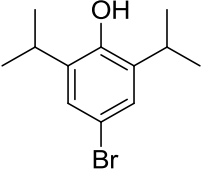
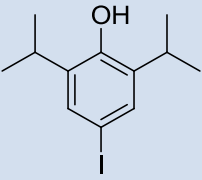


- 8,** X = Cl
9, X = Br
10, X = I

Figure 2.3. Halogenated propofol

In light of these results it was decided to examine the effect of halogenation at the 4-position of propofol in order to determine if the same increase in potency at the $\alpha 1$ GlyR and reduction in EC_{50} values as seen in the substituted phenol series could be replicated with the parent compound (Table 2.2). The physicochemical parameters of the 4-halogenated compounds were also evaluated *in silico* to determine the potential for good oral absorption, potential toxicity and systemic distribution of the 4-halogenated compounds (8-10).

Table 2.2. Halogenated compounds tested for efficacy against the $\alpha 1$ GlyR¹¹.

Compound	EC_{50} (μM) ^a	ClogP ^b	CogD ^d	LogS	Aq sol (μM)	MW
 8	0.00066 \pm 0.0038	4.49	4.4	-3.68	18.37	212
 9	0.00062 \pm 0.0018	4.63	4.67	-4.0	10.81	257
 10	0.00067 \pm 0.0033	4.82	4.82	-4.23	14.85	304

a, $\alpha 1$ GlyR EC_{50} values determination was carried out at the University of Tübingen under the supervision of Prof. Bodo Laube. **b**, ClogP values were determined using chembiodraw ultra 12 software. **c**, In house algorithm.

The results showed that halogenation at the 4-position of propofol (Table 2.2) could significantly enhance efficacy at the $\alpha 1$ GyR isoform with low nM EC_{50} values giving 1000 fold increase in potency, in comparison with propofol. Halogenation also kept the ClogP value within the acceptable parameters of < 5 ¹². Solubility of any novel drug is an important consideration in the design of a drug candidate. A poorly water soluble drug can lead to slow drug absorption, inadequate or variable bioavailability and, in some cases, gastrointestinal mucosal toxicity. It is, therefore, vital that potential pharmacological agents display optimal solubility parameters to achieve their desired concentration in systemic circulation in order to generate the desired pharmacological response¹³. The halogenated compounds all show poor aqueous solubility of $< 20 \mu\text{M}$, whereas the ideal solubility would be in the region of $> 50 \mu\text{M}$ ¹³⁸.

The low nM EC_{50} values of the halogenated analogues may also confer selectivity, with respect to, the $GABA_A$ R by reducing the dose required to activate the $\alpha 1$ GyR compared to the $GABA_A$ R by ~ 3 orders of magnitude¹⁴. Whilst the ClogP is still on the high side, it was decided to profile compound **8** in pharmacokinetic studies to enable proof of principle studies in a neuropathic pain model to follow should sufficient drug exposure be achieved.

2.2.2 In vivo results of compound 8 (previous work cont)

The pharmacokinetic parameters of 4-chloropropofol were calculated following a formal *in vivo* PK study in the rat (Table 2.3). Analogues were dosed by p.o and i.v. routes in the rat. Whole blood samples were taken from a lateral tail vein for plasma separation at time points 0 min, 30 min, 1 h, 2 h and 4 after p.o. dosing; and 0 min, 15 min, 30 min, 1 h, and 2 h after i.v. dosing, while the terminal samples at time point 6 h after dosing (p.o and i.v.) were taken by cardiac puncture. All experiments were carried out in triplicate.

Table 2.3. Pharmacokinetic profile of compound **8** in the Rat. AUC - area under the concentration time curve, AUC 0-6 - area under the concentration time curve from 0-6hrs, C_{max} – maximum concentration of drug, T_{max} – time to maximum concentration of drug, t_{1/2} – half-life, CL/F – apparent total clearance of drug from plasma after oral admission, CL – drug clearance, Vd/F – volume of distribution of drug after oral admission, Vd - volume of distribution, MRT – mean residence time.

Parameter		i.v.		p.o.		F (%)
		Mean	SE	Mean	SE	
		1 mg/kg		8 mg/kg		
AUC	min*µg/mL	7.39	1.68	42.8	8.78	72.4
AUC 0-6	min*µg/mL	6.29	3.18	18.7	5.8	
C_{max}	µg/mL	0.11	0.03	0.1	0.02	
T_{max}	min	15	0	30	0	
t_{1/2}	min	48.8	18.9	398	96.4	
CL/F	mL/min/kg	14.8	27.8	201	34.3	
CL	mL/min/kg	14.8	27.8	146	24.8	
Vd/F	L/kg	11.8	5.64	110	27.4	
Vd	L/kg	11.8	5.64	79.6	19.8	
MRT	min	48.7	16	609	152	

As can be seen from Table 2.3 an 8mg/kg oral dose of compound **8** demonstrated a very high clearance rate (146 mL/min/kg with ideal values in the rat model of 10-45 mL/min/kg) in comparison to rat liver blood flow (55.2 ml/min)¹¹. Despite the high clearance, the half-life (398 min) is high (ideal in the rat model would be in the range of 30-180 min) which could be due to the high volume of distribution of the compound (80.6 L/kg with the range of 0.5-10 L/kg acceptable)¹¹. The oral bioavailability is high at 72.4% (in the rat model F > 30% is good) and absorption is rapid with the time to achieve maximum concentration of drug (T_{max}) being only 30 min (T_{max} < 3hrs is desirable) which is a desirable attribute for an analgesic agent^{11,15}.

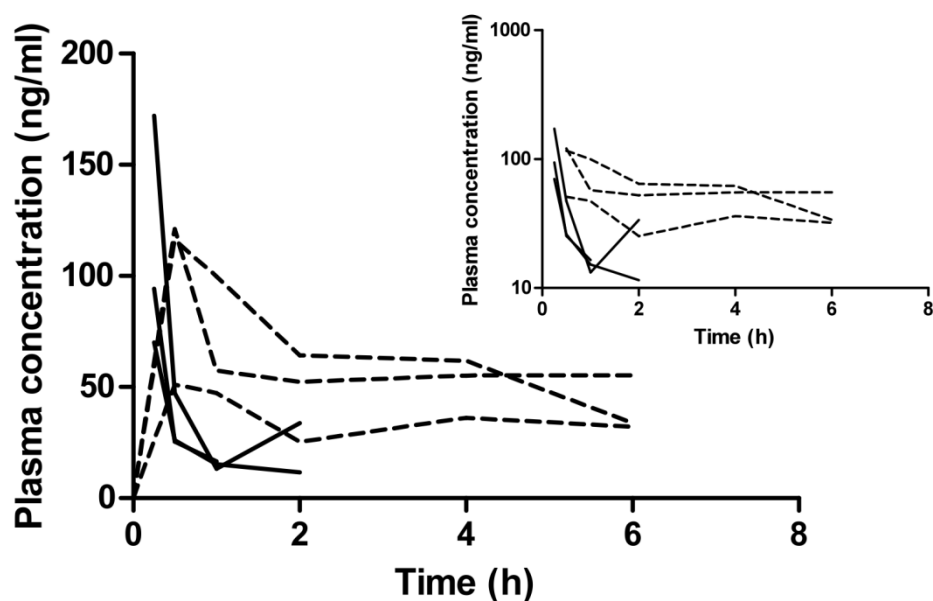


Figure 2.4. Plasma concentrations of individual animals for Compound **8** after p.o. (broken lines) and i.v. (solid lines) administration of 8 mg/kg and 1 mg/kg, respectively. Inset depicts the same data on a semi logarithmic scale.

Figure 2.4 shows the plasma concentrations for the individual test subjects. The apparent limited first pass extraction may be a consequence of the rapid absorption giving rise to a high concentration of drug in the portal vein saturating liver metabolism.

Whilst the results from the electrophysiology testing of compound **8** showed an increase in potency at the $\alpha 1$ GyR (EC_{50} 0.6 nM) and the results from the *in vivo* studies from the rat indicated good oral bioavailability (72.4%) and rapid absorption (T_{max} = 30 min), the validity of the $\alpha 1$ GyR as an analgesic target had still to be demonstrated *in vivo*.

Due to the innate solubility issues seen with propofol and the halogenated analogues, it was decided to include a water soluble phosphate prodrug of compound **8** (Figure 2.6) in the *in vivo* testing.

Several water soluble propofol prodrugs have previously been synthesised including fospropofol (**11**), propofol ethyl dioxy phosphate (**12**) and propofol phosphate (**13**) (Figure 2.5)¹⁶⁻¹⁸.

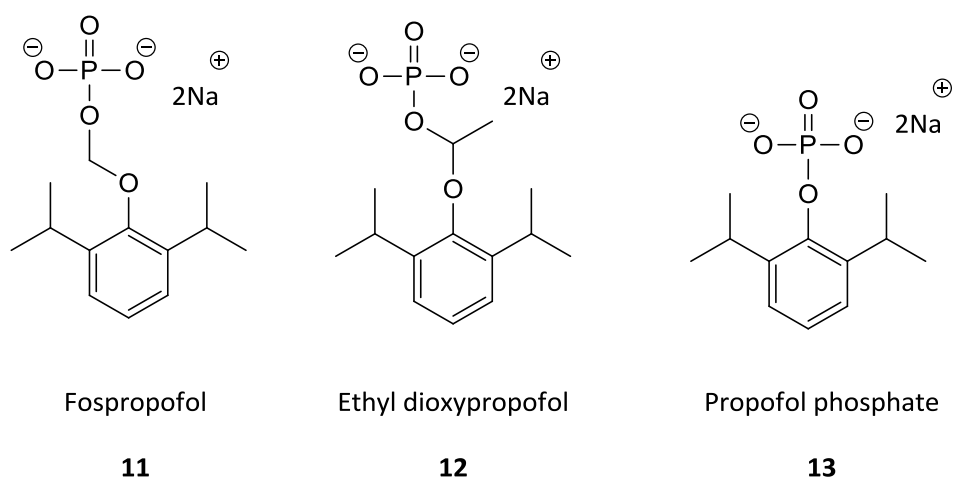
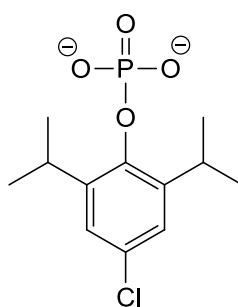


Figure 2.5. Propofol prodrugs.

Both Fospropofol and propofol ethyl dioxy phosphate release toxic compounds (acetone and acetaldehyde respectively) upon enzymatic activation, whereas propofol phosphate only releases inorganic phosphate. Propofol phosphate however, does have a slower onset of action compared to the fospropofol and propofol ethyl dioxy phosphate¹⁹.

To date Fospropofol is the only propofol prodrug licensed by the Food and Drug Administration (FDA) for monitored anaesthesia care²⁰. Fospropofol itself is an inactive form of the drug, and as such, fospropofol relies upon enzymatic cleavage of the phosphate moiety by endothelial cell alkaline phosphatases to release the active compound²¹. Addition of the phosphate moiety to propofol has been shown to increase the solubility by ~3 orders of magnitude from 0.15 mg/mL for propofol to 500mg/mL for fospropofol¹⁸.

Therefore it was decided to determine the effects, not only of compound **8** but, in an effort to increase anticipated oral bioavailability, the effects of the phosphate prodrug of compound **8** (Figure 2.6) were also tested for *in vivo* activity against hyperalgesia, the increased sensitivity to a painful stimulus, and allodynia, the painful response to normally innocuous stimuli²².



14

Figure 2.6. Phosphate prodrug of compound **8**.

The *in vivo* pharmacodynamic investigation was carried out by Dr Laiche Djouhri in the Department of Pharmacology at the University of Liverpool, using the Chung lesion rat model of neuropathic pain.

Neuropathic pain was induced in the animals by partial ligation of the sciatic nerve as set out by Chung¹⁴ and co-workers/. For thermal hyperalgesia the animals were placed on a hot plate set at a predetermined temperature and the animals were observed for paw withdrawal behaviours of the injured limb, the time taken to withdraw the injured limb is given as the paw withdrawal latency. Mechanical allodynia was examined by measuring paw withdrawal thresholds (PWT) to increasing mechanical force applied to the dorsal surface of the rat paw.

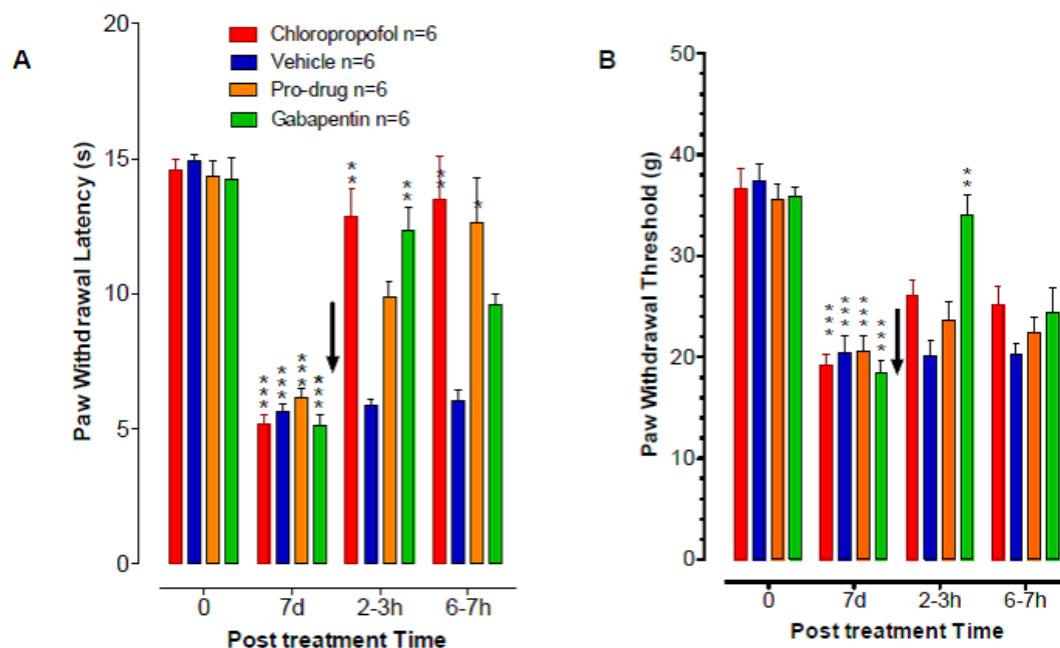


Figure 2.7. Effects of oral administrations of Compound **8** (8mg/Kg, n=6) and prodrug (8mg/Kg, n=6) were compared with those of vehicle (control) and gabapentin (positive control, 30mg/Kg, i.p). data are expressed as mean \pm SEM and comparisons between pre spinal nerve axotomy (SNA) (time 0) and post SNA (7 days) values were made with one way repeated measures ANOVA with Dunnett's multiple comparison. Comparisons between post drug values and vehicle values were made with two way repeated measures ANOVA followed by post Bonferroni tests (* = $P \leq 0.05$, ** = $P \leq 0.01$, *** = $P \leq 0.001$)

As can be seen from Figure 2.7 (A), compound **8** reversed heat hyperalgesia and was as effective, as the current 'gold standard' treatment for neuropathic pain, gabapentin at 2-3 hours post dosing and outperformed gabapentin at 6-7 hours post dosing. The prodrug of compound **8**, predictably had a slower onset of action due to the fact that the prodrug relies upon enzymatic cleavage of the phosphate moiety by alkaline phosphatases in the liver to release the active drug. At 6-7 hours post dosing the prodrug was also more effective than gabapentin.

The results of the mechanical allodynia test (Figure 2.7, B) showed that compound **8** had no effect in the paw withdrawal threshold levels indicating no analgesic activity in the mechanical allodynia arm of the study.

Crucially during these tests no sedation was observed in any of the rats. This is strongly supportive of the fact that 4-chloropropofol is selectively targeting the GlyR not the GABA_AR, achieving analgesic activity without producing the sedative or hypnotic side effects seen with other therapeutics used to treat neuropathic pain i.e. amitriptyline and gabapentin.

2.3 Substituted bi-phenyl series (previous work cont)

With the results from the initial electrophysiology and *in vivo* studies of the halogenated compounds showing that substitution at the 4-position of propofol could substantially increase Cl⁻ current and reduce the EC₅₀ value by ~3 orders of magnitude at the GlyR, it was decided to explore further the effects of substitution at the 4-position. It can be seen from the results of the electrophysiology assays with compound **10** that larger groups can be tolerated at the 4-position. The van der Waals volume of the iodo group is approximately 34.78 Å³, therefore, in order to probe the constraints of the hypothetical binding pocket a series of phenyl analogues were synthesised (Van der Waals volume 99.17 Å^{3*}, Figure 2.8).

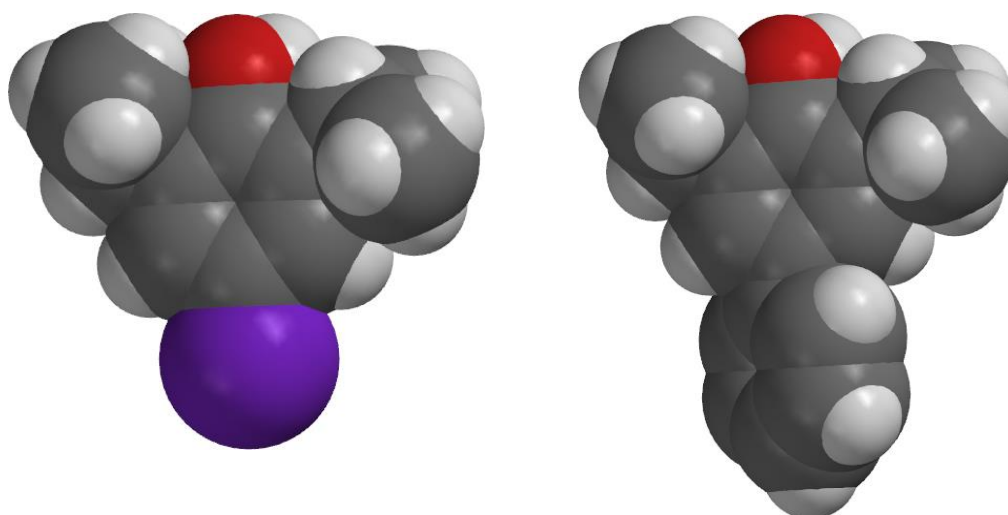


Figure 2.8. Space filled models of the 4-iodo propofol and 4-phenyl propofol showing the similarity in size of iodine and phenyl groups. *Values measured using Spartan 14 software.

The number of possible analogues of substituted aromatic rings with accessible functional groups is extremely large. Therefore in order to explore the chemical space based upon substitution of the phenyl ring, a rational approach in deciding which substituents to use was employed in the form of the Craig plot (Figure 2.10).

2.3.1 The Craig plot (previous work cont)

Craig plots can be utilised to give a visual representation of the relative independence or interdependence of a range of physicochemical parameters including electronic effects (σ) hydrophobic effects (π), molar refractivity (MR) and steric effects (E_s)²³. The Craig plot was used to determine the electronic effects (σ , y axis) vs. the hydrophobic effects (π , x axes) of variety of possible substituents. From this plot it is possible to visualise the various combinations of both electronic and hydrophobic contributions each substituent will make when attached to the benzene ring. There are many examples in the literature of the Craig plot being utilised to drive compound design and selection forward²⁴⁻²⁸. Most of the substituents chosen for this study resided in the top right quadrant of the plot, such as the halogens and trifluoromethyl ether. These substituents have positive σ values and positive π values ($+\sigma$, $+\pi$) which show an increase in both electron withdrawing and hydrophobic effects compared with hydrogen.

Substituents in the in the lower right quadrant (Me, Et, NMe₂) show an increasing electron donating effect while the hydrophobic effect remains positive ($-\sigma$, $+\pi$). These substituents tend to be unstable to metabolism when on aromatic rings; therefore, they were not included in this investigation. Those substituents (OH, NH₂, OCH₃) residing in the lower left quadrant ($-\sigma$, $-\pi$) of the plot were also disregarded due to possible formation of toxic metabolites, such as benzoquinone imines (**15**) and quinones (**16**) when introduced *para* to a hydroxyl group, (Figure 2.9)^{29,30}.

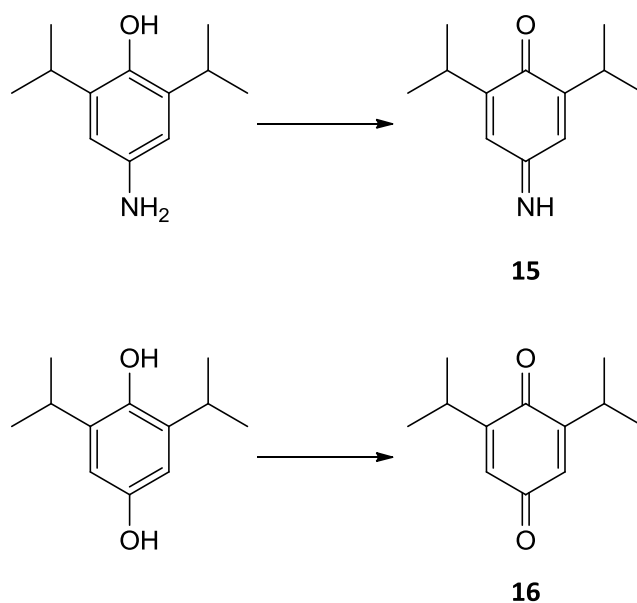


Figure 2.9. Toxic metabolites, quinone (top) and quinoneimine (bottom) formed from *para* hydroxylation or *para* amination of a phenol.

The electron withdrawing, less hydrophobic substitutes ($+\sigma$, $-\pi$) in the top left quadrant were due to be incorporated but the project moved in a different direction and other target compounds were developed.

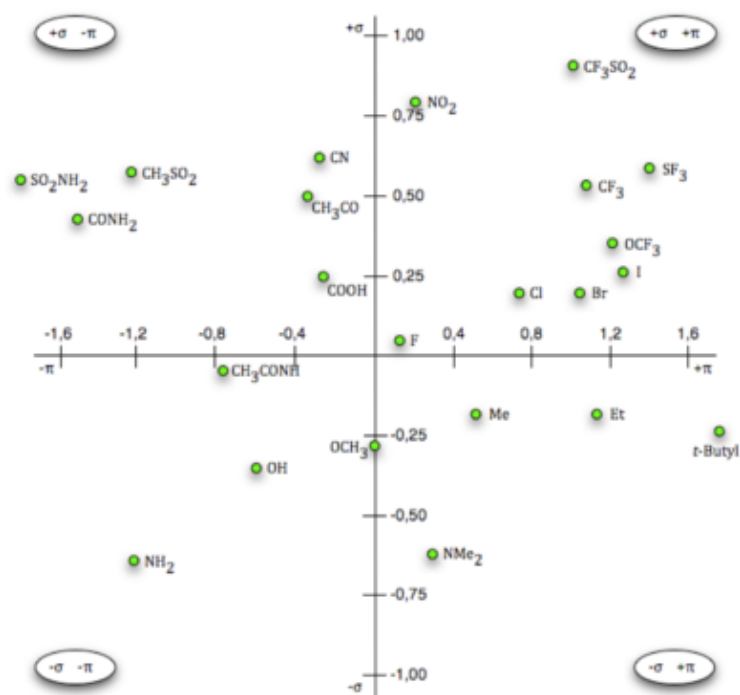


Figure 2.10. The Craig plot¹⁴.

2.3.2 Biological results of the bi-phenyl series (previous work cont)

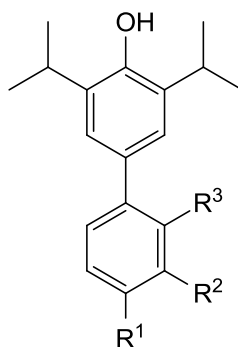


Figure 2.11. Bi-phenyl template

Several of the bi-phenyl series showed remarkable *in vitro* potency against the $\alpha 1$ GlyR, with EC_{50} values in the low picomolar range. Again compounds with chloro substituents at the 4-position, in this case of the terminal ring, were among the most potent compounds.

Table 2.4. Biological results of bi-phenyl compounds previously synthesised within the group.

Compound	R ¹	R ²	R ³	ClogP ^a	EC ₅₀ (μM) ^b
17	Cl	H	H	6.5	0.0002 ± 0.0003
18	t-Butyl	H	H	7.6	0.00005 ± 0.03
19	Cl	F	H	6.7	0.00007 ± 0.00025
20	H	F	H	4.9	0.00014 ± 0.00009
21	Ph	H	H	7.7	0.0008 ± 0.0002
22	Cl	Cl	H	7.2	0.00063 ± 0.00012
23	H	F	F	6.1	0.00038 ± 0.00039

a, ClogP values were determined using chembiodraw ultra 12 software. **b**, $\alpha 1$ GlyR EC_{50} values determination was carried out at the University of Tübingen under the supervision of Prof. Bodo Laube.

The di-halogenated 4-chloro-5-fluoro-diphenyl analogue (**19**) was the most potent compound with an EC₅₀ value of 70 picomolar.

Interestingly compound **18** containing the 4- t-butyl moiety which is electron donating and hydrophobic, as can be seen from the Craig plot (Figure 2.10), was also extremely potent (EC₅₀ 50 pM) indicating the possibility of a large hydrophobic binding pocket for these molecules.

Although several of the bi-phenyl series showed remarkable *in vitro* potency against the α 1 GlyR, with Ec50 values in the low picomolar range (Table 2.4), some of the physicochemical properties of the compounds fall outside the optimal ranges (Table 2.4). In particular the ClogP values of these highly lipophilic molecules are all >6.0 with the optimal range being <5.0¹². The pharmacokinetic profile of the most potent of the bi-phenyl analogue (compound **19**) was investigated in the same *in vivo* model as compound **8** (Table 2.5).

Table 2.5. Pharmacokinetic profile of compound **19** in the Rat. Analogues were dosed p.o and i.v. into the rat. Whole blood samples were taken from a lateral tail vein for plasma separation at time points 0 min, 30 min, 1 h, 2 h and 4 after p.o. dosing; and 0 min, 15 min, 30 min, 1 h, and 2 h after i.v. dosing, while the terminal samples at time point 6 h after dosing (p.o and i.v.) were taken by cardiac puncture. All experiments were carried out in triplicate.

Parameter		i.v		p.o		F (%)
		Mean	SE	Mean	SE	
		2 mg/kg		20 mg/kg		
AUC	min* $\mu\text{g/mL}$	69.2	5.72	123	42	17.8
AUC 0-6	min* $\mu\text{g/mL}$	64.1	6.88	34.6	12.6	
C_{max}	$\mu\text{g/mL}$	0.77	0.17	0.15	0.04	
Tmax	min	15	0	30	0	
t_{1/2}	min	91	5.01	789	185	
CL/F	mL/min/kg	29.3	2.28	231	103	
CL	mL/min/kg	29.3	2.28	41.1	18.3	
Vd/F	L/kg	3.87	0.5	306	195	
Vd	L/kg	3.87	0.5	54.4	34.7	
MRT	min	104	19.1	1160	256	

The results of the *in vivo* testing show that compound **19** is poorly absorbed with a low AUC giving a bioavailability of ~ 18%. Clearance (CL) and volume of distribution (Vd) are both reduced whilst the plasma concentrations are increased ($t_{1/2} > 780$ mins), with respect to compound **8**. The reduced CL and Vd could be due to the poor solubility of compound **19**.

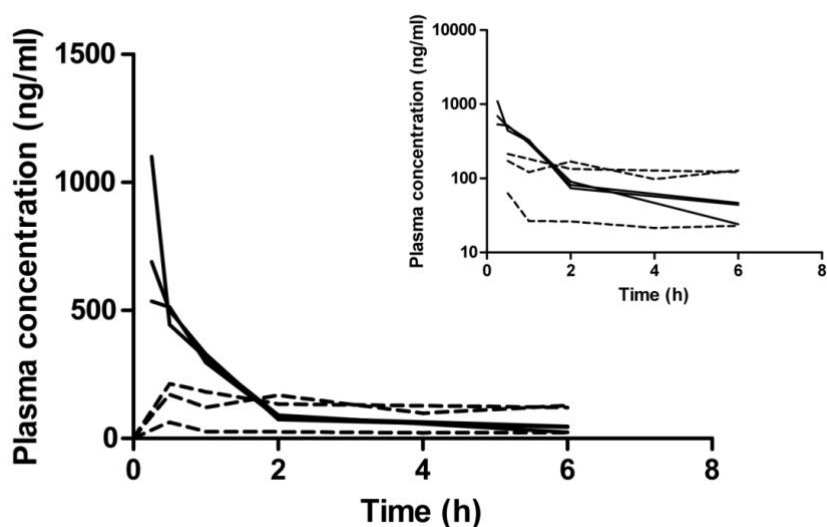


Figure 2.12. Plasma concentrations of individual animals for **19** after p.o. (broken lines) and i.v. (solid lines) administration of 20 mg/kg and 2 mg/kg, respectively. Inset depicts the same data on a semi logarithmic scale.

Figure 2.12 shows the poor absorption of compound **19** leading a low C_{max} (0.15 $\mu\text{g}/\text{mL}$). From the pharmacokinetic data it appears that compound **19** suffers from solubility limited absorption as the compound appears to flat line at around 2 hours.

2.4 Results and discussion

The optimisation of propofol (Figure 2.13) has led to the generation of an extremely potent hit compound with an EC_{50} value of 70pM against the $\alpha 1$ GlyR. From preliminary animal studies it was apparent that the ClogP needed to be reduced and that the aqueous solubility needed to be improved in order to increase bioavailability.

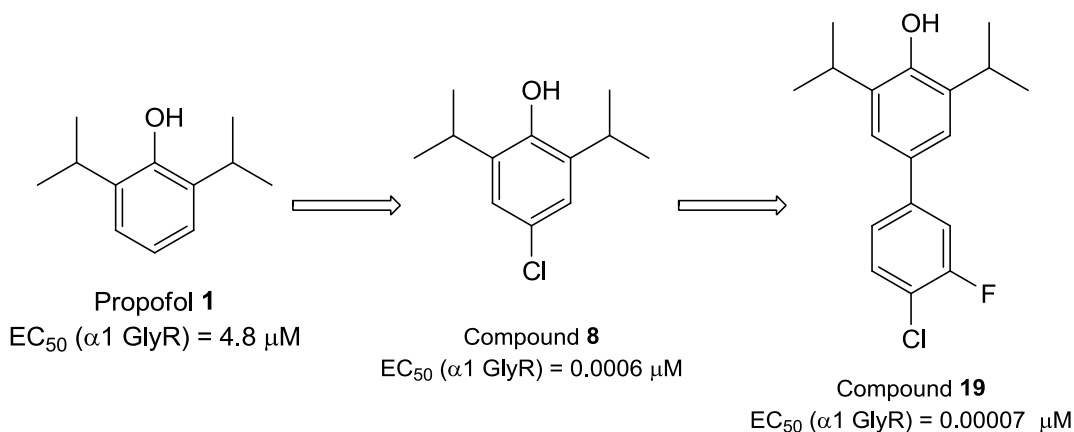


Figure 2.13. Optimisation of propofol to early lead generation.

The α1 GlyR is predominantly found within the CNS of the mammalian system. In order for a therapeutic agent to successfully cross the blood brain barrier (BBB) and enter the CNS the guidelines for the pharmacokinetic parameters are different to the standard Lipinski's guidelines (Table 2.6)^{12,31}.

Table 2.6. Comparison of Lipinski's guidelines and those for CNS penetration. ClogP is the calculated partition coefficient; this gives a measure of the hydrophobicity of a compound. ClogD is the calculated distribution coefficient; this gives a measure of the distribution of a compound throughout various biological systems. Topological polar surface area (TPSA) is the surface sum of all polar atoms, this gives a measure of a compounds ability to permeate cells. MW is the molecular weight of the compound. Hydrogen bond donors (HBD) is the sum of all of the oxygen-hydrogen and nitrogen-hydrogen bonds, whereas hydrogen bond acceptors (HBA) is the sum of all of the oxygen and nitrogen atoms within the compound. pKa gives a measure of the acidity of the compound. Rotatable bond is any single non-ring bond, bounded to nonterminal heavy (i.e., non-hydrogen) atom.

PK Parameter	Lipinski's guidelines	CNS Penetrant guidelines
ClogP	≤5	≤5
ClogD		≤3
TPSA		60-70Å ²
MW _(Da)	≤500	≤450
HBD	≤5	≤3
HBA	≤10	≤7
pKa		7.5-10.5
Number of rotatable Bonds		≤8

The preliminary studies have shown that substitution at the 4-position of propofol can dramatically increase potency at the α 1GlyR, although it is apparent from Table 2.7 that the predicted pharmacokinetic and physicochemical parameters of the templates need to be improved in order to deliver a metabolically stable and orally available analgesic compound. As hepatic metabolism is the primary elimination pathway for the majority of drugs it is, therefore, vital that new chemical entities are tested against liver microsomes and hepatocytes to determine their stability to metabolic degradation^{32,33}.

Hepatic metabolism impacts oral bioavailability and the half-life of a drug which in turn affects the dose and frequency of administration. Microsomes are generally inexpensive and robust; therefore, they are typically used in high throughput screens. Microsomes contain both CYP 450's and UDP-glucouronosyltransferases enzymes which are responsible for the metabolism of the many drug compounds. Hepatocytes contain the full complement of both phase I and phase II metabolising enzymes including cytosolic enzymes such as, methyltransferases and aldehyde oxidases³⁵. The ideal rate of clearance would be below 15 μ l/min/mg for microsomes and below 20 μ l/min/ 10^6 cells for hepatocytes¹¹.

The radar plots give a good visual representation of the ideal values vs. the predicted values for ClogD, solubility, human microsomes and rat hepatocytes. Figure 2.14 shows an ideal radar plot, the shaded area represents where the optimum values for each parameter would lie whilst the red line represents the calculated value for each parameter. If the line falls outside of the shaded areas this shows the predicted value lies outside of the optimal range for that particular parameter.

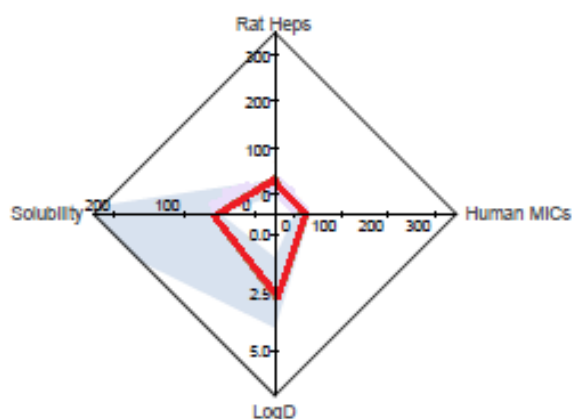
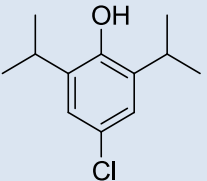
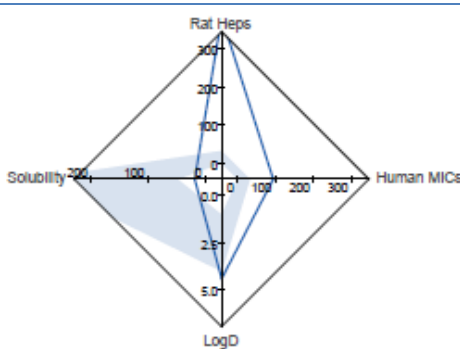
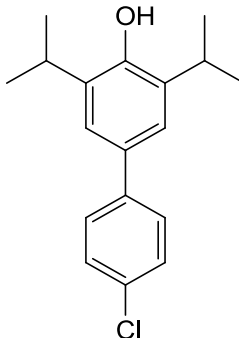
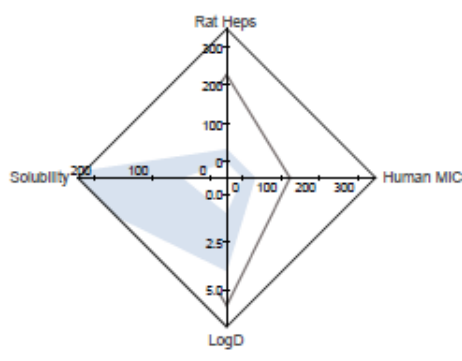
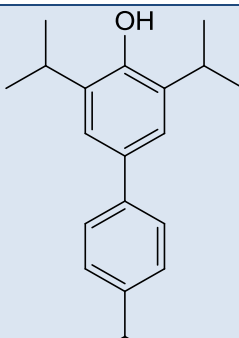
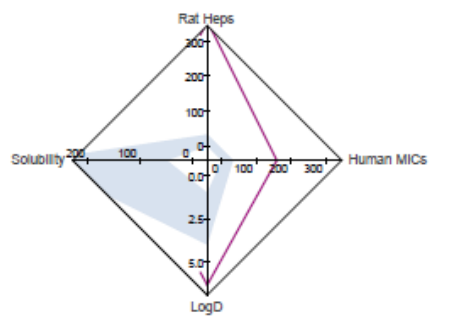
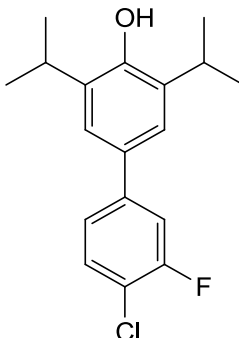
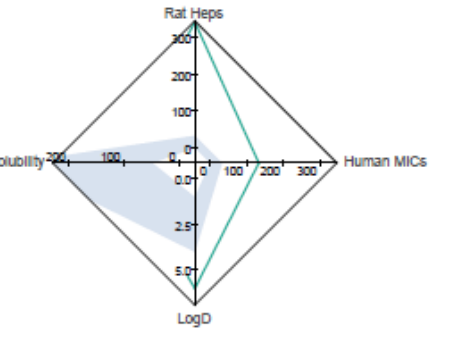


Figure 2.14. An Ideal radar plot

Table 2.7. Pharmacokinetic and physicochemical parameters of compound **8** and the most potent bi-phenyl analogues¹¹. Human Microsomes, 0-30 green, 30-60 yellow, 60 and above red. Rat Hepatocytes, 0-30 green, 30-60 orange, 60 and above red. ClogD 7.4, 1-4 green, <1 OR >4 red.

Compound	Parameters	Radar plot
 <p>8</p>	ClogD 7.4	4.4
	Human Mic ($\mu\text{l}/\text{min}/\text{mg}$)	91.87
	Rat Hep ($\mu\text{l}/\text{min}/1\text{E}6$)	386.8
		

Compound	Parameters		Radar plot
 <p>17</p>	ClogD 7.4	5.84	
	Human Mic (μl/min/mg)	121	
	Rat Hep (μl/min/1E6)	226	
 <p>18</p>	ClogD 7.4	5.84	
	Human Mic (μl/min/mg)	121	
	Rat Hep (μl/min/1E6)	226	
 <p>19</p>	ClogD 7.4	6.0	
	Human Mic (μl/min/mg)	131	
	Rat Hep (μl/min/1E6)	343.5	

In particular the lipophilicity coefficient, ClogP, the 4-aryl series needs to be reduced. Highly lipophilic molecules are, in general, poorly absorbed, have low solubility and have a high metabolic turnover and therefore have a low bioavailability.

Highly lipophilic molecules also have a higher probability of becoming partitioned in lipid membranes and being retained there. If the ClogP values are too low the compounds will not pass through the blood brain barrier in sufficient concentration to achieve therapeutic levels at the site of action. Ideally for maximum probability of CNS penetration the ClogP needs to be between 1.5- 3.0³¹.

The consideration of ClogP values is of vital importance to the medicinal chemist when designing a new molecular entity; but ClogP values do have their limitations. ClogP measurements do not consider the ionisation of a molecule. Many novel drug candidates contain basic or acidic centres which can become ionised as they pass through various biological systems i.e. stomach and gastrointestinal tract (pH-1-2), blood plasma (pH-7.4). Therefore it is important to measure a distribution ratio (ClogD) which takes into account the ratio of ionised/unionised compound at various pH values. To ensure maximum penetration of the BBB the ClogD values should be kept between 1-3^{36,37}.

Topological polar surface area (TPSA) is defined as the sum of contributions to the molecular surface area of polar atoms, such as oxygen and nitrogen. In order to maximise the chances of intestinal absorption the TPSA of a molecule should be in the region of 60-140 Å². Once again the values for optimal CNS penetration are more stringent at <90 Å²,^{36,38}.

Therefore, this study will focus upon optimisation of the 4-substituted propofol template and will aim to drive the compound not only to increased potency but also to correlate activity with improved physicochemical characteristics such as ClogP, ClogD, TPSA in order to maximise the potential for CNS penetration.

2.4.1 Toxicological screening

Toxicological adverse events are one of the primary reasons for compound attrition within the drug discovery pipeline. Therefore our lead compounds will be screened for potential adverse effects in several toxicity assays. The following sections give an overview of the key points the toxicological screens will cover.

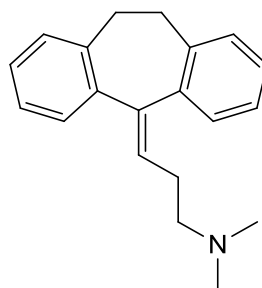
2.4.2 hERG testing

To investigate possible cardiotoxic effects the lead compounds will be tested in the human ether a-go-go related gene (hERG) assay. hERG encodes the inward rectifying voltage-gated potassium channel in the heart (IKr) which is involved in cardiac repolarisation. Inhibition of the hERG current causes QT interval prolongation (the QT interval represents electrical depolarisation and repolarisation of the ventricles) resulting in potentially fatal ventricular tachyarrhythmia called Torsade de Pointes (TdP). A number of drugs have been withdrawn from the market (prenylamine, terodiline, sertindole and astemizole) due to these cardiotoxic effects, therefore it is important to identify inhibitors as early as possible in the drug discovery process³⁹. The data from hERG assays is usually categorised into the following classification bands (Table 2.8).

Table 2.8. Classification bands for hERG IC₅₀ values.

Highly potent	IC ₅₀ < 0.1µM
Potent	IC ₅₀ between 0.1 - 1µM
Moderately potent	IC ₅₀ between 1µM - 10µM
Weak or no inhibition	IC ₅₀ >10µM

Amitriptyline (**24**), a tricyclic antidepressant prescribed for the treatment of neuropathic pain (Figure 2.15), is known to be a moderately potent hERG channel blocker with an IC₅₀ 4.78 µM. As such patients prescribed amitriptyline need to have regular check-ups to assess whether the medication is affecting their QT interval^{40,41}.



Amitriptyline
24

Figure 2.15. Tricyclic antidepressant amitriptyline (**24**); a known hERG blocker

2.4.3 The Ames test

The Ames assay is designed to examine possible mutagenic/carcinogenic effects of chemical compounds. The Ames Salmonella/microsome mutagenicity assay is a short-term bacterial reverse mutation assay. It has been specifically designed to detect a wide range of chemical substances that can produce genetic damage leading to gene mutations. The test uses several histidine dependent Salmonella strains each carrying different mutations in various genes in the histidine operon. These mutations act as hot spots for mutagens that cause DNA damage. When the Salmonella tester strains are grown on an agar plate containing a trace of histidine, only those bacteria that revert to histidine independence (his(+)) are able to form colonies. However, when a mutagen is added to the plate, the number of revertant colonies per plate is increased, usually in a dose-related manner. The Ames test is used world-wide as an initial screen to determine the mutagenic potential of new chemicals and drugs⁴².

2.4.4 Cytotoxicity

In vitro cytotoxicity is an effective indicator of human toxicity potential that must be addressed early in the drug discovery pipeline in order to maximise the successful progression of compounds into development. Our compounds will be screened for cytotoxic effects in hepatocytes (hepG2) assays to evaluate for key toxicity markers including, cell number, nuclear condensation, total nuclear intensity, cell permeability, mitochondrial membrane potential and cytochrome C release^{35,43}

2.4.5 Metabolism and adverse drug reactions

Metabolism serves the important function of chemically modifying a compound to make it more polar and, therefore, more readily cleared into the bile and urine. An unfortunate consequence of metabolism is the possible formation of a reactive metabolite or metabolic intermediate which can lead to toxicity⁴⁴. The occurrence of idiosyncratic adverse drug reactions (ADRs) during late clinical trials or after a drug has been released can lead to a severe restriction in its use and even in its withdrawal. Metabolic activation of relatively inert functional groups to reactive electrophilic intermediates is considered to be an essential component in many drug-induced adverse reactions. A thorough examination of the biochemical reactivity of functional groups in all new drug candidates is essential from a safety viewpoint⁴⁵.

Modifications of proteins can elicit many ADRs from DNA mutations (with carcinogenic outcomes) to immune responses, causing severe hypersensitivity reactions (skin rashes) as in the case of the sulphonamide containing drug Sulfamethoxazole (**25**) and the antiretroviral drug abacavir (**26**) (Figure 2.16)^{46,47}.

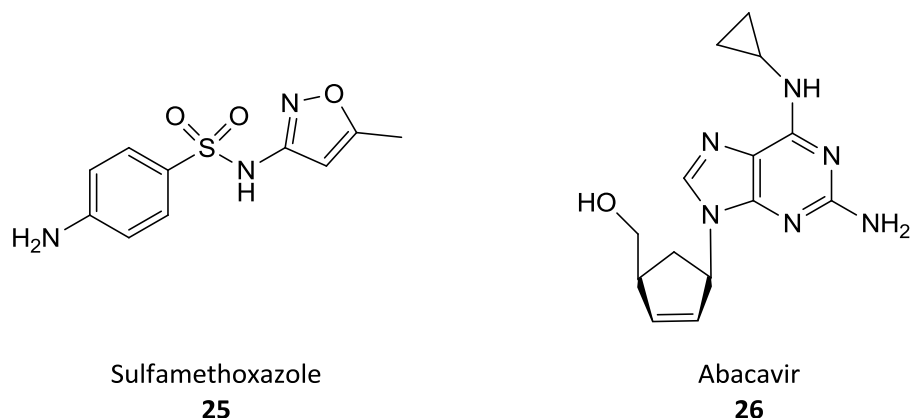


Figure 2.16. Sulfamethoxazole and abacavir, both drugs are responsible for hypersensitivity reactions.

Often ADRs occur in the liver, leading to hepatotoxicity, but the reactive metabolites can also cause damage at distal sites. There are many publications detailing the biochemical activation pathways of common functional groups utilised in drug discovery⁴⁸⁻⁵⁰;

Table 2.9 contains a partial list of structural motifs that may initiate toxicity⁴⁴.

Table 2.9. A partial list of structural motifs that may result in toxic metabolites.

Substrate	Proposed reactive metabolite
Aromatic amine	Hydroxyl amine, nitroso, quinone-imine
Hydroxyl amine	Nitroso
Aromatic nitro	Nitroso
Alkyl halide	Acylhalide
Hydroquinones	p-Benzoquinone
Acetamide	Radical
Thioamide	Thiourea

A target product profile outlining the desired criterion for our novel analgesic compound was developed taking in to account the CNS penetrant physicochemical properties described in Table 2.16, the selectivity required for the GlyR over the GABA_A R to ensure no sedative effects, the desirable pharmacokinetic parameters to ensure maximum absorption with minimum metabolism and to reduce the possibility of attrition due to safety issues as described in section 2.4.1.¹¹

Table 2.10. Target product profile for novel analgesic compounds

Assay/Model	Desired Criterion
Physicochemical properties	
Aqueous solubility	>0.05 mg/mL (pH 7.4)
ClogP	<4
MW	<450 (Da)
TPSA	< 90Å ²
Number of rotatable bonds	<8
ClogD	1-3
Pka	3-9
Selectivity	
GABA _A R (EC ₅₀)	GABA _A EC ₅₀ >100x GlyR EC ₅₀
Pharmacokinetics	
Oral bioavailability (rat)	>20%
Stability rat liver microsomes	T _{1/2} >60 mins
Stability human hepatocytes	T _{1/2} >30 mins
Brain CSF levels	3xEC ₅₀ (free) at 2-3 hrs at 1-3 mg/kg
<i>In vitro</i> plasma protein binding (rat)	<99.5%
Safety	
Functional hERG assay	IC ₅₀ > 10µM
Cytotoxicity HepG2 cells	No cytotoxicity at 500x EC ₅₀ GlyR EC ₅₀
Genotoxicity: Ames	Negative
Absence of metabolic alerts	No alerts

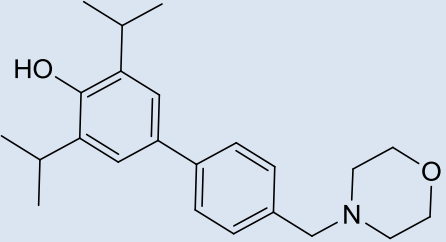
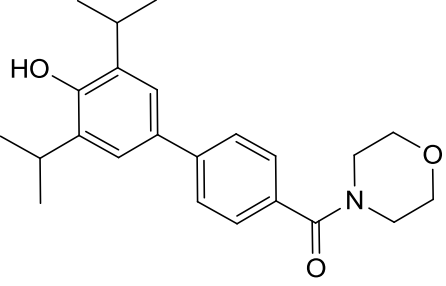
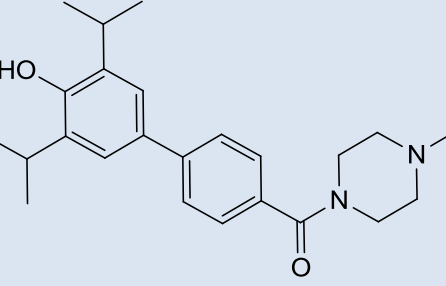
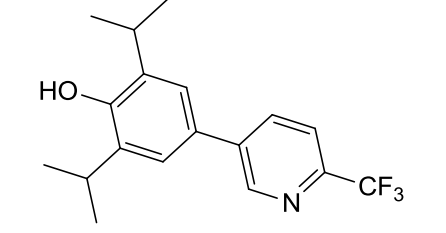
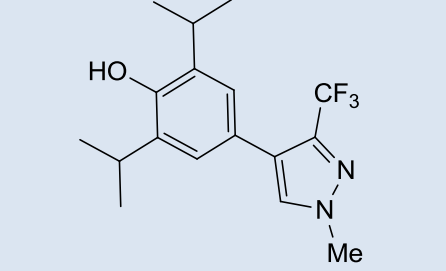
2.5 Heterocycles and Solubilising groups (novel work)

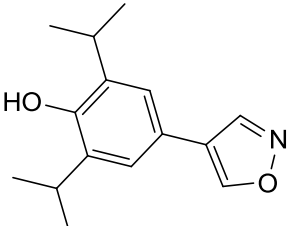
Previous work by Mohammadi, Bahram. Haeseler, Gertrud. Leuwer, Martin. Dengler, Reinhard. Krampfl, Klaus. & Bufler, Johannes³. has demonstrated that halogenation of phenols could significantly increase their potency at the GABA_AR. This work was built upon by previous members of the group who demonstrated that halogenated propofol analogues (compounds **8-10**) could target the α 1 GlyR with EC₅₀ values in the low nM region (compound **8** EC₅₀ = 0.6 nM). This work led to the investigation of a series of bi-phenyl compounds (**17-23**), this progression improved the efficacy at the α 1 GlyR as exemplified by compound **19** with an EC₅₀ = 70pM. From the initial *in vitro* studies of compound **19** it was apparent that solubility was an issue, with the compound being poorly absorbed (Figure 2.12).

Therefore, in an effort to improve the physicochemical parameters, aqueous solubility and optimise CNS penetration of the propofol analogues, this study will focus on a series of bi-phenyl and direct linked heterocyclic substituents incorporated at the 4-position of propofol. Addition of heterocyclic substituents and protonatable groups can improve TPSA, reduce ClogP and improve solubility. With this in mind a small library of novel target molecules was decided upon and their physicochemical parameters were evaluated (Table 2.11).

As can be seen from Table 2.11, whilst the ClogP and ClogD of the proposed compounds (**28,32,33,40,41,44**) have improved with respect to the bi-phenyl compounds they are still suboptimal for the highest probability of CNS penetration. It was decided that at this stage of the project it was important to synthesise these compounds and to subject them to the electrophysiology assays to determine their EC₅₀ values. This would give a greater understanding of the SAR tolerance surrounding substitution at the 4-position and allow us to further probe the binding pocket for these analogues in terms of size, shape and the tolerance of chemical functionality (Table 2.11).

Table 2.11. Proposed heterocyclic analogues. ClogP, TPSA & MW values were generated using ChemBiodraw ultra 12.0. ClogD was data was generated using ACD labs.

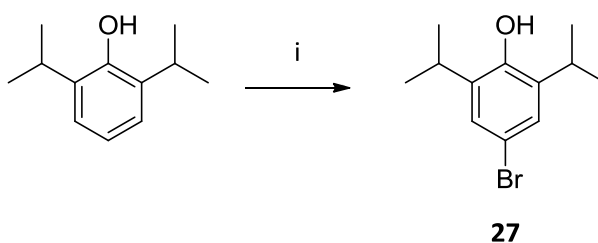
Compound	Structure	Parameters	
		ClogP	ClogD
28		ClogP	5.56
		ClogD	4.70
		TPSA	32.70
		MW	353.30
32		ClogP	4.56
		ClogD	3.90
		TPSA	49.77
		MW	367.48
33		ClogP	5.0
		ClogD	3.40
		TPSA	43.78
		MW	380.52
40		ClogP	5.55
		ClogD	3.70
		TPSA	33.12
		MW	323.35
41		ClogP	5.02
		ClogD	5.70
		TPSA	38.04
		MW	326.36

44		ClogP	3.98
		ClogD	3.40
		TPSA	46.26
		MW	254.32

2.6 Synthesis

The synthesis of **28** began with bromination of propofol followed by Suzuki coupling with the appropriate boronic acid.

Bromine was added drop wise to a solution of propofol in acetic acid to form 4-bromopropofol in 75-80% yields (Scheme 2.1). Mass spectrometry showed characteristic isotopic peaks relating to Br 79 & 81 incorporated into the product.



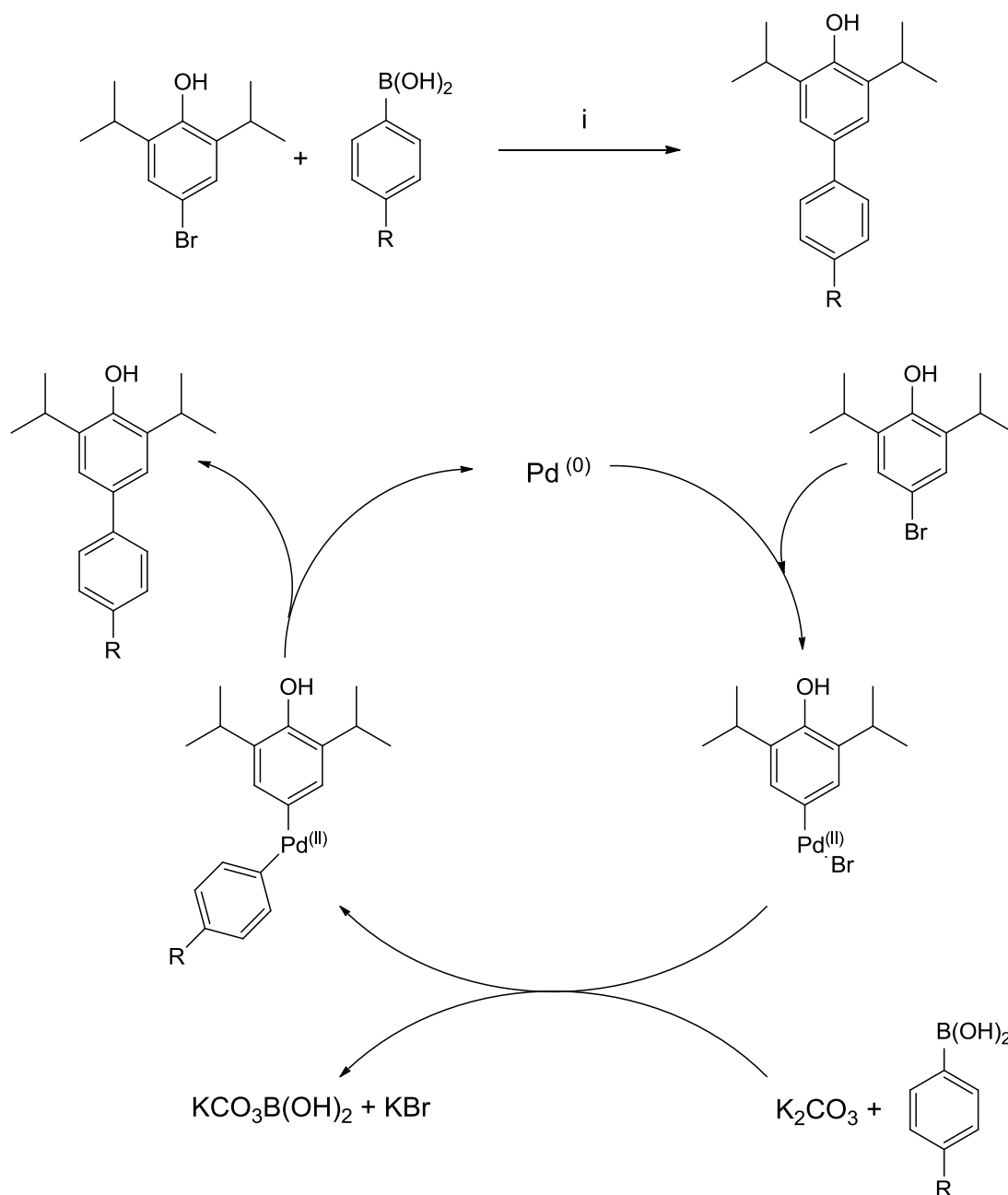
Scheme 2.1. *Reagents and conditions:* i) Bromine, AcOH, RT, 2hrs, 80% yield.

2.6.1 Suzuki Coupling

4-Bromopropofol was reacted with the appropriate commercially available boronic acid under Suzuki conditions to give compound **28** in 48% yield. The Suzuki coupling is one of the most reliable methods for the preparation of bi-aryl containing compounds⁵¹.

The first step in the mechanism of the Suzuki reaction is the oxidative addition of the aryl halide to the palladium (0) complex generating a palladium (II) intermediate. The next step is transmetalation; this involves transfer of the aryl group from the boronic acid to the palladium complex with the loss of the halide. Finally reductive elimination sees the product released and the palladium complex

reduced back to a palladium⁽⁰⁾ species ready for the next round of catalysis (Scheme 2.2).

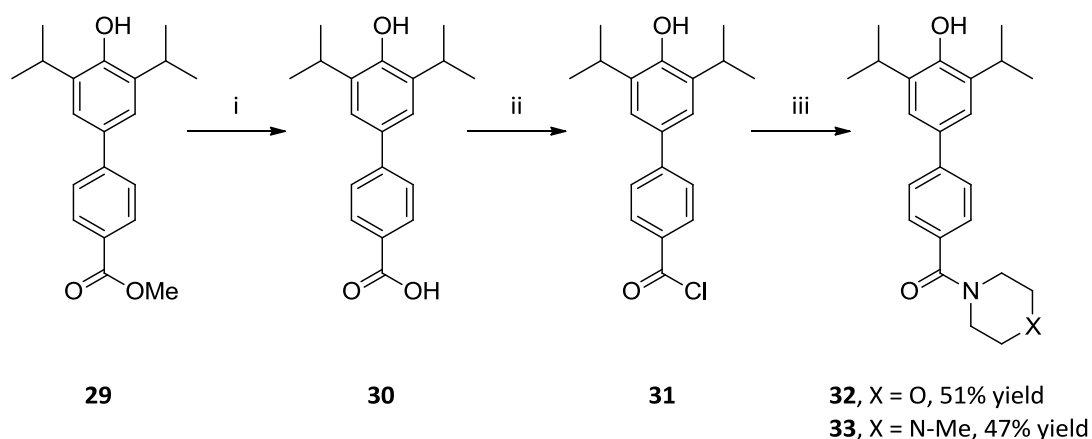


Scheme 2.2. Reagents and conditions: i) Pd(PPh₃)₄, K₂CO₃, THF/H₂O, 80°C, 24hrs, 48-60% yields.

2.6.2 Bi-Phenyl Amide Synthesis

In order to synthesise amide analogues **32** & **33**, 4-bromopropofol was subjected to the Suzuki conditions outlined in scheme 2.2 with the commercially available 4-methoxyphenyl boronic acid to yield the methyl ester (60% yield) which was subsequently hydrolysed to the carboxylic acid by treatment with NaOH in MeOH. The acid chloride was obtained via addition of oxalyl chloride to a solution of carboxylic acid in anhydrous DCM in the presence of catalytic quantities of DMF. The acid chloride was not isolated from the reaction mixture but was placed under reduced vacuum to remove any traces of unreacted oxalyl chloride.

Compounds **32** & **33** were prepared in moderate yields (47%-51%) by addition of the appropriate morpholino analogue to acid chloride (**31**) in anhydrous DCM in the presence of Et₃N⁵³ (Scheme 2.2).

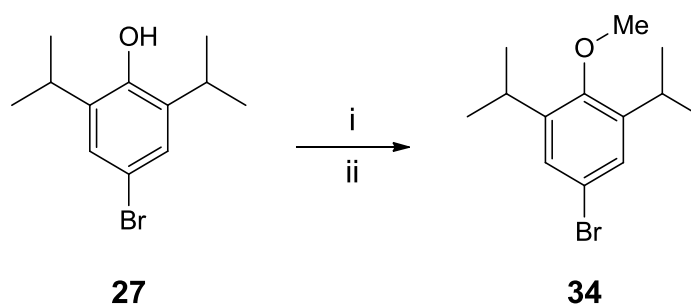


Scheme 2.2. Reagents and conditions: i) NaOH (2M), MeOH, RT, 18hrs, 67% yield; ii) oxalyl chloride, DMF (1 drop), DCM, RT, 2hrs; iii) corresponding amine, Et₃N, DCM, RT, 18hrs⁵².

2.6.3 Heterocycle synthesis

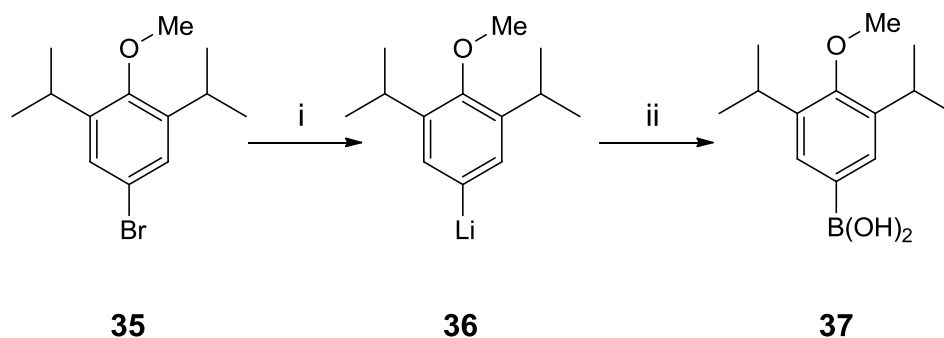
In the case of compounds **40,41 & 44** the corresponding boronic acids of the heterocycles were either not commercially available or they were prohibitively expensive. The halogenated analogues of the heterocycles were commercially available however, therefore, it was decided to synthesise the 4-boronic acid analogue of propofol and utilise the halogenated heterocycle in a Suzuki reaction to afford the desired products.

The first step in this synthetic pathway was to protect the phenolic oxygen. The protecting group chosen was a methyl ether. Addition of the protecting group was facilitated by addition of NaH to a solution of 4-bromopropofol in THF at 0°C. After 10 minutes MeI was added and the reaction was left to stir for 3 hours giving the product in excellent yields (99%)⁵⁴. The product was confirmed by the loss of the hydrogen atom at 4.81 ppm and the addition of a singlet peak at 3.71 ppm integrating for 3 protons in the ¹HNMR (Scheme 2.3).



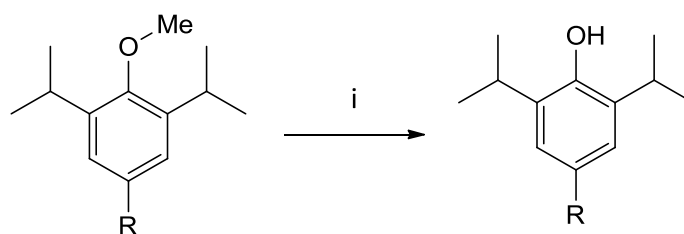
Scheme 2.3. Reagents and conditions: i) NaH, THF, 0°C, 10min; ii) MeI, 0°C, 3hrs, 99% yield.

The synthesis of the boronic acid was completed by lithium halogen exchange using n-butyl lithium to displace bromine and triisopropyl borate was utilised to trap out the lithiated species (Scheme 2.5).



Scheme 2.4. Reagents and conditions: i) n-BuLi 2.5 M, THF, -78°C , 1hr; ii) triisopropyl borate, -78°C -RT, THF, 18hrs⁵⁵.

The boronic acid and the corresponding halogenated heterocycles were subjected to the Suzuki conditions outlined in scheme 2.3. Demethylation was performed with 1.0 M boron tribromide solution in dichloromethane at room temperature for 5 hours to give desired products **40& 41**, (Scheme 2.5).



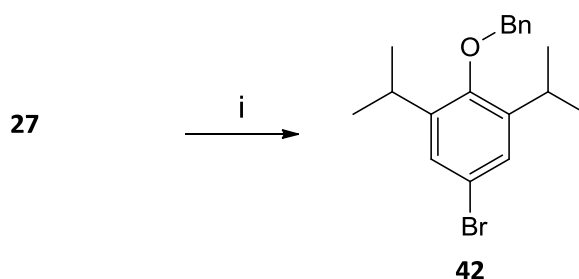
38, R = 2-(trifluoromethyl)pyridine
33, R = 1-methyl-3-(trifluoromethyl)
 -1H-pyrazole

40, R = 2-(trifluoromethyl)pyridine,
 48% yield
41, R = 1-methyl-3-(trifluoromethyl)
 -1H-pyrazole, 68% yield

Scheme 2.5. Reagents and conditions: i) BBr₃, DCM, 0°C , 5hrs⁵⁶.

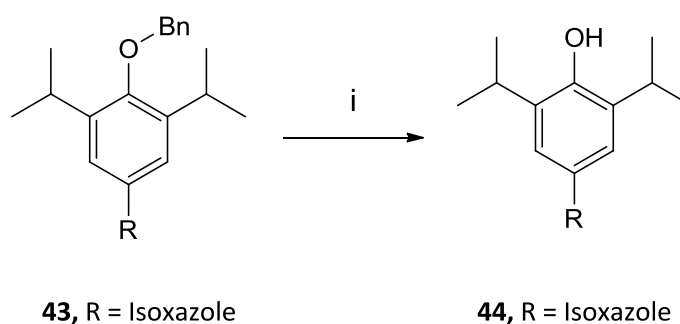
In the case of the isoxazole analogue **44**, it was found that when subjected to the demethylation conditions outlined in Scheme 2.5 the reaction failed to give the desired products.

To overcome this problem a benzyl ether protecting group was employed. The benzyl ether was added to 4-bromopropofol by addition of benzyl bromide and potassium carbonate in acetone at room temperature overnight (Scheme 2.6).



Scheme 2.6. Reagents and conditions: i) BnBr, acetone, K₂CO₃, RT, 18hrs⁵⁷.

The benzyl protected 4-bromopropofol was subjected to the lithium halogen exchange and subsequent trapping conditions outlined in Scheme 2. 4 to form the benzyl protected boronic acid (**37a**). The Suzuki product was formed utilising conditions shown in scheme 2.2, whilst benzyl deprotection was afforded by using hydrogen and palladium/carbon in methanol (Scheme 2.7) to give compound **44**.



Scheme 2.7. Reagents and conditions: i) H₂, Pd/C, MeOH, 18hrs 42% yield⁵⁸.

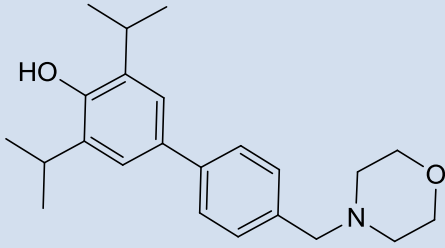
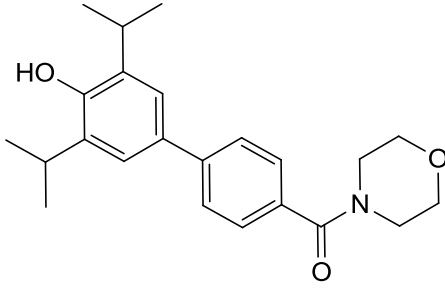
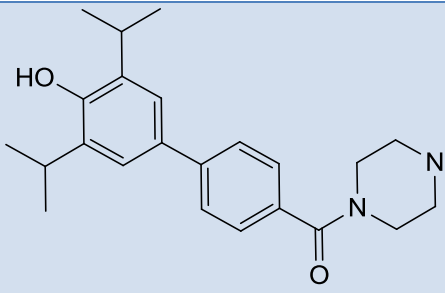
2.7 Biological Data

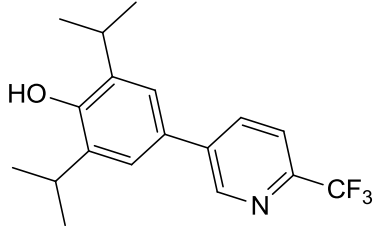
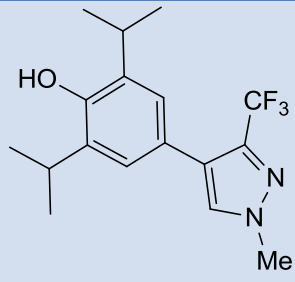
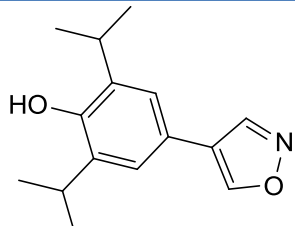
Compounds **28**, **32**, **33**, **40**, **41** & **44** were tested for efficacy at the α 1 GlyR,

Table 2.12 shows EC₅₀ values and physicochemical parameters for the phenyl and direct linked heterocycles.

To evaluate the potential for off target toxicity, compounds from both the biphenyl and heterocyclic templates were sent for testing against the GABA_AR.

Table 2.12. *In vitro* EC₅₀ values for heterocyclic compounds tested against the recombinant α 1GlyR

Compound	α 1 GlyR EC ₅₀ (μ M) ^a	ClogP ^b	ClogD ^c	GABA _A EC ₅₀ (μ M) ^d
 28	>1 μ M	5.56	4.70	NT
 32	ip	4.56	3.90	NT
 33	ip	5.0	3.40	3.33 \pm 0.058

 <p style="text-align: center;">40</p>	0.0001	5.55	3.70	0.12 ± 0.679
 <p style="text-align: center;">41</p>	>1 μM	5.02	5.70	3.33 ± 0.177
 <p style="text-align: center;">44</p>	ip	3.98	3.40	NT

a, $\alpha 1$ GlyR EC_{50} values determination was carried out at the University of Tübingen under the supervision of Prof. Bodo Laube. **b**, ClogP values were determined using chembiodraw ultra 12 software. **c**, In house algorithm. **d**, GABA_A selectivity testing was carried out at BioFocus®, Chesterford Research Park, Saffron Walden, UK. Ip, denotes compounds awaiting testing (in progress).

Of those compounds tested so far, only compound **40** has shown the low nanomolar activity seen with the compounds synthesised previously within the group. Compound **40** was also tested for activity at the GABA_AR, it was found to be a highly potent modulator of the GABA_A $\alpha 1\beta 2\gamma 3$ isoform with an $EC_{50} = 0.12 \mu M$. This is a highly undesirable attribute due to the off target effects seen with compounds that modulate the GABA_AR such as dizziness, drowsiness and sedation. Therefore due to the combination of a lack of efficacy at the $\alpha 1$ GlyR, off target activity and unfavourable physicochemical properties, the decision was taken to terminate this series.

2.8 Multiparameter Optimisation

During the synthesis of **28**, **32**, **33**, **40**, **41** & **44** a team at Pfizer headed by Villalobos⁵⁹ released a series of papers describing the development and use of a multiparameter optimisation (MPO) tool, to aid in the development of drugs acting at sites within the central nervous system. The following is a review of the Pfizer papers and a discussion of how the MPO approach was used as a key element in the design of “pre-optimised compounds”.

2.8.1 MPO Review

The drug discovery process is a highly complex, slow and risky enterprise. On average it takes around 10-15 years and costs in the region of 1 billion US dollars to advance a drug from preclinical discovery to regulatory approval. The pharmaceutical industry faces substantial attrition rates of candidate drugs. Approximately only 1 in 10 drugs entering clinical development actually reaches the market place.

As a result of this high failure rate the pharmaceutical industry faces a huge amount of pressure to not only cut the cost but also the timeframe for drug discovery. Drug discovery is an iterative process of candidate selection, synthesis, testing and optimisation of the candidate’s pharmacological profile. Merely the fact that a compound shows potency against a therapeutic target is not sufficient for a candidate to progress through the drug development process. From an early stage a drug candidate must display favourable physicochemical properties i.e. absorption, distribution, metabolism and excretion (ADME) and exhibit a low risk of possible toxicologically adverse events.

The rate of novel drugs successfully entering development over the last 20 years has remained unchanged at around 11%. Whilst many of the clinical failures can be attributed to a lack of efficacy at unvalidated targets, significant amounts were due to inadequate pharmacokinetic (PK) parameters. Interestingly a report published by Kola and Landis⁶⁰, showed the clinical attrition rate due to poor PK had dropped from 40% in 1991 to 10% in 2000 with failure rates due to safety and toxicology doubling to 30% over the same period. The fall in clinical attrition rates due to poor PK was associated with an increase in failure rates at earlier developmental stages driven by the introduction of *in silico* predictive models and the use of high-throughput assays.

There are several protocols already in use to help the medicinal chemist assess the druglikeness of a novel compound before the expensive and time consuming synthesis/optimisation iterative cycle begins, possibly the most well-known being Lipinski's rule of 5 (which was described earlier).

These guidelines have been used with great success by medicinal chemists since they were introduced in the late 1990s and have spawned many more such "rules of thumb" for drug design including, Glaxo Smith Kline's 4/400, which relates to compounds with a ClogP less than 4 and a MW less than 400 and how on average they have a more favourable ADMET profile⁶¹ and Pfizer's 3/75 rule, which states that compounds that have a ClogP < 3 and TPSA > 75 gave a 6-fold reduction in prevalence of *in vivo* toxicity versus compounds with ClogP > 3 and TPSA < 75 (Table 2.13)^{62,63}.

Table 2.13. Pfizer 3/75 rule for increased toxicity odds with TPSA and ClogP (data from ref.⁶²)

Toxicity	Total-drug		Free-drug	
	TPSA > 75	TPSA < 75	TPSA > 75	TPSA < 75
ClogP < 3	0.39 (57)	1.08 (27)	0.38 (44)	0.5 (27)
ClogP > 3	0.41 (38)	2.4 (85)	0.81 (29)	2.59 (61)

Whilst these rules are easy to understand, calculate and apply, they should be used with an air of caution. All the above mentioned guidelines utilise hard cut-offs in their approach to drug design, this can draw artificially tough distinctions between compounds with similar chemical properties. The use of desirability functions, however, is one approach which could avoid the harsh cut-offs seen with the application of simple filters such as Lipinski's guidelines.

Desirability functions mathematically transform the value of a given property e.g. ClogP or MW into a dimensionless number between 0-1, with 0 being the least desirable outcome and 1 being the ideal. This method can be applied to a variety of PK properties with the summation of each of the desirability functions giving an overall desirability value. This method allows for a more holistic approach to drug design by allowing the refinement of multiple properties without applying the harsh cut-offs seen with single parameter evaluation methods.

This method was exemplified by Villalobos, who whilst investigating the use of a multiparameter optimisation calculator (MPO) for optimal CNS penetration defined desirability scores for six key physicochemical parameters, ClogP, ClogD, MW, HBD, TPSA, and pKa. Each parameter was subjected to a desirability function and was assigned a desirability indices based upon a series of inflection points which serves to delineate the desirable regions from the undesirable regions (Figure 2.14).

ClogP, ClogD, MW, HBD, and pKa were subjected to a monotonic decreasing function whilst TPSA was subjected to a hump function, each of the transformed values were equally weighted. The summation of each of the desirability indices gives the overall CNS MPO score.

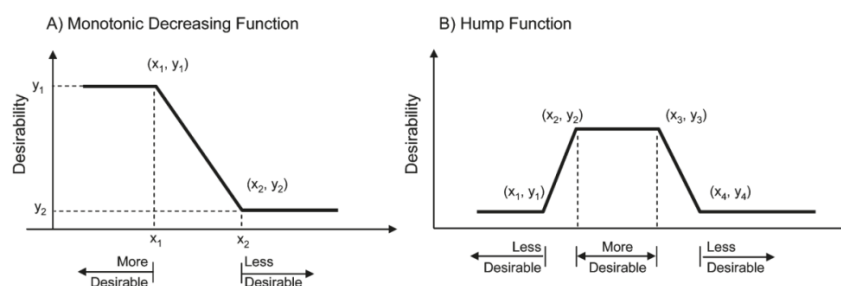


Figure 2.14. Desirability functions, (A) showing a monotonic function which is defined by a desirable region of the property ($x \leq x_1$) and an undesirable region ($x \geq x_2$). A linear transformation is applied between the two inflection points ($x_1 < x \leq x_2$) with those parameters whose values lie closer to x_2 having lower transformed values and are, therefore, less desirable. (B) a hump function, a desirable region flanked by two undesirable regions with linear transformation between the inflection points. Taken from ref ⁵⁹

The authors investigated the MPO score comparisons between 119 marketed CNS targeted drugs and 108 Pfizer CNS candidate drugs. It was found that of the 119 marketed CNS drug set 74% had a CNS MPO score ≥ 4.0 whilst only 60% of the 108 Pfizer candidate drugs had a CNS MPO score ≥ 4.0 . This statistically significant difference shows the MPO calculator could possibly be used to identify compounds which could have a higher probability for success. The flexibility of the MPO calculator was demonstrated with three compounds contained in the Pfizer candidate set.

Each of the compounds has PK parameters outside the optimal values for design space, if traditional rules of thumb were followed i.e. 3/75 rule, yet each compound has a MPO composite score of ≥ 4.5 . This is because the CNS MPO score balances multiple variables without utilising hard cut-offs seen with single value evaluation methods (Figure 2.15).

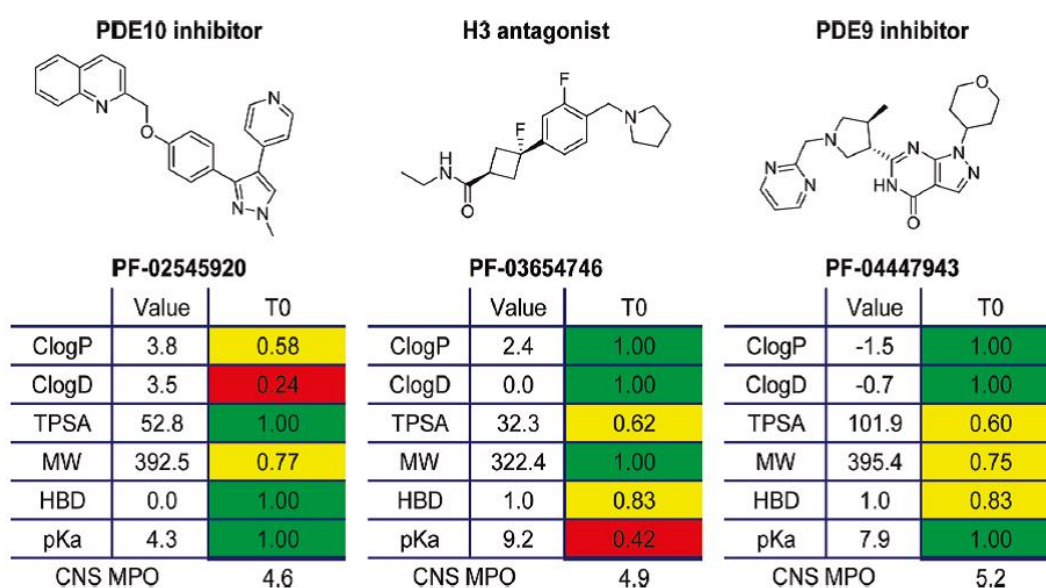


Figure 2.15. Compounds displaying optimal MPO values, would not have been synthesised if traditional guidelines had been followed. Taken from ref ⁵⁹

All of these compounds have completed preclinical toxicological assessment and have entered phase II clinical trials, yet they may not have been synthesised at all if hard cut-offs for $\text{ClogP} \leq 3$ (3/75 rule) or $\text{TPSA} \leq 100$ rule for greater CNS penetration, had been applied.

In addition, the authors also investigated the relationship between the CNS MPO score and four key ADME and safety endpoints, membrane permeability (apparent permeability (P_{app}) measured in the Madin-Darby canine kidney (MDCK) cell line), P-glycoprotein (P-gp) efflux liability (measured in MDCK cells transfected with the MDR1 gene), metabolic stability in human liver microsomes (HLM) (unbound intrinsic clearance), and general cellular toxicity (measured in a THLE Cv assay).

It was found that for both the marketed drug set ($n = 119$) and the candidate set ($n = 108$) compounds with a higher CNS MPO score (≥ 5) had significantly increased chances of favourable outcomes in each assay. It was shown that $> 90\%$ of the compounds in the marketed drug set with CNS MPO scores > 5 demonstrated high P_{app} , low P-gp liability, high cellular viability and favourable metabolic stability, 77% of these compounds displayed all three ADME attributes in one compound.

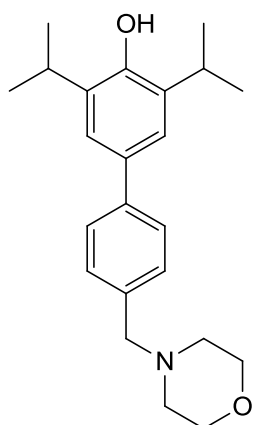
Finally the MPO algorithm was used to evaluate a larger set of 11303 Pfizer compounds in order to extensively cover property space. Once again the CNS MPO scores of the compounds were plotted and the ADME endpoints were assessed as described earlier, with the addition of a dofetilide (Dof) binding assay to assess potential hERG effects. Again a high concordance was found with compounds with higher MPO values (> 5) showing the most desired attributes of ADME properties, 82% showed high P_{app} , 78% had low P-gp, 69% with low $Cl_{int,u}$ and a low Dof liability of 67% . It was also noted that compounds with a high MPO score were found to have a greater chance of achieving favourable results in all four of the *in vitro* endpoints simultaneously.

These results show that the CNS MPO calculator is a useful tool for evaluating design ideas for all compounds not just those designed for CNS penetration. The use of the MPO calculator provides a holistic and flexible approach to drug design and increases the chances of discovering compounds with all the desired ADME and safety attributes aligned in one entity.

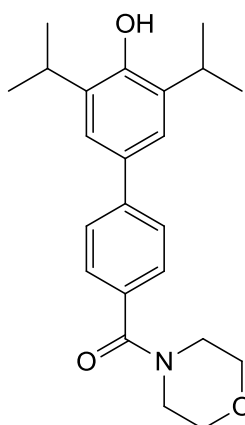
2.8.2 MPO evaluation of heterocyclic compounds

After evaluating the heterocycles synthesised so far it can be seen from Table 2.14 that only one compound (**22**) meets the MPO criteria for a high probability of CNS penetration. Unfortunately this compound does not show activity below $1 \mu\text{M}$ at the $\alpha 1$ GlyR.

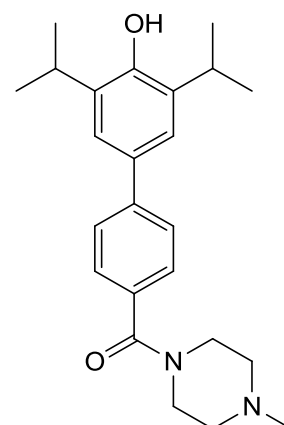
The rest of the compounds have a low MPO score (<4) and do not meet the criteria for a high probability of CNS penetration (MPO score 4-6). Due to the colour coded nature of the MPO calculator (red = poor, yellow = moderate, green = good) for the transformed values, those parameters which fall short of the desired criteria are easily identified. From Table 2.14 it can be seen that the molecular weight, topological surface area and hydrogen bond donor values for the compounds are good to moderate. Those values that consistently fail are ClogP, ClogD and pKa.



28



32

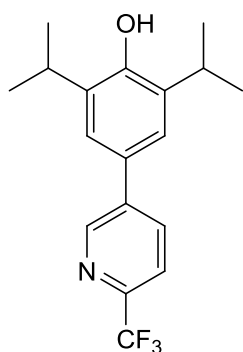
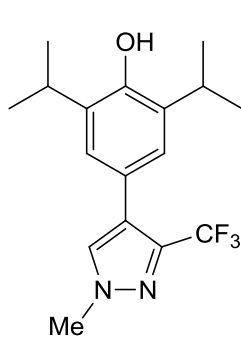
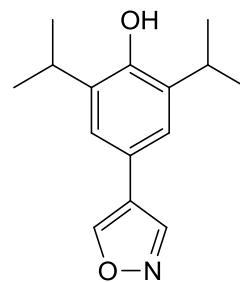


33

Property	Value	T0
ClogP	5.56	0.000
ClogD	4.7	0.000
TPSA	32.7	0.635
MW	353.5	1.000
HBD	1	0.833
pKa	10.93	0.000
CNS MPO		2.5

Property	Value	T0
ClogP	4.56	0.220
ClogD	3.9	0.050
TPSA	49.77	1.000
MW	367.48	0.947
HBD	1	0.833
pKa	10.81	0.000
CNS MPO		3.0

Property	Value	T0
ClogP	5	0.000
ClogD	3.4	0.300
TPSA	43.78	1.000
MW	380.52	0.853
HBD	1	0.833
pKa	10.82	0.000
CNS MPO		3.0

**40****41****44**

Property	Value	T0
ClogP	5.55	0.000
ClogD	3.7	0.150
TPSA	33.12	0.656
MW	323.35	1.000
HBD	1	0.833
pKa	9.22	0.390
CNS MPO		3.0

Property	Value	T0
ClogP	5.02	0.000
ClogD	5.7	0.000
TPSA	38.04	0.902
MW	326.36	1.000
HBD	1	0.833
pKa	10.17	0.000
CNS MPO		2.7

Property	Value	T0
ClogP	3.98	0.510
ClogD	3.4	0.300
TPSA	46.26	1.000
MW	245.32	1.000
HBD	1	0.833
pKa	10.25	0.000
CNS MPO		3.6

Table 2.14. MPO evaluation of heterocyclic compounds.

Table 2.14 shows that all of the compounds synthesised so far have poor ClogP, ClogD and pKa values leading to low MPO scores and consequently, a reduced probability of CNS penetration. The decision was, therefore, taken to reassess the design approach to these molecules with respect to, the MPO calculator in an effort to increase the probability of CNS penetration and to increase the efficacy and metabolic stability of future analogues.

2.9 Summary

In summary this chapter has shown the progression from propofol > halogenated series > 4-aryl series > 4- hetero/bi-phenyl series (Figure 2.16).

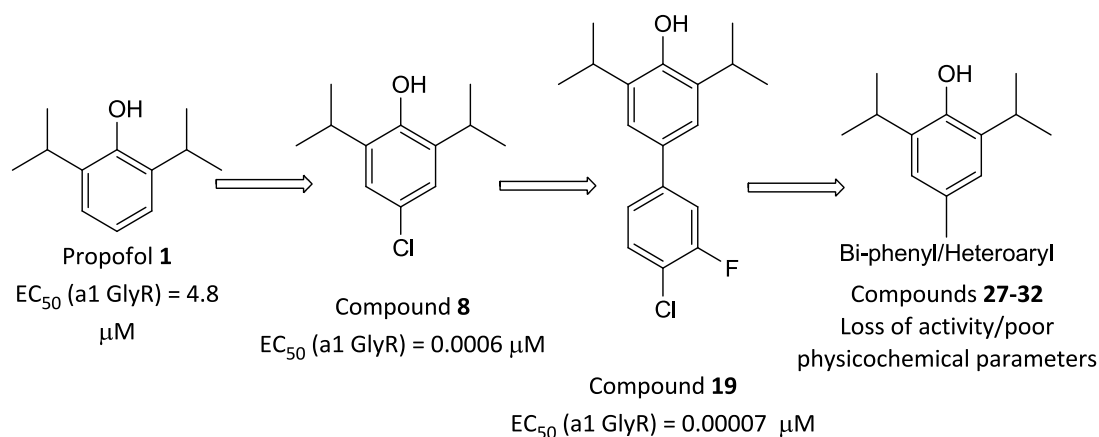


Figure 2.16. Optimisation of propofol analogues targeting the α 1 GlyR.

Building upon work by Mohammadi, Bahram. Haeseler, Gertrud. Leuwer, Martin. Dengler, Reinhard. Krampfl, Klaus. & Bufler, Johannes.³ previous work within the group showed that halogenation at the 4-position of propofol could increase the efficacy for the α 1 GlyR by \sim 3 orders of magnitude. This led to further exploration of the binding pocket tolerances with respect to steric, electronic and hydrophobic interactions by incorporating a series of substituted aryl moieties at the 4-position (compounds **17-23**). These compounds showed excellent *in vivo* activity with EC_{50} values in the low nM/high pM region, exemplified by compound **19** (EC_{50} 70pM). However, from the preliminary animal studies it was evident that the aqueous solubility needed to be enhanced in order to improve the pharmacokinetic profile of these compounds.

A series of morpholino-bi-phenyl and heterocyclic containing compounds were synthesised in an effort to improve the physicochemical properties seen with the previous series, whilst retaining/improving efficacy at the α 1 GlyR (Table 2.12).

From the compounds in this series tested so far only one compound (**30**) showed the low nM activity seen with the previous series.

This compound has subsequently been tested for activity at the GABA_A receptor and has been found to be an agonist at GABA_A with an EC₅₀ = 0.12 μM, rendering it unsuitable for this project.

Evaluation of compounds **28, 32, 33, 40, 41 & 44** with the Pfizer MPO calculator has shown they all fall below the required score of ≥4 indicating a low probability of CNS penetration. With this in mind the decision was taken to redesign the series in order to synthesise molecules that retain low nM efficacy at the α1 GlyR and achieve MPO scores ≥4.

The following chapters describe the rational design of a new series of compounds targeting the α1 GlyR from hit to lead optimisation.

2.10 References

- 1 Dutertre, S., Becker, C.-M. & Betz, H. Inhibitory Glycine Receptors: An Update. *Journal of Biological Chemistry* **287**, 40216-40223 (2012).
- 2 Harvey, R. J. Depner, U. B. Wässle, H., *et al.* GlyR alpha3: an essential target for spinal PGE2-mediated inflammatory pain sensitization. *Science (New York, N.Y.)* **304**, 884-887 (2004).
- 3 Mohammadi, B. Haeseler, G. Leuwer, M. Dengler, E. Krampfl, K. & Bufler, J. Structural requirements of phenol derivatives for direct activation of chloride currents via GABA(A) receptors. *European Journal of Pharmacology* **421**, 85-91 (2001).
- 4 Belelli, D., Pistis, M., Peters, J. A. & Lambert, J. J. The interaction of general anaesthetics and neurosteroids with GABAA and glycine receptors. *Neurochemistry International* **34**, 447-452 (1999).
- 5 Lynch, J. W. Molecular structure and function of the glycine receptor chloride channel. *Physiological Reviews* **84**, 1051-1095 (2004).
- 6 Dong, X. P. & Xu, T. L. The actions of propofol on gamma-aminobutyric acid-A and glycine receptors in acutely dissociated spinal dorsal horn neurons of the rat. *Anesthesia and Analgesia* **95**, 907-914 (2002).
- 7 Hales, T. G. & Lambert, J. J. The actions of propofol on inhibitory amino-acid receptors of bovine adrenomedullary chromaffin cells and rodent central neurons. *British Journal of Pharmacology* **104**, 619-628 (1991).
- 8 Grasshoff, C. Drexler, B. Rudolph, U. Antkowiak, B. Anaesthetic Drugs: Linking Molecular Actions to Clinical Effects. *Current Pharmaceutical Design* **12**, 3665-3679 (2006).
- 9 Helfenbein, J., Lartigue, C. Noirault, E. Azim, E. Legailiard, J. Galmier, M. J. Madelmont, J. C., Isotopic Effect Study of Propofol Deuteration on the Metabolism, Activity, and Toxicity of the Anesthetic. *Journal of Medicinal Chemistry* **45**, 5806-5808 (2002).
- 10 Lin, A. L., Shangari, N., Chan, T. S., Ramirez, D. & O'Brien, P. J. Herbal monoterpene alcohols inhibit propofol metabolism and prolong anesthesia time. *Life Sciences* **79**, 21-29 (2006).
- 11 Personal Communication.
- 12 Lipinski, C. A., Lombardo, F., Dominy, B. W. & Feeney, P. J. Experimental and computational approaches to estimate solubility and permeability in drug discovery and development settings. *Advanced Drug Delivery Reviews* **23**, 3-25 (1997).
- 13 Savjani, K. T., Gajjar, A. K. & Savjani, J. K. Drug solubility: importance and enhancement techniques. *ISRN pharmaceuticals* **2012**, 195727-195727 (2012).
- 14 Trapani, G., Latrofa, A., Franco, M., Altomare, C., Sanna, E., Usala, M., Biggio, G., Liso, G. Propofol Analogues. Synthesis, Relationships between Structure and Affinity at GABAA Receptor in Rat Brain, and Differential

- Electrophysiological Profile at Recombinant Human GABAA Receptors. *Journal of Medicinal Chemistry* **41**, 1846-1854 (1998).
- 15 Moore, N. D. In search of an ideal analgesic for common acute pain. **11**, 129-137 (2009).
- 16 Fechner, J., Ihmsen, H., Jeleazcov, C. & Schüttler, J. Fospropofol disodium, a water-soluble prodrug of the intravenous anesthetic propofol (2,6-diisopropylphenol). *Expert Opinion on Investigational Drugs* **18**, 1565-1571 (2009).
- 17 Welliver, M. & Rugari, S. M. New drug, fospropofol disodium: a propofol prodrug. *AANA journal* **77**, 301-308 (2009).
- 18 Rautio, J. Kumpulainen H, Heimbach T, Oliyai R, Oh D, Järvinen T, Savolainen J. Prodrugs: design and clinical applications. *Nat Rev Drug Discov* **7**, 255-270 (2008).
- 19 Banaszczyk, M. G. Carlo, A. T., Millan, V., Lindsey, A., Moss, R., Carlo, D. J., Hendler, S. Propofol phosphate, a water-soluble propofol prodrug: in vivo evaluation. *Anesthesia & Analgesia* **95**, 1285-1292 (2002).
- 20 injection., P. i. L. f. d. *Research Triangle Park, NC: Eisai Corp* (December 12, 2008).
- 21 Moore, G. D., Walker, A. M. & MacLaren, R. Fospropofol: a new sedative-hypnotic agent for monitored anesthesia care. *The Annals of Pharmacotherapy* **43**, 1802-1808 (2009).
- 22 Ji, R.-R., Kohno, T., Moore, K. A. & Woolf, C. J. Central sensitization and LTP: do pain and memory share similar mechanisms? *Trends in Neurosciences* **26**, 696-705 (2003).
- 23 Craig, P. N. Interdependence between physical parameters and selection of substituent groups for correlation studies. *Journal of Medicinal Chemistry* **14**, 680-684 (1971).
- 24 Wang, F. Wang, F., Good, J. A. D., Rath, O., Kaan, Hung Yi K., Sutcliffe, O. B., Mackay, S. P., Kozielski, F. Triphenylbutanamines: Kinesin Spindle Protein Inhibitors with in Vivo Antitumor Activity. *Journal of Medicinal Chemistry* **55**, 1511-1525 (2012).
- 25 Khanfar, M. A., Hill, R. A., Kaddoumi, A. & El Sayed, K. A. Discovery of Novel GSK-3 β Inhibitors with Potent in Vitro and in Vivo Activities and Excellent Brain Permeability Using Combined Ligand- and Structure-Based Virtual Screening. *Journal of Medicinal Chemistry* **53**, 8534-8545 (2010).
- 26 Scott, K. R. Rankin, G. O., Stables, J. P. Synthesis and Anticonvulsant Activity of Enaminones. 3. Investigations on 4'-, 3'-, and 2'-Substituted and Polysubstituted Anilino Compounds, Sodium Channel Binding Studies, and Toxicity Evaluations^{1,2}. *Journal of Medicinal Chemistry* **38**, 4033-4043 (1995).
- 27 Siener, T., Cambareri, A., Kuhl, U., Englberger, W., Haurand, M., Kögel, B., Holzgrabe, U.. Synthesis and Opioid Receptor Affinity of a Series of 2,4-

- Diaryl-Substituted 3,7-Diazabicyclononanones. *Journal of Medicinal Chemistry* **43**, 3746-37514 (2000).
- 28 Thenmozhiyal, J. C., Wong, P. T.-H. & Chui, W.-K. Anticonvulsant Activity of Phenylmethylethylhydantoin: A Structure–Activity Relationship Study. *Journal of Medicinal Chemistry* **47**, 1527-1535c (2004).
- 29 Toteva, M. M. & Richard, J. P. in *Advances in Physical Organic Chemistry* Vol. Volume 45 (ed P. Richard John) 39-91 (Academic Press, 2011).
- 30 Srivastava, A., Ramachandran, S., Hameed, S. P., Ahuja, V. & Hosagrahara, V. P. Identification and Mitigation of a Reactive Metabolite Liability Associated with Aminoimidazoles. *Chemical Research in Toxicology* **27**, 1586-1597 (2014).
- 31 Pajouhesh, H. & Lenz, G. R. Medicinal chemical properties of successful central nervous system drugs. *NeuroRx : the journal of the American Society for Experimental NeuroTherapeutics* **2**, 541-553 .2.4.541 (2005).
- 32 Williams, R. Hepatic metabolism of drugs. *Gut* **13**, 579-585 (1972).
- 33 Benet, L. Z., Izumi, T., Zhang, Y., Silverman, J. A. & Wachter, V. J. Intestinal MDR transport proteins and P-450 enzymes as barriers to oral drug delivery. *Journal of Controlled Release* **62**, 25-31 (1999).
- 34 Li, A. P. Screening for human ADME/Tox drug properties in drug discovery. *Drug Discovery Today* **6**, 357-366 (2001).
- 35 <http://www.cyprotex.com>.
- 36 Waterbeemd, H., Camenisch, G., Folkers, G., Chretien, J. R. & Raevsky, O. A. Estimation of Blood-Brain Barrier Crossing of Drugs Using Molecular Size and Shape, and H-Bonding Descriptors. *Journal of Drug Targeting* **6**, 151-165 (1998).
- 37 Fichert, T., Yazdani, M. & Proudfoot, J. R. A structure–Permeability study of small drug-like molecules. *Bioorganic & Medicinal Chemistry Letters* **13**, 719-722 (2003).
- 38 Kelder, J., Grootenhuys, P. J., Bayada, D., Delbressine, L. C. & Ploemen, J.-P. Polar Molecular Surface as a Dominating Determinant for Oral Absorption and Brain Penetration of Drugs. *Pharm Res* **16**, 1514-1519 (1999).
- 39 Haverkamp, W., Breithardt, G., Camm, A.J., *et al.* The potential for QT prolongation and pro-arrhythmia by non-anti-arrhythmic drugs: Clinical and regulatory implications. Vol. 47 (2000).
- 40 Walia, K. S., Khan, E. A., Ko, D. H., Raza, S. S. & Khan, Y. N. Side Effects of Antiepileptics— A Review. *Pain Practice* **4**, 194-203 (2004).
- 41 Jo, S.-H., Youm, J. B., Lee, C. O., Earm, Y. E. & Ho, W.-K. Blockade of the HERG human cardiac K⁺ channel by the antidepressant drug amitriptyline. *British Journal of Pharmacology* **129**, 1474-1480 (2000).
- 42 Mortelmans, K. & Zeiger, E. The Ames Salmonella/microsome mutagenicity assay. *Mutation Research/Fundamental and Molecular Mechanisms of Mutagenesis* **455**, 29-60 (2000).
- 43 Taylor, D. L., Haskins, J. R. & Giuliano, K. A. *High content screening [electronic book] : a powerful approach to systems cell biology and drug discovery /*

- edited by D. Lansing Taylor, Jeffrey R. Haskins, Kenneth A. Giuliano. (Totowa, N.J. : Humana Press, 2007., 2007).
- 44 Kerns, E. H. & Di, L. in *Drug-like Properties: Concepts, Structure Design and Methods* (eds Edward H. Kerns & Li Di) 215-223 (Academic Press, 2008).
- 45 Kalgutkar, A. S., Gardner, I., Obach S. R., *et al.* A Comprehensive Listing of Bioactivation Pathways of Organic Functional Groups. *Current Drug Metabolism* **6**, 161-225 (2005).
- 46 Scholar, E. in *xPharm: The Comprehensive Pharmacology Reference* (eds S. J. Enna & David B. Bylund) 1-5 (Elsevier, 2007).
- 47 Arrieta-Bolaños, E., Madrigal, J. A., Marsh, S. G. E., Shaw, B. E. & Salazar-Sánchez, L. The frequency of HLA-B*57:01 and the risk of abacavir hypersensitivity reactions in the majority population of Costa Rica. *Human Immunology*.
- 48 Uetrecht, J. Screening for the potential of a drug candidate to cause idiosyncratic drug reactions. *Drug Discovery Today* **8**, 832-837 (2003).
- 49 Nassar, A.-E. F., Kamel, A. M. & Clarimont, C. Improving the decision-making process in structural modification of drug candidates: reducing toxicity. *Drug Discovery Today* **9**, 1055-1064 (2004).
- 50 Nelson, S. D. Molecular mechanisms of adverse drug reactions. *Current Therapeutic Research* **62**, 885-899 (2001).
- 51 Miyaura, N. & Suzuki, A. palladium-catalyzed cross-coupling reactions of organoboron compounds. *Chemical Reviews* **95**, 2457-2483 (1995).
- 52 Mullican, m.d., Wilson, M. W., Connor, D. T., Kostlan, C. R., Schrier, D. J., Dyer, R. D. design of 5-(3,5-di-tert-butyl-4-hydroxyphenyl)-1,3,4-thiadiazoles, 5-(3,5-di-tert-butyl-4-hydroxyphenyl)-1,3,4-oxadiazoles, and 5-(3,5-di-tert-butyl-4-hydroxyphenyl)-1,2,4-triazoles as orally-active, nonulcerogenic antiinflammatory agents. *Journal of medicinal chemistry* **36**, 1090-1099 (1993).
- 53 Ziakas, G.N., Rekka, E.A., Gavalas, A.M., Eleftheriou, P.T. & Kourounakis, P.N. New analogues of butylated hydroxytoluene as anti-inflammatory and antioxidant agents. *Bioorganic & Medicinal Chemistry* **14**, 5616-5624 (2006).
- 54 Stoochnoff, B.A., Benoiton, N.L. The methylation of some phenols and alcohols with sodium hydride / methyl iodide in tetrahydrofuran at room temperature. *Tetrahedron Letters* **14**, 21-24 (1973).
- 55 Ueda, A., Nishida, S., Fukui, K., *et al.* Three-Dimensional Intramolecular Exchange Interaction in a Curved and Nonalternant π -Conjugated System: Corannulene with Two Phenoxy Radicals. *Angewandte Chemie International Edition* **49**, 1678-1682 (2010)
- 56 McOmie, J.F.W., Watts, M.L. & West, D.E. Demethylation of aryl methyl ethers by boron tribromide. *Tetrahedron* **24**, 2289-2292 (1968).

- 57 Wuts, P.G.M. & Greene, T.W. Protection for Phenols and Catechols. in Greene's Protective Groups in Organic Synthesis 367-430 (John Wiley & Sons, Inc., 2006).
- 58 Martinez-Solorio, D. & Jennings, M.P. Convergent Formal Syntheses of (±)-Brussonol and (±)-Abrotanone via an Intramolecular Marson-Type Cyclization. *Organic Letters* **11**, 189-192 (2008).
- 59 Wager, T.T., Hou, X., Verhoest, P.R. & Villalobos, A. Moving beyond Rules: The Development of a Central Nervous System Multiparameter Optimization (CNS MPO) Approach To Enable Alignment of Druglike Properties. *ACS Chemical Neuroscience* **1**, 435-449 (2010).
- 60 Kola, I. & Landis, J. Can the pharmaceutical industry reduce attrition rates? *Nat Rev Drug Discov* **3**, 711-716 (2004).
- 61 Gleeson, M. P. Generation of a Set of Simple, Interpretable ADMET Rules of Thumb. *Journal of Medicinal Chemistry* **51**, 817-834 (2008).
- 62 Hughes, J. D., Blagg, J., Price, D. A., *et al.* Physicochemical drug properties associated with in vivo toxicological outcomes. *Bioorganic & Medicinal Chemistry Letters* **18**, 4872-4875 (2008).
- 63 Hann, M. M. Molecular obesity, potency and other addictions in drug discovery. *MedChemComm* **2**, 349-355 (2011).

Chapter III

Lead Generation

Contents

3.0	Introduction	106
3.1	Mannich side chain.....	108
3.1.1	In silico testing.....	113
3.1.2	<i>Tert</i> -butyl analogues with Mannich side chains	116
3.1.3	<i>In silico</i> testing.....	119
3.1.4	Biological results and MPO evaluation	121
3.1.5	Quinone methides.....	127
3.2	Amide morpholino analogues	133
3.2.1	<i>i</i> -pr-Amide <i>in silico</i> testing.....	139
3.2.2	<i>Tert</i> -butyl amide analogues.	141
3.2.3	<i>Tert</i> -butyl in silico testing.....	142
3.3	Biological results.....	147
3.3.1	Metabolic stability studies	149
3.3.2	<i>In vivo</i> pharmacokinetic studies (rat).....	151
3.3.3	<i>In vivo</i> neuropathic pain testing (Chung lesion model in the rat)	152
3.4	Summary.....	160
3.5	References	162

3 Introduction

It is evident from the previous chapter that the morpholino bi-phenyl and heterocyclic propofol analogues did not show desired efficacy at the α 1 GlyR with only one compound (**40**) showing the low nanomolar activity seen with the halogenated and early biphenyl compounds.

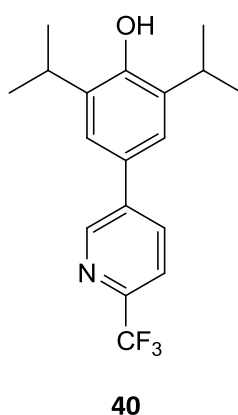


Figure 3.1. Compound **30** $EC_{50} = 0.0001 \mu\text{M}$ at α 1GlyR.

It was also shown in the previous chapter, via the MPO calculator, that the morpholino bi-phenyl and heterocyclic compounds had low probability of CNS penetration¹. It was noted that the ClogP and ClogD of the compounds was, in general, too high (>5 & >3 respectively) and that this could have a negative effect on solubility and consequently oral bioavailability².

In order to identify molecules with a better profile we initially added solubilising groups to propofol in the form of morpholino substituents attached directly to the core of the propofol scaffold. We had incorporated morpholines to several of the bi-phenyl compounds seen in the previous chapter (Table 2.12) but they were highly lipophilic and did not show any activity up to 1 μM at the α 1 GlyR.

We decided we wanted to keep the favourable solubilising properties of the morpholines but to remove the B-ring in an effort to lower ClogP and to reduce the overall steric bulk of the molecules. With this in mind, a review of the literature revealed a paper by Cooke, Anderson and Buchanan *et al*³. that described a series of propofol analogues containing *para*-aminoalkyl substituents (Figure 3.2). These molecules were designed as water-soluble versions of propofol targeting the GABA receptor³.

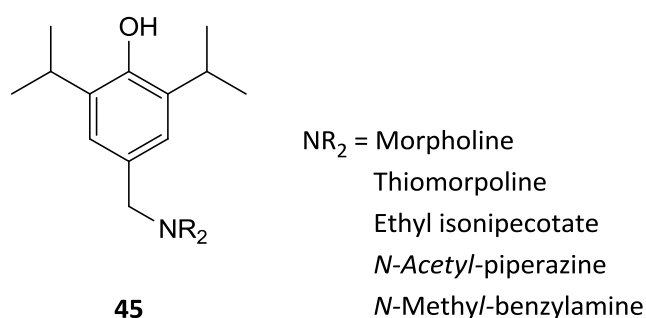
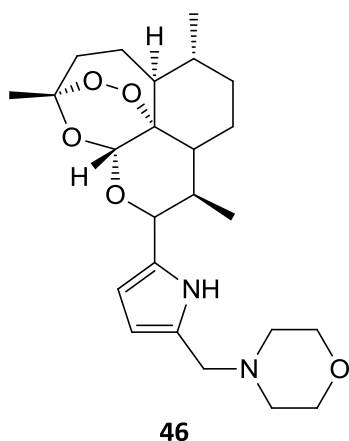


Figure 3.2. *Para*-aminoalkyl substituents described by Cooke and co-workers.

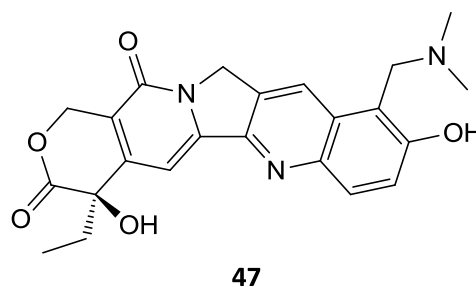
In this work it was shown that whilst several *para* aminoalkyl analogues retained some hypnotic effect in mice (albeit with HD₅₀ values in micromolar range), the *para* aminoalkyl analogues did not target the GABA_A receptor indicating the hypnotic effect was not mediated by the GABA_A receptor as expected. It is also of interest to note that none of the *para* aminoalkyl analogues synthesised by Cooke, Anderson and Buchanan *et al.* were tested for efficacy at the GlyR. It was thought that if the *para* aminoalkyl propofol analogues were active at the GlyR in the low nanomolar range, as seen with the halogenated and biphenyl series, this could confer selectivity over the GABA_A receptor and significantly reduce off target hypnotic activity. It was therefore decided to synthesise a series of propofol analogues with *para* aminoalkyl groups for testing against the α 1 GlyR. One of the ways in which the amino functionality can be introduced into the propofol core is via the Mannich reaction.

3.1 Mannich side chain

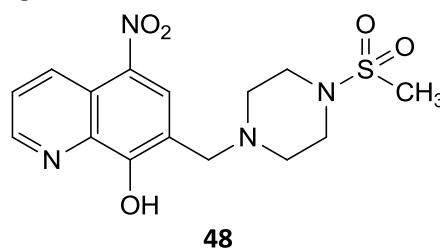
The Mannich reaction is one of the most important and versatile C-C bond forming reactions in organic synthetic chemistry⁴. The widespread use of the Mannich reaction is undoubtedly due to the diversity of functional groups tolerated and the variety of applications found for this robust reaction⁵. The introduction of Mannich side chains to biologically active compounds has been shown to improve solubility, bioavailability and, in some cases such as artemisinin (**46**), topotecan (**47**), and clioquinol (**48**), can result in increased potency⁶⁻⁹.



Artemisinin analogue with Mannich side chain
3x more potent than parent drug



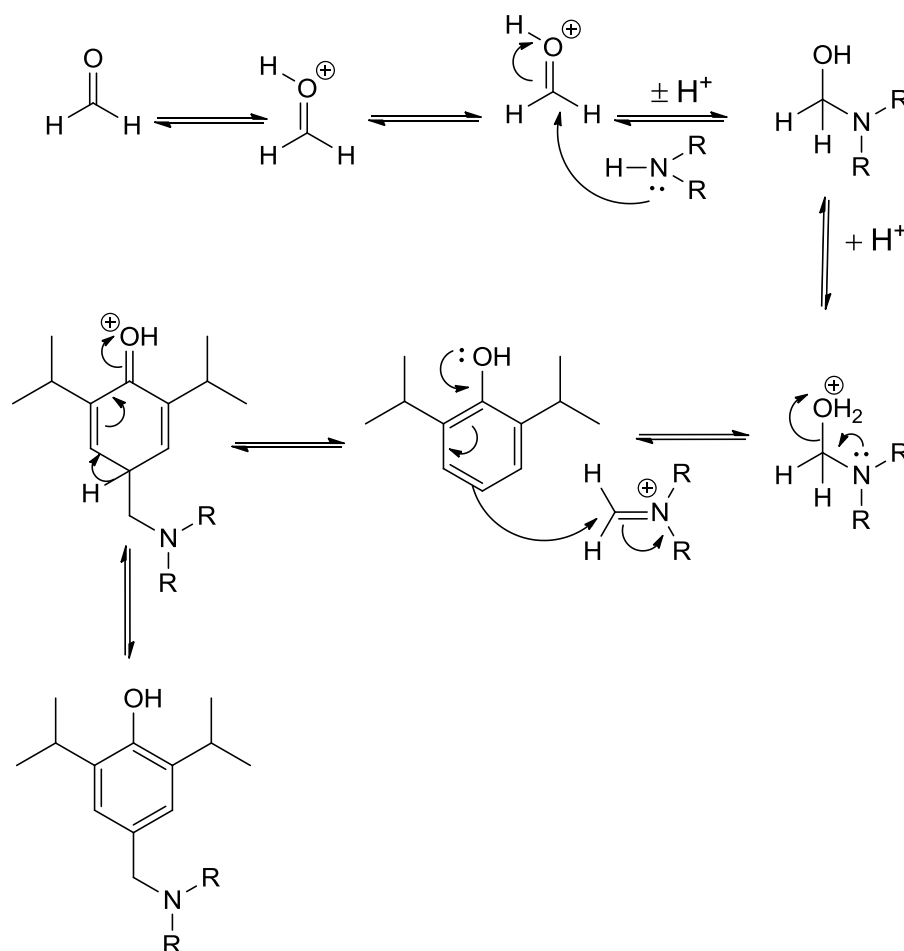
Mannich derivitised Topotecan,
water soluble antitumour agent



Clioquinol Mannich derivative, improved antiproliferic properties

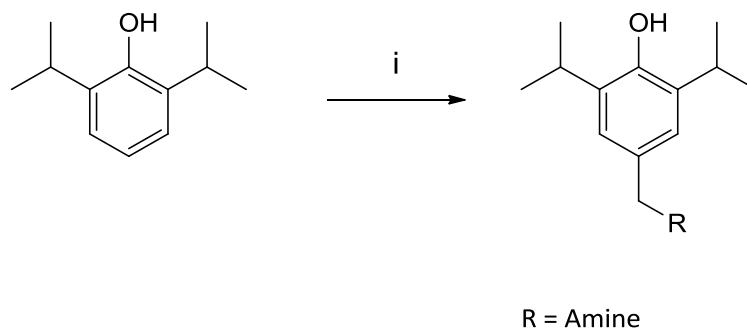
Figure 3.3. Mannich derivatives with increased biological activity with respect to parent compounds

The mechanism of the Mannich reaction proceeds via the formation of an imine salt from the amine and formaldehyde with the elimination of water. The electrophilic salt is then able to add into the phenolic ring (Scheme 3. 1).



Scheme 3. 1. Mechanism of the Mannich reaction.

The Mannich reaction can be accomplished in a variety of different ways¹⁰⁻¹²; we performed the reaction by sequentially adding propofol, the secondary amine of choice and formaldehyde to aqueous ethanol. The reaction mixture was heated to reflux for ~16 hours before being quenched with water, extracted with ethyl acetate and washed with brine (Scheme 3.2)



Scheme 3.2. Reagents and conditions: i) CH_2O , secondary amine, EtOH/ H_2O , reflux 16hrs 70-89% yields.

Flash column chromatography gave the desired Mannich products, compounds **49-55** (Figure 3.4).

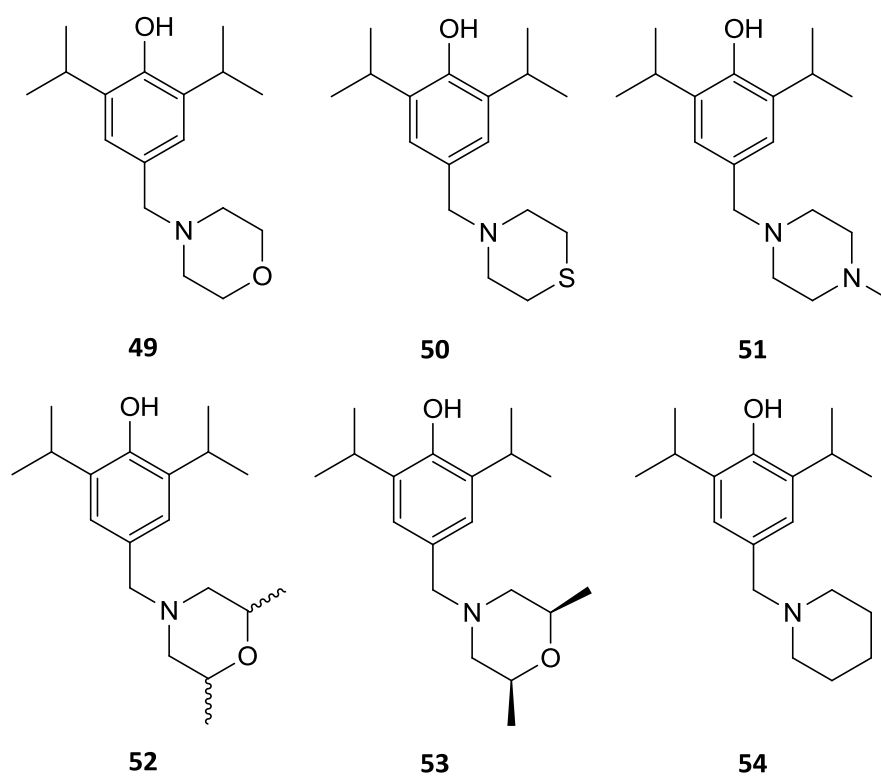
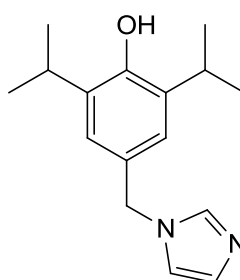


Figure 3.4. Mannich products.

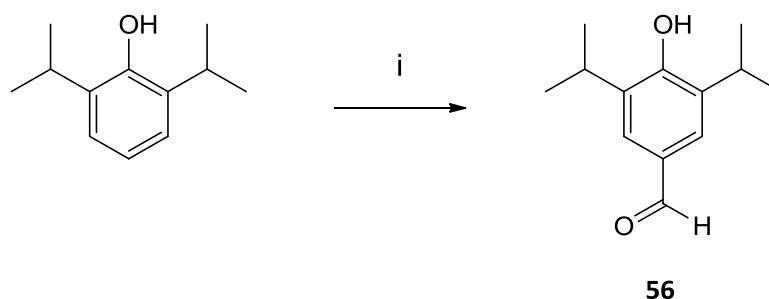
In addition to saturated small molecule heterocycles we also considered the use of basic heterocycles. Imidazoles are present in many natural and synthetic pharmacologically active compounds including, antibacterial, antifungal, anticancer and anti-HIV agents. These nitrogen containing aromatic heterocycles are often incorporated into medicinal compounds where their polar and ionisable characteristics can optimise the solubility and bioavailability parameters of poorly soluble compounds^{13,14} (Figure 3.5).



55

Figure 3.5. Imidazole Mannich side chain.

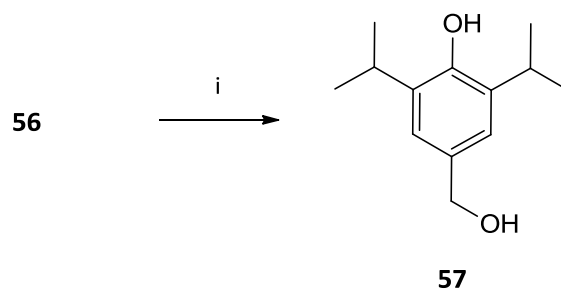
The synthesis of the imidazole Mannich side chain began with the formylation of propofol. 4-Formyl propofol was prepared by addition of hexamethylenetetramine to a solution of propofol dissolved in acetic acid (Scheme 3.3)^{15,16}. The reaction proceeded in good yields without the need for purification. The presence of the product was confirmed by a signature aldehyde shift at 10 ppm in the ¹HNMR¹⁷.



56

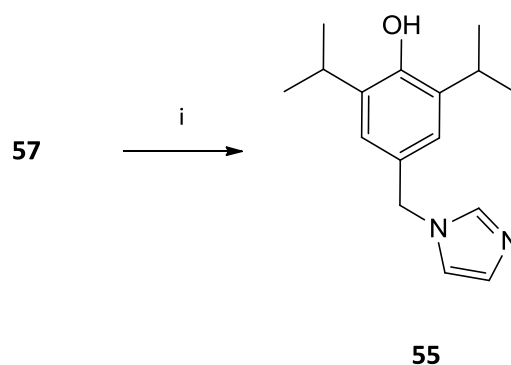
Scheme 3.3. Reagents and conditions: i) Hexamethylenetetramine, AcOH, reflux 16hrs, 89% yield.

The aldehyde **56** was then reduced to the benzyl alcohol **57** using lithium aluminium hydride, this reaction was carried out in anhydrous THF at 0°C (Scheme 3.4). The newly formed alcohol was characterised by the loss of the aldehyde singlet at 10ppm and by the appearance of a new singlet at 4.52ppm in the ¹HNMR integrating for two protons corresponding to the benzyl alcohol linker.



Scheme 3.4. Reagents and conditions: i) LiAlH₄, anhydrous THF, 0°C, 30min 80% yield.

Addition of the imidazole ring was afforded by allowing the alcohol to stir in the presence of excess imidazole at 160°C to give compound **55** in 50% yield.

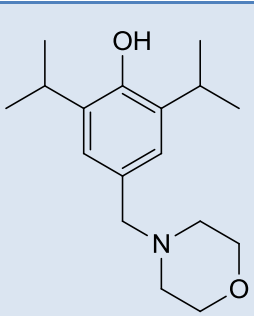
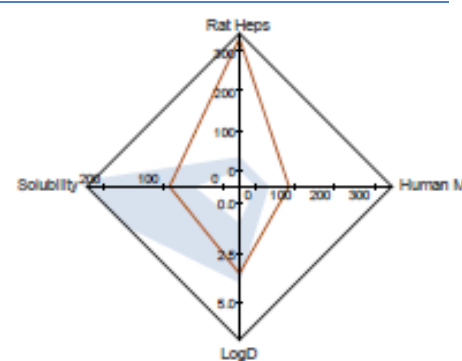
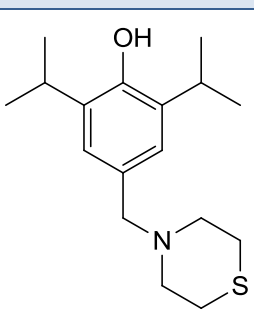
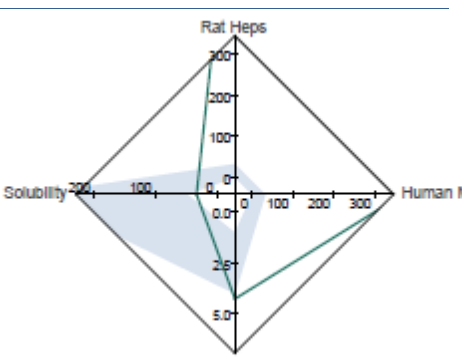


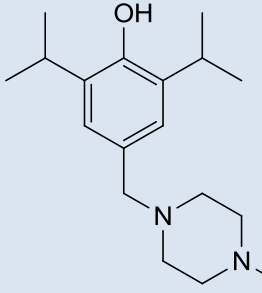
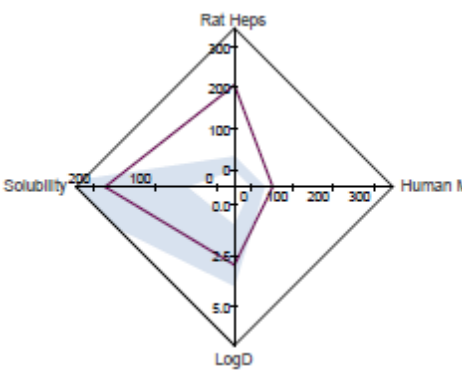
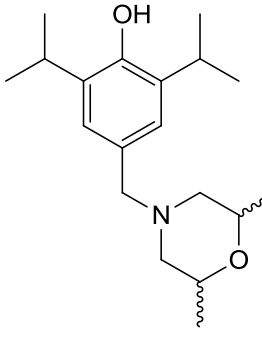
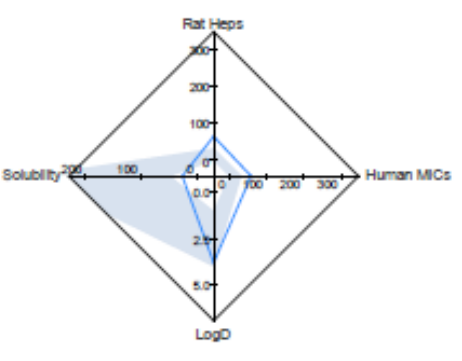
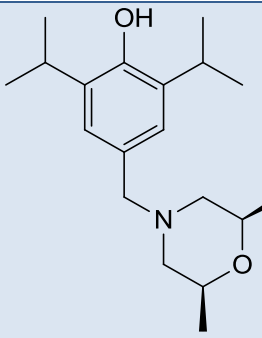
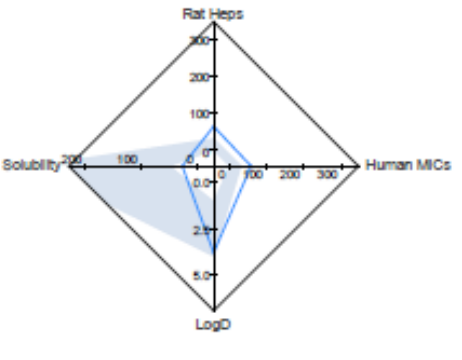
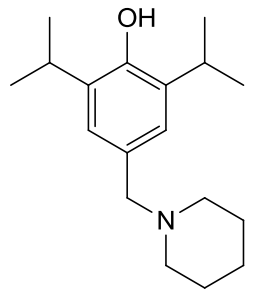
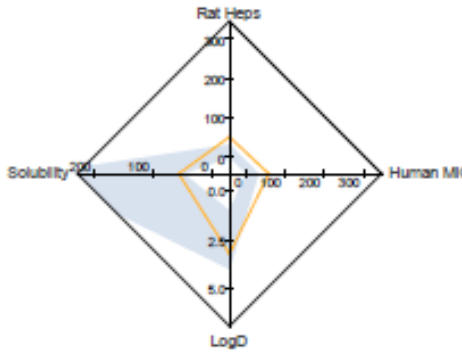
Scheme 3.5. Reagents and conditions: i) Imidazole, 160°C, 2hrs, 50% yield¹⁸.

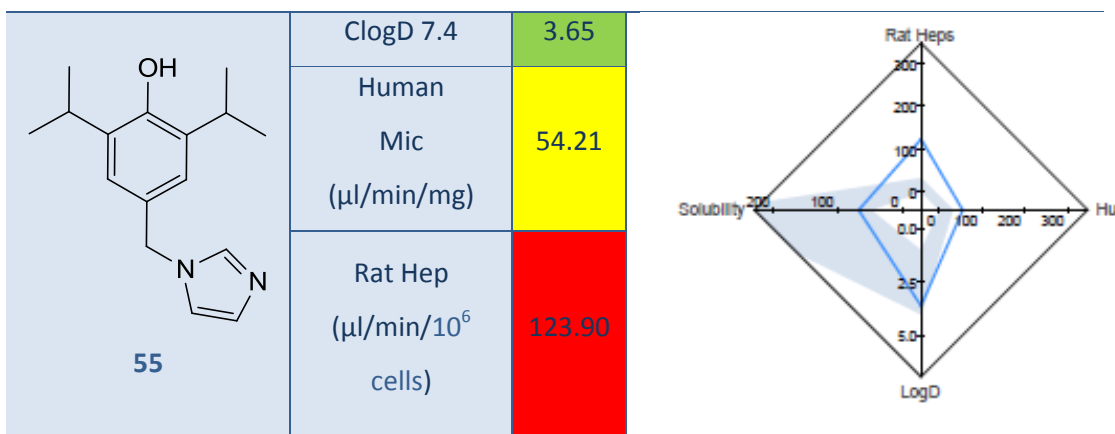
3.1.1 In silico testing

Before being sent for in vitro testing against the $\alpha 1$ GlyR compounds **49-55** were screened in silico in order to predict their physicochemical parameters, ClogP, ClogD, aqueous solubility and for their predicted clearance from human microsomes and rat hepatocytes (Table 3.1)¹⁹. *In silico* QSAR models were built and validated (using cross validation) using a set of descriptors (structural counts, topological indices and physicochemical property descriptors) and standard statistical tools: a Support Vector Machine (SVM), partial least squares (PLS) and Random Forest (RF) models. QSAR modelling and validation practice maximizes the robustness of models that are built and selected for use. Following thorough analyses of historical data, the parameters for the statistical methods used in have been empirically chosen and fixed to maximize performance and reliability.

Table 3.1. *In silico* prediction of physicochemical and pharmacokinetic parameters of benzyl compounds. Human Microsomes, 0-30 green, 30-60 yellow, 60 and above red. Rat Hepatocytes, 0-30 green, 30-60 orange, 60 and above red. ClogD7.4, 1-4 green, <1 OR >4 red.

Compound	Parameters	Radar plot	
 49	ClogD 7.4	3.45	
	Human Mic ($\mu\text{l}/\text{min}/\text{mg}$)	84.35	
	Rat Hep ($\mu\text{l}/\text{min}/10^6$ cells)	333.5	
 50	ClogD 7.4	4.26	
	Human Mic ($\mu\text{l}/\text{min}/\text{mg}$)	368	
	Rat Hep ($\mu\text{l}/\text{min}/10^6$ cells)	83.50	

 <p>51</p>	ClogD 7.4	2.95	
	Human Mic (μl/min/mg)	51.37	
	Rat Hep (μl/min/10 ⁶)	205.3	
 <p>52</p>	ClogD 7.4	3.82	
	Human Mic (μl/min/mg)	57.90	
	Rat Hep (μl/min/10 ⁶ cells)	62.55	
 <p>53</p>	ClogD 7.4	3.82	
	Human Mic (μl/min/mg)	57.90	
	Rat Hep (μl/min/10 ⁶ cells)	62.55	
 <p>54</p>	ClogD 7.4	3.22	
	Human Mic (μl/min/mg)	57.17	
	Rat Hep (μl/min/10 ⁶ cells)	50.82	



It can be seen from . In *silico* QSAR models were built and validated (using cross validation) using a set of descriptors (structural counts, topological indices and physicochemical property descriptors) and standard statistical tools: a Support Vector Machine (SVM), partial least squares (PLS) and Random Forest (RF) models. QSAR modelling and validation practice maximizes the robustness of models that are built and selected for use. Following thorough analyses of historical data, the parameters for the statistical methods used in have been empirically chosen and fixed to maximize performance and reliability.

Table 3.1 that ClogD remains high in many of the compounds with only **51** showing a ClogD value within the acceptable parameter of <3 . Therefore more work needs to be done to lower the ClogD and this could be achieved by the addition of more polar substituents. The aqueous solubility of many of the compounds is high ($>50 \mu\text{M}$), as expected those compounds with higher ClogP values (**50**, **52** & **53**,) typically fall below the optimal solubility value as can be seen in the radar plots (Table 3.1). The radar plots give a good visual representation of the ideal values vs. the predicted values for ClogD, solubility, human microsomes and rat hepatocytes. The shaded areas of the plots show where the ideal values for each parameter should lie.

The predicted rate of clearance in both human liver microsomes (for phase I metabolism) and rat hepatocytes (phase I and phase II metabolism) was evaluated using our metabolism prediction software. It can be seen from Table 3.1 that all of the compounds are extensively metabolised in both models. It is thought that phase I metabolism would occur predominantly at the benzylic linker, with minor contributions from hydroxylation of the isopropyl and morpholino substituents^{20,21}, whereas phase II metabolism would be mediated through glucuronidation (by uridine diphosphate glucuronosyltransferases) of both the phenolic hydroxyl group and the hydroxy products of phase I metabolism.

In addition to the 2,6-diisopropyl series we also examined a series of bis-*tert*-butyl propofol analogues since as it had previously been shown that 2,6-di-*tert*-butylphenol displays no anaesthetic properties²².

3.1.2 *Tert*-butyl analogues with Mannich side chains

In a 2001 study by Krasowski and co-workers, 27 different propofol analogues were screened for anaesthetic activity and for potentiation of the most common GABA_A subtype ($\alpha_1\beta_2\gamma_{2s}$)²³. Anaesthetic activity was determined by loss of righting reflex (LRR) in *Xenopus laevis* tadpoles, whilst GABA potentiation was determined via electrophysiological studies using HEK 293 cells^{24,25}. 2,6-di-*tert*-butylphenol (Figure 3.6), was one of the compounds chosen by Krasowski for this study not only because it is one of the closest structural analogues of propofol but also because it had shown no anaesthetic properties in mice in previous studies by Glen and co-workers²⁶.

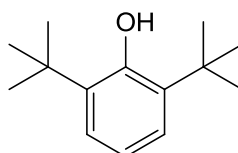


Figure 3.6. 2,6-Di-*tert*-butylphenol.

The results of the study by Krasowski showed that 2,6-di-tert-butylphenol did not display any anaesthetic activity in the *Xenopus laevis* tadpoles, but crucially electrophysiological results showed that **56** did not potentiate the GABA_AR, either directly or by co-activation.

These results lend weight to the hypothesis that alteration of GABA functionality is, at least in part, responsible for the anaesthetic effects of propofol. This hypothesis was tested once again by Ahrens and co-workers who tested 2,6-di-tert-butylphenol against rat GABA receptors within a mammalian expression system (HEK 293 cells). Once again it was determined that it showed no potentiation of GABA current²².

In an earlier publication, Ahrens and co-workers had compared the effects of both propofol and 2,6-di-tert-butylphenol at the rat α 1 GlyR (in HEK 93 cells)²⁷.

From this study it was determined that propofol has the ability to both directly activate and co-activate the α 1 GlyR ($EC_{50} = 12.5 \mu\text{M}$), addition of the GlyR antagonist strychnine increased the immobilising EC_{50} of propofol by $\sim 50\%$ whereas addition of GABA antagonist picrotoxin (**57 & 58**) or gabazine (**59**), gave a 400% increase in propofol's immobilising EC_{50} (Figure 3.7).

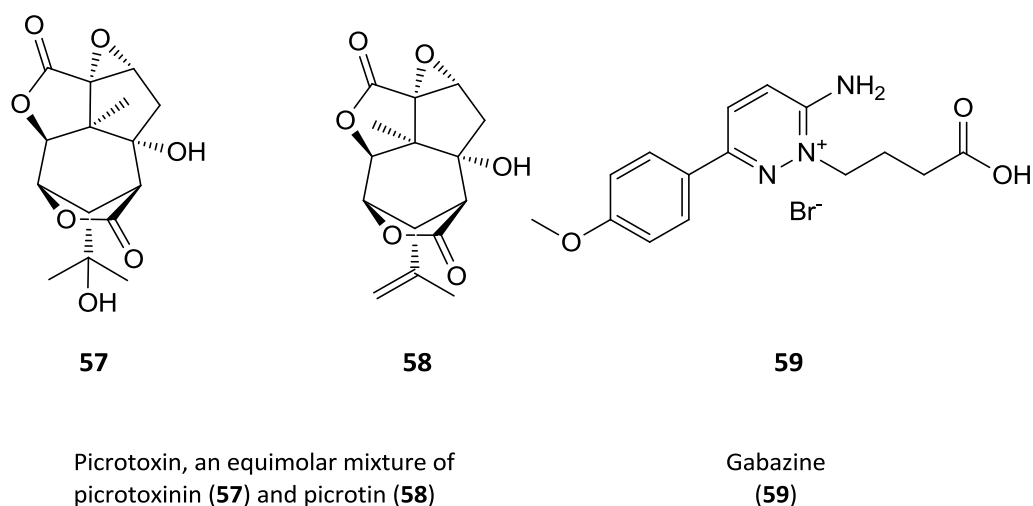
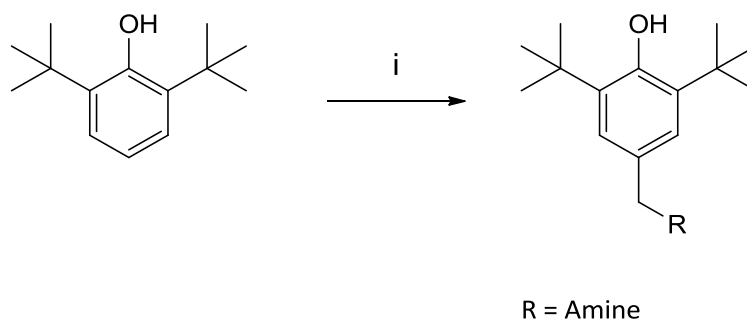


Figure 3.7. Gaba antagonists picrotoxin (**57 & 58**) and gabazine (**59**).

These results give credence to the hypothesis that glycine potentiation is not required for the immobilising effects of propofol. Importantly this study also shows that the propofol analogue 2,6-di-tert-butylphenol can co-activate and directly activate the $\alpha 1$ GlyR ($EC_{50} = 9.4 \mu\text{M}$) from a distinct binding site (allosterically).

Armed with the knowledge that 2,6-di-tert-butylphenol could selectively target the GlyR, with respect to the GABA_AR , it was decided to synthesise a number of 2,6-di-tert-butylphenol analogues with the Mannich side chains seen with the propofol analogues (Figure 3.4).

Synthesis of the 2,6-di-tert-butylphenol Mannich analogues (Scheme 3.6) is analogous to that seen in Scheme 3.2¹⁰.



Scheme 3.6. *Reagents and conditions:* i) CH_2O , secondary amine, EtOH/ H_2O , reflux 16hrs 70-89% yields.

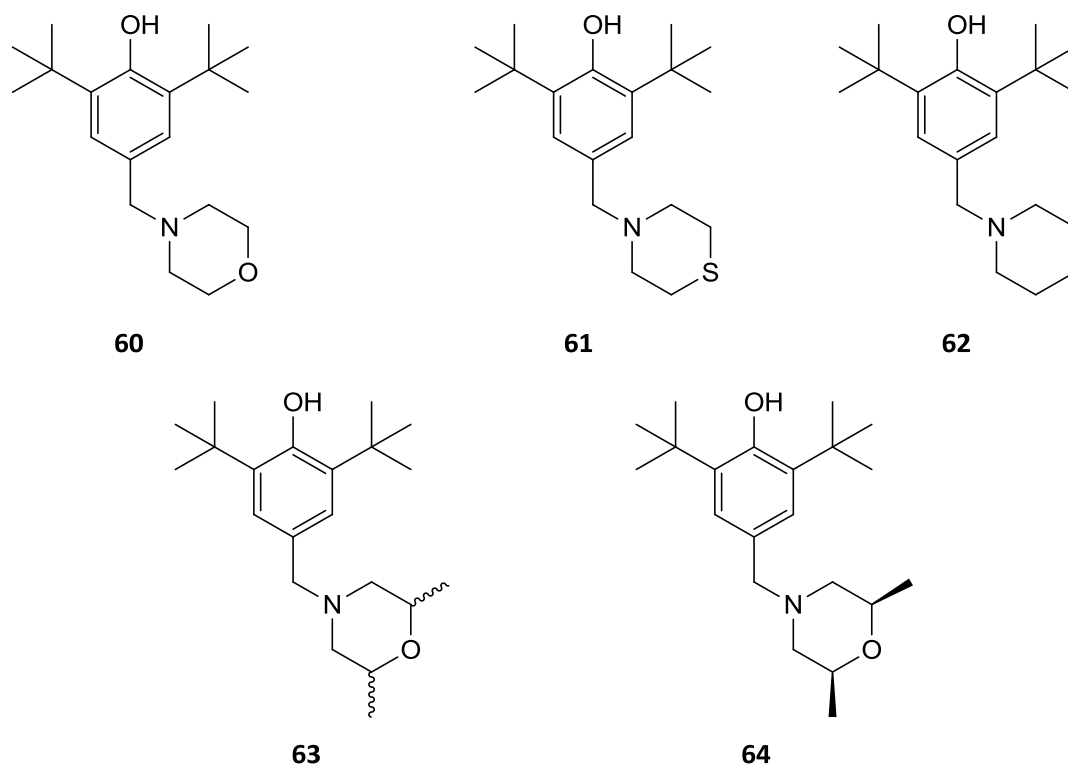
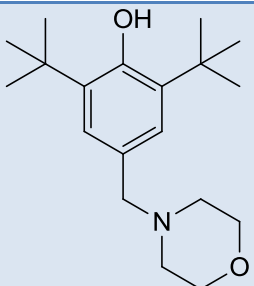
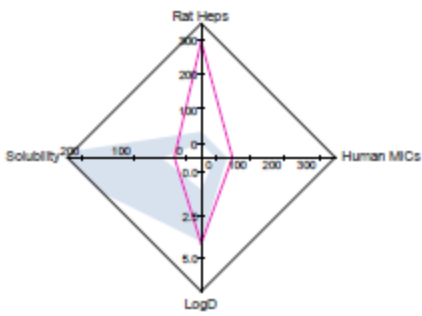
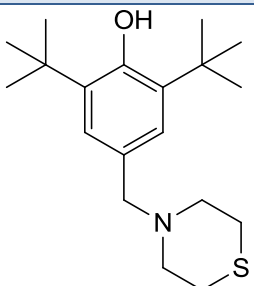
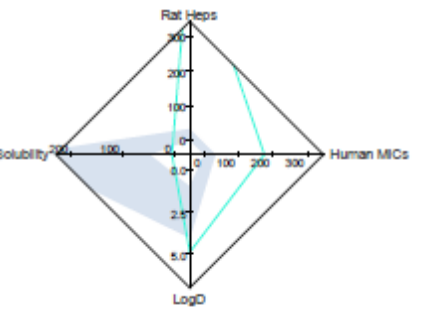
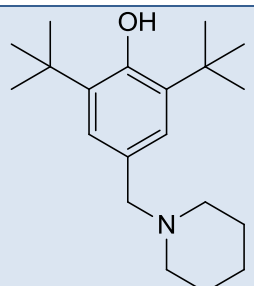
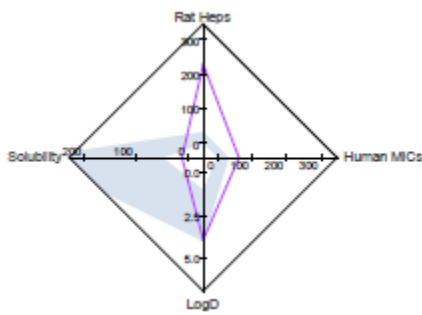
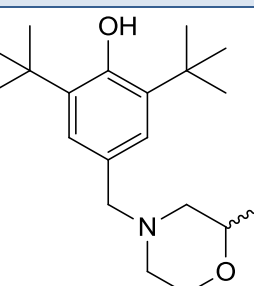
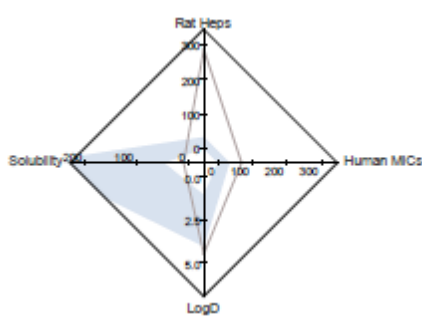


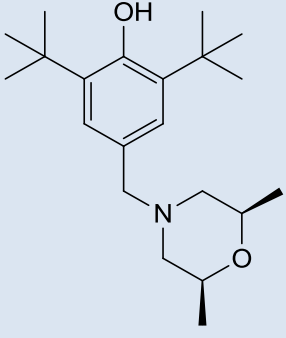
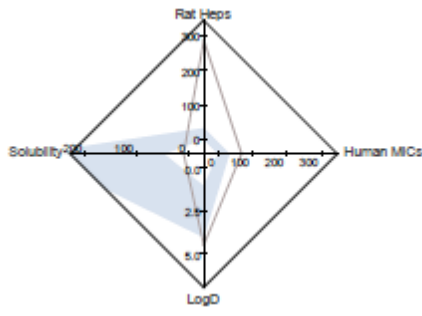
Figure 3.8. 2,6-Di-*tert*-butyl Mannich analogues.

3.1.3 *In silico* testing

The 2,6-di-*tert*-butyl Mannich analogues were also subjected to the same *in silico* prediction model as the 2,6-di-*i*-pr Mannich analogues in an effort to determine the effect of adding the increasingly lipophilic *tert*-butyl groups upon the ColgP, ClogD, solubility and metabolism of the compounds (Table 3.2).

Table 3.2. *In silico* prediction of *tert*-butyl morpholino analogues.

Compound	Parameters		Radar plot
 60	ClogD 7.4	4.14	
	Human Mic (μl/min/mg)	48.81	
	Rat Hep (μl/min/10 ⁶ cells)	293.6	
 61	ClogD 7.4	4.82	
	Human Mic (μl/min/mg)	175.3	
	Rat Hep (μl/min/10 ⁶ cells)	592.4	
 62	ClogD 7.4	3.93	
	Human Mic (μl/min/mg)	60.92	
	Rat Hep (μl/min/10 ⁶ cells)	228.0	
 63	ClogD 7.4	4.48	
	Human Mic (μl/min/mg)	67.37	
	Rat Hep (μl/min/10 ⁶ cells)	288.8	

 <p style="text-align: center;">64</p>	ClogD 7.4	4.48	
	Human Mic (µl/min/mg)	67.37	
	Rat Hep (µl/min/10 ⁶ cells)	288.8	

As can be seen from Table 3.2 the addition of the *tert*-butyl group had a negative effect upon the distribution co-efficient with ClogD increasing to unacceptable levels. There is, in general no difference in the TPSA of the molecules as the overall polarity of the compounds has remained unchanged (Table 3.5) but the increased lipophilicity has had a detrimental effect upon the solubility of the compounds to such an extent that none of the compounds now hit the 50 µM solubility target. The phase I metabolism (human microsomes) of the compounds remains broadly similar to that of the *i*-pr-Mannich analogues with only slight reduction.

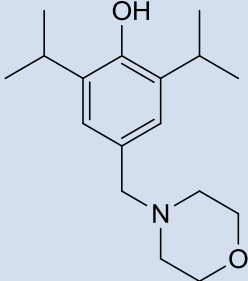
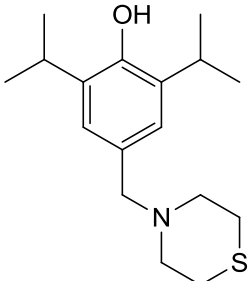
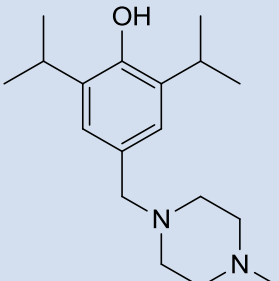
Predicted phase II clearance (see predicted hepatocyte clearance data) for **60** and **61**, indicated some improvements compared with analogues **49** and **50**. This reduction in predicted clearance could be due to the increased steric bulk of the *tert*-butyl group preventing glucuronidation of the phenolic hydroxyl group.

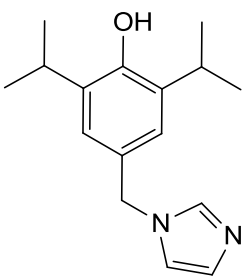
3.1.4 Biological results and MPO evaluation

Due to the time consuming nature of developing a stable cell line and the large amounts of cells required for electrophysiological testing, only a small selection of compounds synthesised were able to be tested. Several Mannich compounds were selected for testing against α1 GlyR, their EC₅₀ values are shown in Table 3.3. In order to prevent the unwanted side effects seen with compounds that target the GABA_AR, selected compounds were be tested for efficacy against the GABA_AR

($\alpha 1\beta 2\gamma 3$ subtype). Compounds that are selective need to display a 100 fold more efficacious EC_{50} at the GlyR than the $GABA_A$ receptor.

Table 3.3. EC_{50} results from electrophysiology testing of compounds **49-51** & **55**.

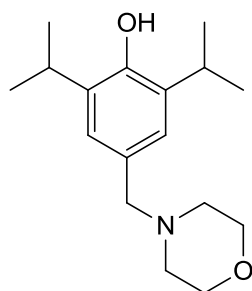
Compound	EC_{50} (μM) ^a	ClogP ^b	ClogD ^c	$GABA_A$ EC_{50} (μM) ^d
 49	>1	3.68	2.70	30 $\mu M \pm 0.120$
 50	>1	4.41	4.10	NT
 51	>1	4.21	2.70	NT

 55	>1	3.84	3.60	NT
---	----	------	------	----

a, α 1 GlyR EC₅₀ values determination was carried out at the University of Tübingen under the supervision of Prof. Bodo Laube. **b**, ClogP values were determined using chembiodraw ultra 12 software. **c**, In house algorithm. **d**, GABA_A selectivity testing was carried out at BioFocus®, Chesterford Research Park, Saffron Walden, UK.

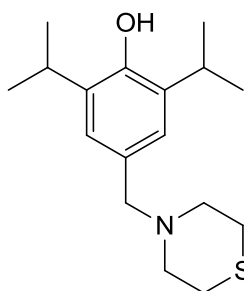
Disappointingly it can be seen from Table 3.3 that none of the Mannich base analogues have activity below 1 μ M at the α 1 GlyR. We decided to examine the MPO scores of the both the *i*-pr and *tert*-butyl Mannich compounds in order to ascertain how their physicochemical parameters differ from the bi-phenyl compounds shown in chapter II. The results of the MPO evaluation for the *i*-pr and *tert*-butyl are shown in Table 3.4 and Table 3.5 respectively.

Table 3.4. MPO evaluation of benzyl amine compounds.



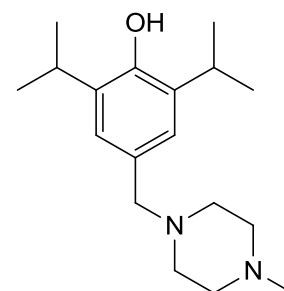
49

Property	Value	T0
ClogP	3.6	0.700
ClogD	2.7	0.650
TPSA	32.70	0.635
MW	277.4	1.000
HBD	1	0.833
pKa	10.89	0.000
CNS MPO		3.8



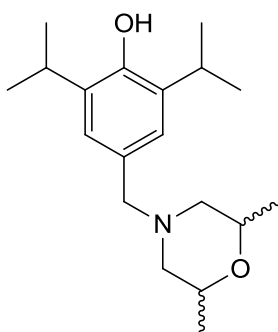
50

Property	Value	T0
ClogP	4.41	0.295
ClogD	4.10	0.000
TPSA	23.47	0.174
MW	293.47	1.000
HBD	1	0.833
pKa	10.89	0.000
CNS MPO		2.3



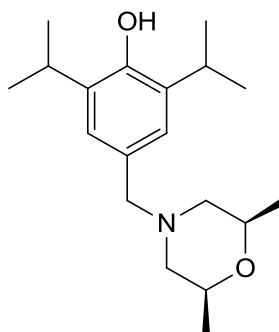
51

Property	Value	T0
ClogP	3.6	0.700
ClogD	2.7	0.650
TPSA	26.71	0.336
MW	277.4	1.000
HBD	1	0.833
pKa	10.89	0.000
CNS MPO		3.5



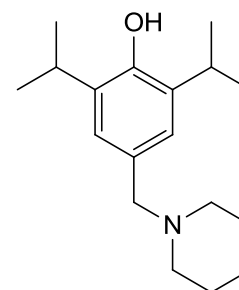
52

Property	Value	T0
ClogP	4.7	0.150
ClogD	3.2	0.150
TPSA	32.70	0.635
MW	305.45	1.000
HBD	1	0.833
pKa	10.89	0.000
CNS MPO		3.0



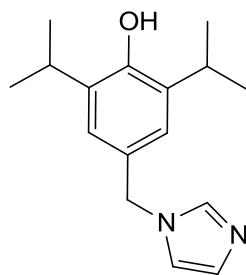
53

Property	Value	T0
ClogP	4.7	0.150
ClogD	3.2	0.150
TPSA	32.70	0.635
MW	305.45	1.000
HBD	1	0.833
pKa	10.89	0.000
CNS MPO		3.0



54

Property	Value	T0
ClogP	4.9	0.050
ClogD	2.7	0.650
TPSA	23.47	0.174
MW	275.4	1.000
HBD	1	0.833
pKa	10.93	0.000
CNS MPO		2.7

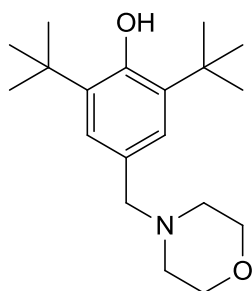


55

Property	Value	T0
ClogP	3.54	0.729
ClogD	3.6	0.200
TPSA	38.04	0.902
MW	258.4	1.000
HBD	1	0.833
pKa	10.98	0.000
CNS MPO		3.7

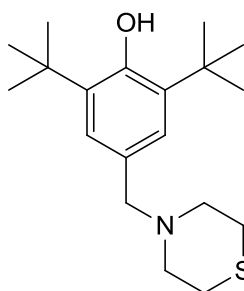
Table 3.4 depicts the MPO evaluations for the benzyl amine series. As can be seen from the table none of the compounds meet the criteria for optimal probability of CNS penetration (for optimal probability of CNS penetration the overall CNS MPO should be score >4)¹⁵⁸. From the breakdown of the parameters for each compound it can be seen that the ClogP and ClogD values are marginally too high (transformed value, T0 of 1.000 is the optimal value) whilst the TPSA of the compounds is too low. The TPSA for many of the compounds falls outside the acceptable range of 40-120 Å (the ideal range being 60-90 Å)¹⁵⁸. The TPSA is defined as the contributions of all of the polar atoms in a given molecule, therefore, addition of O or N bearing substituents could be incorporated in an effort to bring the TPSA above the acceptable parameters. The molecular weight (MW) of the compounds is in the optimal region but the hydrogen donor contribution of the compounds could be improved. The pKa of the compounds is also consistently too high, the optimal value for BBB penetration and, therefore, access to the CNS is between 4-10^{28,29}.

The pKa of the compounds can be modulated by addition of either an electron withdrawing group (NO₂, CN, CO₂Me) which can reduce the nucleophilicity of the hydroxyl group via the inductive effect when added *ortho* or *para* to the hydroxyl group.

Table 3.5. MPO evaluation of *tert*-butyl amine analogue

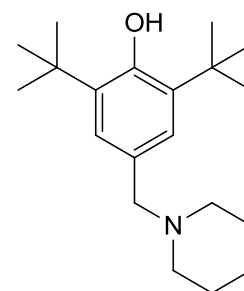
60

Property	Value	T0
ClogP	4.67	0.165
ClogD	3.5	0.250
TPSA	32.70	0.635
MW	305.45	1.000
HBD	1	0.833
pKa	12.01	0.000
CNS MPO		2.9



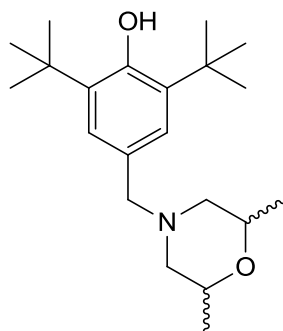
61

Property	Value	T0
ClogP	5.41	0.000
ClogD	5.0	0.000
TPSA	23.47	0.174
MW	321.52	1.000
HBD	1	0.833
pKa	12.01	0.000
CNS MPO		2.0



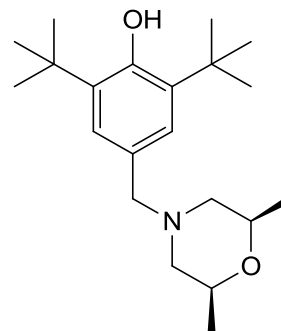
62

Property	Value	T0
ClogP	5.95	0.000
ClogD	3.6	0.200
TPSA	23.47	0.174
MW	303.48	1.000
HBD	1	0.833
pKa	12.09	0.000
CNS MPO		2.2



63

Property	Value	T0
ClogP	5.71	0.000
ClogD	4.5	0.000
TPSA	32.70	0.635
MW	333.51	1.000
HBD	1	0.833
pKa	12.01	0.000
CNS MPO		2.5



64

Property	Value	T0
ClogP	5.71	0.000
ClogD	4.5	0.000
TPSA	32.70	0.635
MW	333.51	1.000
HBD	1	0.833
pKa	12.01	0.000
CNS MPO		2.5

Table 3.5 shows the substantial deleterious effects on the MPO scores of a simple substitution from an isopropyl to a *tert*-butyl group. The ClogP, ClogD and pKa values have all increased leading to a significant reduction in MPO scores. None of the compounds have MPO scores >3 which leads to a reduction in the probability of any of these compounds passing the BBB and reaching the target α 1 GlyR located within the CNS.

It is clear from the *in silico* screening EC₅₀ results and MPO evaluations that none of the compounds synthesised in the Mannich series have the physicochemical characteristics (ClogP <3, ClogD <3), the optimal MPO scores (>4) or the potency to be viable CNS penetrant analgesic drugs targeting the α 1 GlyR¹. These compounds are also predicted to be highly susceptible to both phase I & phase II metabolic clearance. As the data recorded in Table 3.3 reveals that this template has poor allosteric glycinergic activity making the decision to terminate this series relatively easy. An additional potential liability with this template is outlined in the following section.

3.1.5 Quinone methides

The benzyl amines depicted above (**49-55 & 60-64**) have a structural alert for the formation of a quinone methide reactive metabolic intermediate.

Quinone methides (QM's) (Figure 3.9) are reactive metabolites of a variety of ortho or para alkyl substituted phenolic compounds. QM's are thought to be responsible for the cytotoxic/genotoxic effects of the parent compounds such as drug-induced liver injury (DILI) or idiosyncratic adverse drug reactions (IADR's)^{30,31}.

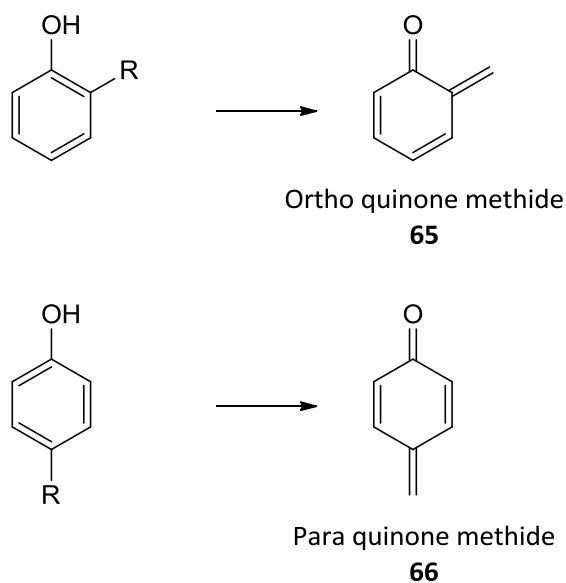
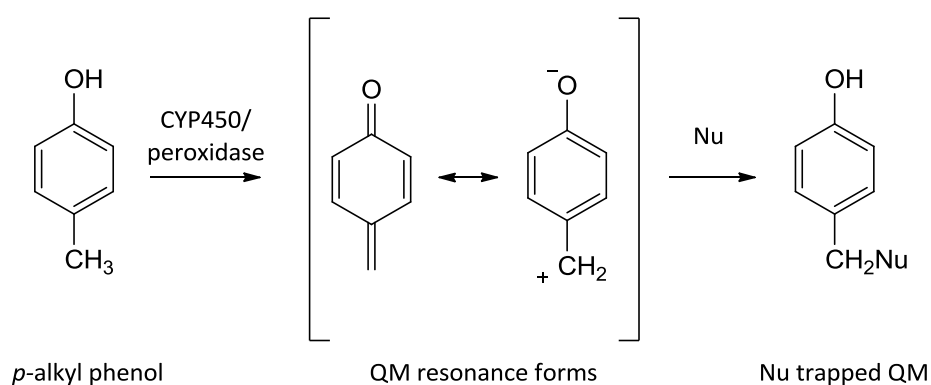


Figure 3.9. *Ortho* and *para* quinone methides.

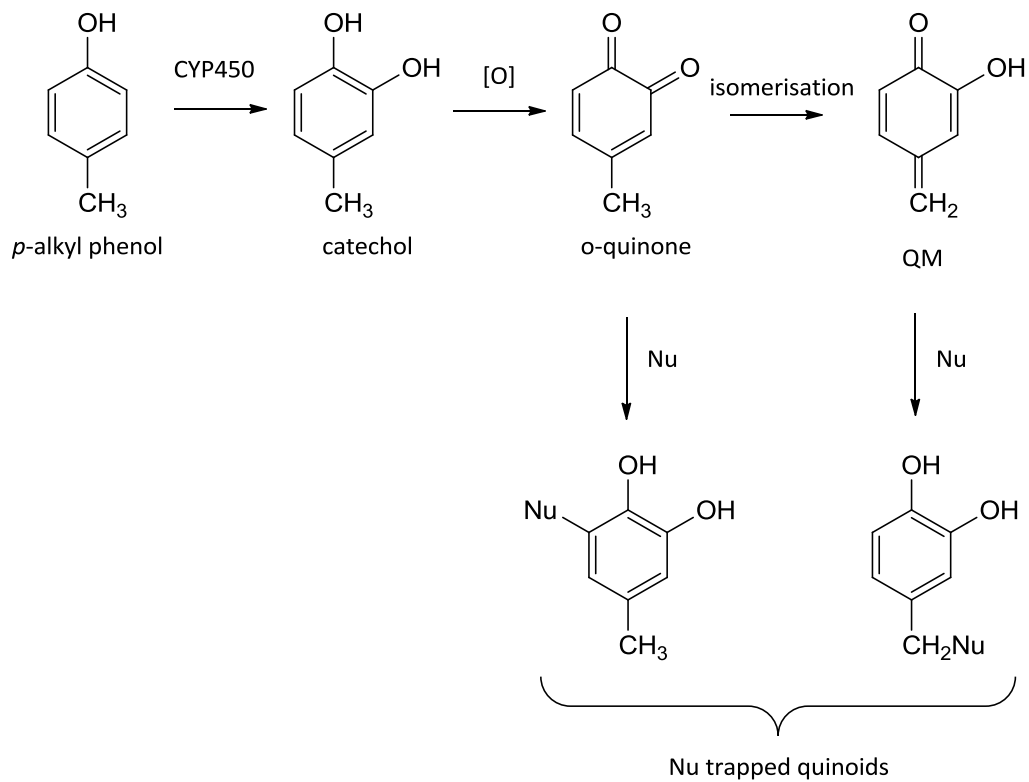
QM's are highly reactive electrophilic species that react rapidly with a variety of biologically relevant nucleophiles including alcohols, thiols, proteins, water, and DNA. Due to their reactivity QM's often go undetected, but their formation has been inferred by trapping them out with reactive nucleophiles such as N-acetylcysteine or glutathione^{32,33}.

QM intermediates can be formed by three major pathways (Scheme 3. 7);

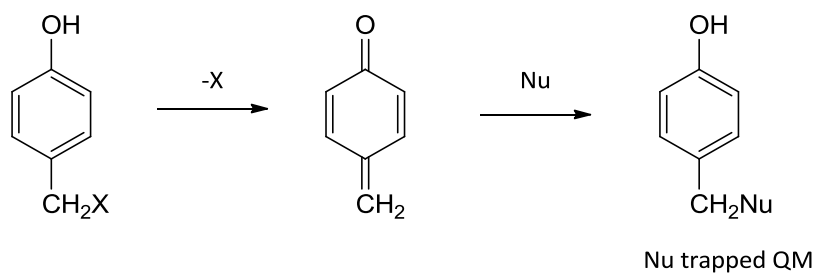
1) Two electron enzymatic oxidation



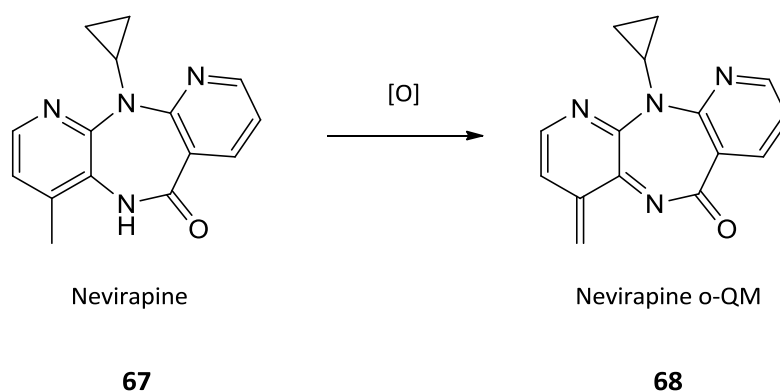
2) Ortho-quinone isomerisation



3) Elimination of a leaving group

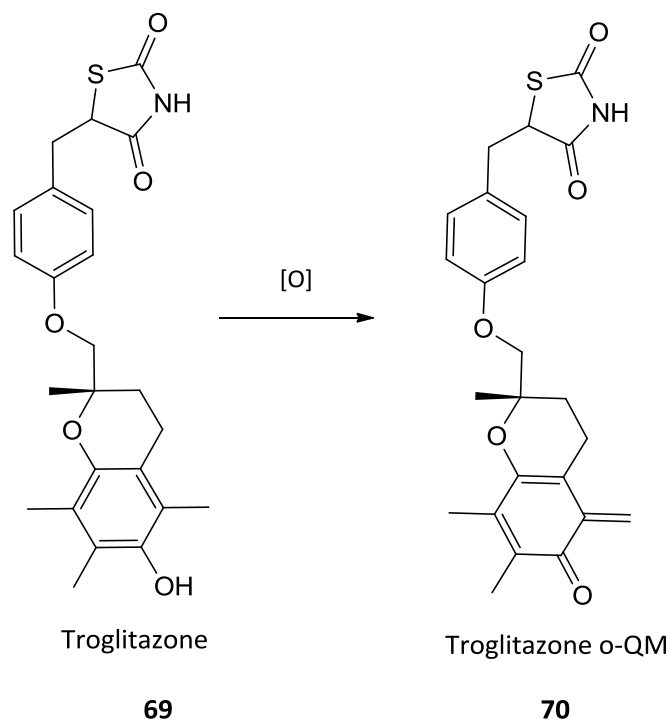
Scheme 3. 7. 3 major pathways of QM formation (adapted from Bolton ³²)

QM formation has been implicated in the hepatotoxicity or IADR's of several marketed drugs. Nevirapine (**67**) is a non-nucleoside reverse transcription inhibitor (NNRTI) used in the treatment of HIV-1 and AIDS³⁴. Nevirapine is known to cause idiosyncratic hepatotoxicity and adverse skin reactions. In 2000 the FDA issued a black box warning on nevirapine, warning that it could cause severe liver damage including liver failure³⁵. It is thought that both mechanisms of toxicity could be due to the formation of o-QM intermediates (**68**) formed during the bioactivation of nevirapine (Scheme 3.8)^{36,37}.



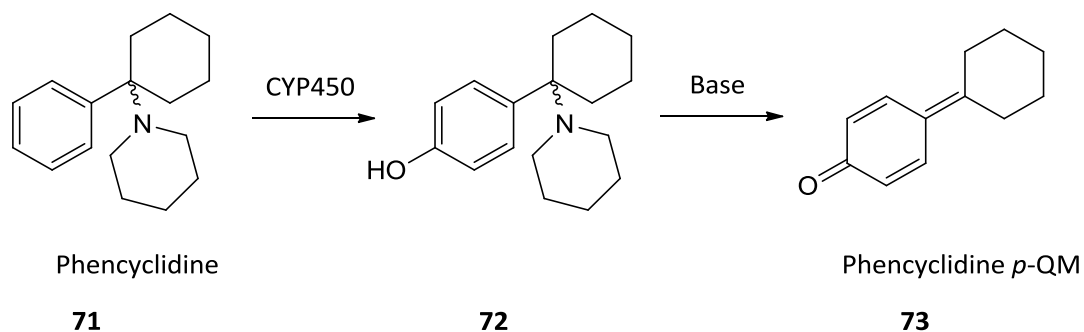
Scheme 3.8. Two electron oxidation of nevirapine to the QM intermediate.

The antidiabetic and anti-inflammatory agent troglitazone (**59**) was withdrawn from the market after reports of idiosyncratic adverse reactions leading to drug induced hepatitis and liver failure³⁸. The hepatotoxicity of troglitazone has also been ascribed to the formation of reactive o-QM metabolites (**70**) (Scheme 3.9)³⁹.



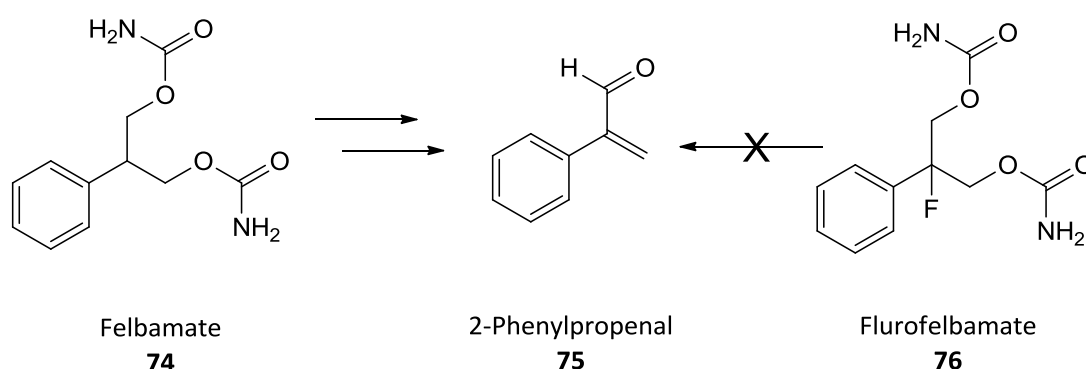
Scheme 3.9. Two electron oxidation of troglitazone to the QM intermediate

Similarly the anaesthetic agent phencyclidine (PCP, **71**) was withdrawn from the market soon after introduction due to the emergence of adverse drug reactions which included a schizophrenia like psychosis⁴⁰. It is thought the psychosis may be induced by the binding of reactive metabolites of PCP to crucial proteins within the CNS. Phencyclidine is also known to be a potent inhibitor of CYP450-2B6, it is thought that the formation of *p*-QM metabolites of PCP is responsible for both mechanisms of toxicity (Scheme 3.10)^{41,42}.



Scheme 3.10. CYP450 mediated hydroxylation and subsequent base catalysed elimination of piperidine to form the *p*-QM of PCP.

Therefore, in order to mitigate against potential *p*-QM formation we decided to introduce a substituent at the methylene position to block the formation of the reactive metabolite. There are several strategies available for blockade of the metabolic activation pathway including, introduction of steric hindrance in the vicinity of metabolic degradation⁴³, structural modification in order to redirect metabolism⁴⁴, or the introduction of a metabolically stable substituent at the site of metabolism, as seen with the fluorination of the antiepileptic agent felbamate (Scheme 3.11).



Scheme 3.11. Fluorination at the site of metabolic transformation of felbamate prevents formation of the toxic metabolite 2-phenylpropenal³³.

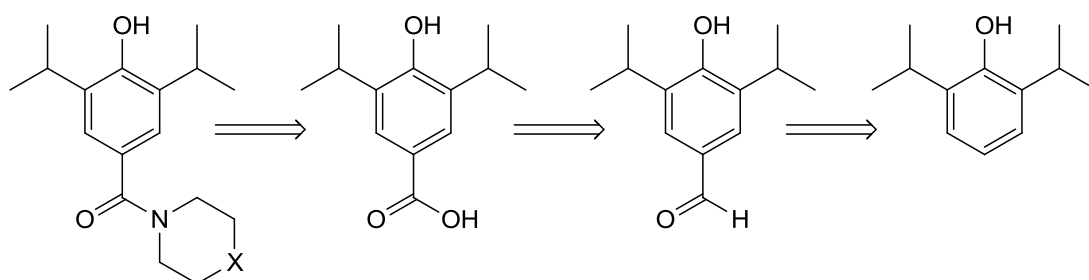
It was, therefore, decided that in order to block the potential formation of the reactive QM intermediate we would introduce a carbonyl function at the site of the methylene linker.

The introduction of an amide functionality will not only mitigate against the formation of the reactive intermediate but addition of the polar carbonyl group will also lower the lipophilicity of the molecules and increase the overall TPSA. The presence of the carbonyl might also influence the pKa and reduce the rate of phase II clearance by reduction of the nucleophilicity of the phenolic hydroxyl group.

3.2 Amide morpholino analogues

Based upon the rationale noted above, we designed a series of series of amide analogues of the benzylamino series (**49-54**). A retrosynthetic analysis is depicted in Scheme 3.12 where disconnection takes us back to propofol as a starting material. It was proposed that formylation of propofol, oxidation and amide coupling of the acid would furnish the desired targets.

The acid can then undergo an amide coupling reaction with the appropriate secondary amine to form the desired amide (Scheme 3.12).



77, X = O

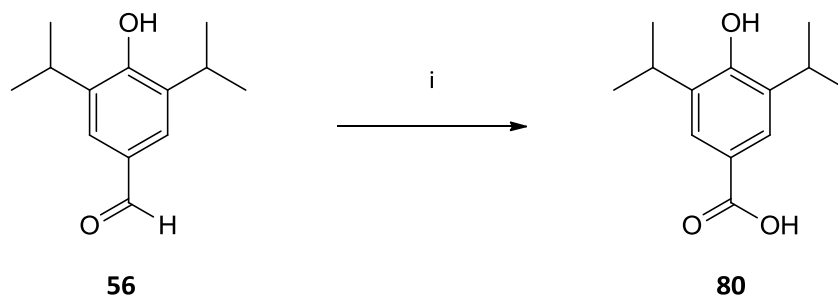
78, X = NMe

79, X = S

Scheme 3.12. Retrosynthetic analysis.

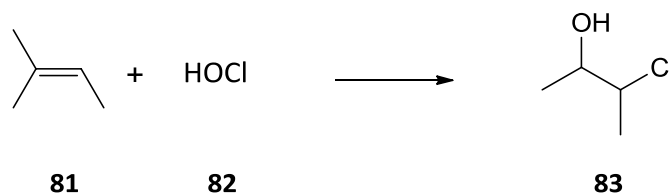
Target synthesis began with the formylation of propofol (as shown in Scheme 3.3). The next step was to oxidise the aldehyde (**56**) to the carboxylic acid (**80**).

Initial studies employed a Pinnick oxidation using sodium chlorite (NaClO_2) (Scheme 3.13)^{45,46} This reaction was first performed without the inclusion of 2-methyl-2-butene. Whilst the reaction was successful the yield of the carboxylic acid was very poor, ~10%.



Scheme 3.13. Reagents and conditions: i) NaClO_2 , t-BuOH, NaH_2PO_4 , 2-methyl-2-butene, RT, 16hrs 40% yield.

It is thought that during the oxidation, hypochlorous acid (HOCl , **83**) is formed which reacts with the NaClO_2 rendering it unable to oxidise the aldehyde (**44**). To prevent this possible side reaction 2-methyl-2-butene (**81**) is added as a scavenger. HOCl reacts with double bonds of the 2-methyl-2-butene (**81**) via a halohydrin formation reaction and, therefore, HOCl reacts with the sacrificial 2-methyl-2-butene before it can react with NaClO_2 (Scheme 3.14).

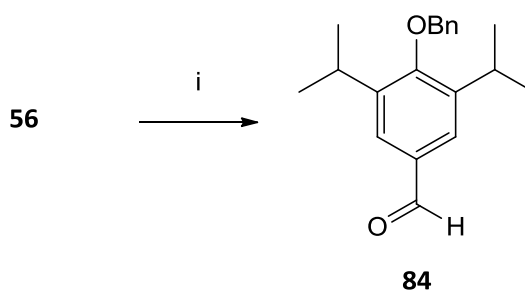


Scheme 3.14. Reaction of 2-methyl-2-butene scavenger with HOCl to form halohydrin.

When the reaction was subsequently performed with the alkene scavenger present the yield did improve somewhat, giving ~40% yields. It was noted however, that there were many side products also formed in the reaction and purification of the carboxylic acid was very difficult. It was, therefore, decided to find a different route to oxidation of the aldehyde (**56**).

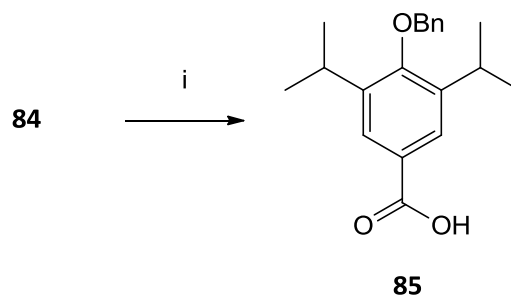
A search of the literature found an oxidation method using catalytic quantities of selenium (IV) oxide in hydrogen peroxide⁴⁷. The first step in the reaction sequence was to protect the phenolic hydroxyl group of the aldehyde as a benzyl ether (**84**).

The benzyl ether protecting group was chosen because it is stable to both acidic and basic conditions and it is also resistant to many oxidants such as KMnO_4 , OsO_4 and CrO_3 ⁴⁸. Protection of the hydroxyl group was afforded by addition of benzyl bromide to a solution of aldehyde in acetone, in the presence of potassium carbonate. The facile reaction proceeded in high yields⁴⁸ (>70%) (Scheme 3.15).



Scheme 3.15. *Reagents and conditions:* i) BnBr, K₂CO₃, acetone, RT, 18hrs, 88% yield.

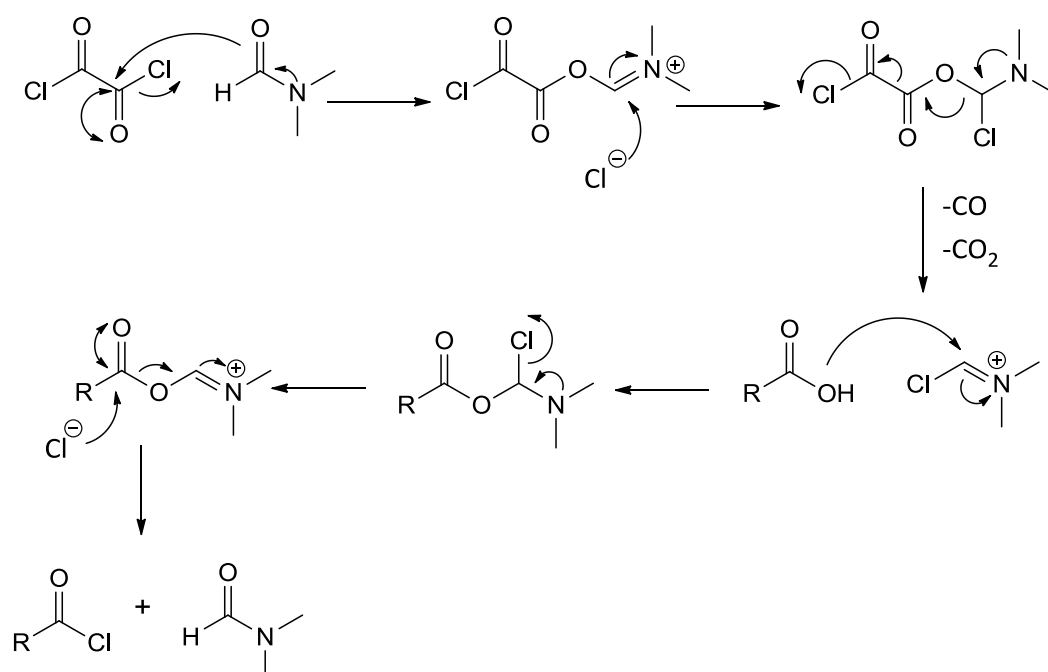
The oxidation of the benzyl protected aldehyde (**84**) was carried out with hydrogen peroxide (27% solution) in the presence of catalytic amounts of Selenium (IV) oxide. The reaction was allowed to heat overnight and upon completion the remaining oxidant was quenched with palladium/carbon. The reaction proceeded well and gave the desired carboxylic acid (**85**) in good yields 70% (Scheme 3.16).



Scheme 3.16. Reagents and conditions: i) SeO_2 , H_2O_2 , THF, reflux, 18hrs 70% yield.

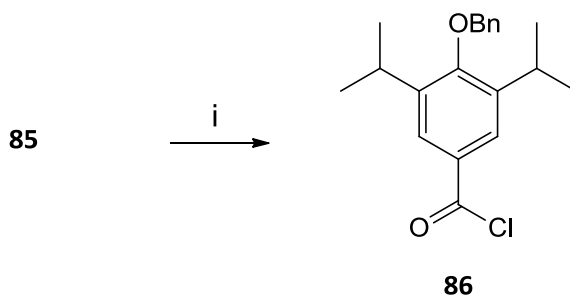
The amide bond was formed by the condensation of an acid chloride with the amine of choice. The first step in the amide formation was to synthesise the acid chloride⁴⁹.

This was achieved by addition of oxalyl chloride to a solution of **85** in the presence of triethylamine. The reaction is promoted by catalytic quantities of dimethylformamide (DMF), the catalytic role of DMF is shown in Scheme 3.17.



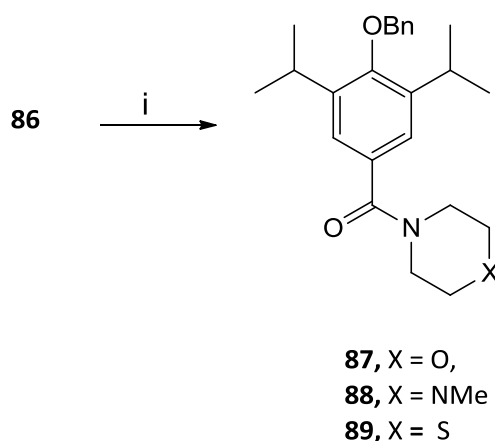
Scheme 3.17. The catalytic role of dimethylformamide.

The acid chloride (**86**) is a very reactive species and, therefore, was not isolated and was taken through to the next stage (Scheme 3.18).



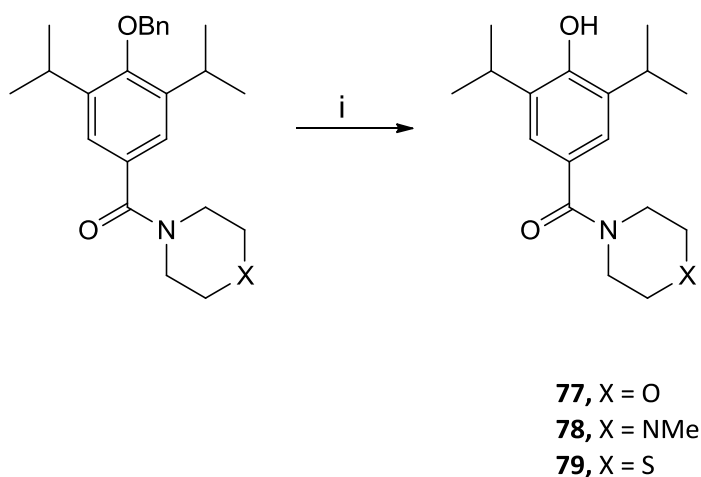
Scheme 3.18. *Reagents and conditions:* i) Benzyl protected acid, oxalyl chloride, Et₃N, DMF, DCM, RT, 2hrs.

The amide coupling began with the addition of the amine of choice to a solution of acid chloride (**86**) and triethylamine in dichloromethane. The reaction was allowed to stir at room temperature overnight (Scheme 3.19).



Scheme 3.19. *Reagents and conditions:* i) Secondary amine, Et₃N, DCM, RT, 18hr 65-70% yields⁵⁰.

There are several methods for benzyl deprotection including the use of strong acids or via oxidation of the benzyl to the benzoate and subsequent hydrolysis under basic conditions^{51,52}. We chose to deprotect the amide analogues by palladium catalysed hydrogenation, delivering the free phenol and toluene (Scheme 3.20). This is a very simple easy method of deprotection which gave the desired product in very high yields (>95%)⁵³.

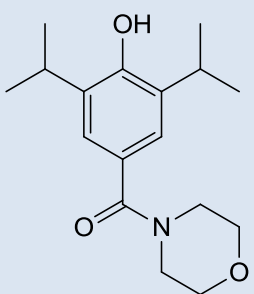
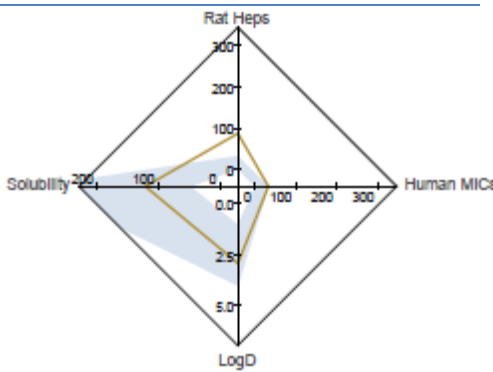
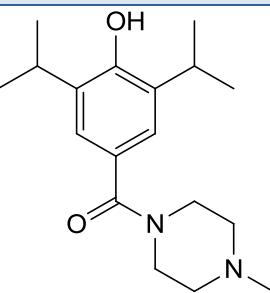
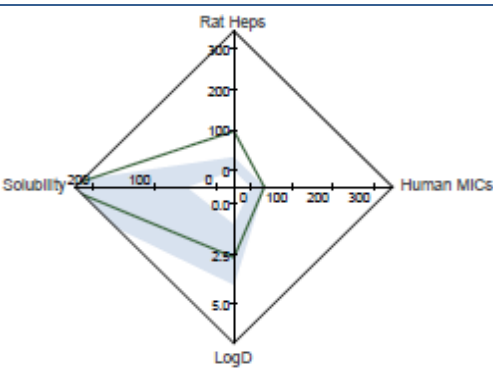
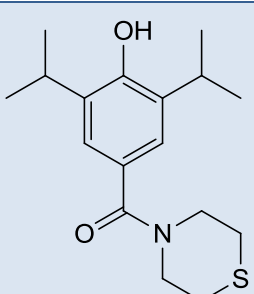
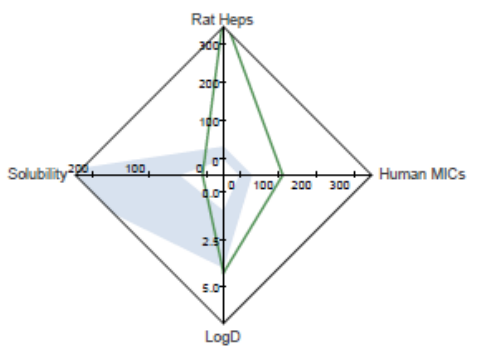


Scheme 3.20. *Reagents and conditions:* i) Pd/C, H₂, MeOH, RT, 18hrs, 95-98% yields.

3.2.1 *i-pr*-Amide *in silico* testing

The *i-pr*-amide analogues (**77-79**) were also screened *in silico* to determine the predicted physicochemical and metabolic stability parameters.

Table 3.6. *In silico* predictions of the *i-pr*-amide analogues.

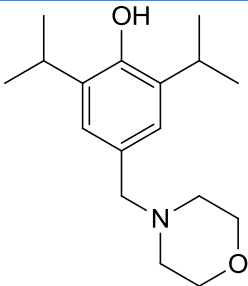
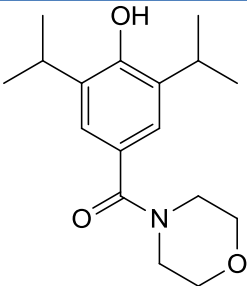
Compound	Parameters		Radar
 77	ClogD 7.4	2.88	
	Human Mic ($\mu\text{l}/\text{min}/\text{mg}$)	31.21	
	Rat Hep ($\mu\text{l}/\text{min}/10^6$ cells)	67.41	
 78	ClogD 7.4	2.67	
	Human Mic ($\mu\text{l}/\text{min}/\text{mg}$)	30.28	
	Rat Hep ($\mu\text{l}/\text{min}/10^6$ cells)	97.44	
 79	ClogD 7.4	3.46	
	Human Mic ($\mu\text{l}/\text{min}/\text{mg}$)	93.33	
	Rat Hep ($\mu\text{l}/\text{min}/10^6$ cells)	39.81	

As expected addition of the carbonyl group has had the desired effect of reducing the predicted physicochemical parameters of ClogP and ClogD as well as increasing the TPSA.

Inclusion of the amide functionality has also improved the predicted physicochemical properties and rate of metabolic turnover for the proposed target molecules.

Table 3.7 shows a direct comparison between compounds **49** & **77**. It can be seen that the ClogP of **77** has been reduced to 3.10, the ClogD has been reduced to 2.88 whilst the TPSA has been increased to 49.80. This should enable better absorption membrane permeability and CNS penetration⁵⁴⁻⁵⁶. Predicted metabolism of **77** also has been significantly reduced in both microsomes and hepatocytes.

Table 3.7. Direct comparison of physicochemical and metabolic predicted parameters for compounds **49** & **77**.

		
49		77
3.67	ClogP	3.10
3.45	ClogD 7.4	2.88
32.70	TPSA	49.80
84.35	Human Mic ($\mu\text{l}/\text{min}/\text{mg}$)	31.21
333.5	Rat Hep ($\mu\text{l}/\text{min}/10^6$ cells)	87.41

The MPO scores of the *i*-pr-amide analogues were examined in order to determine their probability for BBB penetration (Table 3.8).

Table 3.8. MPO evaluation of the *i*-pr-amide analogues

Property	Value	T0
ClogP	3.10	0.950
ClogD	2.80	0.600
TPSA	49.80	1.000
MW	291.0	1.000
HBD	1	0.833
pKa	10.10	0.000
CNS MPO		4.4

Property	Value	T0
ClogP	3.54	0.729
ClogD	2.30	0.850
TPSA	43.78	1.000
MW	304.43	1.000
HBD	1	0.833
pKa	10.14	0.000
CNS MPO		4.4

Property	Value	T0
ClogP	3.83	0.583
ClogD	4.40	0.000
TPSA	65.84	1.000
MW	307.45	1.000
HBD	1	0.833
pKa	10.08	0.000
CNS MPO		3.4

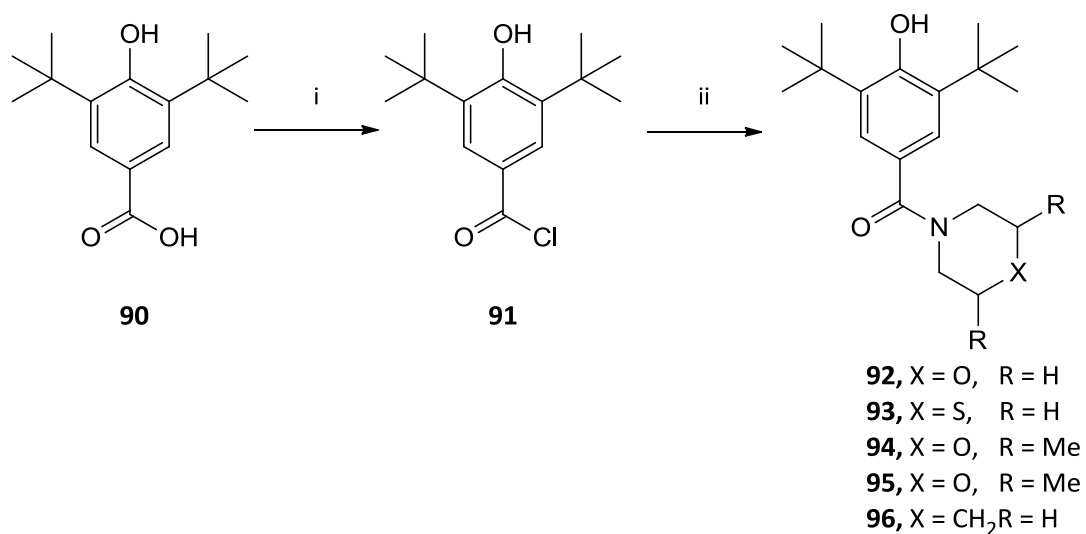
With the reduction in both ClogP and ClogD increase in TPSA compounds **77** & **78** now meet the criteria for optimal CNS penetration with overall CNS MPO scores >4¹.

3.2.2 *Tert*-butyl amide analogues.

With the improvements seen in the predicted physicochemical parameters and metabolic stability of the *i*-pr-amide compounds, it was decided to also synthesise several di-*tert*-butyl amide analogues in an effort to both improve the predicted properties and to confer selectivity for the GlyR as discussed earlier (**section 3.1.2**).

The synthesis of the di-*tert*-butyl amide analogues began with the commercially available 3,5-di-*tert*-butyl-4-hydroxybenzoic acid.

The benzoic acid was first converted to the acid chloride using the same conditions seen in Scheme 3.18, before being subjected to the amide coupling conditions analogous to Scheme 3.19 (Scheme 3.21).

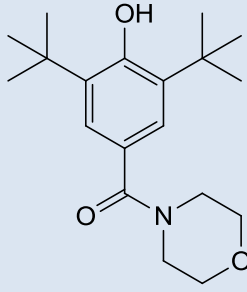
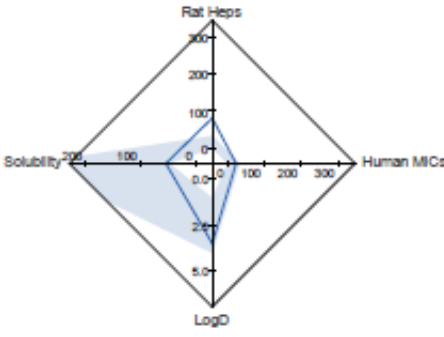
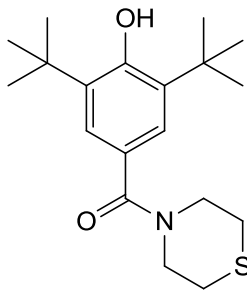
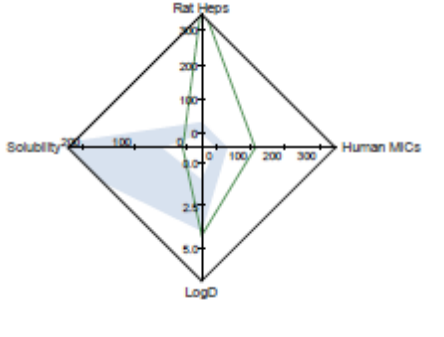
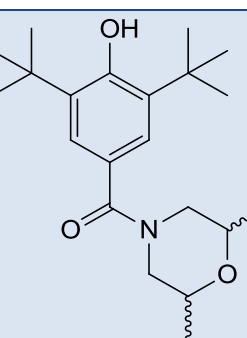
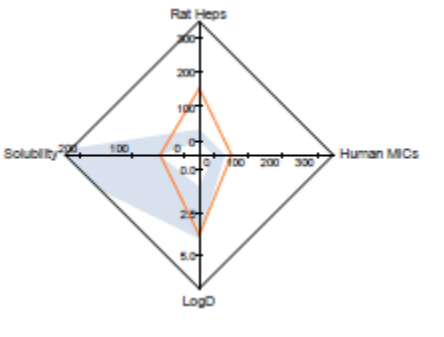


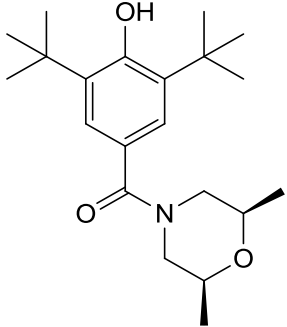
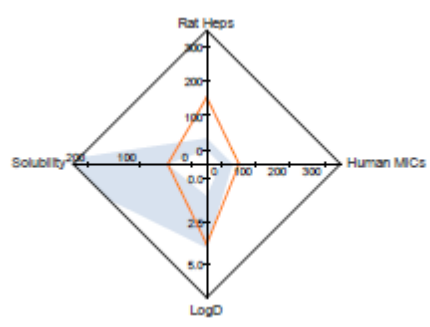
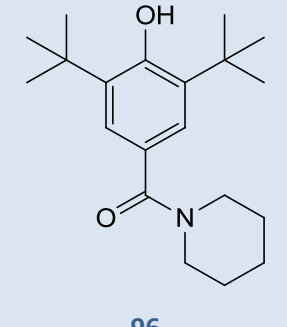
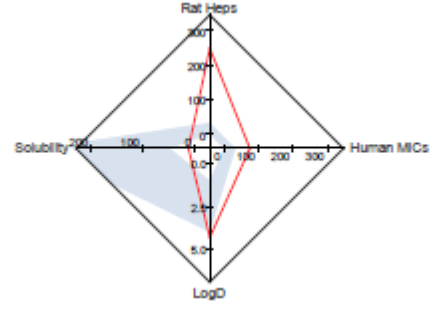
Scheme 3.21. *Reagents and conditions:* i) Oxalyl chloride, Et₃N, DMF, DCM, RT, 2hrs. ii) Acid chloride, amine, Et₃N, DCM, RT, 18hrs, 68-91 % yields.

3.2.3 Tert-butyl in silico testing

The tert-butyl amide compounds **92-96** were also put through the in silico screen to determine their predicted physicochemical and metabolic stability parameters (Table 3.9).

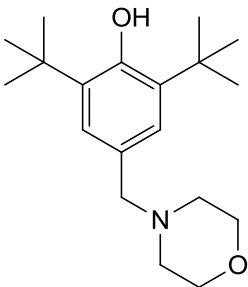
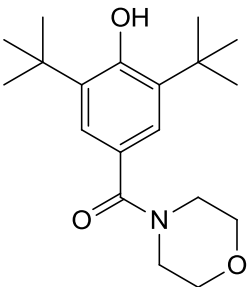
Table 3.9. *In silico* predictions of the *tert*-butyl amide analogues.

Compound	Parameters		Radar plot
 92	ClogD 7.4	3.51	
	Human Mic ($\mu\text{l}/\text{min}/\text{mg}$)	22.35	
	Rat Hep ($\mu\text{l}/\text{min}/10^6$ cells)	78.68	
 93	ClogD 7.4	4.26	
	Human Mic ($\mu\text{l}/\text{min}/\text{mg}$)	112.9	
	Rat Hep ($\mu\text{l}/\text{min}/10^6$ cells)	378	
 94	ClogD 7.4	3.80	
	Human Mic ($\mu\text{l}/\text{min}/\text{mg}$)	49.48	
	Rat Hep ($\mu\text{l}/\text{min}/10^6$ cells)	152.7	

 <p style="text-align: center;">95</p>	ClogD 7.4	3.80	
	Human Mic ($\mu\text{l}/\text{min}/\text{mg}$)	49.48	
	Rat Hep ($\mu\text{l}/\text{min}/10^6$)	152.7	
 <p style="text-align: center;">96</p>	ClogD 7.4	4.33	
	Human Mic ($\mu\text{l}/\text{min}/\text{mg}$)	73.85	
	Rat Hep ($\mu\text{l}/\text{min}/10^6$)	250.5	

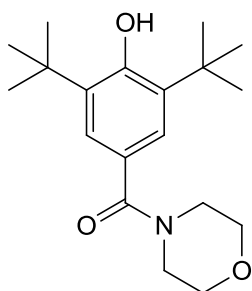
Again Table 3.9 shows that, in general, the addition of the amide function has reduced the ClogP and ClogD of compounds **92-96** and increased the TPSA. The predicted metabolic stability of **82**, **83** & **86** has also improved, but interestingly compounds **94** & **95** (with the di-methyl morpholine substituents) have seen a predicted increase in their metabolic degradation. Table 3.10 shows a direct comparison between the predicted physicochemical and metabolic parameters of the *tert*-butyl Mannich morpholine and the *tert*-butyl amide morpholine.

Table 3.10. Direct comparison of the predicted physicochemical and metabolic parameters of the *tert*-butyl Mannich and amide morpholines.

 60		 92	
4.67	ClogP	4.10	
4.14	ClogD 7.4	3.51	
32.70	TPSA	49.77	
48.81	Human Mic ($\mu\text{l}/\text{min}/\text{mg}$)	22.35	
293.6	Rat Hep ($\mu\text{l}/\text{min}/10^6$)	78.68	

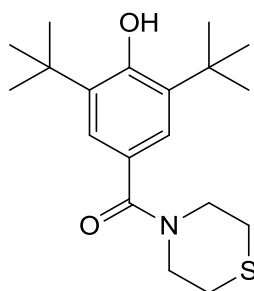
The same trend can be seen with the *tert*-butyl compounds **90** & **92** as was shown in Table 3.7 for the *i*-pr compounds **49** & **77**, that is to say, a decrease in both predicted ClogP and ClogD values and an increase in TPSA.

Although an improvement has been seen with the physicochemical parameters ClogP and ClogD they both still exceed the optimal values of <3 for maximum probability of CNS penetration². The TPSA has also improved although again it falls below the ideal value of >60 Å it is now above the >40 Å minimum cut-off¹⁴⁶. Again the metabolic stability for compound **92** has improved with respect to **49**, with a predicted reduction in both phase I and phase II metabolic degradation. The MPO scores of the *tert*-butyl amide compounds **92-96** were also evaluated (Table 3.11).

Table 3.11. MPO evaluation of the *tert*-butyl amide analogues

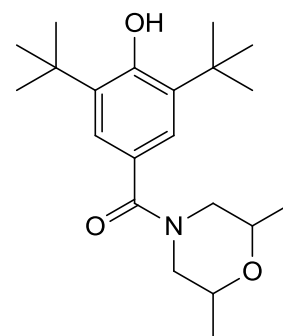
92

Property	Value	T0
ClogP	4.10	0.450
ClogD	4.70	0.000
TPSA	49.77	1.000
MW	319.44	1.000
HBD	1	0.833
pKa	10.52	0.000
CNS MPO		3.3



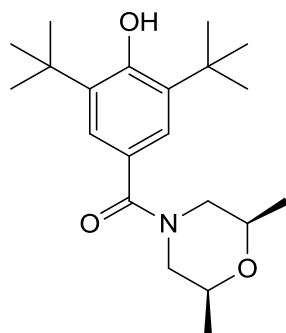
93

Property	Value	T0
ClogP	4.83	0.085
ClogD	5.20	0.000
TPSA	40.54	1.000
MW	335.5	1.000
HBD	1	0.833
pKa	10.52	0.000
CNS MPO		2.9



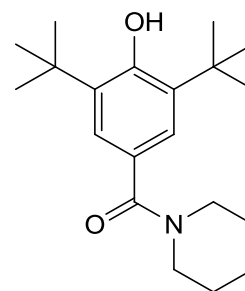
94

Property	Value	T0
ClogP	5.14	0.000
ClogD	4.70	0.000
TPSA	49.77	1.000
MW	347.45	1.000
HBD	1	0.833
pKa	10.52	0.000
CNS MPO		2.8



95

Property	Value	T0
ClogP	5.14	0.000
ClogD	4.70	0.000
TPSA	49.77	1.000
MW	347.45	1.000
HBD	1	0.833
pKa	10.52	0.000
CNS MPO		2.8



96

Property	Value	T0
ClogP	5.13	0.000
ClogD	3.70	0.150
TPSA	40.54	1.000
MW	317.47	1.000
HBD	1	0.833
pKa	10.70	0.000
CNS MPO		3.0

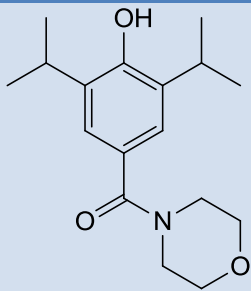
As can be seen from Table 3.11 the improvements in the physicochemical parameters ClogP and ClogD and an increase in the TPSA has improved the MPO scores, with respect to the *tert*-butyl Mannich analogues **60-64** (Table 3.5). But all of the compounds still fall short of reaching the optimal score of >4. For all of the compounds in the *tert*-butyl amide series **92-96**, the ClogP and ClogD still exceed the optimal value <3, although the TPSA, MW and HBD values are in acceptable ranges the pKa values are also too high.

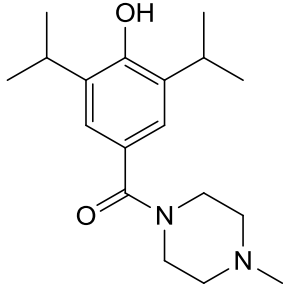
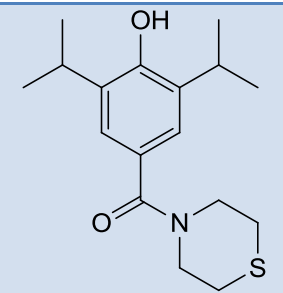
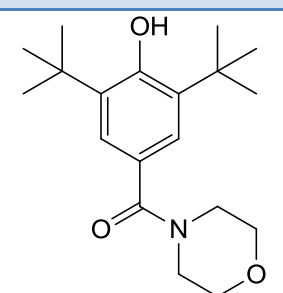
Many of the compounds synthesised so far fall short of the desired criteria, in terms of the physicochemical parameters ClogP <3, ClogD >3, the pKa ≤8 and the overall MPO score ≥4. It is, however, important to subject these compounds to the α1 GlyR *in vitro* assay in an effort to identify an early lead compound which could be taken through to a lead optimisation programme.

3.3 Biological results

The *in vitro* activities of compounds **77-79** & **92** were evaluated in the electrophysiology whole-cell voltage-clamp assay using HEK293 cell as described in chapter II. The results of the *in vitro* studies are shown in Table 3.12.

Table 3.12. *In vitro* EC₅₀ values for amide linked compounds tested against the recombinant α1GlyR

Structure	EC ₅₀ (μM) ^a	ClogP ^b	ClogD ^c	GABA _A (μM) ^d
 <p style="text-align: center;">77</p>	0.00035 ± 0.00002	3.10	2.80	30 ± 0.120

 <p>78</p>	0.0000012 ± 0.4	3.54	2.30	NT
 <p>79</p>	>1	3.83	4.40	NT
 <p>92</p>	0.00046 ± 0.0002	4.10	4.70	30 ± 0.145

a, α 1 GlyR EC₅₀ values determination was carried out at the University of Tübingen under the supervision of Prof. Bodo Laube. **b**, ClogP values were determined using chembiodraw ultra 12 software. **c**, In house algorithm **d**, GABA_A selectivity testing was carried out at BioFocus®, Chesterford Research Park, Saffron Walden, UK. NT = not tested.

It can be seen from Table 3.12, several of the amide analogues (**77**, **78** & **92**) have shown low nM efficacy at the α 1GlyR. It was therefore, decided to send these compounds for further studies in order to assess their susceptibility to metabolism.

3.3.1 Metabolic stability studies

Encouraged by the low EC_{50} values of *i*-pr-amides **77** & **78**, and *tert*-butyl amide **92**, these compounds were selected for further *in vitro* metabolism studies. Microsomal stability studies were carried out at the Liverpool School of Tropical Medicine. These investigations utilised human (HLM) and rat (RLM) liver microsomes (1mg/mL) at a concentration of 1 μ M in the presence of NADPH for 0, 10, 30 and 60 mins (Figure 3.10).

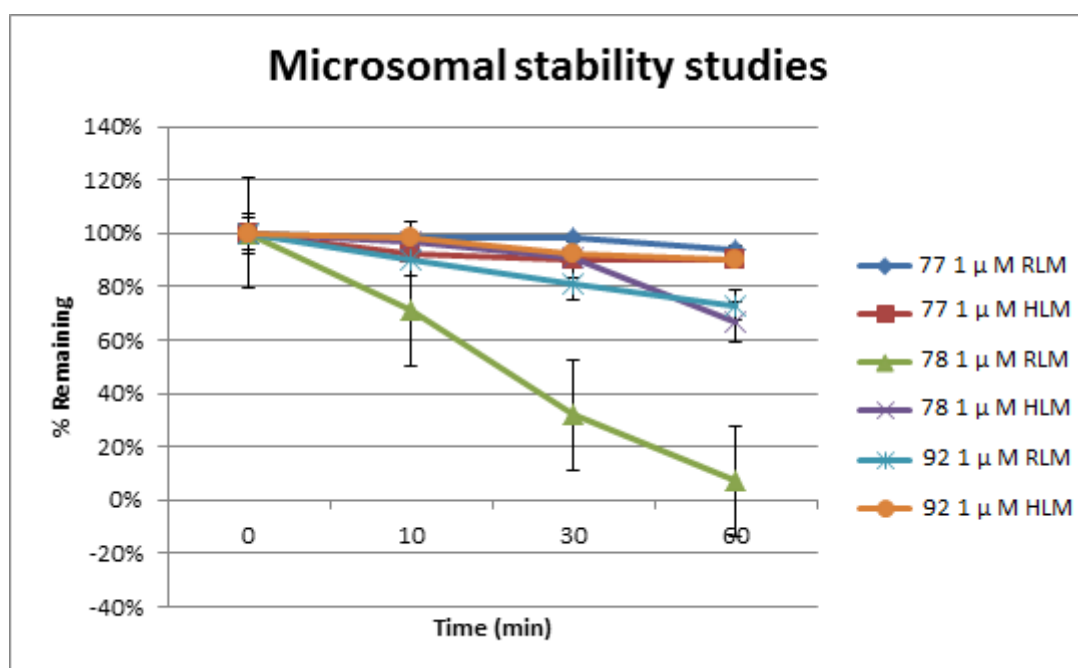


Figure 3.10. *in vitro* metabolism studies for compounds **77**, **78** & **92** in human and rat liver microsomes.

Figure 3.10 shows that compound **78** is extensively metabolised in HLM with only 7% remaining after 60 mins. It is thought that the high rate of turnover seen with **78** is a consequence of metabolism at the N-methyl moiety.

Compounds **77** & **92** are relatively stable in both systems with **92** having 73% remaining in RLM and 90% remaining in HLM. Compound **77** proved to be the most resistant to phase I metabolic degradation with 94 % remaining in RLM and 90% in HLM. The *in vitro* half-lives and intrinsic clearance values are recorded in Table 3.13.

Table 3.13. Metabolic stability of compounds **77**, **78** & **92** in human and rat microsomes. Human and rat liver microsomes (1mg/mL) at a concentration of 1 μ M in the presence of NADPH for 0, 10, 30 and 60 mins, n = 2. Studies carried out at the Liverpool School of Tropical Medicine.

Compound	<i>In vitro</i> half-life $t_{1/2}$ (min)		Intrinsic clearance mL/min/kg	
	RLM	HLM	RLM	HLM
77	770	495	1.6	1.75
78	46	126	26.88	6.9
92	165	407	7.5	2.1

Compounds **77** & **92** were selected to undergo further *in vitro* stability studies with human and rat liver hepatocytes to determine the extent of both phase I and phase II metabolism. These studies were carried out with human and rat hepatocytes at a concentration of 1 μ M for 0, 15, 30, 60, and 120 mins*.

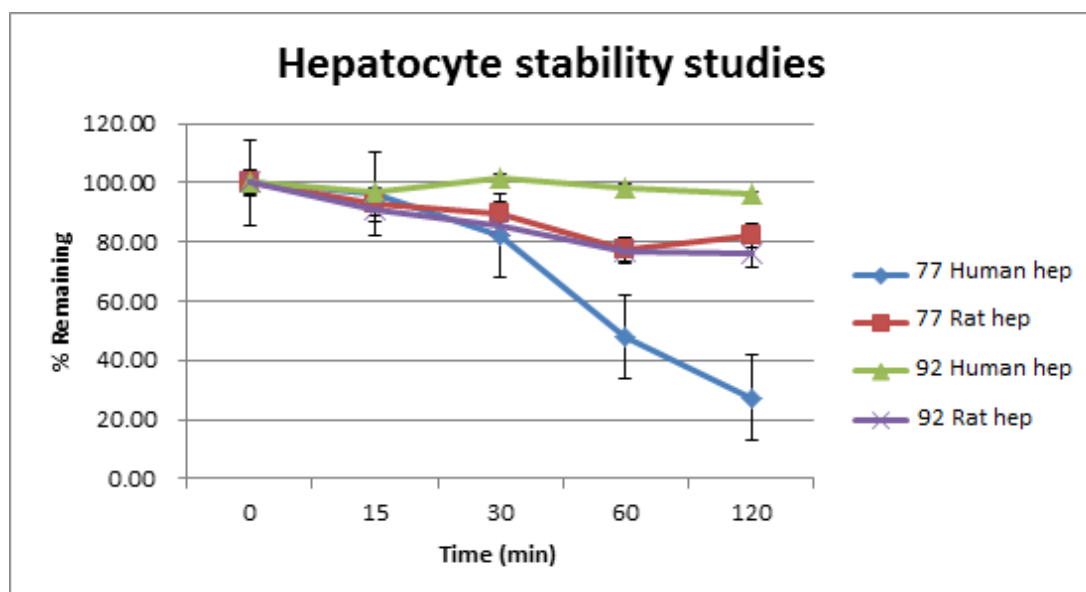


Figure 3.11. *in vitro* metabolism studies for compounds **77** & **92** in human and rat hepatocytes. *These investigations were carried out by ChemPartners, Cai Lun Rd, Pudong, Shanghai, 201203, P.R. China.

The hepatocyte stability studies have shown that compound **77** is metabolised more quickly than **92** in human hepatocytes, which could be due to extensive glucuronidation of the hydroxyl moiety. Compound **92** is more sterically hindered around the hydroxyl group which may be preventing a high rate of metabolic turnover. The *in vitro* half-life and intrinsic clearance values from the hepatocyte studies are recorded in Table 3.14.

Table 3.14. Metabolic stability of compounds **77** & **92** in human and rat hepatocytes. Human and rat hepatocytes concentration 1 μ M, n=2.*These investigations were carried out by ChemPartners, Cai Lun Rd, Pudong, Shanghai, 201203, P.R. China.

Compound	<i>In vitro</i> half-life $t_{1/2}$ (min)		Intrinsic clearance mL/min/kg	
	Human	Rat	Human	Rat
77	59	429	28.69	7.55
92	2387	324	0.72	9.99

There appears to be inconsistencies between the *in silico* predicted data (Table 3.6) and the *in vivo data* for the clearance values in rat hepatocytes for this series (Table 3.14). Therefore, future predicted hepatocyte data will be interpreted cautiously.

3.3.2 *In vivo* pharmacokinetic studies (rat)

The *in vivo* pharmacokinetic (PK) parameters of compounds **77**, **78**, and **92** were also studied. The pharmacokinetic parameters of the *i*-pr-benzyl morpholine compound (**49**) were also studied to give a direct comparison between the *i*-pr-amine and amide morpholine analogues (**49** & **77**). Compounds **77** and **92** stand out with excellent oral bio-availabilities, drug exposures and terminal half-lives.

Table 3.15. Pharmacokinetic profiles of compounds **49**, **77**, **78** and **92** in the rat (oral dose 10 mg/kg). Fasted, male, SD rats. n = 3/group. Vehicle: 10% DMSO, 10% Solutol HS15 and 80% saline at 1 mg/mL. *These investigations were carried out by ChemPartners, , Cai Lun Rd, Pudong, Shanghai, 201203, P.R. China.

Compound	Pharmacokinetic parameters				
	T _{max} (hr)	C _{max} (ng/mL)	AUC (hr*ng/mL)	T _{1/2} (hr)	F (%)
49	0.5	429 ± 30.4	1242 ± 219	2.45 ± 0.833	35.8 ± 6.28
77	0.5	4605 ± 745	20135 ± 826	2.58 ± 0.289	85.9 ± 3.63
78	0.5	1533 ± 477	1556 ± 541	1.96 ± 0.619	38.1 ± 13.0
92	3.00	2130 ± 133	16616 ± 1144	4.74 ± 0.316	129 ± 9.88

3.3.3 *In vivo* neuropathic pain testing (Chung lesion model in the rat)

The *i-pr*-amide compounds **77**, **78** and the *tert*-butyl amide compound **92** were further selected to undergo *in vivo* studies in the Chung lesion model of chronic neuropathic pain (as described in Ch II, section **2.2.3**)⁵⁷. All *in vitro* neuropathic pain testing was carried out at King's College London, under the supervision of Prof. S. McMahon. Groups of 6 rats were administered doses of 3, 10 and 30 mg/mg of each of the compounds being tested (**77**, **78**, & **92**). Each compound was tested at 1, 3, 6 and 24hr time points for reversal of mechanical allodynia and hyperalgesia.

% Reversal of mechanical allodynia

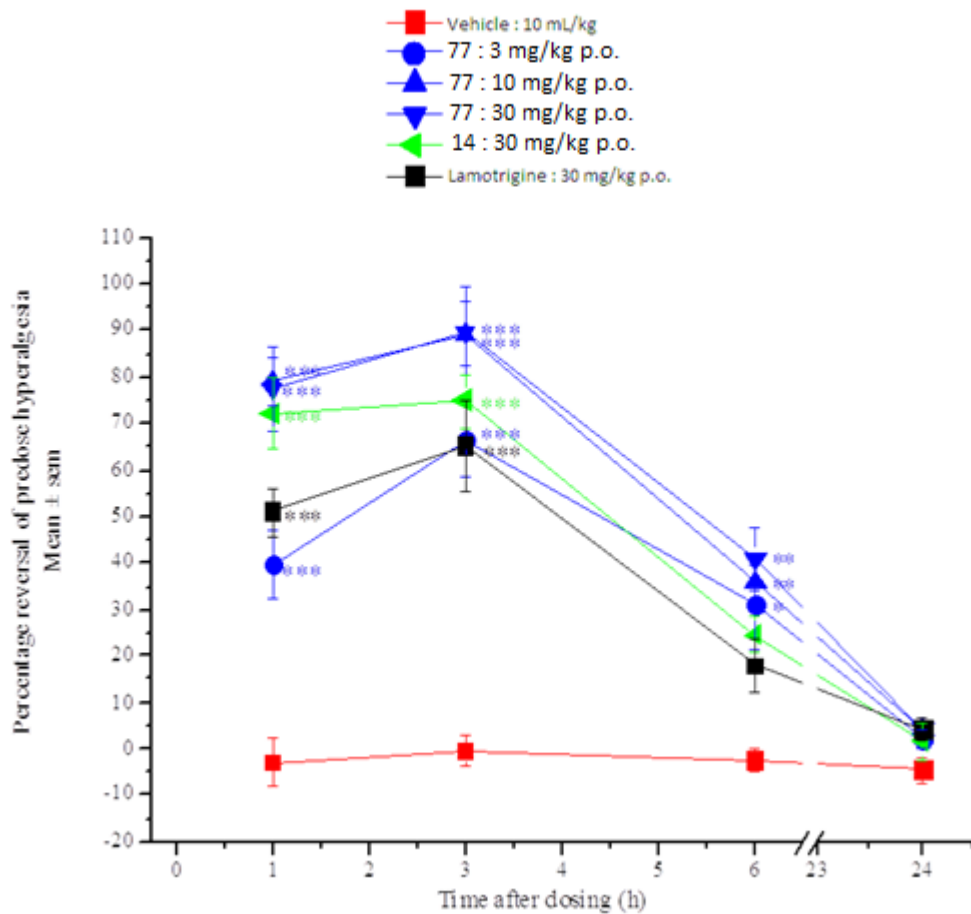


Figure 3. 12. The effect of compound **77** on ipsilateral paw withdrawal thresholds to mechanical pressure in neuropathic rats. In comparison with lamotrigine. Fasted, male, Wistar rats. n = 6/group. Vehicle: 10% DMSO/10% Solutol HS15/80% saline. 10ml/kg p.o. One-way ANOVA, comparison with time-matched vehicle group using Tukey's HSD test, * p < 0.05, ** p < 0.01, *** p < 0.001.

The results from the mechanical allodynia test (Figure 3.12) show that compound **77** is absorbed rapidly, reaching an 80% reversal of painful symptoms 1 hour after a dose of 10 mg/kg. After 3 hours, compound **77** gives a maximum of 90% reversal of neuropathic pain symptoms at 10 mg/kg.

No increase in the maximum reversal is seen at the highest dose of 30 mg/kg. The positive control (lamotrigine, 30 mg/kg) reaches a maximum reversal of only 60 % after 3 hours which is consistent with the lowest dose of **77** administered (3 mg/kg).

% Reversal of cold hyperalgesia

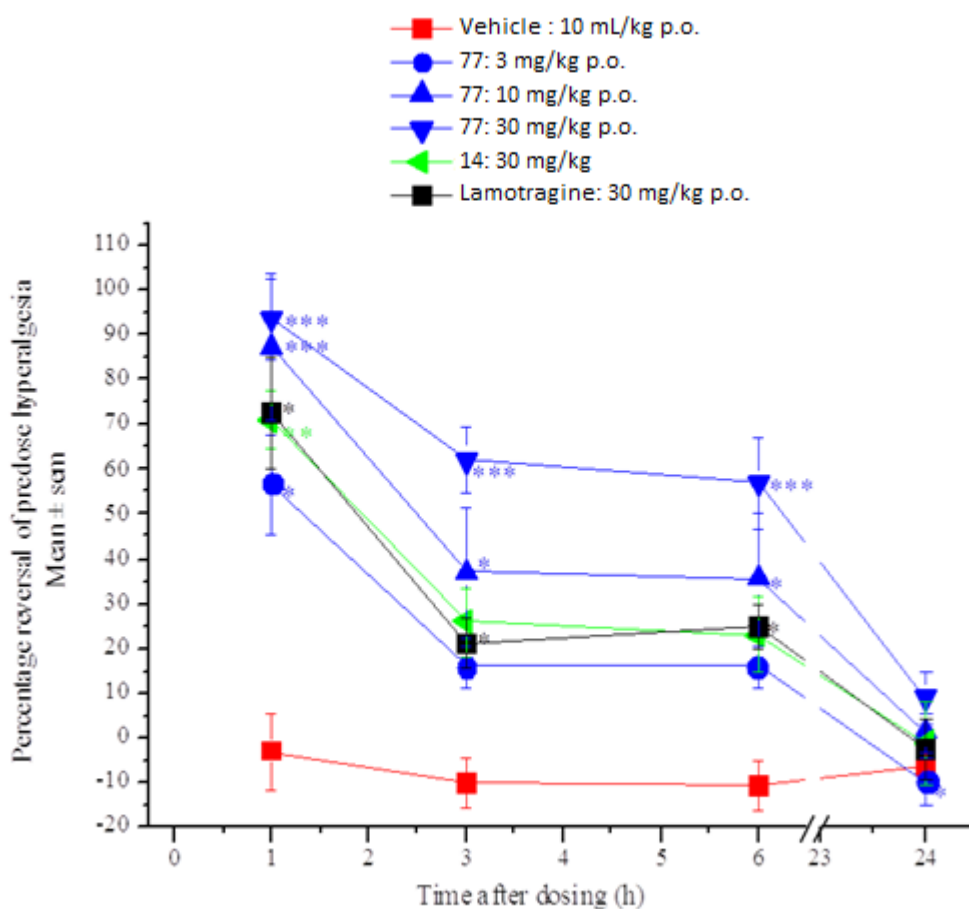


Figure 3. 13. The effect of compound **77** on ipsilateral paw withdrawal thresholds to a cold (10°C) stimulus in neuropathic rats. In comparison with lamotrigine. Fasted, male, Wistar rats. n = 6/group. Vehicle: 10% DMSO/10% Solutol HS15/80% saline. 10ml/kg p.o. One-way ANOVA, comparison with time-matched vehicle group using Tukey's HSD test, * p < 0.05, ** p < 0.01, *** p < 0.001

The results for the cold hyperalgesia test show that compound **77** reached peak reversal for all three doses at 1 hour. The peak analgesic effect for compound **77** was 95% reversal at 30 mg/kg.

The analgesic effect for **77** declined slowly but after 6 hours there was still a 60% reversal of painful symptoms, this is consistent with a long half-life ($t_{1/2}$ 2.98hr) and a high exposure (AUC 20135 hr*ng/mL, (Table 3.15) seen with compound **77**.

At the 3 hour time point compound **77** is more than 3 times as effective as the positive control (lamotrigine) for comparable doses (Figure 3.13).

% Reversal of mechanical allodynia

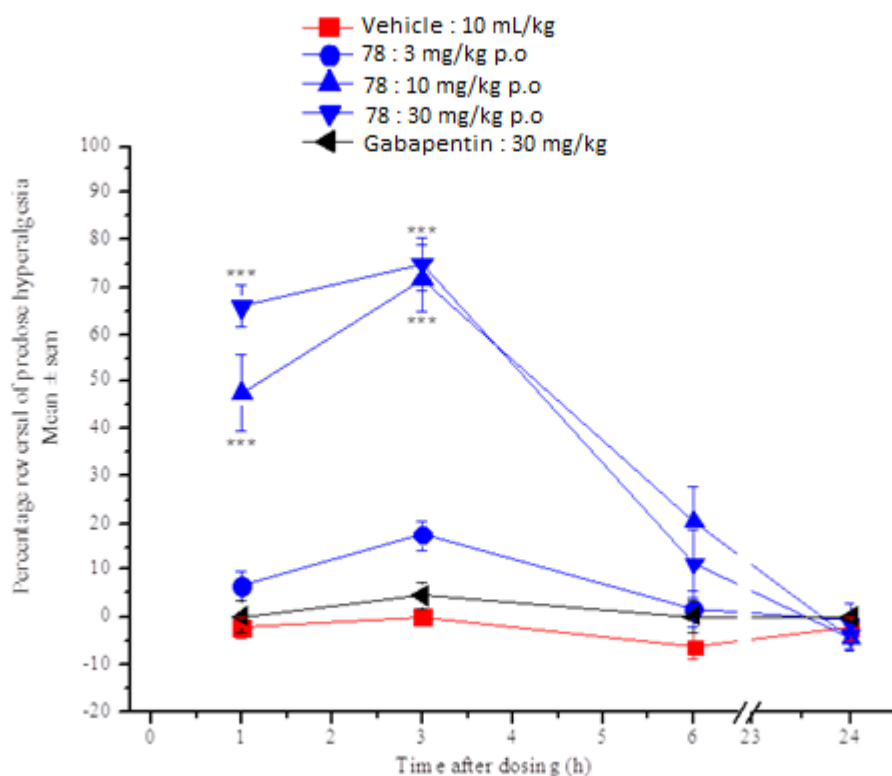


Figure 3.14. The effect of compound **78** on ipsilateral paw withdrawal thresholds to mechanical pressure in neuropathic rats. In comparison with gabapentin. Fasted, male, Wistar rats. $n = 6/\text{group}$. Vehicle: 10% DMSO/10% Solutol HS15/80% saline. 10ml/kg p.o. One-way ANOVA, comparison with time-matched vehicle group using Tukey's HSD test, * $p < 0.05$, ** $p < 0.01$, *** $p < 0.001$

Compound **78** achieved a maximum reversal of 75% after 3 hours at the highest dose of 30 mg/kg in the test for mechanical pressure. After 6 hours, however, the reversal of painful symptoms has dropped to 10%, which is consistent with the low half-life ($t_{1/2}$ in 2.5 hr) and high rate of metabolism (CL 2.5 L/hr/kg) seen with compound **78** in rat pharmacokinetic studies (Table 3.15). At the lowest dose of 3 mg/kg compound **78** gave more than double the analgesic effect of the positive control gabapentin, considered the 'gold standard' of care for neuropathic pain, which only achieved a 10% reversal of painful symptoms (Figure 3.14)

% Reversal of cold hyperalgesia

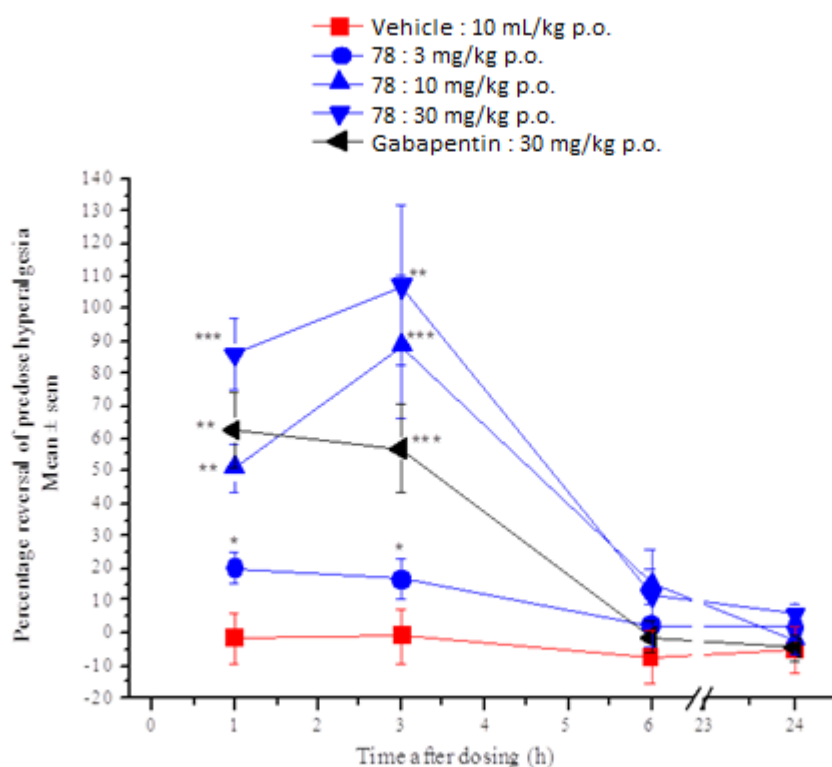


Figure 3.15. The effect of compound **78** on ipsilateral paw withdrawal thresholds to a cold (10°C) stimulus in neuropathic rats. In comparison with gabapentin. Fasted, male, Wistar rats. n = 6/group. Vehicle: 10% DMSO/10% Solutol HS15/80% saline. 10ml/kg p.o. One-way ANOVA, comparison with time-matched vehicle group using Tukey's HSD test, * p < 0.05, ** p < 0.01, *** p < 0.001

Compound **78** again showed a rapid onset of action with a 30 mg/kg dose reaching 90% reversal of painful symptoms after 1 hour and reaching a maximum analgesic effect at 3 hours with a 105% reversal in pain symptoms. This effect was short lived however, as after 6 hours the effect had dropped to just 20%. Once again compound **78** outperformed gabapentin which reached a maximum of 65% reversal at 1 hour (Figure 3.15).

% Reversal of mechanical allodynia

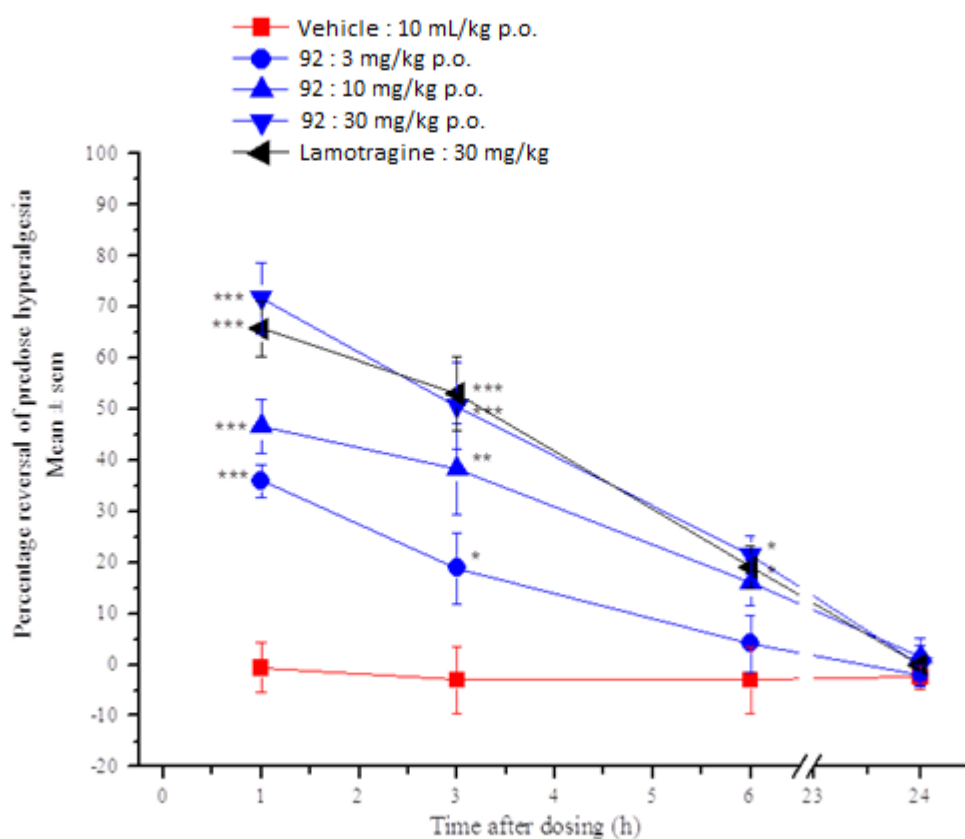


Figure 3.16. The effect of compound **92** on ipsilateral paw withdrawal thresholds to mechanical pressure in neuropathic rats. In comparison with lamotragine. Fasted, male, Wistar rats. $n = 6/\text{group}$. Vehicle: 10% DMSO/10% Solutol HS15/80% saline. 10ml/kg p.o. One-way ANOVA, comparison with time-matched vehicle group using Tukey's HSD test, * $p < 0.05$, ** $p < 0.01$, *** $p < 0.001$

Although the pharmacokinetic data for compound **92** would suggest it is absorbed slowly (T_{max} 3hr, Table 3.15) a dose of 30 mg/kg reached a peak reversal of 75% after only 1 hour. Reversal of analgesic effects drops steadily for compound **92** and at 6 hours post dosing the reversal effect is only 20%. This could be a consequence of compound **92** not achieving the concentration levels seen with compound **77** (C_{max} 4605 for **77**, C_{max} 2130 for **77**, Table 3.15).

Figure 3.16 shows that compound **92** is as effective as the positive control in reversing the effects of mechanical allodynia at a dose of 30 mg/kg.

% Reversal of cold hyperalgesia

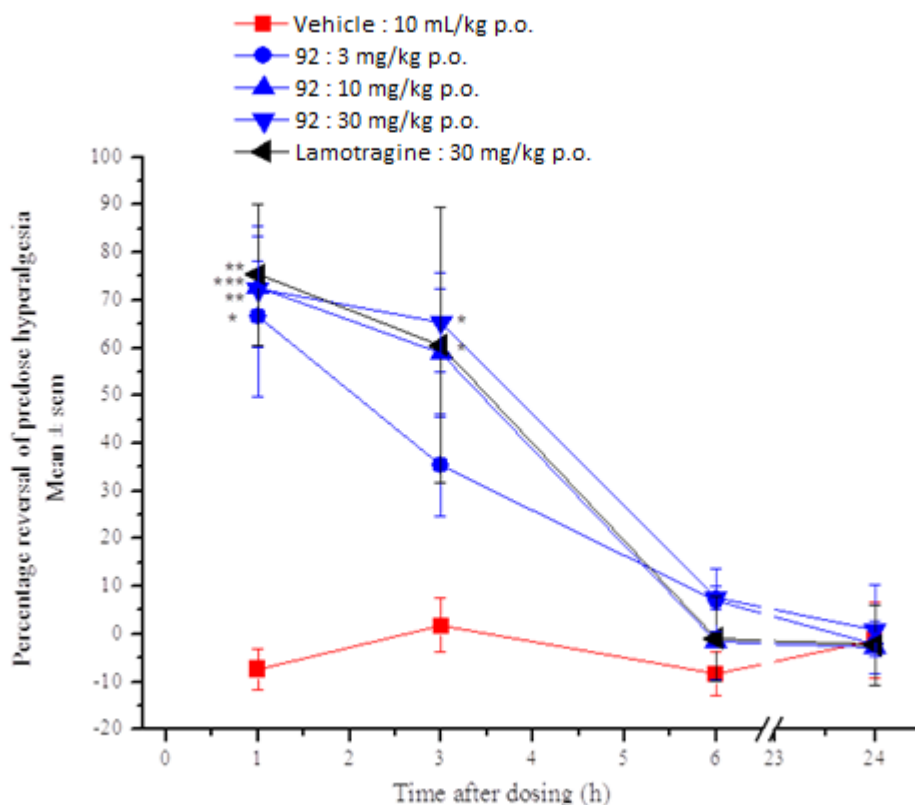


Figure 3.17. The effect of compound **92** on ipsilateral paw withdrawal thresholds to a cold (10°C) stimulus in neuropathic rats. In comparison with lamotragine. Fasted, male, Wistar rats. n = 6/group. Vehicle: 10% DMSO/10% Solutol HS15/80% saline. 10ml/kg p.o. One-way ANOVA, comparison with time-matched vehicle group using Tukey's HSD test, * p < 0.05, ** p < 0.01, *** p < 0.001

For the *tert*-butyl amide compound **92**, again onset of analgesia was rapid with a peak reversal of 70% at 1 hour. The analgesic effect remained consistently high at the 3 hour time point but rapidly dropped to only 10% at 6 hours. Once again compound **92** (30 mg/kg dose) was as effective as lamotragine (Figure 3.17). At the 24 hour time point the response to painful stimuli for all compounds, at all doses, had reverted back to pre-dosing levels.

This indicates that after 24 hours the concentration of all the compounds, even at the highest doses, had fallen below the therapeutic window⁵⁸.

The results of the *in vivo* tests for mechanical allodynia and cold hyperalgesia are summarised in tables Table 3.16 and Table 3.17 respectively.

Table 3.16. *In vivo* results of the mechanical allodynia test, in the Chung lesion model of neuropathic pain.

		77			78			92		
		3	10	30	3	10	30	3	10	30
		mg/kg	mg/kg	mg/kg	mg/kg	mg/kg	mg/kg	mg/kg	mg/kg	mg/kg
% Reversal	1hr	40	80	80	5	45	65	35	45	70
	3hr	70	90	90	20	70	75	20	40	50
	6hr	30	40	40	0	20	10	15	25	20
	24hr	0	0	0	0	0	0	0	0	0

Table 3.17. *In vivo* results of the cold hyperalgesia test, in the Chung lesion model of neuropathic pain.

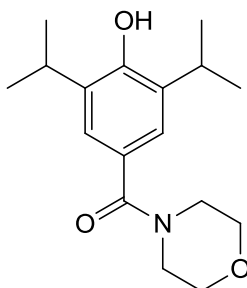
		77			78			92		
		3	10	30	3	10	30	3	10	30
		mg/kg	mg/kg	mg/kg	mg/kg	mg/kg	mg/kg	mg/kg	mg/kg	mg/kg
% Reversal	1hr	60	85	95	20	50	90	65	70	70
	3hr	20	35	65	15	90	105	35	60	65
	6hr	20	35	60	0	20	20	10	10	10
	24hr	0	0	0	0	0	0	0	0	0

3.4 Summary

This chapter has highlighted the synthesis and biological evaluation of a range of novel compounds targeting the α 1 GlyR. Initial studies focused on the synthesis of a series of 2,6-diisopropyl and 2,6-di-*tert*-butylphenol analogues containing *para*-amino alkyl substituents (**49-55** & **60-64** respectively). Compounds **49-51** & **55** were tested for efficacy at the α 1 GlyR, however, none of the compounds tested showed any activity below 1 μ M. *In silico* screening of the *para*-amino series also highlighted problems of a predicted high rate of clearance from both human microsomes and rat hepatocytes. Compounds **49-55** & **60-64** also displayed poor physicochemical properties, low MPO scores, which highlighted potential problems with CNS penetration, and the compounds also had the potential to form toxic quinone methide intermediates. All the factors detailed above made the decision to terminate this series easy.

In an effort to improve the issues seen with the *para*-amino series we decided to install a carbonyl group at the site of quinone methide formation. In general the amide series (**77-79** & **92-96**) showed improved physicochemical properties, reduced metabolism and greater MPO scores than the *para*-amino alkyl analogues.

Among the compounds synthesised we have identified several highly potent allosteric modulators of the α 1 GlyR (**77**, **78**, & **92**), exemplified by the morpholine amide **77** (EC_{50} = 3.5 nM).



77

Figure 3.18. Morpholine amide compound **77**.

The *i*-pr-amide morpholine compound **77** has been shown to be extremely potent at the α 1 GlyR with an EC₅₀ 3.5 nM (Table 3.12). It has also displayed a favourable physicochemical (Table 3.7) and pharmacokinetic profile (Table 3.15). MPO evaluation of compound **77** shows that it possesses the attributes required for a high level of CNS penetration (MPO score 4.4, Table 3.8) and the *in vivo* results from the Chung lesion model of chronic neuropathic pain show a peak of \geq 90% reversal of painful symptoms in both mechanical allodynia and cold hyperalgesia.

Pharmacokinetic studies show that an oral dose of **67** (10 mg/kg) has a high level of absorption (C_{max} = 4605 ng/mL) a large exposure (AUC = 20135 hr*ng/mL) a moderate half-life (2.58 hr) and a high bioavailability (F = 85%) (Table 3.15).

With an overall CNS MPO score for of 4.4 for compound **77** was thought to have a high probability of crossing the BBB and entering the CNS to target the α 1 GlyR.

In vivo testing in the Chung lesion model for neuropathic pain showed that a dose 10 mg/kg of compound **77** could perform better than the positive control (lamotrigine at 30 mg/kg) delivering 90% reversal of painful symptoms for mechanical allodynia and 30 mg/kg gave 95% reversal for cold hyperalgesia.

Chapter IV details the lead optimisation of the propofol amide scaffold.

3.5 References

- 1 Wager, T. T., Hou, X., Verhoest, P. R. & Villalobos, A. Moving beyond Rules: The Development of a Central Nervous System Multiparameter Optimization (CNS MPO) Approach To Enable Alignment of Druglike Properties. *ACS Chemical Neuroscience* **1**, 435-449, (2010).
- 2 Pajouhesh, H. & Lenz, G. R. Medicinal chemical properties of successful central nervous system drugs. *NeuroRx : the journal of the American Society for Experimental NeuroTherapeutics* **2**, 541-553, (2005).
- 3 Cooke, A., Anderson, A., Buchanan, K., *et al.* Water-soluble propofol analogues with intravenous anaesthetic activity. *Bioorganic & Medicinal Chemistry Letters* **11**, 927-930, (2001).
- 4 Mannich, C. & Krösche, W. Ueber ein Kondensationsprodukt aus Formaldehyd, Ammoniak und Antipyrin. *Archiv der Pharmazie* **250**, 647-667, (1912).
- 5 Subramaniapillai, S. Mannich reaction: A versatile and convenient approach to bioactive skeletons. *J Chem Sci* **125**, 467-482, (2013).
- 6 Pacorel, B., Fisher, N., Shone, A. E. *et al.* Modular Synthesis and in Vitro and in Vivo Antimalarial Assessment of C-10 Pyrrole Mannich Base Derivatives of Artemisinin. *Journal of Medicinal Chemistry* **53**, 633-640, (2009).
- 7 Yogeewari, P., Sriram, D., Kavya, R. & Tiwari, S. Synthesis and in-vitro cytotoxicity evaluation of gatifloxacin Mannich bases. *Biomedicine & pharmacotherapy* **59**, 501-510 (2005).
- 8 A, K. & S, P. K. a. P. N. R. *Int. J. Pharm.* **127**, 229 (1996).
- 9 Chen, H.-L. Chang, Chun-Yi., Lee, Hsun-Tzu., Lin, Hua-Hsuan., Lu, Pei-Jung., Yang, Chia-Ning., Shiao, Chung-Wai., Shaw, Arthur Y.. Synthesis and pharmacological exploitation of clioquinol-derived copper-binding apoptosis inducers triggering reactive oxygen species generation and MAPK pathway activation. *Bioorganic & Medicinal Chemistry* **17**, 7239-7247, (2009).
- 10 Nie, J., Guo, H.-C., Cahard, D. & Ma, J.-A. Asymmetric Construction of Stereogenic Carbon Centers Featuring a Trifluoromethyl Group from Prochiral Trifluoromethylated Substrates. *Chemical Reviews* **111**, 455-529, (2010).
- 11 Kobayashi, S., Mori, Y., Fossey, J. S. & Salter, M. M. Catalytic Enantioselective Formation of C–C Bonds by Addition to Imines and Hydrazones: A Ten-Year Update. *Chemical Reviews* **111**, 2626-2704, (2011).
- 12 Liu, Y., Liu, J., Huang, Y. & Qing, F.-L. Lewis acid-catalyzed regioselective synthesis of chiral [small alpha]-fluoroalkyl amines via asymmetric addition of silyl dienolates to fluorinated sulfinylimines. *Chemical Communications* **49**, 7492-7494, (2013).
- 13 Srivastava, A., Ramachandran, S., Hameed, S. P., Ahuja, V. & Hosagrahara, V. P. Identification and Mitigation of a Reactive Metabolite Liability Associated

- with Aminoimidazoles. *Chemical Research in Toxicology* **27**, 1586-1597, (2014).
- 14 Zhang, L., Peng, X.-M., Damu, G. L. V., Geng, R.-X. & Zhou, C.-H. Comprehensive Review in Current Developments of Imidazole-Based Medicinal Chemistry. *Medicinal Research Reviews* **34**, 340-437, (2014).
- 15 Bills, E. J. Reactions between hexamethylenetetramine and phenolic compounds Part I A new method for the preparation of 3-and 5-aldehydosalicylic acids. *Journal of the Chemical Society*, 1987-1987 (1932).
- 16 Roth, B. Baccanari, D. P., Sigel, C. W., Hubbell, J. P., Eaddy, J., Kao, J. C., Grace, M. E., Rauckman, B. S.. 2,4-diamino-5-benzylpyrimidines and analogs as antibacterial agents .9. lipophilic trimethoprim analogs as antigonococcal agents. *Journal of Medicinal Chemistry* **31**, 122-129, (1988).
- 17 Duff, J. C. 96. A new general method for the preparation of o-hydroxyaldehydes from phenols and hexamethylenetetramine. *Journal of the Chemical Society (Resumed)*, 547-550, (1941).
- 18 Ahmed, S., Shahid, I., Dhanani, S. & Owen, C. P. Synthesis and biochemical evaluation of a range of sulfonated derivatives of 4-hydroxybenzyl imidazole as highly potent inhibitors of rat testicular 17 α -hydroxylase/17,20-lyase (P-45017 α). *Bioorganic & Medicinal Chemistry Letters* **19**, 4698-4701, (2009).
- 19 Personal Communication.
- 20 Betts, A. Atkinson, F., Gardner, I., Fox, D., Webster, R., Beaumont, K., Morgan, P.. Impact of Physicochemical and Structural Properties on the Pharmacokinetics of a Series of α 1L-Adrenoceptor Antagonists. *Drug Metabolism and Disposition* **35**, 1435-1445, (2007).
- 21 Murayama, N., Minoshima, M., Shimizu, M., Guengerich, F. P. & Yamazaki, H. Involvement of human cytochrome P450 2B6 in the ω - and 4-hydroxylation of the anesthetic agent propofol. *Xenobiotica* **37**, 717-724, (2007).
- 22 Ahrens, J. Leuwer, M., de la Roche, J., Foadi, N., Krampfl, K., Haeseler, G. The Non-Anaesthetic Propofol Analogue 2,6-Di-tert-Butylphenol Fails to Modulate GABA_A Receptor Function. *Pharmacology* **83**, 95-98 (2009).
- 23 Krasowski, M. D., Jenkins, A., Flood, P., Kung, A. Y., Hopfinger, A. J., Harrison, N. L. General Anesthetic Potencies of a Series of Propofol Analogs Correlate with Potency for Potentiation of γ -Aminobutyric Acid (GABA) Current at the GABAA Receptor but Not with Lipid Solubility. *Journal of Pharmacology and Experimental Therapeutics* **297**, 338-351 (2001).
- 24 Collins, J. G., Kendig, J. J. & Mason, P. Anesthetic actions within the spinal cord: contributions to the state of general anesthesia. *Trends in Neurosciences* **18**, 549-553, (1995).
- 25 Downes, H. & Courogen, P. M. Contrasting effects of anesthetics in tadpole bioassays. *Journal of Pharmacology and Experimental Therapeutics* **278**, 284-296 (1996).

- 26 James, R. & Glen, J. B. Synthesis, biological evaluation, and preliminary structure-activity considerations of a series of alkylphenols as intravenous anesthetic agents. *Journal of Medicinal Chemistry* **23**, 1350-1357, (1980).
- 27 Ahrens, J., Haeseler, G., Leuwer, M., Mohammadi, B., Krampfl, K., Dengler, R., Bufler, J. 2,6 Di-tert-butylphenol, a Nonanesthetic Propofol Analog, Modulates $\alpha 1\beta$ Glycine Receptor Function in a Manner Distinct from Propofol. *Anesthesia & Analgesia* **99**, 91-96 (2004).
- 28 Fischer, H., Gottschlich, R. & Seelig, A. Blood-brain barrier permeation: molecular parameters governing passive diffusion. *The Journal of membrane biology* **165**, 201-211 (1998).
- 29 Palm, K., Luthman, K., Ros, J., Gråsjö, J. & Artursson, P. Effect of molecular charge on intestinal epithelial drug transport: pH-dependent transport of cationic drugs. *Journal of Pharmacology and Experimental Therapeutics* **291**, 435-443 (1999).
- 30 Leung, L., Kalgutkar, A. S. & Obach, R. S. Metabolic activation in drug-induced liver injury. *Drug Metabolism Reviews* **44**, 18-33, (2012).
- 31 Monks, T. J. & Jones, D. C. The Metabolism and Toxicity of Quinones, Quinonimines, Quinone Methides, and Quinone-Thioethers. *Current Drug Metabolism* **3**, 425-438, (2002).
- 32 Bolton, J. L. Quinone Methide Bioactivation Pathway: Contribution to Toxicity and/or Cytoprotection? *Curr. Org. Chem.* **18**, 61-69, (2014).
- 33 Stachulski, A. V., Baillie, T. A., Kevin P. B., *et al.* The Generation, Detection, and Effects of Reactive Drug Metabolites. *Medicinal Research Reviews* **33**, 985-1080, (2013).
- 34 Dias, C. G., Marinho, A. T., Caixas, U., Faustino, I., Antunes, A. M. M., Matilde M. M., Monteiro, E. C., Pereira, S. A. Thiol status in HIV-infected patients: The effect of nevirapine metabolism. *Toxicology Letters* **229, Supplement**, S95, (2014).
- 35 <http://www.fda.gov/safety/medwatch/safetyinformation/safetyalertsforhumanmedicalproducts/ucm173102.htm> > (
- 36 Chen, J., Mannargudi, B. M., Xu, L. & Uetrecht, J. Demonstration of the Metabolic Pathway Responsible for Nevirapine-Induced Skin Rash. *Chemical Research in Toxicology* **21**, 1862-1870, (2008).
- 37 Sharma, A. M., Li, Y., Novalen, M., Hayes, M. A. & Uetrecht, J. Bioactivation of Nevirapine to a Reactive Quinone Methide: Implications for Liver Injury. *Chemical Research in Toxicology* **25**, 1708-1719, (2012).
- 38 Watkins, P. B. & Whitcomb, R. W. Hepatic Dysfunction Associated with Troglitazone. *New England Journal of Medicine* **338**, 916-917, (1998).
- 39 Kassahun, K., Pearson, P. G., Tang, W., *et al.* Studies on the Metabolism of Troglitazone to Reactive Intermediates in Vitro and in Vivo. Evidence for Novel Biotransformation Pathways Involving Quinone Methide Formation

- and Thiazolidinedione Ring Scission†. *Chemical Research in Toxicology* **14**, 62-70, (2000).
- 40 Fuman, B., Aldinger, G., Fauman, M. & Rosen, P. Psychiatric sequelae of phencyclidine abuse. *Clin Toxicol.* **9**, 529-538 (1976).
- 41 Shebley, M., Kent, U. M., Ballou, D. P. & Hollenberg, P. F. Mechanistic Analysis of the Inactivation of Cytochrome P450 2B6 by Phencyclidine: Effects on Substrate Binding, Electron Transfer, and Uncoupling. *Drug Metabolism and Disposition* **37**, 745-752, (2009).
- 42 Driscoll, J. P., Kornecki, K., Wolkwski, J. P., Chupak, L., Kalgutkar, A. S., O'Donnell, J.P. Bioactivation of Phencyclidine in Rat and Human Liver Microsomes and Recombinant P450 2B Enzymes: Evidence for the Formation of a Novel Quinone Methide Intermediate. *Chemical Research in Toxicology* **20**, 1488-1497, (2007).
- 43 Roy, P., Brideau, C., Chan, C. C. *et al.* A new series of selective COX-2 inhibitors: 5,6-diarylthiazolo[3,2-b][1,2,4]triazoles. *Bioorganic & Medicinal Chemistry Letters* **7**, 57-62, (1997).
- 44 Obach, R. S., Kalgutkar, A. S., Ryder, T. F. & Walker, G. S. In Vitro Metabolism and Covalent Binding of Enol-Carboxamide Derivatives and Anti-Inflammatory Agents Sudoxicam and Meloxicam: Insights into the Hepatotoxicity of Sudoxicam. *Chemical Research in Toxicology* **21**, 1890-1899, (2008).
- 45 Yadav, J. S., Rajendar, G., Rao, R. S. & Pabbaraja, S. Total Synthesis of Nhatrangin A. *The Journal of Organic Chemistry* **78**, 8524-8530, (2013).
- 46 Bal, B. S., Childers, W. E. & Pinnick, H. W. Oxidation of α,β -unsaturated aldehydes. *Tetrahedron* **37**, 2091-2096, d (1981).
- 47 Brzasczcz, M., Kloc, K., Maposah, M. & Mlochowski, J. Selenium(IV) Oxide Catalyzed Oxidation of Aldehydes to Carboxylic Acids with Hydrogen Peroxide. *Synthetic Communications* **30**, 4425-4434,
- 48 Wuts, P. G. M. & Greene, T. W. in *Greene's Protective Groups in Organic Synthesis* 367-430 (John Wiley & Sons, Inc., 2006).
- 49 Mullican, m.d., Wilson, M. W., Connor, D. T., Kostlan, C. R., Schrier, D. J., Dyer, R. D. design of 5-(3,5-di-tert-butyl-4-hydroxyphenyl)-1,3,4-thiadiazoles, 5-(3,5-di-tert-butyl-4-hydroxyphenyl)-1,3,4-oxadiazoles, and 5-(3,5-di-tert-butyl-4-hydroxyphenyl)-1,2,4-triazoles as orally-active, nonulcerogenic antiinflammatory agents. *journal of medicinal chemistry* **36**, 1090-1099 (1993).
- 49 Boovanahalli, S. K., Kim, D. W. & Chi, D. Y. Application of Ionic Liquid Halide Nucleophilicity for the Cleavage of Ethers: A Green Protocol for the Regeneration of Phenols from Ethers. *The Journal of Organic Chemistry* **69**, 3340-3344, (2004).

- 50 Ziakas, G.N., Rekka, E.A., Gavalas, A.M., Eleftheriou, P.T. & Kourounakis, P.N. New analogues of butylated hydroxytoluene as anti-inflammatory and antioxidant agents. *Bioorganic & Medicinal Chemistry* **14**, 5616-5624 (2006).
- 51 Angibeaud, P., Defaye, J., Gadelle, A. & Uille, J.-P. Mild Deprotection of Benzyl Ether Protective Groups with Ozone. *Synthesis* **1985**, 1123-1125, (1985).
- 52 Boovanahalli, S. K., Kim, D. W. & Chi, D. Y. Application of Ionic Liquid Halide Nucleophilicity for the Cleavage of Ethers: A Green Protocol for the Regeneration of Phenols from Ethers. *The Journal of Organic Chemistry* **69**, 3340-3344
- 53 Martinez-Solorio, D. & Jennings, M.P. Convergent Formal Syntheses of (\pm)-Brussonol and (\pm)-Abrotanone via an Intramolecular Marson-Type Cyclization. *Organic Letters* **11**, 189-192 (2008).
- 54 Ertl, P., Rohde, B. & Selzer, P. Fast Calculation of Molecular Polar Surface Area as a Sum of Fragment-Based Contributions and Its Application to the Prediction of Drug Transport Properties. *Journal of Medicinal Chemistry* **43**, 3714-3717, (2000).
- 55 Van de Waterbeemd, H., Camenisch, G., Folkers, G., Chretien, J. R. & Raevsky, O. A. Estimation of Blood-Brain Barrier Crossing of Drugs Using Molecular Size and Shape, and H-Bonding Descriptors. *Journal of Drug Targeting* **6**, 151-165, (1998).
- 56 Hansch, C., Steward, A. R., Anderson, S. M. & Bentley, D. L. Parabolic dependence of drug action upon lipophilic character as revealed by a study of hypnotics. *Journal of Medicinal Chemistry* **11**, 1-11, (1968).
- 57 Yoon, C., Young Wook, Y., Heung Sik, N., Sun Ho, K. & Jin Mo, C. Behavioral signs of ongoing pain and cold allodynia in a rat model of neuropathic pain. *Pain* **59**, 369-376, (1994).
- 58 Coleman, M. D. *Human Drug Metabolism: An Introduction*. (Wiley, 2010).

Chapter IV

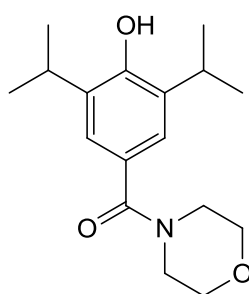
Lead Optimisation

Contents

4.0	Introduction	169
4.1	Amide synthesis.....	171
4.1.1	Trifluoromethylation	179
4.2	<i>In silico</i> testing	182
4.2.1	Biological results	186
4.2.2	MPO evaluation.....	189
4.2.3	<i>In vivo</i> pharmacokinetic studies (rat).....	192
4.2.4	<i>In vivo</i> neuropathic pain testing (Chung lesion model in the rat)	192
4.3	Target product profile	195
4.4	Summary.....	197
4.5	References.....	199

4 Introduction

The previous chapter detailed the design and synthesis of a series of novel amide propofol analogues exemplified by compound **77** (Figure 4.1). **77** displayed low nM activity at the α 1 GlyR, favourable physicochemical and pharmacokinetic profiles and has an MPO score >4.



77

Figure 4.1. Amide morpholine compound **77**.

Encouraged by these favourable results we embarked upon a lead expansion programme based around the *i*-pr-amide morpholine. Morpholino substituents were chosen to explore the steric and electronic constraints of the active site in an effort to gain a greater understanding of the SAR surrounding the α 1 GlyR (Figure 4.1). The pKa of all of the compounds synthesised thus far has exceeded the optimal value, which according to reports by Fischer and co-workers and Palm co-workers, should be kept between 4-10. However Villalobos recommend that for maximum probability of CNS penetration the pKa should not exceed 8¹⁻³.

Therefore in order to reduce the pKa of our compounds it was decided to include a variety of electronegative substituents at *para* positions of the propofol core in an effort to reduce electron density at the phenolic hydroxyl group (Figure 4.2)

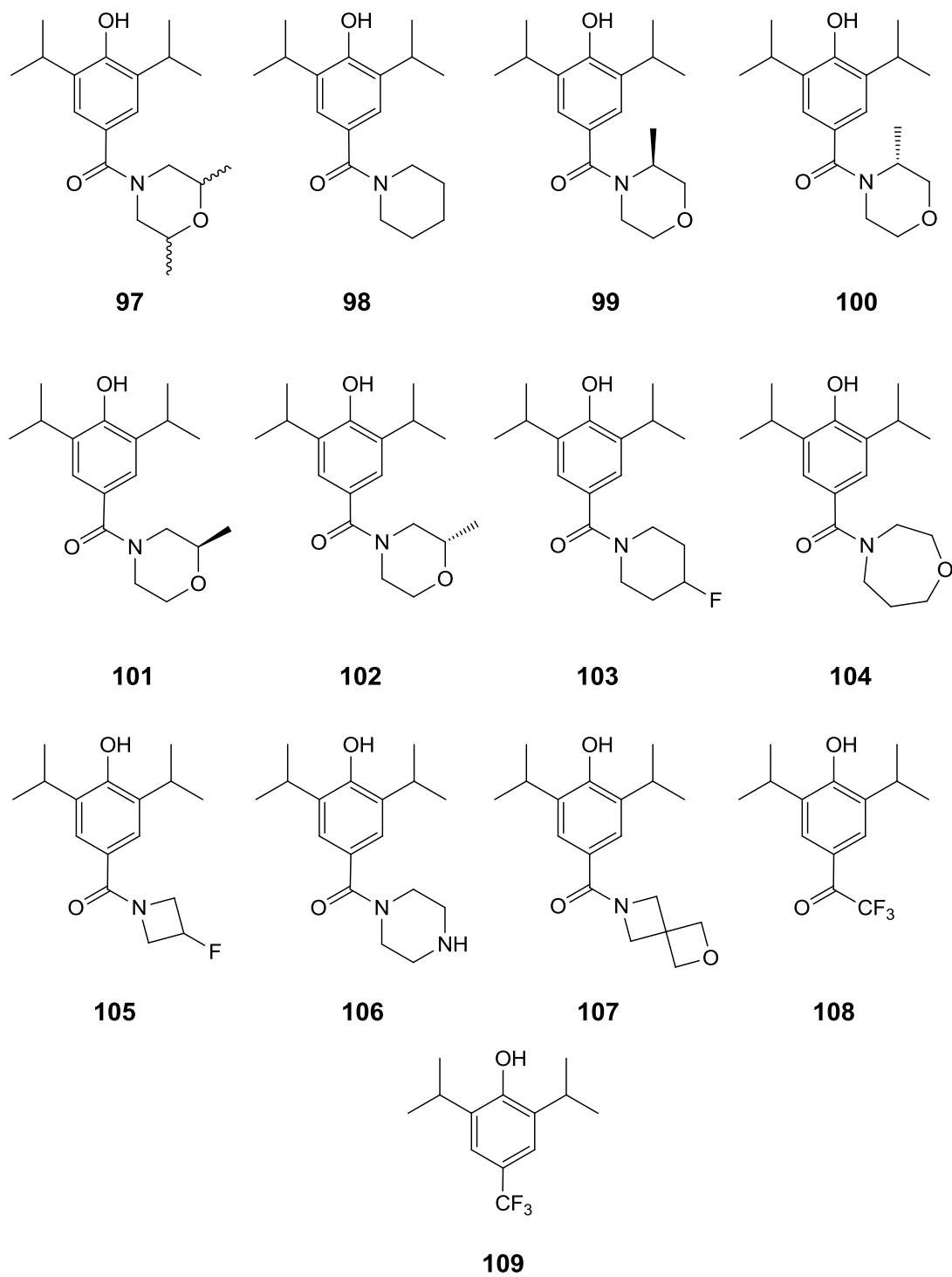
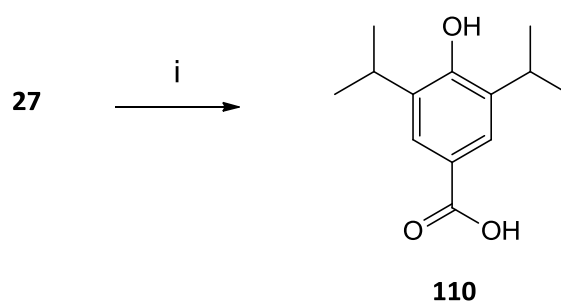


Figure 4.2. Proposed lead optimisation compounds.

4.1 Amide synthesis

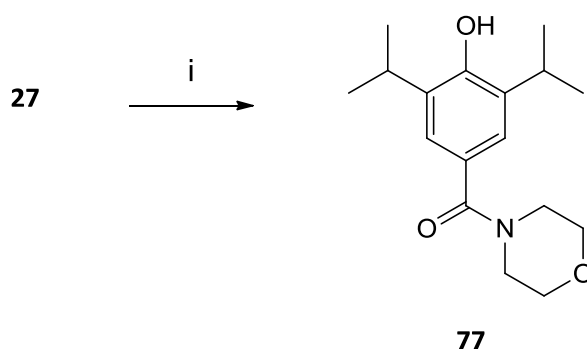
During a search of the literature a report by Wu and co-workers was found which detailed the conversion of aryl bromides into secondary and tertiary benzamides. Aminocarbonylation was afforded by metal catalysed (Herrmann's catalyst) carbonylation in microwave heated water, using $\text{Mo}(\text{CO})_6$ as the source of carbon monoxide⁴. If this method could be utilised to synthesise our proposed morpholino compounds (**97-105**) it would reduce the number of synthetic steps from 6 to 2. However, when this method was employed to resynthesize compound **77**, we found these conditions gave only the benzoic acid (**110**) derivative shown in Scheme 4.1^{5,6}



Scheme 4.1. *Reagents and conditions:* i) Morpholine, Na_2CO_3 , *trans*-bis(acetate)bis[o-(di-o-tolylphosphino)benzyl]dipaladium(II), $\text{Mo}(\text{CO})_6$, H_2O , microwave, 165°C , 10mins.

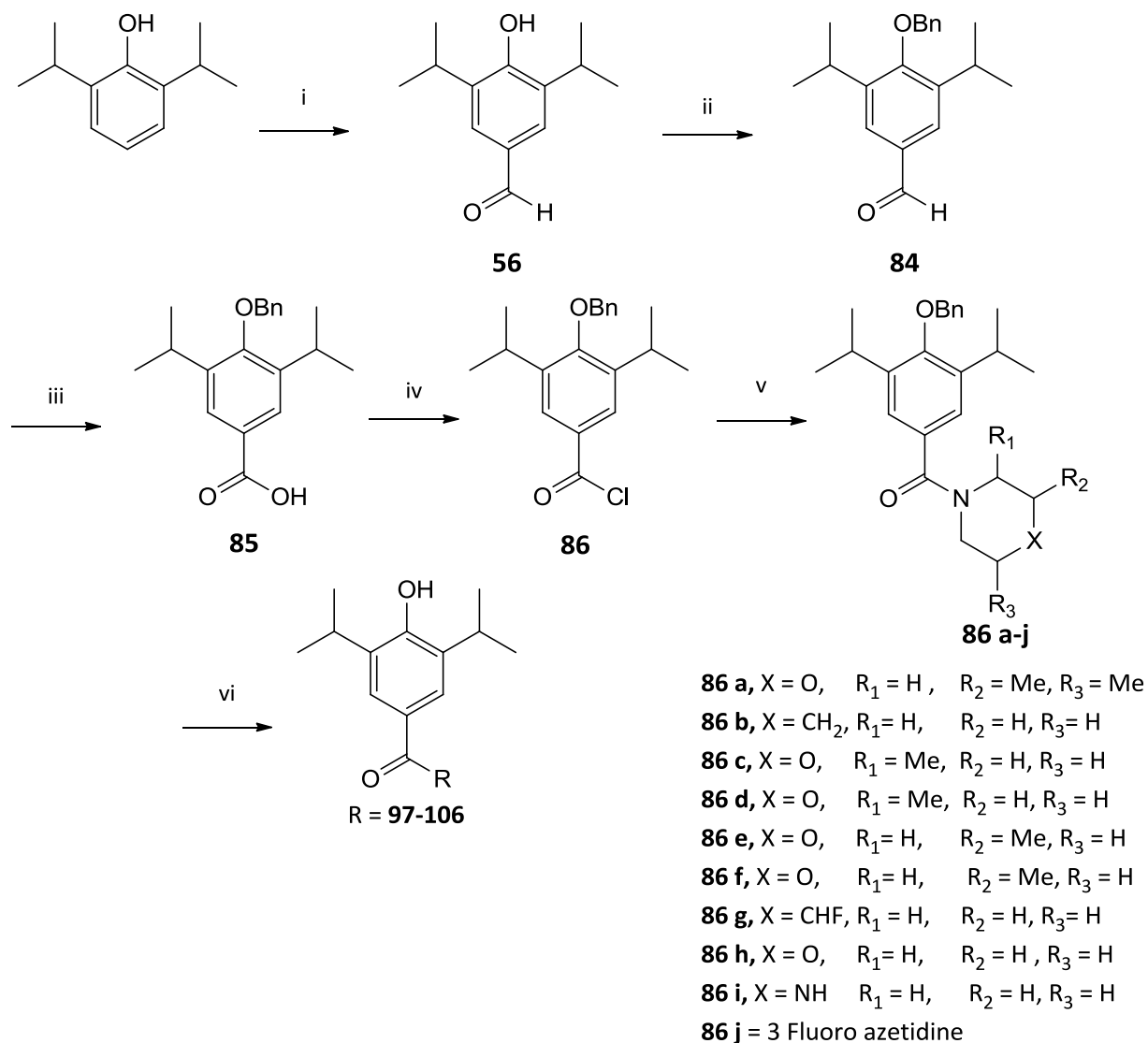
It was thought that the presence of water as the solvent may be responsible for the formation of the hydroxycarbonylation product (**110**) (Scheme 4.1).

Therefore, in an effort to mitigate against the formation of the unwanted product the aprotic solvent 1,4-dioxane was employed as the solvent instead of water (Scheme 4.2).



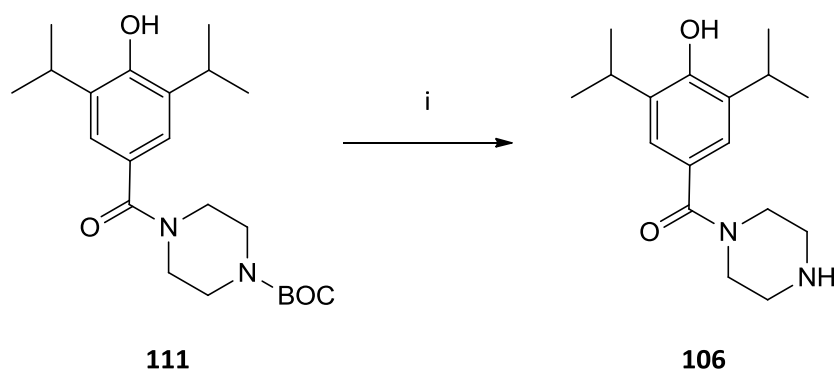
Scheme 4.2. *Reagents and conditions:* i) Morpholine, Na_2CO_3 , *trans*-bis(acetate)bis[o-(di-o-tolylphosphino)benzyl]dipaladium(II), $\text{Mo}(\text{CO})_6$, 1,4-dioxane, microwave, 165°C , 10mins, 60% yield.

The change of solvent solved the problem and the aminocarbonylation product was afforded in 60% yield (after purification). However, when this method was utilised to synthesise compound **97** it was found that the reaction failed to produce the desired product. It was also noted that no hydroxycarbonylation was detected either. This reaction was tried several times with substituted morpholines **100-106** to no avail. It was, therefore, decided to revert back to the original 6 step synthetic scheme to synthesise compounds **97-105** (Scheme 4.3).



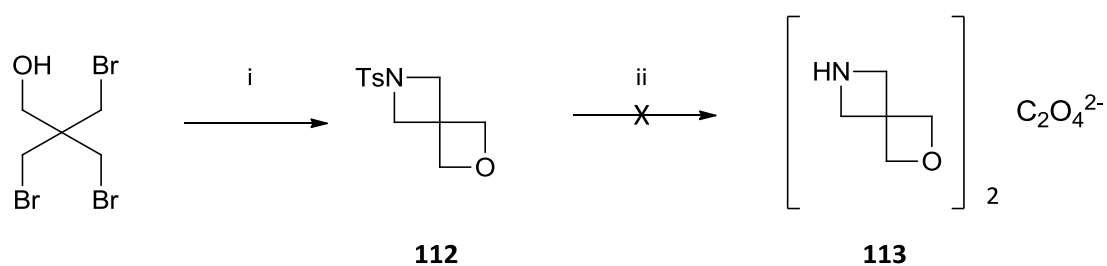
Scheme 4.3. *Reagents and conditions:* i) Hexamethylenetetramine, AcOH, reflux 16hrs, 89% yield⁷. ii) BnBr, K₂CO₃, acetone, RT, 18hrs, 88% yield⁸. iii) SeO₂, H₂O₂, THF, reflux, 18hrs 70% yield⁹. iv) Oxalyl chloride, Et₃N, DMF, DCM, RT, 2hrs¹⁰. v) Secondary amine, Et₃N, DCM, RT, 18hr 42-95% yields¹¹. vi) Pd/C, H₂, MeOH, RT, 18hrs, 95-98% yields¹².

Synthesis of piperazine compound **106** followed Scheme 4.3 to produce BOC-protected piperazine (**111**) which was further subjected to BOC deprotection using trifluoroacetic acid (TFA) in DCM (Scheme 4.4).



Scheme 4.4. Reagents and conditions: i) TFAA, DCM, 18 hrs, RT, 60% yield¹³.

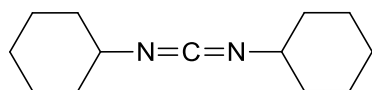
In an attempt to further increase the metabolic stability of our compounds it was decided to include a spirocyclic analogue of morpholine (**107**). The initial synthesis of spirocyclic analogue **107** began with the synthesis of the 2-oxa-6-azaspiro[3.3]heptane moiety (**112**). Tribromopentaerythritol and tosylamide were stirred in the presence of KOH for 5 days to give **112**. This was then to be converted to the oxalate salt via cleavage of the tosylamide with Mg/MeOH and treatment with oxalic acid to give compound **113** (Scheme 4.5).



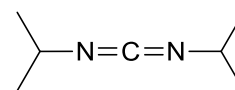
Scheme 4.5. Reagents and conditions: i) Tosylamide, KOH, EtOH, 120hrs, reflux 55% yield. ii) Mg, Na₂SO₄·10H₂O, oxalic acid, MeOH, sonicate 1hr¹⁴.

Compound **112** was produced in reasonable yields (55%) and was characterised by ¹HNMR showing doublets at 7.71 ppm and 7.37 ppm integrating to 2 protons each corresponding to the aromatic protons on the tosylamide group, a singlet at 4.6 ppm integrating for 4 protons corresponding to the O-(CH₂)₂ and another singlet at 3.91 ppm integrating for 4 protons corresponding to the N-(CH₂)₂. However, when we attempted to convert compound **103** to the oxalate salt the reaction failed and only the starting material was recovered. This reaction was repeated several times varying the length of sonication time, using fresh Mg (granules) and employing anhydrous methanol all to no avail. Therefore we decided to find a commercial supplier for compound **113**.

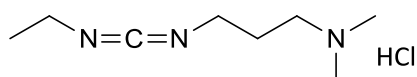
Once compound **113** was in hand it was subjected to the amide coupling conditions outlined in. Unfortunately the reaction failed and only starting material was recovered. The reaction was repeated several times with varying equivalents of triethylamine to mop up the oxalate salt and the HCl produced from the coupling of the acid chloride and amide. Again the reaction was unsuccessful. We, therefore, decided to investigate the use of carbodiimides as coupling reagents. Dicyclohexyl carbodiimide (DCC, **114**), diisopropyl carbodiimide (DIC, **115**) and 1-ethyl-3-(3'-dimethylamino) (EDC, **116**) carbodiimide HCl salt are amongst the most frequently used carbodiimides for amide bond formation (Figure 4.3)¹⁵.



DCC

114

DIC

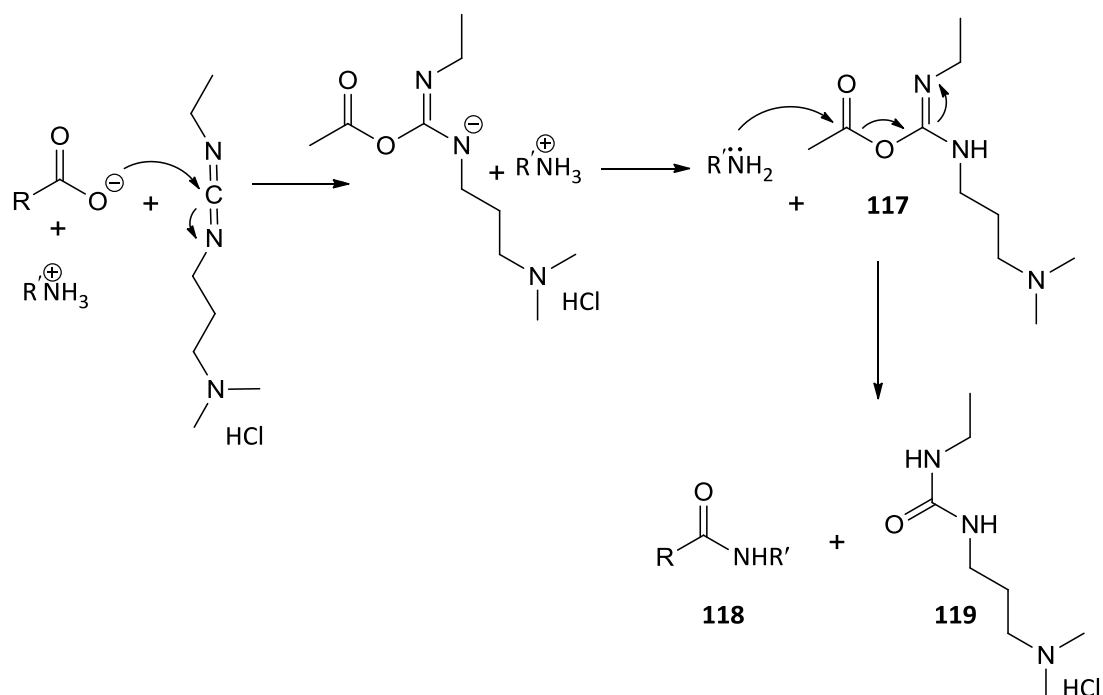
115

EDC

116

Figure 4.3. DCC, DIC and EDC the most common carbodiimide reagents used in amide bond formation.

The carbodiimide reacts with the carboxylic acid to form the O-acylisourea mixed anhydride (**117**). This intermediate can then react with the amine to yield the desired amide (**118**) and the urea by-product (**119**) (Figure 4.3)¹⁶.



Scheme 4.6. Amide bond formation using carbodiimide (EDC).

Often acyl transfer to the unreactive N-acylurea can be observed, to counter this, the reaction mixture is often cooled to 0°C before the amine is added. In order to further mitigate the unwanted acyl transfer a nucleophile (dimethylamino pyridine **120** or hydroxybenzotriazole **110**, Figure 4.4) is often added to the reaction mixture which reacts faster than the acyl transfer but generates an intermediate still active enough to couple with the amine¹⁷.

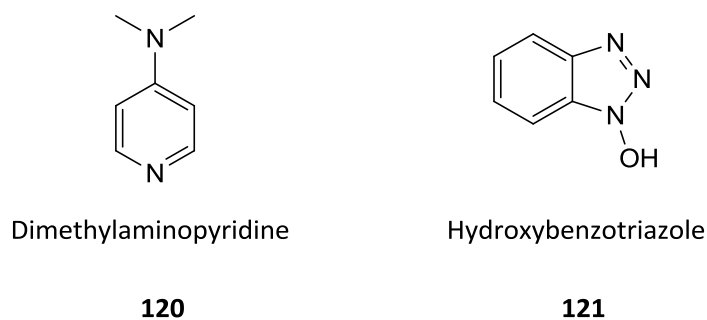
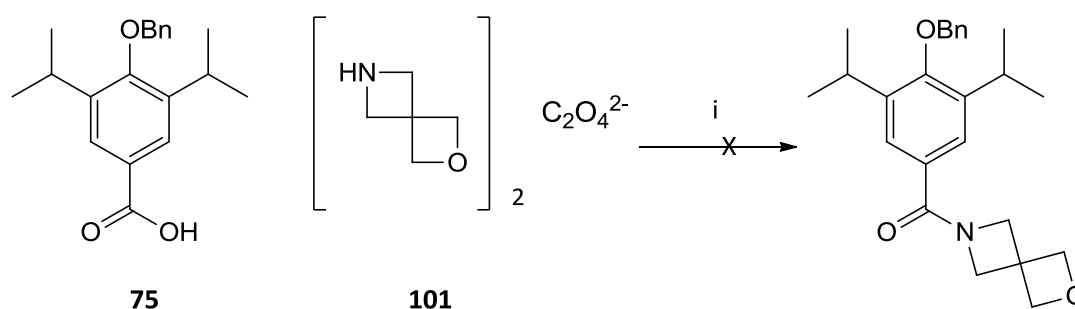


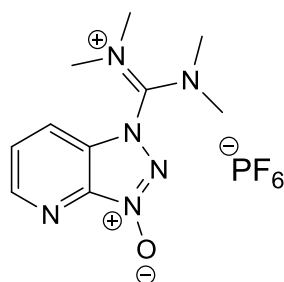
Figure 4.4. Nucleophiles Dmap and HOBt used to minimise N-acylurea formation.

However, when we subjected the spirocyclic amine (**113**) and carboxylic acid (**85**) to the coupling conditions shown in Scheme 4.7 the desired amide product was not observed.

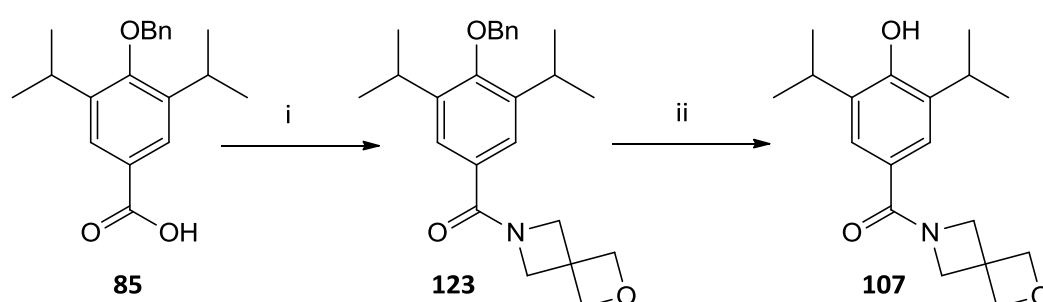


Scheme 4.7. Reagents and conditions: i) Carboxylic acid, EDC, HOBt, spirocyclic oxalate salt, DMF, NMM, 0°C.

We therefore turned our attention to another coupling reagent, (1-[Bis(dimethylamino)methylene]-1H-1,2,3-triazolo[4,5-b]pyridinium3-oxid hexafluorophosphate) (HATU, Figure 4.5). HATU (**122**) has been shown to be very efficient in the synthesis of sterically hindered amide bonds¹⁶.

**122****Figure 4.5.** HATU.

The spirocyclic amine (**113**) and the carboxylic acid (**85**) were dissolved in DMF before HATU (**122**) was added. The reaction mixture was allowed to stir at room for 1 hour before TLC revealed that the reaction had been successful giving the desired amide (**123**) in 50% yield. Subsequent de-protection furnished the desired amide **107** in excellent yields (Scheme 4.8).

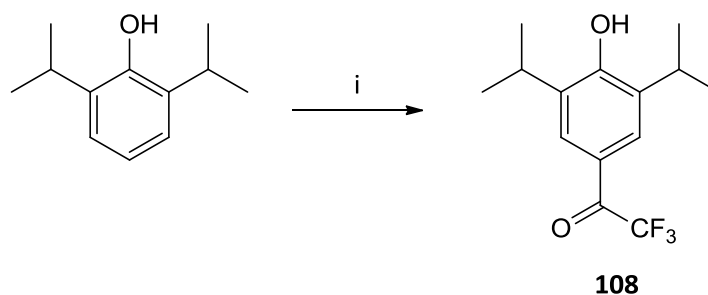


Scheme 4.8. Reagents and conditions: i) Spirocyclic amine, HATU, K₂CO₃, DMF, RT, 1hr¹⁶. ii) Benzyl protected spirocyclic amide, Pd/C, H₂, MeOH, RT, 18hrs, 99% yield¹².

4.1.1 Trifluoromethylation

Incorporation of fluorine into drug candidates has become commonplace. Fluorine can impart a variety of properties to a new chemical entity including, metabolic stability, enhanced binding interactions and changes in physicochemical properties. The strongly electron withdrawing nature of the trifluoromethyl group (CF_3) can have a dramatic effect upon the acidity of carboxylic acids, alcohols, heterocycles and phenols. Therefore, we decided to introduce a CF_3 group to our compounds in an effort to reduce the pK_a of the phenolic hydroxyl group. It is thought that the reduction in the nucleophilicity of the hydroxyl group will, in turn, reduce the rate of phase II clearance.

For the synthesis of compound **108** we utilised Friedel-Crafts acylation, employing trifluoroacetic anhydride to install the carbonyl CF_3 group and aluminium trichloride (AlCl_3) as the Lewis acid catalyst¹⁸.

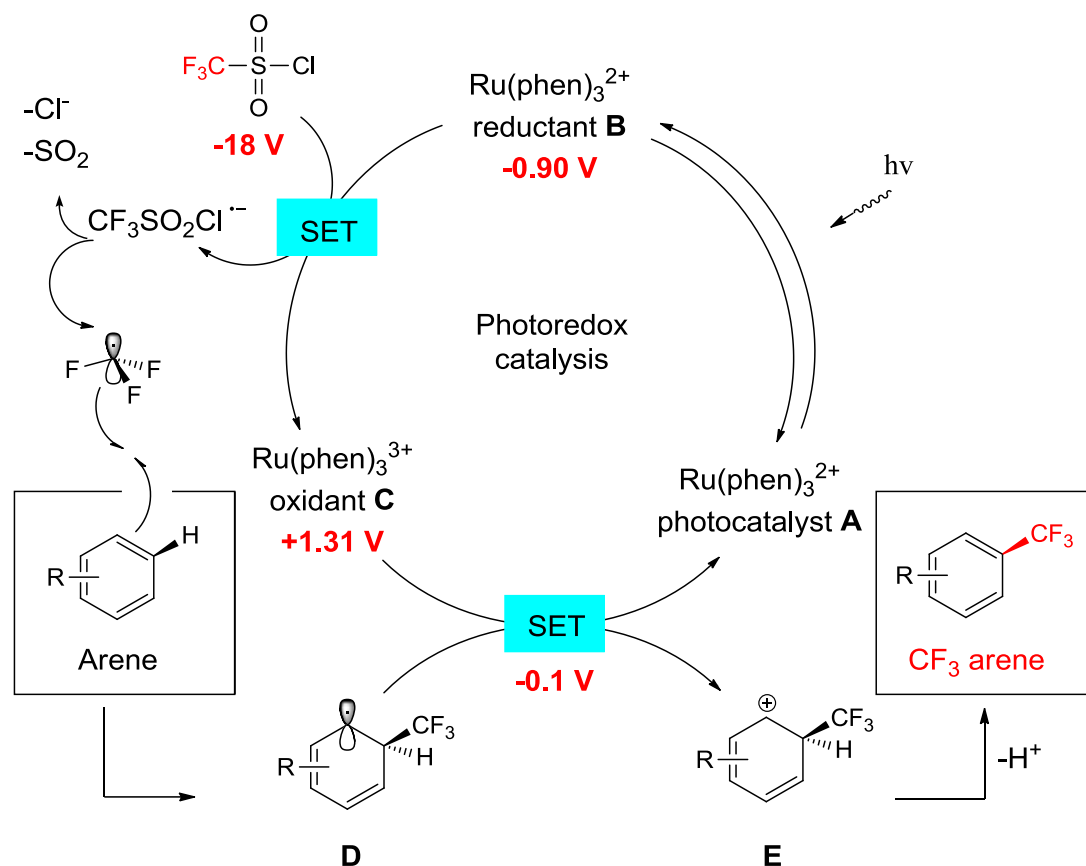


Scheme 4.9. *Reagents and conditions:* i) Trifluoroacetic anhydride, AlCl_3 , DCM, -48°C -RT, 18hrs, 45% yield¹⁸.

The installation of a CF_3 moiety on an arene is typically carried out via cross coupling reactions catalysed by stoichiometric quantities metal salts or organometallic complexes of transition metals¹⁹.

More recently copper and palladium complexes have been successful in enabling this transformation in a catalytic fashion, using an electrophilic or nucleophilic source of CF_3 (Umemoto's or Ruppert-Prakash reagent respectively)²⁰.

However these methods rely on the Pre-functionalisation of the arene with activating groups such as Cl, I or $\text{B}(\text{OH})$ ²¹⁻²⁴. Nagib and MacMillan recently devised a method of direct trifluoromethylation of non-activated arenes by using photoredox catalysis to generate electrophilic CF_3 radicals. Nagib and co-workers utilised $\text{Ru}(\text{phen})_3\text{Cl}_2$, a polypyridyl organometallic complex which is excited by visible light (household light bulb) at room temperature to provide a strongly oxidising or reducing catalyst. Trifluoromethanesulphonyl chloride (TfCl) was chosen as the source of the CF_3 radical due to the ease of handling and relative cost of the reagent (Scheme 4.10)²⁵.

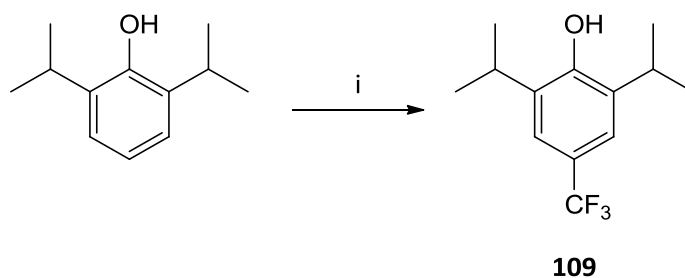


Scheme 4.10. Proposed mechanism for the direct trifluoromethylation of unfunctionalised arenes via photoredox catalysis (reproduced from Nagib²⁵)

The mechanism of the reaction is thought to proceed via excitation of the photocatalyst (**A**) to the higher energy excited state (**B**) by light.

TfCl is reduced by **B** (via single electron transfer SET) to give the radical anion and oxidant **C**. The anion is thought to collapse to give the CF₃ radical which combines with the aromatic system to give **D**. Oxidation of the radical arene by **3** (SET) and facile deprotonation of the resulting cation **E** provides the desired trifluoromethylated arene whilst restoring the catalyst (**A**).

For the synthesis of compound **99** we followed the protocol devised by Nagib and co-workers²²⁴. The catalyst (Ru(phen)₃Cl₂) was added to a vial along with K₂HPO₄ under a blanket of N₂. MeCN, propofol and the TfCl reagent were added to the vial via syringe in order to maintain the anhydrous atmosphere. The vial was placed ~2 cm from a 26 W household light bulb, and the reaction was allowed to stir for 24 hrs. Upon completion the reaction was quenched with water and extracted into EtOAc. Flash chromatography gave the desired product in reasonable yield (42%).

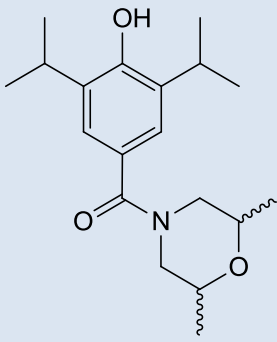
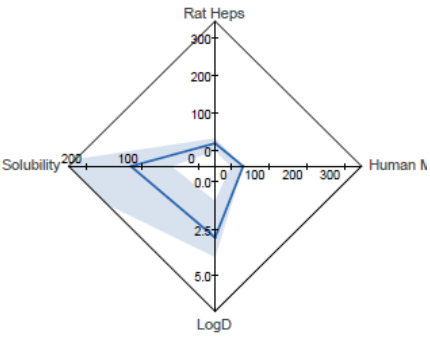
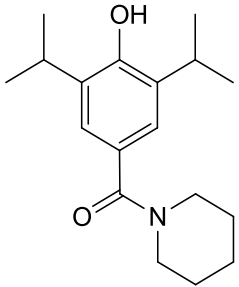
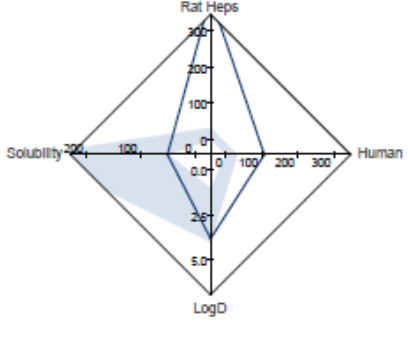
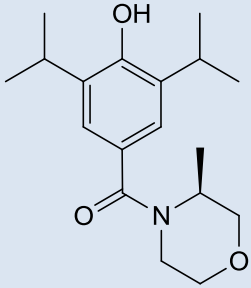
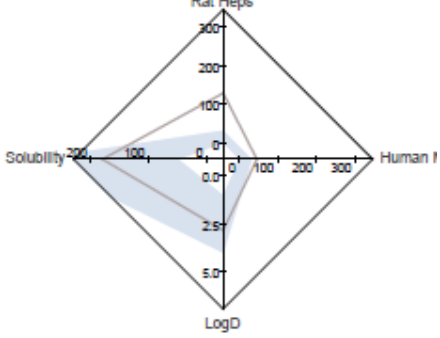


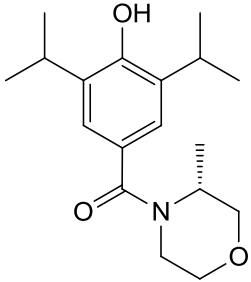
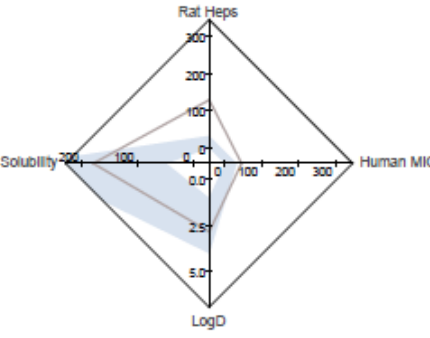
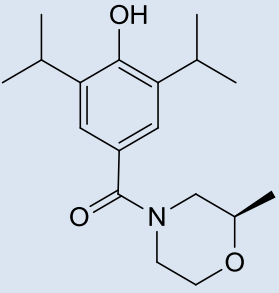
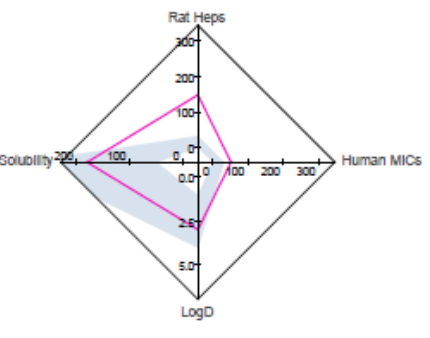
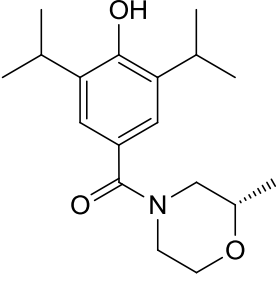
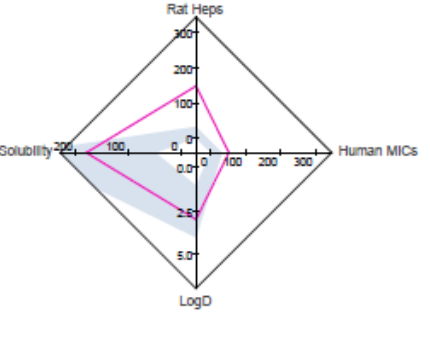
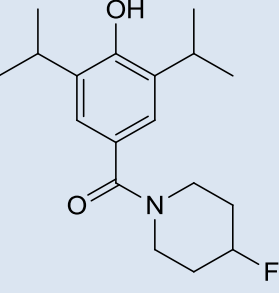
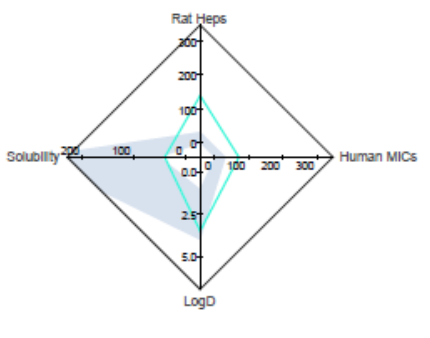
Scheme 4.11. Reagents and conditions: i) Propofol, TfCl, Ru(phen)₃Cl₂, K₂HPO₄, MeCN, 26-W light source, RT, 24 hrs, 42% yield²⁵.

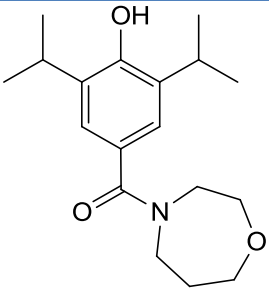
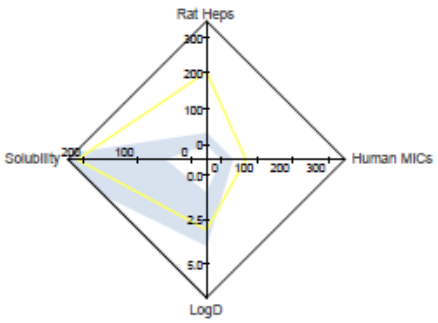
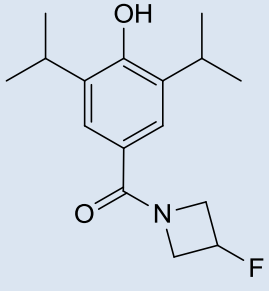
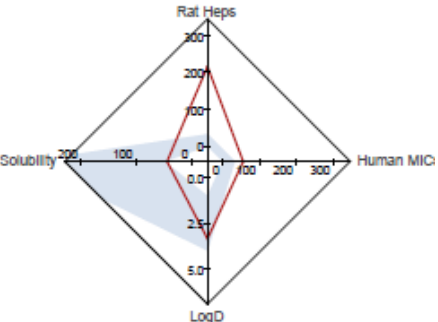
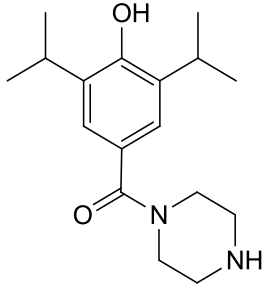
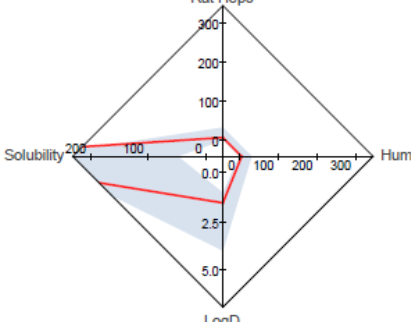
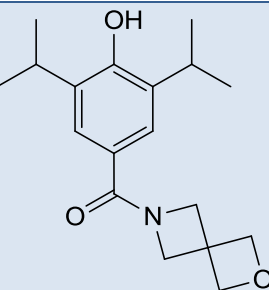
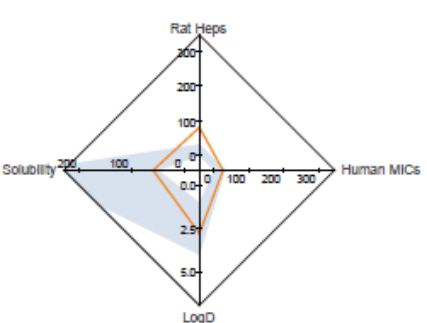
4.2 *In silico* testing

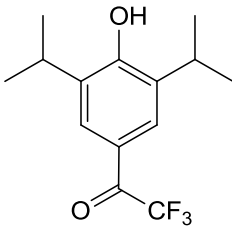
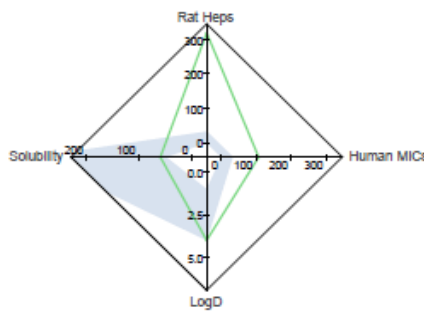
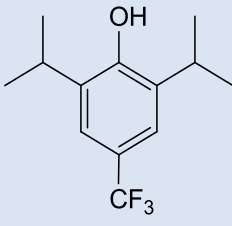
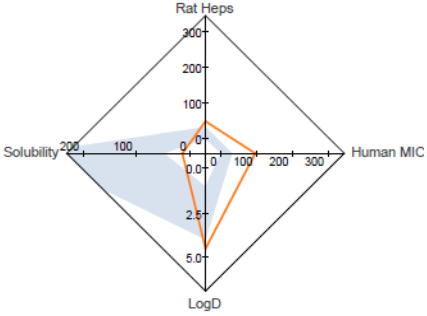
Compounds **97-109** were screened *in silico* in order to ascertain their predicted metabolic stability, aqueous solubility and their distribution co-efficient, ClogD.

Table 4.1. *In silico*^c predictions for compounds **97-109**

Compound	Parameters		Radar plot
 97	ClogD 7.4	2.99	
	Human Mic ($\mu\text{l}/\text{min}/\text{mg}$)	32.36	
	Rat Hep ($\mu\text{l}/\text{min}/10^6$ cells)	19.05	
 98	ClogD 7.4	3.81	
	Human Mic ($\mu\text{l}/\text{min}/\text{mg}$)	107.7	
	Rat Hep ($\mu\text{l}/\text{min}/10^6$ cells)	396.6	
 99	ClogD 7.4	2.81	
	Human Mic ($\mu\text{l}/\text{min}/\text{mg}$)	44.02	
	Rat Hep ($\mu\text{l}/\text{min}/10^6$ cells)	127.9	

 <p>100</p>	ClogD 7.4	2.81	
	Human Mic ($\mu\text{l}/\text{min}/\text{mg}$)	44.02	
	Rat Hep ($\mu\text{l}/\text{min}/10^6$ cells)	127.9	
 <p>101</p>	ClogD 7.4	3.0	
	Human Mic ($\mu\text{l}/\text{min}/\text{mg}$)	52.61	
	Rat Hep ($\mu\text{l}/\text{min}/10^6$ cells)	147.1	
 <p>102</p>	ClogD 7.4	3.0	
	Human Mic ($\mu\text{l}/\text{min}/\text{mg}$)	52.61	
	Rat Hep ($\mu\text{l}/\text{min}/10^6$ cells)	147.1	
 <p>103</p>	ClogD 7.4	3.48	
	Human Mic ($\mu\text{l}/\text{min}/\text{mg}$)	71.13	
	Rat Hep ($\mu\text{l}/\text{min}/10^6$ cells)	138.9	

 <p>104</p>	ClogD 7.4	3.12	
	Human Mic ($\mu\text{l}/\text{min}/\text{mg}$)	68.21	
	Rat Hep ($\mu\text{l}/\text{min}/10^6$ cells)	203.3	
 <p>105</p>	ClogD 7.4	3.38	
	Human Mic ($\mu\text{l}/\text{min}/\text{mg}$)	54.95	
	Rat Hep ($\mu\text{l}/\text{min}/10^6$ cells)	217.5	
 <p>106</p>	ClogD 7.4	1.54	
	Human Mic ($\mu\text{l}/\text{min}/\text{mg}$)	6.92	
	Rat Hep ($\mu\text{l}/\text{min}/10^6$ cells)	4.27	
 <p>107</p>	ClogD 7.4	2.8	
	Human Mic ($\mu\text{l}/\text{min}/\text{mg}$)	23.25	
	Rat Hep ($\mu\text{l}/\text{min}/10^6$ cells)	79.12	

 <p style="text-align: center;">108</p>	ClogD 7.4	4.02	
	Human Mic ($\mu\text{l}/\text{min}/\text{mg}$)	106.3	
	Rat Hep ($\mu\text{l}/\text{min}/10^6$ cells)	321.8	
 <p style="text-align: center;">109</p>	ClogD 7.4	2.54	
	Human Mic ($\mu\text{l}/\text{min}/\text{mg}$)	95.50	
	Rat Hep ($\mu\text{l}/\text{min}/10^6$ cells)	47.86	

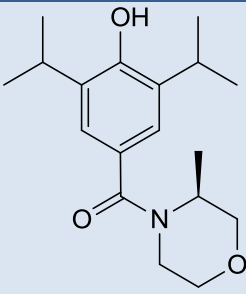
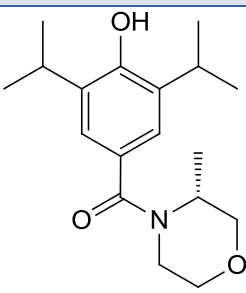
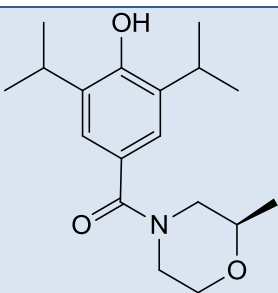
c, In house algorithm.

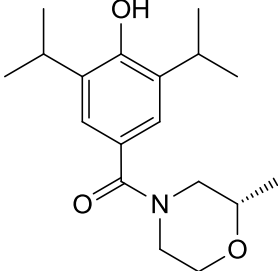
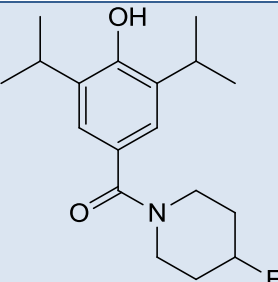
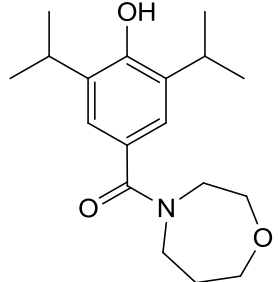
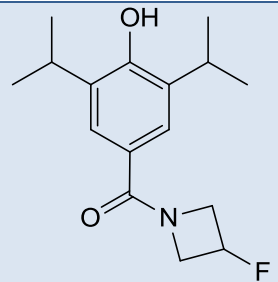
It can be seen from Table 4.1 that several of the compounds screened (**97, 99-102 & 105-107**) are predicted to have an improved rate of phase I clearance, with respect to the previous series. As was noted in the previous chapter the data for the predicted rate of phase II metabolic clearance (rat hepatocytes) should be treated with caution as it does not appear consistent with *in vitro* clearance values. Substituted morpholines **97** and **99-102** appear to have a reduced metabolic liability in human liver microsomes when compared to the unsubstituted morpholines. This may be due to the blockade of CYP450 hydroxylation seen in the phase I metabolism of morpholino compounds²⁶. All the compounds shown in Table 4.1 have ClogD 7.4 values below 4, with several compounds (**97-102, 106, 107 & 109**) now in the optimal range of 1.5-3.0²⁷.

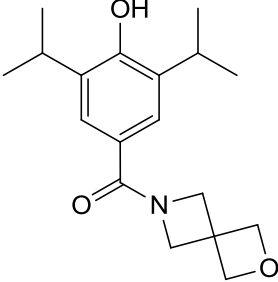
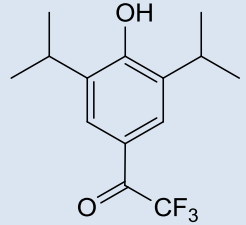
4.2.1 Biological results

Several compounds were selected for testing against $\alpha 1$ GlyR, their EC₅₀ values are shown in Table 4.2

Table 4.2. EC₅₀ values and physicochemical properties for compounds **99-105, 107 &108.**

Compound	$\alpha 1$ GlyR EC ₅₀ (μ M) ^a	ClogP ^b	ClogD ^c	GABA _A EC ₅₀ (μ M) ^d
 99	>1	3.60	2.81	NT
 100	>1	3.60	2.81	NT
 101	0.00006 ± 2.6	3.60	2.81	30 ± 0.159

 102	>1	3.60	2.81	No effect at the highest conc: 30
 103	>1	3.80	3.48	3.3 ± 0.162
 104	>1	2.90	3.12	NT
 105	0.0000012 ± 0.016	3.30	3.38	NT

 <p>107</p>	0.0000016 ± 0.04	3.30	2.80	NT
 <p>188</p>	0.00022	4.46	4.02	3.3 ± 0.489

a, $\alpha 1$ GlyR EC_{50} values determination was carried out at the University of Tübingen under the supervision of Prof. Bodo Laube. **b**, ClogP values were determined using chembiodraw ultra 12 software. **c**, In house algorithm. **d**, GABA_A selectivity testing was carried out at BioFocus®, Chesterford Research Park, Saffron Walden, UK. NT = not tested.

It can be seen from Table 4.2 that of the four monomethyl analogues tested compounds **99**, **100** & **102** ((s)-3 monomethyl, (R)-3-monomethyl and (S)-2-monomethyl morpholine respectively) show no activity below 1 μ M at the $\alpha 1$ GlyR. However, compound **101** ((R)-2-monomethyl shows remarkable activity with an EC_{50} 60 pM. One explanation for this profound increase in activity could be that the (R)-stereochemistry of the methyl group on compound **101** allows it to align with a hydrophobic pocket in the active site boosting potency²⁸.

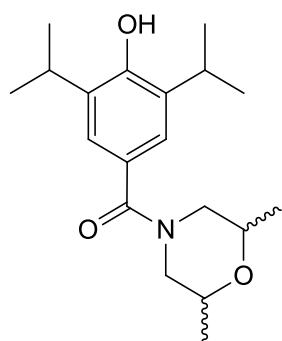
It is also possible that the increased affinity could stem from an increase in shape complementarity between compound **101** and the active site of the $\alpha 1$ GlyR in the bound state, thus reducing the conformational reordering of the active site upon binding of the substrate^{29,30}. Interestingly ring expansion by only one methylene unit, from morpholine (**77**) to homo-morpholine (**104**) has reduced activity from 0.35 nM (**77**) to >1 μ M (**104**).

This could possibly be a consequence of a very constrained binding site. 4-Fluoropiperidine analogue **103** was also shown to be devoid of activity below 1 μM , however, when the ring size was reduced to the more constrained 3-fluoroazetidine analogue, it was found to increase activity to give an EC_{50} of 1.2 μM . Compounds **107** (the spirocyclic surrogate for morpholine) and **108** (trifluoromethyl) were also found to be extremely potent with EC_{50} values of 1.2 μM and 0.22nM respectively.

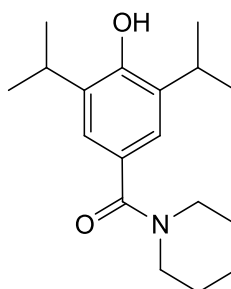
4.2.2 MPO evaluation

The MPO scores of compounds **97-109** were also evaluated to estimate their potential for CNS penetration (Table 4.3).

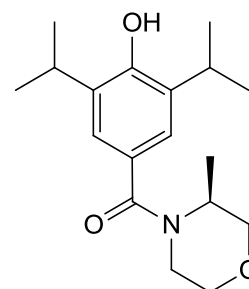
Table 4.3. MPO evaluation for compounds **97-109**.



97



98

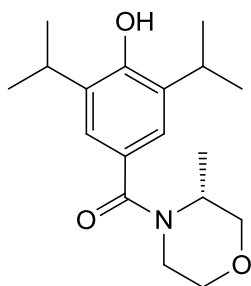


99

Property	Value	T0
ClogP	4.14	0.430
ClogD	4.13	0.000
TPSA	49.77	1.000
MW	319.44	1.000
HBD	1	0.833
pKa	10.08	0.000
CNS MPO		3.3

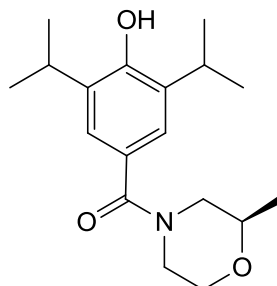
Property	Value	T0
ClogP	4.13	0.435
ClogD	4.48	0.000
TPSA	40.54	1.000
MW	289.41	1.000
HBD	1	0.833
pKa	10.18	0.000
CNS MPO		3.3

Property	Value	T0
ClogP	3.6	0.700
ClogD	3.9	0.050
TPSA	49.77	1.000
MW	305.41	1.000
HBD	1	0.833
pKa	10.08	0.000
CNS MPO		3.6



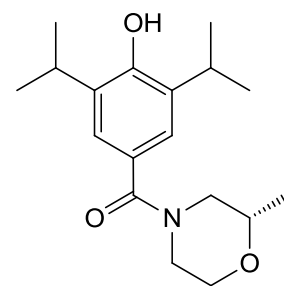
100

Property	Value	T0
ClogP	3.6	0.700
ClogD	3.9	0.050
TPSA	49.77	1.000
MW	305.41	1.000
HBD	1	0.833
pKa	10.08	0.000
CNS MPO		3.6



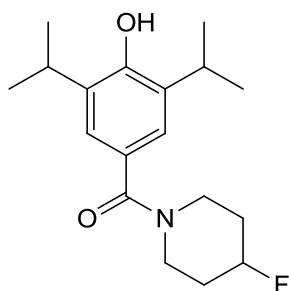
101

Property	Value	T0
ClogP	3.6	0.700
ClogD	3.9	0.050
TPSA	49.77	1.000
MW	305.41	1.000
HBD	1	0.833
pKa	10.08	0.000
CNS MPO		3.6



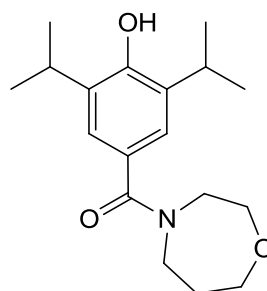
102

Property	Value	T0
ClogP	3.6	0.700
ClogD	3.9	0.050
TPSA	49.77	1.000
MW	305.41	1.000
HBD	1	0.833
pKa	10.08	0.000
CNS MPO		3.6



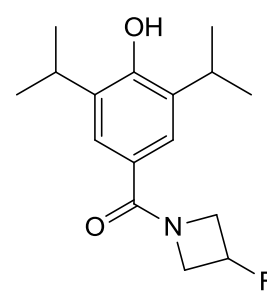
103

Property	Value	T0
ClogP	3.80	0.600
ClogD	4.32	0.000
TPSA	40.54	1.000
MW	307.4	1.000
HBD	1	0.833
pKa	10.18	0.000
CNS MPO		3.4



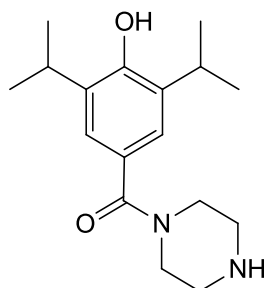
104

Property	Value	T0
ClogP	2.9	1.000
ClogD	3.86	0.070
TPSA	49.77	1.000
MW	305.41	1.000
HBD	1	0.833
pKa	10.13	0.000
CNS MPO		3.9

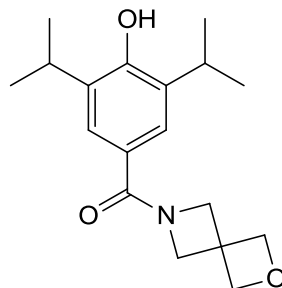


105

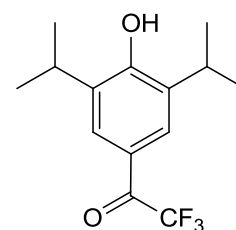
Property	Value	T0
ClogP	3.3	0.850
ClogD	3.57	0.215
TPSA	40.54	1.000
MW	279.35	1.000
HBD	1	0.833
pKa	9.77	0.115
CNS MPO		4.0



106



107

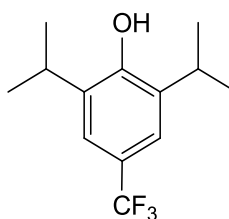


108

Property	Value	T0
ClogP	3.08	0.960
ClogD	1.92	1.000
TPSA	52.57	1.000
MW	290.40	1.000
HBD	1	0.833
pKa	10.14	0.000
CNS MPO		4.8

Property	Value	T0
ClogP	3.30	0.850
ClogD	3.93	0.035
TPSA	49.77	1.000
MW	303.34	1.000
HBD	1	0.833
pKa	10.10	0.000
CNS MPO		3.7

Property	Value	T0
ClogP	4.46	0.270
ClogD	4.0	0.000
TPSA	37.30	0.865
MW	274.30	1.000
HBD	1	0.833
pKa	8.7	0.650
CNS MPO		3.6



109

Property	Value	T0
ClogP	5.33	0.000
ClogD	4.50	0.000
TPSA	20.23	0.012
MW	246.20	1.000
HBD	1	0.833
pKa	9.62	0.190
CNS MPO		2.0

As can be seen from Table 4.3 many of the compounds synthesised now meet the CNS MPO criteria for ClogP (<4 desirable, <3 optimal¹⁵⁸), TPSA (>40, <120 Å²), and MW (<450), with compounds **105** & **106** achieving an overall CNS MPO score of >4 giving rise to a high probability of CNS penetration.

4.2.3 *In vivo* pharmacokinetic studies (rat)

Encouraged by the results of the *in vitro* electrophysiology studies ($EC_{50} = 1.2 \text{ pM}$) and the high CNS MPO score (≥ 4) compound **105** was selected for *in vitro* PK investigations in the rat (Table 4.4).

Table 4.4. PK parameters of compound **105** in the rat. 10 mg/kg p.o. Fasted, male, SD rats. n = 3/group. Vehicle: 10% DMSO, 10% Solutol HS15 and 80% saline at 1 mg/mL. *These investigations were carried out by ChemPartners, Cai Lun Rd, Pudong, Shanghai, 201203, P.R. China

Compound	Pharmacokinetic parameters				
	T _{max} (hr)	C _{max} (ng/mL)	AUC (hr*ng/mL)	T _{1/2} (hr)	F (%)
105	0.5	995 ± 228	2390 ± 448	2.58 ± 0.308	38.8 ± 6.97

Table 4.4 shows that although compound **105** is a highly potent modulator of the $\alpha 1$ GlyR ($EC_{50} = 1.2 \text{ pM}$) it did not perform as well as compound **77** (chapter III, Table 3.15) in the PK studies. Although both **77** & **105** reached Maximum concentration in 30mins, **105** has a much lower exposure than **77** and less than half the bioavailability.

4.2.4 *In vivo* neuropathic pain testing (Chung lesion model in the rat)

Compound **105** (Table 4.3) was further selected for *in vivo* testing in the Chung lesion model of chronic neuropathic pain³¹ (described in Ch II, section **2.2.3**), groups of 6 rats were administered doses of 3, 10 and 30 mg/mg of compound **105**. The effect of **105** was tested at 1, 3, 6 and 24hr time points for reversal of mechanical allodynia and hyperalgesia. The results of the Chung lesion neuropathic pain test are captured below.

% Reversal of mechanical allodynia

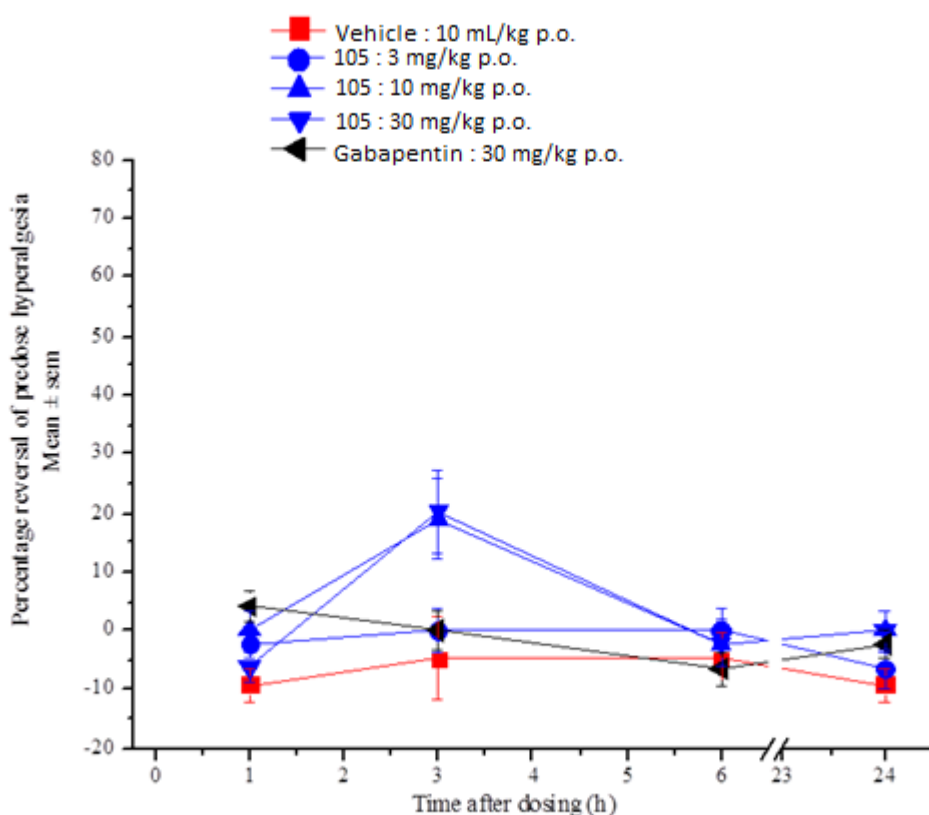


Figure 4.6. The effect of compound **105** on ipsilateral paw withdrawal thresholds to mechanical pressure in neuropathic rats. In comparison with gabapentin. Fasted, male, Wistar rats. n = 6/group. Vehicle: 10% DMSO/10% Solutol HS15/80% saline. 10ml/kg p.o.

The results from the mechanical allodynia test (Figure 4.6) show that compound **105** performed better than the gabapentin at the 3 hour time point (at both 10 & 30 mg/kg) with a 20% reversal of painful symptoms. However, **105** did not perform as well as compound **77** which reached 90% reversal of symptoms at 3 hours post dosing.

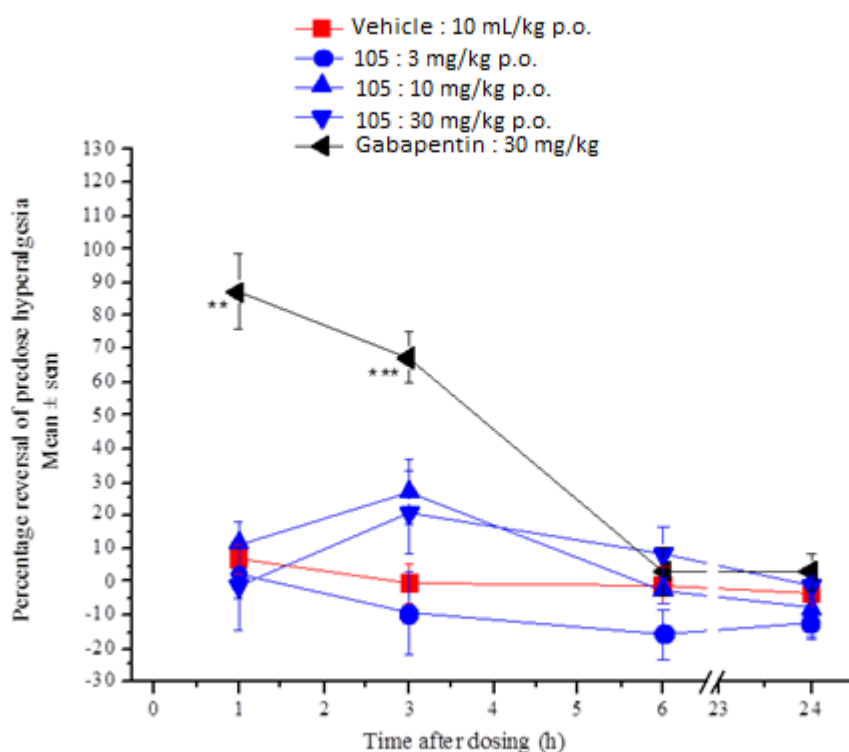
% Reversal of cold hyperalgesia

Figure 4.7. The effect of compound **105** on ipsilateral paw withdrawal thresholds to a cold (10°C) stimulus in neuropathic rats. In comparison with gabapentin. Fasted, male, Wistar rats. n = 6/group. Vehicle: 10% DMSO/10% Solutol HS15/80% saline. 10ml/kg p.o.

In the cold hyperalgesia test compound **105** did not perform as well as compound **77** or the positive control gabapentin. **105** only reached 25% reversal of symptoms at 3 hours, whereas, **77** peaked at 95% and gabapentin reached a maximum of 85% reversal of painful symptoms at the 1hour time point. These results could be a consequence of the lower C_{max}, exposure (AUC) and lower bioavailability of **105** lowering the systemic concentrations of the drug in comparison to **77**.

4.3 Target product profile

The lead optimisation series has identified several highly potent allosteric modulators of the α 1GlyR, exemplified by compound **105**. However, of those compounds that have been examined to date **67** has displayed the most promising results. Encouraged by the potent $EC_{50} = 3.5$ nM at the α 1GlyR, the favourable microsomal stability and PK results both *in vitro* and *in vivo*, the high CNS MPO score (4.4) and also from the high levels of analgesia seen in the Chung lesion neuropathic pain model; compound **77** was chosen to undergo toxicity, cerebrospinal fluid (CSF) and protein binding studies. The results of these tests are summarised in the target product profile table (Table 4.5).

Table 4.5. Target product profile for a novel analgesic compound.

Assay/Model	Desired Criterion	Measured data for Compound 77
Physicochemical properties		
Aqueous solubility ¹	>0.05 mg/mL (pH 7.4)	0.025 mg/mL (pH 7.4)
ClogP ²	<4	3.10
MW ²	<450 (Da)	291 (Da)
TPSA ²	< 90Å ²	49.80 Å ²
Number of rotatable bonds	<8	7
ClogD ³	1-3	2.88
Pka ³	3-9	10.10
Selectivity		
GABA _A R (EC_{50}) ⁴	GABA _A EC_{50} >100x GlyR EC_{50}	30 μ M (>1000x GlyR EC_{50})
Pharmacokinetics		
Oral bioavailability (rat) ¹	>20%	>80%
Stability rat liver ⁵ microsomes	$T_{1/2}$ >60 mins	741 mins
Stability human ¹ hepatocytes	$T_{1/2}$ >30 mins	59 mins

Brain CSF levels ¹	3xEC ₅₀ (free) at 2-3 hrs at 1-3 mg/kg	10 x EC ₅₀
<i>In vitro</i> plasma protein binding (rat) ¹	<99.5%	62%
Safety		
Functional hERG assay ¹	IC ₅₀ > 10µM	IC ₅₀ > 30 µM
Cytotoxicity HepG2 cells ⁶	No cytotoxicity at 500x EC ₅₀ GlyR EC ₅₀	No cytotoxicity below 500 µM
Genotoxicity: Ames ⁶	Negative	Negative
Absence of metabolic alerts	No alerts	No alerts

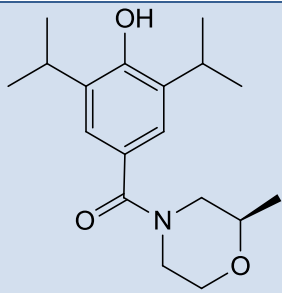
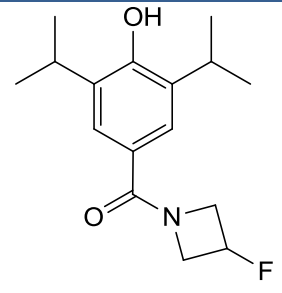
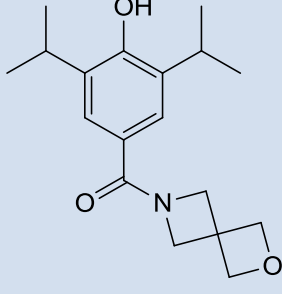
¹Measurements carried out by ChemPartners, Cai Lun Rd, Pudong, Shanghai, 201203, P.R. China. Solubility testing in 100 mM phosphate buffer (pH 7.4), n=2. Oral bioavailability (oral dose 10 mg/kg). Fasted, male, SD rats. n = 3/group. Vehicle: 10% DMSO, 10% Solutol HS15 and 80% saline at 1 mg/mL. Human and rat hepatocytes concentration 1 µM, n=2. Protein binding and CSF, 3 mg/kg dose p.o. vehicle solution in 10%DMSO, 10%Solutol HS 15 and 80%saline at 0.3 mg/mL, n=9. hERG testing using transfected Chinese hamster ovary cells 10⁶. ²Values were determined using chembiowdraw ultra 12 software. ³ Values generated fromACD/labs software. ⁴BioFocus®, Chesterford Research Park, Saffron Walden, UK. 90 mM KCl, 50 mM KF, 11 mM EGTA, 10 mM HEPES, 1 mM MgCl₂, 2 mM Mg-ATP, pH 7.35, n=6. ⁵Human and rat liver microsomes (1mg/mL) at a concentration of 1 µ M in the presence of NADPH for 0, 10, 30 and 60 mins, n = 2. Studies carried out at the Liverpool School of Tropical Medicine. ⁶CHO-K1 cells are incubated with test compound over a 10 point concentration range in duplicate. The *in vitro* micronucleus test (MNT) method uses automated fluorescent cellular imaging (Thermo Scientific Cellomics ArrayScan VTI HCS Reader) to assess cytotoxicity and quantification of micronuclei (genotoxicity). Ames test conc 250 µ/mL of **70** incubated at 37°C for 48hrs with TA98 test strain bacteria, n=6.

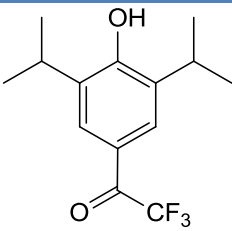
From Table 4.5 it can be seen that the physicochemical properties of compound **77** match our desired criteria with only the solubility falling slightly below the desired level, but it is still within acceptable parameters. Selectivity of **77** for the GlyR against the GABA_A is greater than 1000 fold and the PK parameters all exceed our criteria including the CSF levels (a measure of how much free drug enters the CNS) which are 10 fold higher than the EC₅₀ value (3.5 nM) and protein binding, which is 62%, giving high levels of unbound drug to target the GlyR. The results of the toxicity tests (described in chapter II, section **2.4.1**) are very favourable. The hERG IC₅₀ is 30 µM, 3 times higher than the minimum required, there appears to be no cytotoxicity detected up to the maximum concentration examined (500 µM) and the results of the Ames test showed no genotoxicity.

4.4 Summary

This chapter has highlighted the lead optimisation and biological evaluation of a series of novel propofol amide analogues targeting the $\alpha 1$ GlyR. Among the compounds synthesised we have identified several highly potent allosteric modulators of the $\alpha 1$ GlyR (Table 4.6).

Table 4.6. EC₅₀ values and physicochemical properties for the most potent lead optimised compounds.

Compound	$\alpha 1$ GlyR EC ₅₀ (μ M) ^a	ClogP ^b	ClogD ^c	GABA _A EC ₅₀ (μ M) ^d
 101	0.00006 ± 2.6	3.60	2.81	30 ± 0.159
 105	0.0000012 ± 0.016	3.30	3.38	NT
 107	0.0000016 ± 0.04	3.30	2.80	NT

 <p style="text-align: center;">108</p>	0.00022	4.46	4.02	3.3 ± 0.489
---	---------	------	------	-------------

a, $\alpha 1$ GlyR EC_{50} values determination was carried out at the University of Tübingen under the supervision of Prof. Bodo Laube. **b**, ClogP values were determined using chembiodraw ultra 12 software. **c**, In house algorithm **d**, GABA_A selectivity testing was carried out at BioFocus®, Chesterford Research Park, Saffron Walden, UK.

Lead optimised compounds **97-109** were assessed *in silico* in order to ascertain their predicted metabolic clearance (Table 4.1). As noted earlier the predicted rat hepatocyte data was inconsistent with *in vitro* data, therefore it was treated with caution. In general the predicted microsomal data was improved and the MPO score of one of the most potent compounds **95** is in the optimal range of ≥ 4 .

Pharmacokinetic studies for compound **95** show that although an oral dose of 10 mg/kg is absorbed quickly ($T_{max} = 0.5$ hr) the C_{max} is moderate (995 ng/mL) as is the exposure ($AUC = 2390$ hr*nh/mL) and bioavailability ($F = 38.8\%$).

In vivo testing in the Chung lesion model for neuropathic pain showed a 10 mg/kg dose of compound **105** could outperform a 30 mg/kg dose of the current 'gold standard' treatment for chronic pain, gabapentin, by delivering a 20% reversal of painful symptoms in the mechanical allodynia test. In the cold hyperalgesia test compound **105** showed a 25% reversal of painful symptoms.

At the time of writing this thesis work is on-going with the lead optimised series and we are awaiting further results from the $\alpha 1$ GlyR electrophysiology studies for compounds **97, 98, 106 & 109**.

4.5 References

- 1 Palm, K., Luthman, K., Ros, J., Gråsjö, J. & Artursson, P. Effect of molecular charge on intestinal epithelial drug transport: pH-dependent transport of cationic drugs. *Journal of Pharmacology and Experimental Therapeutics* **291**, 435-443 (1999).
- 2 Fischer, H., Gottschlich, R. & Seelig, A. Blood-brain barrier permeation: molecular parameters governing passive diffusion. *The Journal of membrane biology* **165**, 201-211 (1998).
- 3 Wager, T. T., Hou, X., Verhoest, P. R. & Villalobos, A. Moving beyond Rules: The Development of a Central Nervous System Multiparameter Optimization (CNS MPO) Approach To Enable Alignment of Druglike Properties. *ACS Chemical Neuroscience* **1**, 435-449, (2010).
- 4 Wu, X. & Larhed, M. Microwave-Enhanced Aminocarbonylations in Water. *Organic Letters* **7**, 3327-3329, (2005).
- 5 Cheprakov, A. V., Ponomareva, N. V. & Beletskaya, I. P. Palladium catalyzed carbonylation of iodoarenes in aqueous solubilized systems. *Journal of Organometallic Chemistry* **486**, 297-300, (1995).
- 6 Uozumi, Y. & Watanabe, T. Green Catalysis: Hydroxycarbonylation of Aryl Halides in Water Catalyzed by an Amphiphilic Resin-Supported Phosphine-Palladium Complex. *The Journal of Organic Chemistry* **64**, 6921-6923, (1999).
- 7 Roth, B. Baccanari, D. P., Sigel, C. W., Hubbell, J. P., Eaddy, J., Kao, J. C., Grace, M. E., Rauckman, B. S.. 2,4-diamino-5-benzylpyrimidines and analogs as antibacterial agents .9. lipophilic trimethoprim analogs as antigonococcal agents. *Journal of Medicinal Chemistry* **31**, 122-129, (1988).
- 8 Wuts, P.G.M. & Greene, T.W. Protection for Phenols and Catechols. in *Greene's Protective Groups in Organic Synthesis* 367-430 (John Wiley & Sons, Inc., 2006).
- 9 Brzasczcz, M., Kloc, K., Maposah, M. & Mlochowski, J. Selenium(IV) Oxide Catalyzed Oxidation of Aldehydes to Carboxylic Acids with Hydrogen Peroxide. *Synthetic Communications* **30**, 4425-4434,
- 10 Mullican, m.d., Wilson, M. W., Connor, D. T., Kostlan, C. R., Schrier, D. J., Dyer, R. D . design of 5-(3,5-di-tert-butyl-4-hydroxyphenyl)-1,3,4-thiadiazoles, 5-(3,5-di-tert-butyl-4-hydroxyphenyl)-1,3,4-oxadiazoles, and 5-(3,5-di-tert-butyl-4-hydroxyphenyl)-1,2,4-triazoles as orally-active, nonulcerogenic antiinflammatory agents. *journal of medicinal chemistry* **36**, 1090-1099 (1993).
- 11 Ziakas, G.N., Rekka, E.A., Gavalas, A.M., Eleftheriou, P.T. & Kourounakis, P.N. New analogues of butylated hydroxytoluene as anti-inflammatory and antioxidant agents. *Bioorganic & Medicinal Chemistry* **14**, 5616-5624 (2006).

- 12 Martinez-Solorio, D. & Jennings, M.P. Convergent Formal Syntheses of (±)-Brussonol and (±)-Abrotanone via an Intramolecular Marson-Type Cyclization. *Organic Letters* **11**, 189-192 (2008).
- 13 Fletcher, S. & Gunning, P. T. Mild, efficient and rapid O-debenzylation of ortho-substituted phenols with trifluoroacetic acid. *Tetrahedron Letters* **49**, 4817-4819
- 14 Burkhard, J. A., Wuitschik, G., Rogers-Evans, M., Müller, K. & Carreira, E. M. Oxetanes as Versatile Elements in Drug Discovery and Synthesis. *Angewandte Chemie International Edition* **49**, 9052-9067, (2010)
- 15 Sheehan, J., Cruickshank, P. & Boshart, G. Notes- A Convenient Synthesis of Water-Soluble Carbodiimides. *The Journal of Organic Chemistry* **26**, 2525-2528, (1961). Montalbetti, C. A. G. N. & Falque, V. Amide bond formation and peptide coupling. *Tetrahedron* **61**, 10827-10852, (2005).
- 16 Montalbetti, C. A. G. N. & Falque, V. Amide bond formation and peptide coupling. *Tetrahedron* **61**, 10827-10852,
- 17 Iwasawa, T., Wash, P., Gibson, C. & Rebek, J. Reaction of an Introverted Carboxylic Acid with Carbodiimide. *Tetrahedron* **63**, 6506-6511, (2007).
- 18 Stewart, D. S. Savechenkov, P.Y., Dostalova, Z., Chiara, D.C., Ge, R., Raines, D E., Cohen, J.B., Forman, S. A., Bruzik, K.S., Miller, K.W. p-(4-Azipentyl)propofol: A Potent Photoreactive General Anesthetic Derivative of Propofol. *Journal of Medicinal Chemistry* **54**, 8124-8135, (2011).
- 19 Tomashenko, O. A. & Grushin, V. V. Aromatic Trifluoromethylation with Metal Complexes. *Chemical Reviews* **111**, 4475-4521, (2011).
- 20 Hagmann, W. K. The many roles for fluorine in medicinal chemistry. *Journal of Medicinal Chemistry* **51**, 4359-4369, (2008).
- 21 Furuya, T., Kamlet, A. S. & Ritter, T. Catalysis for fluorination and trifluoromethylation. *Nature* **473**, 470-477, (2011).
- 22 Oishi, M., Kondo, H. & Amii, H. Aromatic trifluoromethylation catalytic in copper. *Chemical Communications*, 1909-1911, (2009).
- 23 Cho, E. J. Senecal, T.D., Kinzel, T., Zhang, Y., Watson, D. A., Buchwald, S. L. The Palladium-Catalyzed Trifluoromethylation of Aryl Chlorides. *Science* **328**, 1679-1681, doi:10.1126/science.1190524 (2010).
- 24 Xu, J. Luo, Dong-Fen., Xiao, Bin., Liu, Zhao-Jing., Gong, Tian-Jun., Fu, Yao., Liu, Lei. Copper-catalyzed trifluoromethylation of aryl boronic acids using a CF₃⁺ reagent. *Chemical Communications* **47**, 4300-4302, (2011).
- 25 Nagib, D. A. & MacMillan, D. W. C. Trifluoromethylation of arenes and heteroarenes by means of photoredox catalysis. *Nature* **480**, 224-228, (2011).
- 26 Combourieu, B., Besse, P., Sancelme, M., Godin, J. P., Monteil, A., Veschambre, H., Delort, A. M. Common degradative pathways of

- morpholine, thiomorpholine, and piperidine by *Mycobacterium aurum* MO1: Evidence from H-1-nuclear magnetic resonance and ionspray mass spectrometry performed directly on the incubation medium. *Applied and Environmental Microbiology* **66**, 3187-3193, (2000).
- 27 Personal Communication.
- 28 Leung, C. S., Leung, S. S. F., Tirado-Rives, J. & Jorgensen, W. L. Methyl Effects on Protein–Ligand Binding. *Journal of Medicinal Chemistry* **55**, 4489-4500, (2012).
- 29 Schärfer, C. Schulz-Gasch, T., Ehrlich, Hans-Christian., Guba, W., Rarey, M., Stahl, M. Torsion Angle Preferences in Druglike Chemical Space: A Comprehensive Guide. *Journal of Medicinal Chemistry* **56**, 2016-2028, (2013).
- 30 Schönherr, H. & Cernak, T. Profound Methyl Effects in Drug Discovery and a Call for New C–H Methylation Reactions. *Angewandte Chemie International Edition* **52**, 12256-12267, (2013).
- 31 Yoon, C., Young Wook, Y., Heung Sik, N., Sun Ho, K. & Jin Mo, C. Behavioral signs of ongoing pain and cold allodynia in a rat model of neuropathic pain. *Pain* **59**, 369-376, (1994).

Chapter V

Conclusions

Contents

5.0 Conclusions 204

5.1 References 213

5 Conclusions

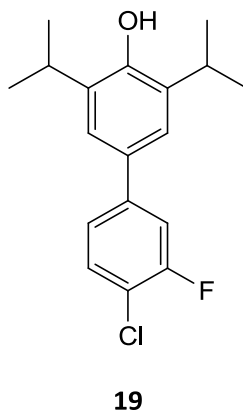
The aims of this thesis were to identify novel analgesic compounds based around a 2,6-diisopropylphenol (propofol) core scaffold, which selectively target the $\alpha 1$ subtype of the strychnine sensitive glycine receptor ($\alpha 1$ GlyR). Our objective was to generate lead optimised compounds which display favourable *in vitro*, *in vivo* activity, acceptable pre-clinical toxicology and ADME properties as defined in our target product profile (Table 5.1).

Table 5.1. Target product profile for a novel analgesic compound

Assay/Model	Desired Criterion
Physicochemical properties	
Aqueous solubility	>0.05 mg/mL (pH 7.4)
ClogP	<4
MW	<450 (Da)
TPSA	< 90Å ²
Number of rotatable bonds	<8
ClogD	1-3
Pka	3-9
Selectivity	
GABA _A R (EC ₅₀)	GABAA EC ₅₀ >100x GlyR EC ₅₀
Pharmacokinetics	
Oral bioavailability (rat)	>20%
Stability rat liver microsomes	T _{1/2} >60 mins
Stability human hepatocytes	T _{1/2} >30 mins
Brain CSF levels	3xEC ₅₀ (free) at 2-3 hrs at 1-3 mg/kg
<i>In vitro</i> plasma protein binding (rat)	<99.5%
Safety	
Functional hERG assay	IC ₅₀ > 10µM
Cytotoxicity HepG2 cells	No cytotoxicity at 500x EC ₅₀ GlyR EC ₅₀
Genotoxicity: Ames	Negative
Absence of metabolic alerts	No alerts

Chapter I described the background to the problem of chronic pain, the deficiencies of the current treatments and the clinical need, not only for new treatments but also for novel therapeutic targets. The $\alpha 1$ GlyR was introduced as one such novel target and the role it plays in the nociceptive system was discussed as were the potential advantages of targeting the $\alpha 1$ GlyR. The anaesthetic compound propofol was shown to be a modulator of the GlyR and the attributes of this compound were discussed in detail as were the potential disadvantages of off target effects at the GABA_AR such as dizziness and sedation. The difficulties of crossing the blood brain barrier and entering the central nervous system to access the $\alpha 1$ GlyR were also presented.

Chapter II focused upon optimising a series of bi-phenyl propofol analogues which had been previously synthesised within the group. Although the bi-phenyl analogues had been shown to be highly potent modulators of the $\alpha 1$ GlyR (exemplified by **19**, Figure 5.1) they demonstrated very poor physicochemical and pharmacokinetic properties.



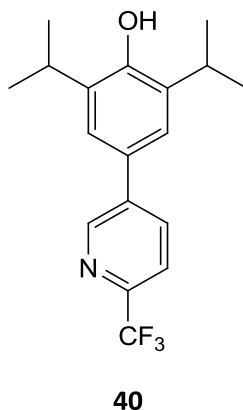
$EC_{50} = 0.00007 \mu\text{M}$

$\text{ClogP} = 6.75$

$\text{ClogD}_{7.4} = 6.0$

Figure 5.1. Compound **19**, the most potent of the bi-phenyl series previously synthesised within the group.

Therefore in an effort to increase solubility, improve physicochemical parameters (ClogP & ClogD) and retain activity, a small library of compounds was synthesised containing 'solubilising' heterocyclic groups (**28-44**, chapter II, section **2.7**). Of the heterocyclic compounds tested only one compound (**40**) showed the low nM activity seen with the previously synthesised bi-phenyl compounds (Figure 5.2).



$EC_{50} = 0.0001 \mu\text{M}$

$\text{ClogP} = 5.55$

$\text{ClogD}_{7.4} = 5.03$

Figure 5.2. Compound **40** the only heterocycle synthesised demonstrating low nM activity at the $\alpha 1$ GlyR.

Although **40** was active against the $\alpha 1$ GlyR, it was apparent that the ClogP and ClogD parameters were still above optimal ($\text{ClogP} < 3$, $\text{ClogD} > 1$, < 3) for maximum probability of crossing the BBB and entering the CNS¹. However, compound **30** did not meet the criteria for GABA_AR selectivity, set out in the target product profile (Table 5.1) as it was found to be a potent modulator of the GABA_AR ($EC_{50} = 0.12 \mu\text{M} \pm 0.012$) and, therefore, was discontinued due to the unwanted sedative effect from this receptor.

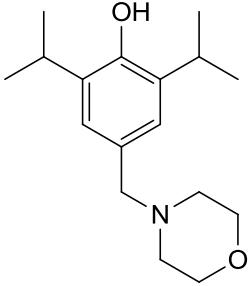
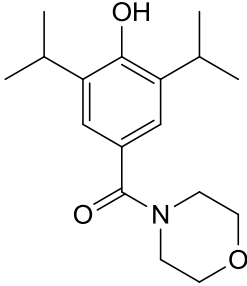
During the development of the heterocyclic compounds (**28-44**) a series of papers from a team at Pfizer were published detailing the use of a multiparameter optimisation (MPO) calculator to aid in the development of drugs acting within the CNS². The CNS MPO calculator gives compounds an overall score based upon the evaluation of six molecular descriptors, ClogP , ClogD , TPSA, MW, HBD and pKa. The summation of the transformed values for these descriptors is given as the overall CNS MPO score, with a score ≥ 4 being required for optimal probability of CNS penetration (chapter II, section 2.8.1).

MPO evaluation of the heterocyclic series showed that none of the compounds synthesised met this criteria, therefore, we terminated the bi-phenyl and heterocycle series and re-evaluated our design strategy.

Chapter III detailed the synthesis of a series of 2,6-diisopropyl and 2,6-di-*tert*-butyl *para*-amino alkyl analogues of propofol (**49-55** & **60-64**). Several of the *para*-amino analogues were tested for efficacy against the α 1 GlyR, however, none of the compounds tested showed activity below 1 μ M. Furthermore MPO evaluation of compounds **49-55** & **60-64** revealed that, there was a low probability of CNS penetration with all compounds recording an overall MPO score <4. An additional potential liability with the *para*-amino alkyl template was the possible formation of a toxic metabolic intermediate (quinone methide)^{3,4}.

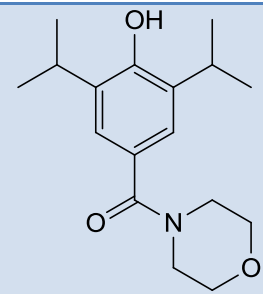
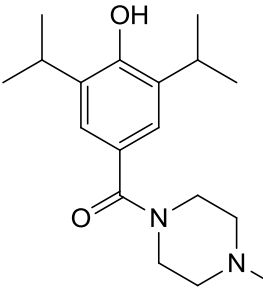
With these facts in mind, the decision was taken to install carbonyl functionality at the site of quinone methide formation to increase predicted metabolic stability and improve the MPO score (Table 5. 2).

Table 5. 2. Improved predicted metabolic stability and MPO for amide analogues.

Compound	Human Mic (μ l/min/mg)	Rat Hep (μ l/min/10 ⁶)	MPO
 49	84.35	333.5	3.8
 77	31.21	87.41	4.4

Upon testing the amide series compounds **77** & **78** were shown to have low nM activity at the α 1 GlyR (Table 5.3).

Table 5.3. *In vitro* EC₅₀ values for amide linked compounds tested against the recombinant α 1GlyR

Structure	EC ₅₀ (μ M)	ClogP	ClogD	MPO
 <p>77</p>	0.00035 \pm 0.00002	3.10	2.80	4.4
 <p>78</p>	0.0000012 \pm 0.4	3.54	2.30	4.4

MPO evaluation of compound **77** revealed a good MPO score of 4.4. *In vivo* pharmacokinetic (PK) analysis (rat) showed that compound **77** is well absorbed (C_{max} = 4605 ng/mL) has a large exposure (AUC = 20135 hr*ng/mL) a moderate half-life (2.58 hr) and a high bioavailability (F = 85%) (chapter III, section 3.3.2). Compound **77** was also tested for off-target activity at the GABA_AR no activity observed below 30 μ M.

In vitro proof of concept studies in the Chung lesion model of neuropathic pain showed compound **77** performed better than the positive control, lamotrigine, with a 10 mg/kg dose reversing the painful symptoms of mechanical allodynia by 90% and reversing the symptoms of cold hyperalgesia by 95% (at a dose of 30 mg/kg).

Chapter IV Lead optimisation of the amide template revealed several more compounds with low nM activity at the $\alpha 1$ GlyR (compounds **101**, **105**, **107** & **108**). Compound **95** was further selected to undergo *in vitro* neuropathic pain studies where it performed better than the current 'gold standard' treatment for chronic neuropathic pain, gabapentin, with a maximum reversal of 20% in the mechanical allodynia test.

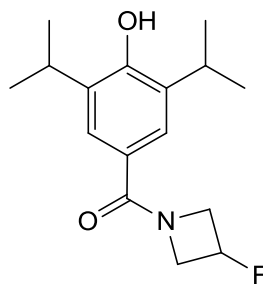


Figure 5.3. Compound **105** EC_{50} = 1.2 pM at the $\alpha 1$ GlyR.

However, compound **105** did not perform as well as the positive control, gabapentin, in the test for cold hyperalgesia, reaching a 25% reversal whereas gabapentin reached a maximum of 90%.

To conclude, we have identified several highly potent allosteric modulators of the $\alpha 1$ GlyR, exemplified by compound **107** (EC_{50} = 3.5 nM), which displays favourable DMPK properties, no toxicity (Table 5.4) and has demonstrated a high level of analgesia (>90% in both mechanical allodynia and cold hyperalgesia) in the Chung lesion model for neuropathic pain.

Table 5.4. Compound **77** mapped onto our target product profile.

Assay/Model	Desired Criterion	Measured data for Compound 67
Physicochemical properties		
Aqueous solubility	>0.05 mg/mL (pH 7.4)	0.025 mg/mL (pH 7.4)
ClogP	<4	3.10
MW	<450 (Da)	291 (Da)
TPSA	< 90Å ²	49.80 Å ²
Number of rotatable bonds	<8	7
ClogD	1-3	2.88
Pka	3-9	10.10
Selectivity		
GABA _A R (EC ₅₀)	GABA _A EC ₅₀ >100x GlyR EC ₅₀	30 µM (>1000x GlyR EC ₅₀)
Pharmacokinetics		
Oral bioavailability (rat)	>20%	>80%
Stability rat liver microsomes	T _{1/2} >60 mins	741 mins
Stability human hepatocytes	T _{1/2} >30 mins	59 mins
Brain CSF levels	3xEC ₅₀ (free) at 2-3 hrs at 1-3 mg/kg	10 x EC ₅₀
<i>In vitro</i> plasma protein binding (rat)	<99.5%	62%
Safety		
Functional hERG assay	IC ₅₀ > 10µM	IC ₅₀ > 30 µM
Cytotoxicity HepG2 cells	No cytotoxicity at 500x EC ₅₀ GlyR EC ₅₀	No cytotoxicity below 500 µM
Genotoxicity: Ames	Negative	Negative
Absence of metabolic alerts	No alerts	No alerts

At the time of writing this thesis compound **77** is undergoing further *in vivo* testing in an animal model of diabetic neuropathy.

This study has also identified several other potential lead compounds with low nM activity at the α 1 GlyR (**101**, **105** & **107**) from the *i*-pr-amide template. Development of these compounds is on-going.

5.1 References

- 1 Pajouhesh, H. & Lenz, G. R. Medicinal chemical properties of successful central nervous system drugs. *NeuroRx : the journal of the American Society for Experimental NeuroTherapeutics* **2**, 541-553, (2005).
- 2 Wager, T. T., Hou, X., Verhoest, P. R. & Villalobos, A. Moving beyond Rules: The Development of a Central Nervous System Multiparameter Optimization (CNS MPO) Approach To Enable Alignment of Druglike Properties. *ACS Chemical Neuroscience* **1**, 435-449, (2010).
- 3 Monks, T. J. & Jones, D. C. The Metabolism and Toxicity of Quinones, Quinonimines, Quinone Methides, and Quinone-Thioethers. *Current Drug Metabolism* **3**, 425-438, (2002).
- 4 Bolton, J. L., Trush, M. A., Penning, T. M., Dryhurst, G. & Monks, T. J. Role of Quinones in Toxicology†. *Chemical Research in Toxicology* **13**, 135-160, (2000).

Chapter VI

Experimental

Chemistry

General

Reactions that were air and moisture sensitive were performed under a nitrogen atmosphere. This was achieved with oven dried or flame dried glassware sealed with a rubber septa. Dry nitrogen gas was introduced *via* a manifold or balloon.

Reactions were stirred using Teflon-coated magnetic stir bars. Organic solutions were concentrated using a Büchi rotary evaporator with a diaphragm vacuum pump. Anhydrous solutions and sensitive liquids were transferred *via* syringe.

Purification of solvents and reagents

Anhydrous solvents were obtained from commercial sources or dried and distilled prior to use. The distillation was under the flow of dry nitrogen. THF was distilled from sodium. Dichloromethane was distilled from calcium hydride. All reagents were purchased from Sigma Aldrich or Alfa Aesar and were used without purification unless otherwise indicated.

Purification of products

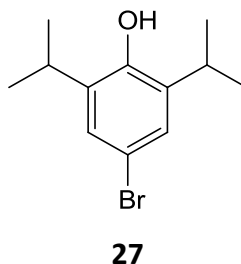
Analytical thin layer chromatography (TLC) was performed with 0.25 mm Merck silica gel 60 F254 plates with 254 nm fluorescent indicator. Plates were visualised by U.V. at 254 nm or treated with *p*-anisaldehyde solution, ninhydrin or potassium permanganate followed by gentle heating. Chromatographic purification of products was accomplished by flash column chromatography unless otherwise indicated.

Analysis

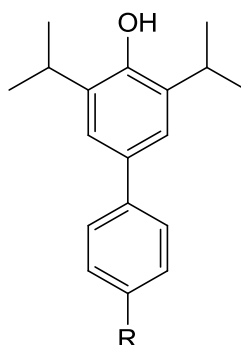
^1H NMR spectra were measured on a Bruker AMX400 (400 MHz) nuclear magnetic resonance spectrometer. The data for ^1H NMR spectra are reported as follows: chemical shifts were described in parts per million (δ , ppm) downfield from an internal reference of trimethylsilane. Integration. Multiplicities: (s = singlet, d = doublet, t = triplet, q = quartet, dd = doublet of doublets, dt = doublet of triplets, td = triplet of doublets, m = multiplet and Hept = heptet). Coupling (J , Hz). ^{13}C NMR spectra were measured on a Bruker AMX400 (100 MHz) and are reported in terms of chemical shift (δ , ppm) relative to residual solvent peak. Mass spectrometry (MS) and High Resolution Mass Spectrometry (HRMS) were recorded on a VG analytical 7070E machine, Frisons TRIO spectrometers or Agilent QTOF 7200 using chemical ionisation (CI) or electron ionisation (EI). Micromass LCT mass spectrometer used electron spray ionisation (ESI). Elemental analysis (%C, %H, %N) were determined by the University of Liverpool Microanalysis Laboratory. Melting points were determined on a Gallenkamp melting point apparatus in degrees Celsius and are uncorrected. Full characterisation was performed on final compounds that were tested in various assays. Intermediates were characterised ^1H NMR ^{13}C NMR and Mass spectrometry techniques.

6.0 Synthesis

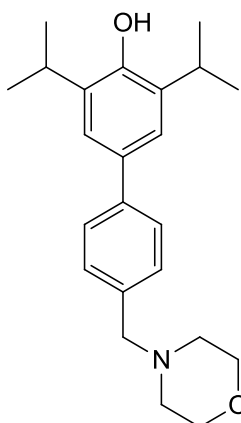
4-Bromo-2,6-diisopropylphenol¹



Bromine (1.2 mL, 24 mmol) was added drop wise to a stirred solution of 2,6-diisopropylphenol (3.7 mL, 20 mmol) in glacial acetic acid (60 mL). The resulting solution was allowed to stir at room temperature for 1 hour. Upon completion the reaction was quenched with H₂O (50 mL), extracted with EtOAc (3 x 50 mL) and washed with brine. The resulting organic extracts were dried over MgSO₄ and concentrated under vacuum. The product was purified by column chromatography (10:90 EtOAc/Hexane) to afford the product as an orange oil (4.0 g, 80% yield) ¹H NMR (400 MHz, CDCl₃) δ 7.14 (s, 2H), 4.81 (s, 1H), 3.12 (hept, *J* = 6.8 Hz, 2H), 1.24 (d, *J* = 6.8 Hz, 12H). ¹³C NMR (101 MHz, CDCl₃) δ 149.43, 136.43, 126.85, 113.57, 27.46, 22.97. MS: [M+H]⁺ C₁₂H₁₈BrO requires: 257.0536, found: 257.0530.

General procedure 1. Suzuki coupling reaction

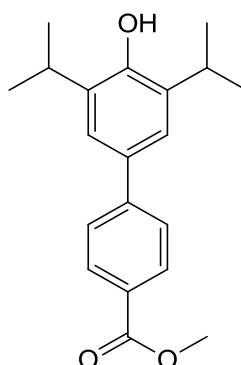
4-Bromo-2,6-diisopropylphenol (1eq) was added to a stirred suspension of substituted boronic acid (2.0 eq), tetrakis(diphenylphosphino)palladium (5 mol%) and potassium carbonate (3.2 eq) in a solution of THF (10 mL/g) and H₂O (5 mL/g) in THF (10 mL/g). The resulting mixture was heated under reflux for 24 hours at 80°C. The reaction was monitored by TLC (EtOAc/n-Hexane) and upon completion the reaction was quenched with HCl (50 mL/g) and was extracted with EtOAc (3 x 30 mL). The combined organic extracts were washed with H₂O, brine, dried over MgSO₄ and concentrated under vacuum. The products were purified by column chromatography (EtOAc/n-Hexane).

3,5-diisopropyl-4-(morpholinomethyl)-(1-1-biphenyl)-4-ol

28

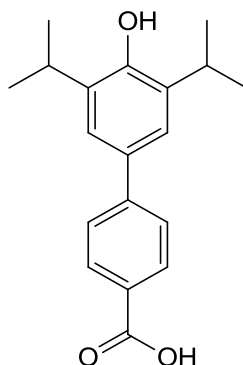
4-Bromo-2,6-diisopropylphenol (318mg, 1.24mmol) was reacted with (4-orpholinomethyl)phenyl)boronic acid (548 mg, 2.47 mmol) according to **general procedure 1**, the crude product was purified by column chromatography (80:20 EtOAc/Hexane) to afford the product as a white solid (210mg, 48% yield). mp = 178-180°C: ^1H NMR (400 MHz, CDCl_3) δ 7.50 (d, $J = 8.2$ Hz, 1H), 7.36 (d, $J = 8.1$ Hz, 1H), 7.26 (s, 2H), 4.87 (s, 1H), 3.74 – 3.71 (m, 4H), 3.21 (hept, $J = 6.8$ Hz, 2H), 2.48 (s, 4H), 1.32 (d, $J = 6.8$ Hz, 12H). ^{13}C NMR (101 MHz, CDCl_3) δ 150.17 – 149.70, 141.12, 134.09, 129.86, 126.94, 122.62, 67.53, 63.59, 54.06, 31.34, 27.73, 22.98. MS:[M+H] $^+$ $\text{C}_{23}\text{H}_{32}\text{NO}_2$ requires: 354.2427, found: 354.2433. CHN requires C: 78.15% H: 8.84% N: 3.96, found C: 77.75% H: 8.81% N: 4.00%

Methyl-4'-hydroxy-3'-5'-diisopropyl-(1-1'-biphenyl)-4-carboxylate



29

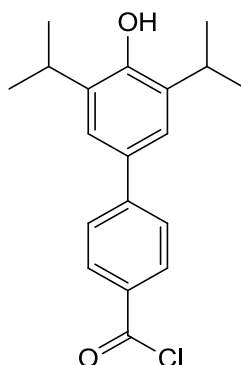
4-Bromo-2,6-diisopropylphenol (500 mg, 1.95 mmol) was reacted with (4-methoxycarbonyl)phenyl) boronic acid (702 mg, 3.90 mmol) according to **general procedure 1**, the crude product was purified by column chromatography (40:60 EtOAc/Hexane) to afford the product as a white solid (365 mg, 60% yield): ^1H NMR (400 MHz, CDCl_3) δ 8.08 (d, $J = 8.3$ Hz, 2H), 7.62 (d, $J = 8.3$ Hz, 2H), 7.32 (s, 2H), 4.94 (s, 1H), 3.94 (s, 3H), 3.27 (hept, $J = 6.8$ Hz, 2H), 1.33 (d, $J = 6.8$ Hz, 12H). MS:[M-H] $^-$, $\text{C}_{20}\text{H}_{23}\text{O}_3$ requires: 311.3954, found: 311.3952.

4'-Hydroxy-3'-5'-diisopropyl-(1-1'-biphenyl)-4-carboxylic acid**30**

To a stirred solution of Methyl-4'-hydroxy-3'-5'-diisopropyl-(1-1'-biphenyl)-4-carboxylate (312 mg, 3.2 mmol) in MeOH (15 mL) was added NaOH (10 mL, 2M). The resulting solution was allowed to stir at room temperature for 18 hours. The reaction was monitored by TLC (40:60 EtOAc/n-Hexane) and upon completion the solution was acidified with HCl (pH 3-4) washed with brine and extracted with EtOAc (3 x 30 mL). The combined organic extracts were dried over MgSO₄ and concentrated under vacuum to afford the product as a white solid (639 mg, 67% yield). ¹H NMR (400 MHz, CDCl₃) δ 8.15 (d, *J* = 8.4 Hz, 2H), 7.67 (d, *J* = 8.4 Hz, 2H), 7.34 (s, 2H), 3.32 (hept, *J* = 6.8 Hz, 2H), 1.34 (d, *J* = 6.8 Hz, 12H). ¹³C NMR (101 MHz, CDCl₃) δ 172.24, 150.61, 147.24, 134.26, 132.28, 130.72, 127.12, 126.78, 122.7, 27.37, 22.78. MS:[M-H]⁻: C₁₉H₂₁O₃ requires: 297.1496, found: 297.1491.

General procedure 2 . Synthesis of acid chlorides

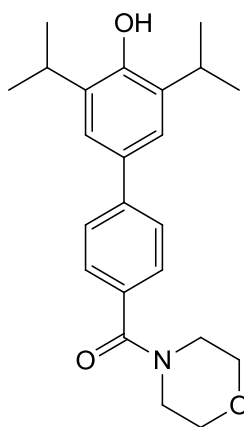
Oxalyl chloride (2.0 eq) was added to a solution of appropriate carboxylic acid (1 eq) in DCM (10 mL/g) at room temperature and under an inert atmosphere. 1 drop of DMF (from a Pasteur pipette) was added. The reaction mixture was allowed to stir for 2 hours. Upon completion the solvent was removed under vacuum. The product from this reaction was not isolated.

4'-Hydroxy-3'-5'-diisopropyl-(1-1'-biphenyl)-4-carbonyl chloride**31**

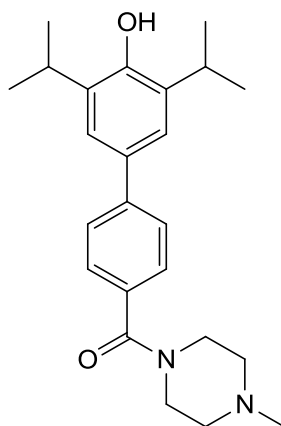
4'-Hydroxy-3'-5'-diisopropyl-(1-1'-biphenyl)-4-carboxylic acid (200 mg, 0.67 mmol) was reacted with oxalyl chloride (169 mg, 1.3 mmol) according to **general procedure 2** to afford the product as a pale yellow oil. The product from this reaction was not isolated and was carried through crude.

General procedure 3 . Amide coupling

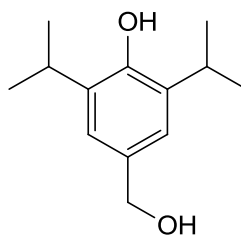
The appropriate morpholine derivative (1.2 eq) was added to a stirred solution of the acid chloride (1.0 eq) dissolved in DCM (10 mL/g). Et₃N (1.5 eq) was added and the resulting solution was allowed to stir at room temperature for 1.5 hours. The reaction was monitored by TLC and upon completion the reaction mixture was quenched with H₂O (50 mL) and extracted with EtOAc (3 x 50 mL). The combined organic extracts were washed with Na₂CO₃, dried over MgSO₄ and the solvent was removed under vacuum.

(4'-Hydroxy-3'-5'-diisopropyl-(1-1'-biphenyl)-4-yl)(morpholino)methanone**32**

4'-Hydroxy-3'-5'-diisopropyl-(1-1'-biphenyl)-4-carbonyl chloride (211 mg, 0.67 mmol) was reacted with morpholine (0.07 mL, 0.80 mmol) according to **general procedure 3**. The crude product was purified by column chromatography (60:40 EtOAc/n-Hexane) to afford the product as a white solid (121 mg, 51% yield). mp = 191-193°C: ^1H NMR (400 MHz, CDCl_3) δ 7.67 d, $J = 8.4$ Hz, 2H), 7.46 (d, $J = 8.4$ Hz, 2H), 7.26 (s, 2H), 5.33 (s, 1H), 3.73 (s, 8H), 3.23 (hept, $J = 6.8$ Hz, 2H), 1.31 (d, $J = 6.8$ Hz, 12H). ^{13}C NMR (101 MHz, CDCl_3) δ 170.98, 150.66, 144.04, 134.82, 133.36, 132.70, 128.07, 127.18, 122.80, 67.35, 60.83, 27.66, 23.21. MS:[M+Na] $^+$ $\text{C}_{23}\text{H}_{29}\text{NNaO}_3$ requires: 390.2045, found: 390.2051. CHN omitted due to inconsistent results.

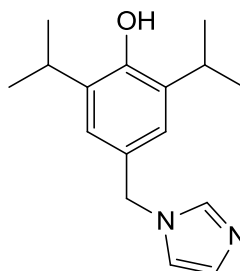
(4'-Hydroxy-3'-5'-diisopropyl-(1-1'-biphenyl)-4-yl)(methylpiperazin-1-yl)methanone**33**

4'-Hydroxy-3'-5'-diisopropyl-(1-1'-biphenyl)-4-carbonyl chloride (200 mg, 0.67 mmol) was reacted with N-methylpiperazine (0.07 mL, 0.80mmol) according to **general procedure 3** . The crude product was purified by column chromatography (60:40 EtOAc/n-Hexane) to afford the product as an off white solid (117 mg, 47% yield). mp = 184-186°C: ^1H NMR (400 MHz, CDCl_3) δ 7.58 – 7.06 (m, 6H), 4.91 (s, 1H), 3.62 (m, 4H), 3.28 (hept, $J = 6.8$ Hz, 2H), 2.40 (m, 4H), 1.23 (d, $J = 6.8$ Hz, 12H). ^{13}C NMR (101 MHz, CDCl_3) δ 170.55, 150.63, 143.95, 134.87, 133.40, 132.93, 128.02, 126.71, 122.79, 55.56, 46.34, 27.78, 23.23. MS:[M+Na] $^+$: $\text{C}_{24}\text{H}_{32}\text{N}_2\text{NaO}_2$ requires: 381.2542, found: 381.2527. CHN omitted due to inconsistent results.

4-(Hydroxymethyl)-2,6-diisopropylphenol²**57**

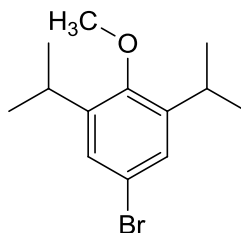
4-Hydroxy-3-5-diisopropylbenzaldehyde (530 mg, 2.5 mmol) was dissolved in dry THF and cooled to 0°C. Lithium aluminium hydride was added (100 mg, 2.5 mmol) and the solution was allowed to stir at 0°C for 1hr. Upon completion acetone (5 mL) was added along with HCl (5 mL, 1 M). The resulting solution was diluted with H₂O (50 mL) and extracted with EtOAc (3 x 50 mL). The combined organic extracts were dried over MgSO₄ and concentrated under vacuum to afford the product as a white solid (415 mg, 80% yield). ¹H NMR (400 MHz, CDCl₃) δ 6.98 (s, 2H), 4.99 (s, 1H), 4.52 (s, 2H), 3.09 (hept, *J* = 6.8 Hz, 2H), 1.18 (d, *J* = 6.8 Hz, 12H). ¹³C NMR (101 MHz, CDCl₃) δ 171.65, 151.45, 133.69, 122.84, 27.14, 22.62, 15.28.

4-((1*H*-imidazol-1-yl)methyl)-2,6-diisopropylphenol

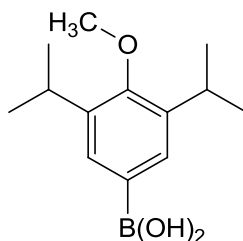


55

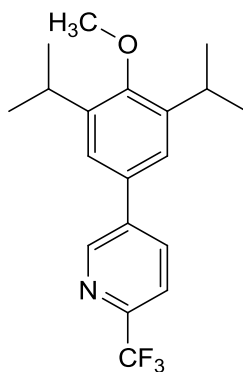
Imidazole (100 mg, 1.6 mmol) was added to 4-(Hydroxymethyl)-2,6-diisopropylphenol (325 mg, 1.6 mmol). The resulting mixture was heated to 160°C and stirred for 2 hours. Upon completion the reaction mixture was cooled and the solid precipitate was isolated. The crude product was purified by column chromatography (20:80 EtOAc/n-Hexane) to give the product as a white solid (205 mg, 50% yield). ¹H NMR (400 MHz, CDCl₃) δ 7.51 (s, 1H), 7.07 (s, 1H), 6.90 (s, 1H), 6.86 (s, 2H), 5.02 (s, 1H), 3.15 (hept, *J* = 6.8Hz, 2H), 1.23 (d, *J* = 6.8 Hz, 12H). mp = 156-158°C: ¹³C NMR (101 MHz, CDCl₃) δ 150.61, 137.39, 135.03, 129.37, 127.82, 123.44, 119.64, 51.60, 27.58, 23.05. MS:[M+H]⁺: C₁₆H₂₃N₂O, requires 259.1810, found 259.1809. CHN omitted due to inconsistent results.

5-Bromo-1,3-diisopropyl-2-methoxybenzene³**34**

4-Bromo-2,6-diisopropylphenol (4.4 g, 17.1 mmol) was dissolved in THF (10 mL) and the resulting solution was cooled to 0°C. NaH (821 mg, 34.22 mmol) was added and the solution was allowed to stir for 10 mins before MeI (3.2 mL, 51.3 mmol) was added. The reaction mixture was stirred for a further 3 hours. The reaction was monitored by TLC and upon completion the reaction mixture was quenched with brine (50 mL), extracted with EtOAc (3x50 mL). The combined extracts were washed with NaOH (50 mL, 1M), dried over MgSO₄ and concentrated under vacuum to afford the product as a pale yellow oil (4.3g, 99% yield). ¹H NMR (400 MHz, CDCl₃) δ 7.18 (s, 2H), 3.71 (s, 3H), 3.28 (hept, *J* = 6.8 Hz, 2H), 1.21 (d, *J* = 6.8 Hz, 12H). ¹³C NMR (101 MHz, CDCl₃) δ 154.03, 144.42, 127.68, 118.04, 62.49, 26.99, 24.17. MS:[M+H]⁺: C₁₃H₂₀BrO, requires: 272.0620, found 272.0614.

(3,5-diisopropyl-4-methoxyphenyl)boronic acid**37**

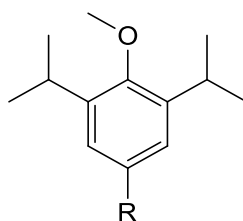
5-Bromo-1,3-diisopropyl-2-methoxybenzene (4.0 g, 14.7 mmol) was dissolved in anhydrous THF (30 mL) under a blanket of N₂. The resulting solution was cooled to -78°C before n-BuLi (9.5 mL, 23.6 mmol, 2.5M) was added. The resulting mixture was allowed to stir at -78°C for 1 hour before B(O-*i*pr)₃ (6.8 mL, 29.5 mmol) was added. The reaction mixture was allowed to stir for 18 hours. Upon completion HCl (30 mL, 2M) was added and the solution was stirred for a further 30 mins. The product was extracted with EtOAc (3x50 mL) and the combined organic extracts were washed with H₂O (50 mL), brine (50 mL), dried over MgSO₄ and the solvent was removed under vacuum. The product from this reaction was not isolated and was carried through crude.

5-(3,5-diisopropyl-4-methoxyphenyl)-2-(trifluoromethyl)pyridine**38**

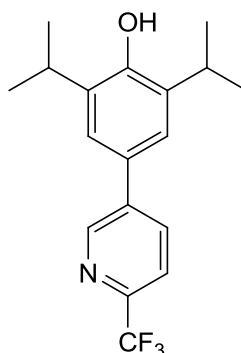
(3,5-Diisopropyl-4-methoxyphenyl)boronic acid (300 mg, 1.27 mmol) was reacted with 5-bromo-2-(trifluoromethyl)pyridine (203 mg, 1.01 mmol) according **general**

procedure 1. The crude product was purified by column chromatography (40:60 EtOAc/n-Hexane) to afford the product as a white solid (234 mg, 69% yield). ^1H NMR (400 MHz, CDCl_3) δ 8.83 (s, 1H), 7.93 (d, $J = 8.1$ Hz, 1H), 7.65 (d, $J = 8.1$ Hz, 1H), 7.22 (s, 2H), 3.72 (s, 3H), 3.32 (hept, $J = 6.8$ Hz, 2H), 1.21 (d, $J = 6.8$ Hz, 12H). ^{13}C NMR (101 MHz, CDCl_3) δ 155.93, 148.78, 146.38, 143.24, 140.19, 135.60, 132.91, 123.75, 120.73, 62.73, 27.00, 24.42. ^{19}F NMR (376 MHz, CDCl_3) δ -68.12. MS: $[\text{M}+\text{H}]^+$ $\text{C}_{19}\text{H}_{23}\text{NOF}_3$, requires: 338.1732, found: 338.1734.

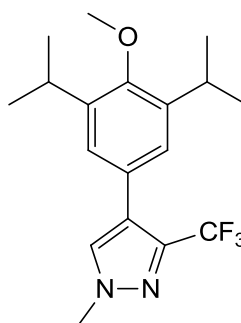
General procedure 4. Demethylation



The appropriately methylated reagent (1eq) was taken in DCM (10 mL/g) and cooled to 0°C before BBr_3 (2.0eq) was added. The resulting solution was allowed to stir for 5 hours. Upon completion the reaction mixture was quenched with methanol (1 mL/g) and water (10 mL/g). The product was extracted with EtOAc (3 x 30 mL) and the combined organic extracts were washed with brine (50 mL), dried over MgSO_4 and concentrated under vacuum. The products were purified by column chromatography (EtOAc/n-Hexane).

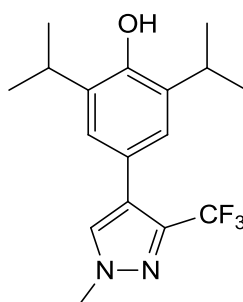
2,6-Diisopropyl-4-(6-(trifluoromethyl)pyridine-3-yl)phenol**40**

5-(3,5-diisopropyl-4-methoxyphenyl)-2-(trifluoromethyl)pyridine (210 mg, 0.62 mmol) was reacted with BBr_3 (0.12 mL, 1.2 mmol) according to **general procedure 4**. The crude product was purified by column chromatography (60:40 EtOAc/n-Hexane) to afford the product as a white solid. (96 mg, 48% yield). mp = 176-178°C: ^1H NMR (400 MHz, CDCl_3) δ 8.90 (s, 1H), 7.99 (d, $J = 8.1$ Hz, 1H), 7.71 (d, $J = 8.1$ Hz, 1H), 7.27 (s, 2H), 5.00 (s, 1H), 3.22 (hept, $J = 6.8$ Hz, 2H), 1.33 (d, $J = 6.8$ Hz, 12H). ^{13}C NMR (101 MHz, CDCl_3) δ 151.54, 148.63, 146.44, 146.10, 145.75, 140.55, 135.42, 135.15, 123.16, 27.75, 23.08. ^{19}F NMR (376 MHz, CDCl_3) δ -67.99. MS:[M-H] $^-$ $\text{C}_{18}\text{H}_{19}\text{NOF}_3$, requires: 322.1419, found: 322.1425. CHN requires C: 66.86%, H: 6.23%, N: 4.33%, found C: 66.86%, H: 6.10%, N: 4.11%.

4-(3,5-Diisopropyl-4-methoxyphenyl)-1-methyl-3-(trifluoromethyl)-1H-pyrazole**39**

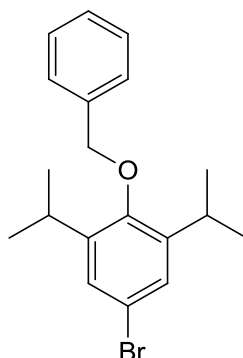
(3,5-Diisopropyl-4-methoxyphenyl)boronic acid (280 mg, 1.20 mmol) was reacted with 4-Bromo-1-methyl-3-(trifluoromethyl)-1*H*-pyrazole (229 mg, 1.0 mmol) according to **general procedure 1**. The crude product was purified by column chromatography (40: 60 EtOAc/n-Hexane) to afford the product as a white solid. (197 mg, 58% yield). ^1H NMR (400 MHz, CDCl_3) δ 7.48 (s, 1H), 7.12 (s, 2H), 3.98 (s, 3H), 3.76 (s, 3H), 3.35 (hept, $J = 6.8$ Hz, 2H), 1.25 (d, $J = 6.8$ Hz, 12H). ^{13}C NMR (101 MHz, CDCl_3) δ 154.52, 142.05, 130.80, 126.90, 124.57, 123.30, 120.76, 62.68, 39.92, 26.89, 24.39. ^{19}F NMR (376 MHz, CDCl_3) δ -59.24. MS:[$\text{M}+\text{H}$] $^+$ $\text{C}_{18}\text{H}_{24}\text{FNO}_2$, requires: 341.1835, found: 341.1837.

2,6-Diisopropyl-4-(1-methyl-3-(trifluoromethyl)-1*H*-pyrazol-4-yl)phenol

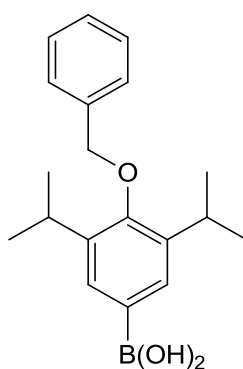


41

4-(3,5-Diisopropyl-4-methoxyphenyl)-1-methyl-3-(trifluoromethyl)-1*H*-pyrazole (120 mg, 0.35 mmol) was reacted with BBr_3 (0.7 mL, 0.70 mmol) according to **general procedure 4**. The crude product was purified by column chromatography (60:40 EtOAc/n-Hexane) to afford the product as a white solid. (78 mg, 68%). mp = 165-167°C: ^1H NMR (400 MHz, CDCl_3) δ 7.46 (s, 1H), 7.09 (s, 2H), 4.87 (s, 1H), 3.98 (s, 3H), 3.17 (hept, $J = 6.8$ Hz, 2H), 1.28 (d, $J = 6.8$ Hz, 12H). ^{13}C NMR (101 MHz, CDCl_3) δ 154.52, 142.05, 130.80, 126.90, 124.57, 62.68, 26.89, 24.39. ^{19}F NMR (376 MHz, CDCl_3) δ -59.25. MS:[$\text{M}-\text{H}$] $^-$ $\text{C}_{17}\text{H}_{20}\text{F}_3\text{N}_2\text{O}$, requires: 325.1528, found: 325.1526. CHN omitted due to inconsistent results.

2-(Benzyloxy)-5-bromo-1,3-diisopropylbenzene⁴**42**

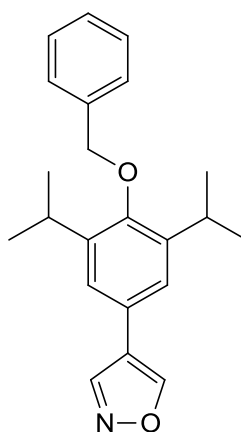
To a solution of 4-bromopropofol (500 mg, 1.44 mmol) in acetone (10 mL) was added BnBr (0.19 mL, 1.59 mmol) and K_2CO_3 (390 mg, 2.88 mmol). The resulting mixture was allowed to stir at room temperature for 18 hours and the reaction was monitored by TLC. Upon completion the mixture was filtered through Celite and the solvent was removed under vacuum to give the product as a white solid. The product was from this reaction was not isolated and was taken through crude.

(4-(Benzyloxy)-3,5-diisopropylphenyl)boronic acid⁴**37a**

4-Bromopropofol (300 mg, 0.96 mmol) was dissolved in anhydrous THF (5 mL) under a blanket of N_2 . The resulting solution was cooled to $-78^\circ C$ before n-BuLi (0.61

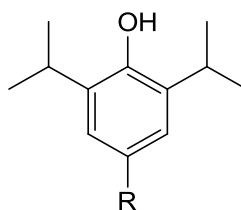
mL, 1.54 mmol, 2.5M) was added. The resulting mixture was allowed to stir at -78°C for 1 hour before $\text{B}(\text{O}-i\text{pr})_3$ (0.44 mL, 1.92 mmol) was added. The reaction mixture was allowed to stir for 18 hours. Upon completion HCl (10 mL, 2M) was added and the solution was stirred for a further 30 mins. The product was extracted with EtOAc (3x30 mL) and the combined organic extracts were washed with H_2O (30 mL), brine (30 mL), dried over MgSO_4 and the solvent was removed under vacuum to give the product as a white solid. The product was from this reaction was not isolated and was taken through crude.

4-(4-(Benzyloxy)-3,5-diisopropylphenyl)isoxazole

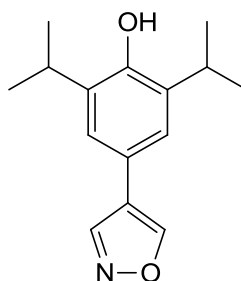


43

(3,5-diisopropyl-4-methoxyphenyl)boronic acid (200 mg, 0.85 mmol) was reacted with 4-bromoisoxazole (103 mg, 0.71 mmol) according to **general procedure 1**. The crude product was purified by column chromatography (30: 70 EtOAc/n-Hexane) to afford the product as an off white solid (32 mg, 62% yield). mp = $171-173^{\circ}\text{C}$: ^1H NMR (400 MHz, CDCl_3) δ 8.64 (s, 1H), 8.54 (s, 1H), 7.56 – 7.30 (m, 5H), 7.20 (s, 2H), 4.82 (s, 2H), 3.42 (hept, $J = 6.8$ Hz, 2H), 1.27 (d, $J = 6.8$ Hz, 12H). ^{13}C NMR (101 MHz, CDCl_3) δ 153.64, 153.41, 148.61, 143.43, 137.78, 129.02, 128.48, 127.81, 125.36, 122.88, 122.05, 31.30, 27.09, 24.42.

General procedure 5. Hydrogenation

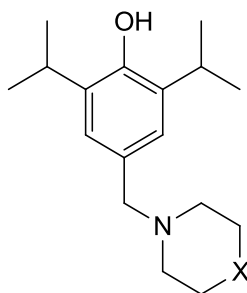
The benzyl protected phenol was dissolved in MeOH (20 mL/g). Pd/C (10 mol%) was added to the solution and the resulting mixture was degassed and placed under a blanket of H₂. The mixture was allowed to stir for 18 hours. The reaction was followed by TLC and upon completion the reaction mixture was filtered through Celite and the solvent was removed under vacuum.

2,6-Diisopropyl-4-(isoxazol-4-yl)phenol**44**

4-(4-(Benzyloxy)-3,5-diisopropylphenyl)isoxazole (180 mg, 0.65 mmol) was reacted with Pd/C (35 mg, 0.03 mmol) according to **general procedure 5**. The crude product was purified by column chromatography (40:60 EtOAc/n-Hexane) to afford the product as a white solid. (80mg, 42% yield). mp = 156-158°C: ¹H NMR (400 MHz, CDCl₃) δ 8.59 (s, 1H), 8.51 (s, 1H), 7.13 (s, 2H), 4.95 (s, 2H), 3.19 (hept, *J* = 6.8 Hz, 5H), 1.30 (d, *J* = 6.8 Hz, 12H). ¹³C NMR (101 MHz, CDCl₃) δ 152.90, 150.70, 149.56,

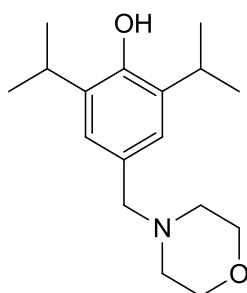
135.01, 128.13, 122.28, 121.25, 27.66, 23.06. MS:[M+H]⁺ C₁₅H₁₉NO₂ requires: 246.1489, found: 246.1490. CHN omitted due to inconsistent results.

General procedure 6. Mannich reaction



To a solution of 2,6-Diisopropylphenol (1 eq) in ethanol/H₂O (70:30) was added the appropriate morpholine derivative (1.5 eq) and paraformaldehyde (1.5 eq). The resulting mixture was heated to reflux under stirring for 16 hours. The reaction was monitored by TLC (EtOAc/n-Hexane) and upon completion the reaction was quenched with H₂O (50 mL/g) and extracted with EtOAc (3 x 30 mL). The combined organic extracts were dried over MgSO₄ and reduced under vacuum. The crude product was purified by column chromatography (EtOAc/n-Hexane).

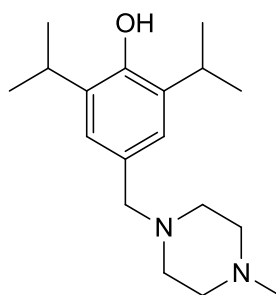
2,6-Diisopropyl-4-(morpholinomethyl)phenol⁵



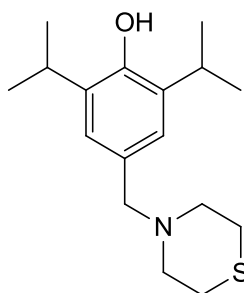
49

2,6-Diisopropylphenol (1 g, 5.6 mmol) was reacted with Morpholine (0.7 mL, 8.4 mmol) and formaldehyde (0.72 mL, 8.4 mmol) according to **general procedure 6**. The crude product was purified by column chromatography (20:80 EtOAc/n-Hexane) to afford the product as a white solid (1.28 g, 83% yield). mp = 122-124°C: ^1H NMR (400 MHz, CDCl_3) δ 6.97 (s, 2H), 4.91 (s, 1H), 3.74 – 3.63 (m, 4H), 3.43 (s, 2H), 3.14 (hept, $J = 6.8$ Hz, 2H), 2.51 – 2.31 (m, 4H), 1.26 (d, $J = 6.8$ Hz, 12H). ^{13}C NMR (101 MHz, CDCl_3) δ 149.48, 133.88, 129.65, 124.89, 67.31, 63.86, 53.59, 27.46, 23.19. MS: $[\text{M}+\text{H}]^+$ $\text{C}_{17}\text{H}_{28}\text{NO}_2$ requires: 278.2120, found: 278.2121. CHN requires C: 73.61%, H: 9.81%, N: 5.05, found C: 73.53%, H: 9.83%, N: 5.03%.

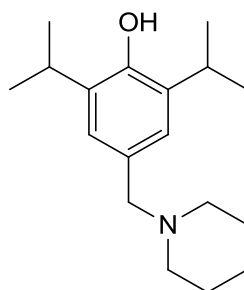
2,6-Diisopropyl-4-((4-methylpiperazin-1-yl)methyl) phenol

**51**

2,6-Diisopropylphenol (1 g, 5.6 mmol) was reacted with N-methylpiperazine (0.9 mL, 8.4 mmol) and formaldehyde (0.72 mL, 8.4 mmol) according to **general procedure 6**. The crude product was purified by column chromatography (20:80 EtOAc/n-Hexane) to afford the product as a brown solid (1.27 g, 78% yield). mp = 128-130°C: ^1H NMR (400 MHz, CDCl_3) δ 6.95 (s, 2H), 3.45 (s, 2H), 3.19 (hept, $J = 6.8$ Hz, 2H), 2.48 (s, 8H), 2.27 (s, 3H), 1.23 (d, $J = 6.8$ Hz, 12H). ^{13}C NMR (101 MHz, CDCl_3) δ 149.69, 134.59, 129.56, 124.78, 63.42, 54.26, 53.00, 46.42, 27.50, 23.34. MS: $[\text{M}+\text{H}]^+$ $\text{C}_{18}\text{H}_{31}\text{N}_2\text{O}$ requires: 291.2436, found: 291.2437. CHN omitted due to inconsistent results.

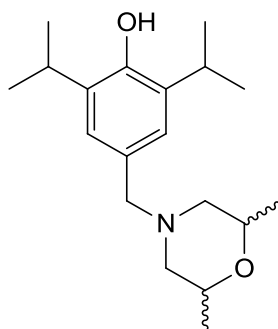
2,6-Diisopropyl-4-(thiomorpholinomethyl) phenol⁵**50**

2,6-Diisopropylphenol (1 g, 5.6 mmol) was reacted with thiomorpholine (0.8 mL, 8.4 mmol) and formaldehyde (0.72 mL, 8.4 mmol) according to **general procedure 6**. The crude product was purified by column chromatography (20:80 EtOAc/n-Hexane) to afford the product as a light green solid (1.4 g, 87% yield). mp = 126-128°C: ¹H NMR (400 MHz, CDCl₃) δ 6.95 (s, 2H), 4.72 (s, 1H), 3.45 (s, 2H), 3.14 (hept, *J* = 6.8 Hz, 2H), 2.68 (s, 8H), 1.26 (d, *J* = 6.8 Hz, 12H). ¹³C NMR (101 MHz, CDCl₃) δ 149.47, 133.82, 124.57, 63.93, 54.87, 28.26, 27.46, 23.19 . MS:[M+H]⁺ C₁₇H₂₈NOS requires: 294.1892, found: 294.1895. CHN requires C: 69.58%, H: 9.27%, N: 4.77, found C: 68.40%, H: 9.32%, N: 4.82%

2,6-Diisopropyl-4-(piperidine-1-ylmethyl)phenol⁶**54**

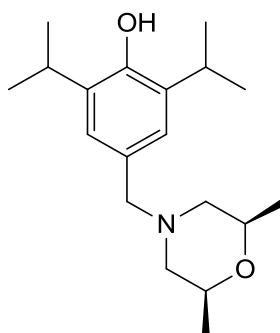
2-6-Diisopropylphenol (1 g, 5.6 mmol) was reacted with piperidine (0.63 mL, 8.4 mmol) and formaldehyde (0.72 mL, 8.4 mmol) according to **general procedure 6**. The crude product was purified by column chromatography (20:80 EtOAc/n-Hexane) to afford the product as a light pink solid (1.17 g, 76% yield). mp = 134-136°C: ^1H NMR (400 MHz, CDCl_3) δ 6.97 (s, 2H), 4.83 (s, 1H), 3.42 (s, 2H), 3.14 (hept, $J = 6.8\text{Hz}$, 2H), 2.36 (s, 4H), 1.62 – 1.52 (m, 4H), 1.42 (s, 2H), 1.26 (d, $J = 6.8\text{ Hz}$, 12H). ^{13}C NMR (101 MHz, CDCl_3) δ 149.47, 133.84, 129.64, 124.81, 72.10, 63.44, 59.58, 27.46, 23.18, 19.38. MS:[M+H] $^+$ $\text{C}_{18}\text{H}_{30}\text{NO}$ requires: 275.2249, found: 275.2242. CHN requires C: 78.49%, H: 10.61%, N: 5.09, found C: 78.19%, H: 10.59%, N: 4.97%.

4-((2,6-Dimethylmorpholino)methyl)-2,6-diisopropylphenol

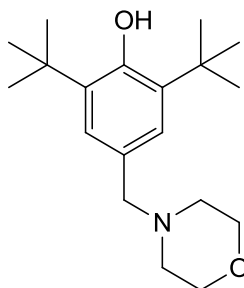


52

2-6-Diisopropylphenol (1 g, 5.6 mmol) was reacted with 2,6-dimethylpiperidine (1.0 mL, 8.4 mmol) and formaldehyde (0.72 mL, 8.4 mmol) according to **general procedure 6**. The crude product was purified by column chromatography (20:80 EtOAc/n-Hexane) to afford the product as an off white solid (1.35 g, 79% yield). mp = 132-134°C: ^1H NMR (400 MHz, CDCl_3) δ 6.97 (s, 2H), 4.86 (s, 1H), 3.72 – 3.66 (m, 2H), 3.41 (s, 2H), 3.15 (hept, $J = 6.8\text{ Hz}$, 2H), 2.71 (d, $J = 10.5\text{ Hz}$, 2H), 1.75 – 1.66 (m, 2H), 1.26 (d, $J = 6.8\text{ Hz}$, 12H), 1.14 (d, $J = 6.3\text{ Hz}$, 6H). ^{13}C NMR (101 MHz, CDCl_3) δ 149.47, 133.84, 129.64, 124.81, 72.10, 63.44, 59.58, 27.46, 23.18, 19.38. MS:[M+H] $^+$ $\text{C}_{19}\text{H}_{32}\text{NO}_2$ requires: 306.2428, found: 306.2423. . CHN omitted due to inconsistent results.

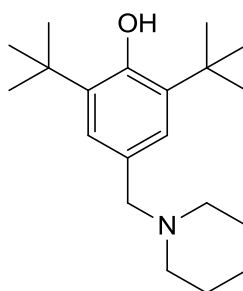
4-(((2S,6R)-2,6-dimethylmorpholino)methyl)-2,6-diisopropylphenol**53**

2,6-Diisopropylphenol (500 mg, 2.8 mmol) was reacted with (2S,6R)-2,6-dimethylmorpholine (0.52 mL, 4.2 mmol) and formaldehyde (0.35 mL, 4.2 mmol) according to **general procedure 6**. The crude product was purified by column chromatography (20:80 EtOAc/n-Hexane) to afford the product as a yellow solid (608 mg, 76% yield). mp = 144-146°C: ^1H NMR (400 MHz, CDCl_3) δ 6.98 (s, 1H), 4.77 (s, 1H), 3.77 – 3.59 (m, 2H), 3.41 (s, 2H), 3.14 (hept, $J = 6.8$ Hz, 2H), 2.71 (d, $J = 10.8$ Hz, 2H), 1.72 (t, $J = 10.7$ Hz, 2H), 1.27 (d, $J = 6.8$ Hz, 12H), 1.14 (d, $J = 6.3$ Hz, 6H). ^{13}C NMR (101 MHz, CDCl_3) δ 148.77, 133.34, 129.23, 124.48, 71.72, 63.06, 59.38, 27.10, 22.80, 19.20. MS: $[\text{M}+\text{H}]^+$ $\text{C}_{19}\text{H}_{32}\text{NO}_2$ requires: 307.2428, found: 307.2421. CHN omitted due to inconsistent results.

2,6-Di-*tert*-butyl-4-(morpholinomethyl)phenol⁶**60**

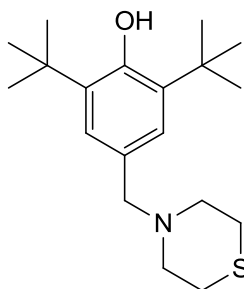
2,6-Di-*tert*-butylphenol (1 g, 4.8 mmol) was reacted with Morpholine (0.6mL, 7.3 mmol) and formaldehyde (0.6 mL, 7.3 mmol) according to **general procedure 6**. The crude product was purified by column chromatography (20:80 EtOAc/*n*-Hexane) to afford the product as a white solid 1.3g, 88% yield). mp = 138-140°C: ^1H NMR (400 MHz, CDCl_3) δ 7.09 (s, 2H), 5.13 (s, 1H), 3.72 (s, 4H), 3.42 (bs, 2H), 2.44 (bs, 4H), 1.44 (s, 18H). ^{13}C NMR (101 MHz, CDCl_3) δ 153.08, 135.85, 128.35, 126.31, 67.48, 63.92, 53.89, 34.69, 30.62. MS $[\text{M}+\text{H}]^+$: $\text{C}_{19}\text{H}_{32}\text{NO}_2$ requires: 306.2433, found: 306.2442. CHN requires C: 74.71%, H: 10.23%, N: 4.59, found C: 74.65%, H: 10.29%, N: 4.92%

2,6-Di-*tert*-butyl-4-(piperidin-1-ylmethyl)phenol⁶

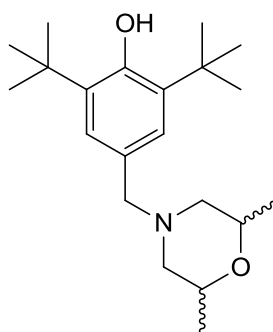


62

2,6-Di-*tert*-butylphenol (1 g, 4.8 mmol) was reacted with piperidine (0.7 mL, 7.3 mmol) and formaldehyde (0.6 mL, 7.3 mmol) according to **general procedure 6**. The crude product was purified by column chromatography (20:80 EtOAc/*n*-Hexane) to afford the product as a white solid (1.2g, 86% yield). mp = 127-129°C: ^1H NMR (400 MHz, CDCl_3) δ 7.08 (s, 2H), 5.11 (s, 1H), 3.40 (bs, 4H), 2.37 (bs, 4H), 1.57 (bs, 4H), 1.44 (s, 18H). ^{13}C NMR (101 MHz, CDCl_3) δ 152.67, 135.32, 128.91, 125.96, 64.04, 54.39, 34.37, 30.46, 26.09, 24.55. . MS $[\text{M}+\text{H}]^+$: $\text{C}_{20}\text{H}_{34}\text{NO}$ requires: 306.2640, found: 306.2635. CHN requires C: 79.15%, H: 10.96%, N: 4.62, found C: 78.98%, H: 10.54%, N: 4.10%

2,6-Di-*tert*-butyl-4-(thiomorpholinomethyl)phenol⁶**61**

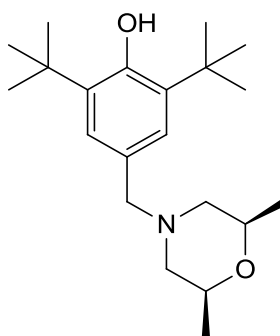
2,6-Di-*tert*-butylphenol (1.0 g, 4.8 mmol) was reacted with thiomorpholine (0.7 mL, 7.3 mmol) and formaldehyde (0.6 mL, 7.3 mmol) according to **general procedure 6**. The crude product was purified by column chromatography (20:80 EtOAc/*n*-Hexane) to afford the product as a white solid. (1.1g, 70% yield). mp = 124-126°C: ¹H NMR (400 MHz, CDCl₃) δ 7.06 (s, 2H), 5.13 (s, 1H), 3.44 (s, 2H), 2.69 (bs, 8H), 1.44 (s, 18H). ¹³C NMR (101 MHz, CDCl₃) δ 153.31, 135.85, 129.90, 126.02, 64.17, 55.08, 34.46, 30.61, 28.26. MS [M+H]⁺: C₁₉H₃₂NOS requires: 322.2205, found: 322.2193. CHN requires C: 70.98%, H: 9.72%, N: 4.36, found C: 70.78%, H: 9.74%, N: 4.32%

2,6-Di-*tert*-butyl-4-(2,6-dimethylmorpholino)phenol**63**

2,6-Di-*tert*-butylphenol (1.0 g, 4.8 mmol) was reacted with 2,6-dimethylmorpholine (830 mg, 7.3 mmol) and formaldehyde (0.6 mL, 7.3 mmol) according to **general**

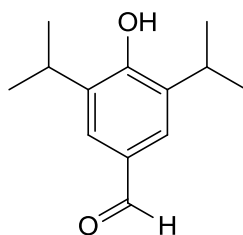
procedure 6. The crude product was purified by column chromatography (20:80 EtOAc/n-Hexane) to afford the product as an off white solid (1.4g, 89% yield). mp = 132-134°C: ^1H NMR (400 MHz, CDCl_3) δ 7.08 (s, 2H), 5.14 (s, 1H), 3.77 – 3.62 (m, 2H), 3.39 (s, 2H), 2.73 (d, J = 12.0 Hz, 2H), 1.73 (t, J = 12.0 Hz, 2H), 1.44 (s, 18H), 1.15 (d, J = 4.0 Hz, 6H). ^{13}C NMR (101 MHz, CDCl_3) δ 153.09, 135.85, 127.39, 126.02, 63.45, 59.88, 34.69, 30.78, 19.61. MS $[\text{M}+\text{H}]^+$: $\text{C}_{21}\text{H}_{36}\text{NO}_2$ requires: 334.2, found: 334.4. CHN requires C: 75.63%, H: 10.58%, N: 4.20, found C: 75.25%, H: 10.63%, N: 4.08%

2,6-Di-*tert*-butyl-4-(((2*S*,6*R*)-2,6-dimethylmorpholino)methyl)phenol

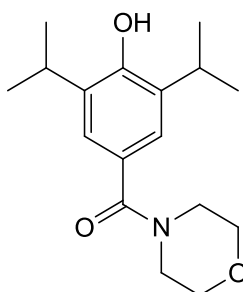


64

2,6-Di-*tert*-butylphenol (500 mg, 2.4 mmol) was reacted with (2*S*,6*R*)-2,6-dimethylmorpholine (0.45 mL, 3.6 mmol) and formaldehyde (0.30 mL, 3.6 mmol) according to **general procedure 6**. The crude product was purified by column chromatography (20:80 EtOAc/n-Hexane) to afford the product as a white solid (608 mg, 76% yield). mp = 138-140°C: ^1H NMR (400 MHz, CDCl_3) δ 7.08 (s, 2H), 5.14 (s, 1H), 3.70-3.63 (m, 2H), 2.89 – 2.79 (m, 4H), , 1.44 (s, 18H), 1.15 (s, 6H). ^{13}C NMR (101 MHz, CDCl_3) δ 152.64, 135.32, 128.24, 125.68, 71.76, 63.03, 59.43, 34.14, 30.28, 18.95. MS $[\text{M}+\text{H}]^+$: $\text{C}_{21}\text{H}_{36}\text{NO}_2$ requires: 334.2732, found: 334.4.2732. CHN requires C: 75.63%, H: 10.58%, N: 4.20, found C: 75.18%, H: 10.48%, N: 4.11%

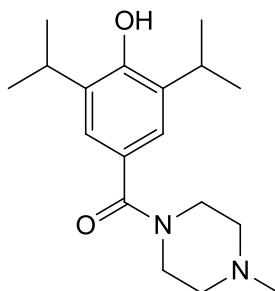
4-Hydroxy-3-5-diisopropylbenzaldehyde⁷**56**

Hexamethylenetetramine (15.8 g, 56 mmol) was added to a solution of 2,6-Diisopropylphenol (10.4 mL) in glacial acetic acid (50 mL) and H₂O (10 mL). The resulting mixture was heated to reflux for 6 hours and the reaction was monitored by TLC. Upon completion of the reaction the solution was cooled to 0°C and the resulting orange precipitate was isolated and washed with H₂O (3 x 50 mL) to afford product as a pale orange solid (10.3 g, 89% yield). ¹H NMR (400 MHz, CDCl₃) δ 9.86 (s, 1H), 7.63 (s, 2H), 5.49 (s, 1H), 3.21 (hept, *J* = 6.8 Hz, 2H), 1.31 (d, *J* = 6.8 Hz, 12H). ¹³C NMR (101 MHz, CDCl₃) δ 191.82, 156.02, 134.45, 129.66, 126.22, 27.06, 22.54. MS:[M+H]⁺ C₁₃H₁₉O₂ requires: 207.1380, found: 207.1378.

(4-Hydroxy-3-5-diisopropylphenyl)(morpholino)methanone**77**

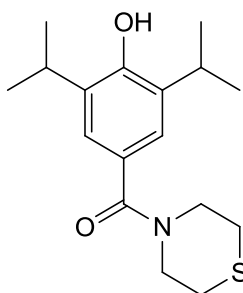
4-Hydroxy-3-5-diisopropylbenzoyl chloride (130 mg, 0.54 mmol) was reacted with morpholine (0.071 mL, 0.81 mmol) according to **general procedure 3** to afford the product as a white solid. The crude product was purified by trituration with EtOAc (120 mg, 76% yield). mp = 162-164°C: ^1H NMR (400 MHz, CDCl_3) δ 7.14 (s, 2H), 5.00 (s, 1H), 3.70 (s, 4), 3.28 (hept, $J = 6.8$ Hz, 2H), 1.56 (s, 4H), 1.27 (d, $J = 6.8$ Hz, 12H). ^{13}C NMR (101 MHz, CDCl_3) δ 134.05, 123.61, 77.74, 77.43, 77.11, 67.36, 27.56, 23.01. MS: $[\text{M}+\text{Na}]^+$ $\text{C}_{17}\text{H}_{25}\text{NNaO}_3$ requires: 314.1740, found: 314.1732. CHN omitted due to inconsistent results.

(4-Hydroxy-3-5-diisopropylphenyl)(4-methylpiperazin-1-yl)methanone

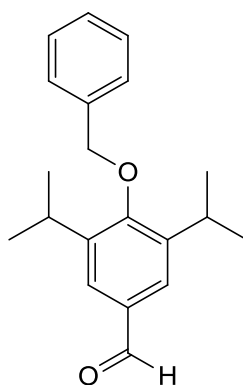


78

4-Hydroxy-3-5-diisopropylbenzoyl chloride (160 mg, 0.66 mmol) was reacted with N-methylpiperazine (0.088 mL, 0.80 mmol) according to **general procedure 3** to afford the product as a brown solid. The crude product was purified by trituration with EtOAc (109mg, 55% yield). mp = 154-156°C: ^1H NMR (400 MHz, CDCl_3) δ 7.13 (s, 2H), 5.18 (s, 1H), 3.74 (s, 4H), 3.16 (hept, $J = 6.8$ Hz, 2H), 2.44 (s, 4H), 1.26 (d, $J = 6.8$ Hz, 12H). ^{13}C NMR (101 MHz, CDCl_3) δ 171.24, 151.59, 133.65, 127.18, 123.19, 65.87, 54.82, 45.78, 27.12, 22.62. MS: $\text{C}_{18}\text{H}_{28}\text{N}_2\text{O}_2$ requires: 305.2229, found: 305.2224. CHN omitted due to inconsistent results.

(4-Hydroxy-3-5-diisopropylphenyl)(thiomorpholino)methanone**79**

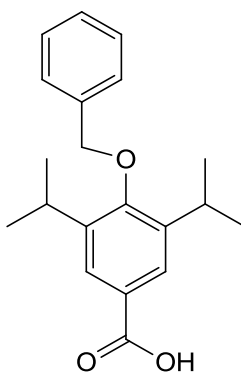
4-Hydroxy-3-5-diisopropylbenzoyl chloride (200 mg, 0.83 mmol) was reacted with thiomorpholine (102 mg, 0.095 mL) according to **general procedure 3** to afford the product as a pale blue solid. The crude product was purified by trituration with EtOAc (153 mg, 60% yield). mp = 122-124°C: ^1H NMR (400 MHz, CDCl_3) δ 7.10 (s, 2H), 5.36 (s, 1H), 3.86 (s, 4H), 3.16 (hept, $J = 6.8$ Hz 2H), 2.66 (s, 4H), 1.24 (d, $J = 6.8$ Hz, 12H). ^{13}C NMR (101 MHz, CDCl_3) δ 171.60, 151.37, 133.69, 127.59, 122.84, 65.87, 27.14, 22.62, 15.28. MS: $\text{C}_{17}\text{H}_{25}\text{NO}_2\text{S}$ requires: 308.1684, found: 308.1672. CHN requires C: 66.41%, H: 8.20%, N: 4.56, found C: 66.13%, H: 8.28%, N: 4.49%.

4-(benzyloxy)-3,5-diisopropylbenzaldehyde⁸**84**

To a solution of 4-Hydroxy-3-5-diisopropylbenzaldehyde (4.18 g, 20.3 mmol) in acetone (50 mL) was added benzyl bromide (2.6 mL, 22.4 mmol) and potassium

carbonate (5.6 g, 40.6 mmol). The resulting mixture was allowed to stir at room temperature for 18 hours and the reaction was monitored by TLC. Upon completion the mixture was filtered through Celite™ and the solvent was removed under vacuum. The product was purified by column chromatography (10:90 EtOAc/n-Hexane) to afford the product as a grey solid (5.3 g, 88% yield). ¹H NMR (400 MHz, CDCl₃) δ 9.96 (s, 1H), 7.69 (s, 2H), 7.55 – 7.30 (m, 5H), 4.85 (s, 2H), 3.40 (hept, *J* = 6.8, 2H), 1.27 (d, *J* = 6.8 Hz, 12H). ¹³C NMR (101 MHz, CDCl₃) δ 192.03, 158.71, 143.34, 136.93, 133.25, 128.70, 128.28, 127.44, 126.35, 66.35, 26.82, 23.92. MS: C₂₀H₂₄O₂ requires: 319.1679, found: 319.1674

4-(benzyloxy)-3,5-diisopropylbenzoic acid

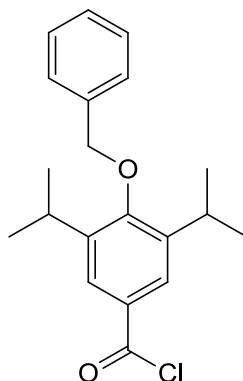


85

4-(benzyloxy)-3,5-diisopropylbenzaldehyde (1.74 g, 5.87 mmol) was dissolved in THF (5 mL) under a blanket of N₂. Selenium dioxide (325 mg, 2.94 mmol) was added to the solution along with hydrogen peroxide (1.5 mL, 27 wt %) and the mixture was heated to reflux for 18 hours. Upon completion Pd/C (10 mg) was added and the reaction mixture was allowed to stir for 10 mins. The mixture was filtered through Celite™ and the solvent was removed under vacuum. The product was purified by column chromatography (80:20 EtOAc/n-Hexane) to afford the product as a white solid (1.6 g, 85% yield). ¹H NMR (400 MHz, CDCl₃) δ 7.92 (s, 2H), 7.57 – 7.27 (m, 5H), 4.85 (s, 2H), 3.40 (hept, *J* = 6.8 Hz, 2H), 1.27 (d, *J* = 6.8 Hz, 12H). ¹³C NMR (101 MHz,

CDCl_3) δ 171.53, 158.06, 142.57, 137.06, 128.65, 128.19, 127.43, 126.77, 125.49, 76.51, 26.76, 23.93. MS $[\text{M}+\text{Na}]^+$: $\text{C}_{20}\text{H}_{24}\text{NaO}_3$ requires: 335.1625, found: 335.1623

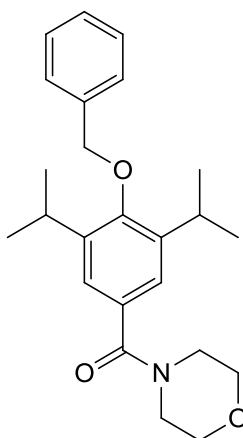
4-(benzyloxy)-3,5-diisopropylbenzoyl chloride



86

4-(benzyloxy)-3,5-diisopropylbenzoic acid (200 mg, 0.6 mmol) was reacted with oxalyl chloride (0.12 mL, 0.72 mmol) according to **general procedure 2**. The product was not isolated and was taken through crude.

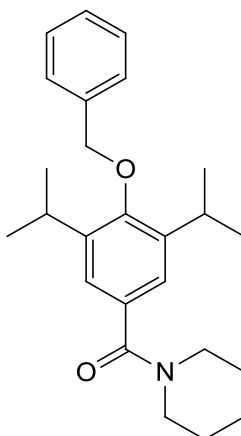
(4-Benzyloxy-3,5-diisopropylphenyl)(morpholino)methanone



87

Morpholine (0.23 mL, 2.25 mmol) was reacted with 4-(benzyloxy)-3,5-diisopropylbenzoyl chloride (500 mg, 1.5 mmol) according to **general procedure 3**. The crude product was purified by column chromatography (20:80 EtOAc/n-Hexane) to afford the product as a white solid (493 mg, 86% yield). ^1H NMR (400 MHz, CDCl_3) δ 7.54 – 7.33 (m, 5H), 7.18 (s, 2H), 4.80 (s, 2H), 3.73 (s, 8H), 3.39 (hept, $J = 6.8$ Hz, 2H), 1.24 (d, $J = 6.8$ Hz, 12H). MS $[\text{M}+\text{Na}]^+$: $\text{C}_{24}\text{H}_{31}\text{NaNO}_3$ requires: 404.2202, found: 404.2196.

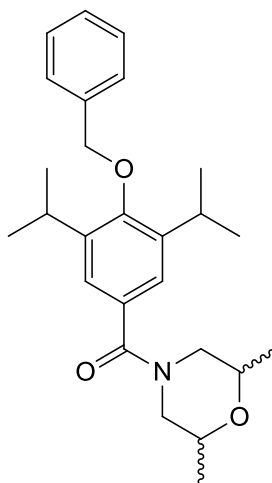
(4-(Benzyloxy)-3,5-diisopropylphenyl)(piperidin-1-yl)methanone



86b

Piperidine (0.23 mL, 2.25 mmol) was reacted with 4-(benzyloxy)-3,5-diisopropylbenzoyl chloride (500 mg, 1.5 mmol) according to **general procedure 3**. The crude product was purified by column chromatography (20:80 EtOAc/n-Hexane) to afford the product as an off white solid (546 mg, 95% yield). ^1H NMR (400 MHz, CDCl_3) δ 7.52-7.32 (m, 5H), 7.16 (s, 2H), 4.80 (s, 1H), 3.71 (s, 4H), 3.39 (hept, $J = 6.8$ Hz, 2H), 1.69 (s, 6H), 1.23 (d, $J = 6.8$ Hz, 12H). ^{13}C NMR (101 MHz, CDCl_3) δ 170.89, 154.06, 142.07, 137.43, 132.63, 128.61, 128.04, 127.39, 123.09, 26.69, 24.70, 24.03. $[\text{M}+\text{H}]^+$: $\text{C}_{25}\text{H}_{34}\text{NNaO}_2$ requires: 380.2590, found: 380.257

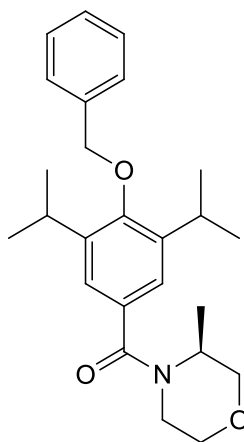
(4-(Benzyloxy)-3,5-diisopropylphenyl)(2,6-dimethylmorpholino)methanone



86a

Dimethylmorpholine (0.28 mL, 2.25 mmol) was reacted with 4-(benzyloxy)-3,5-diisopropylbenzoyl chloride (500 mg, 1.52 mmol) according to **general procedure 3**. The crude product was purified by column chromatography (20:80 EtOAc/n-Hexane) to afford the product as an off white solid (550 mg, 90% yield). ^1H NMR (400 MHz, CDCl_3) δ 7.42(m, 5H), 7.17 (s, 2H), 4.81 (s, 2H), 3.62 (s, 2H), 3.39 (hept, $J = 6.8$ Hz, 2H), 2.57 (s, 4H), 1.23 (d, $J = 6.8$ Hz, 12H), 1.14 (s, 6H). ^{13}C NMR (101 MHz, CDCl_3) δ 170.63, 154.46, 142.33, 137.31, 131.58, 128.63, 128.10, 127.37, 123.52, 72.08, 26.69, 24.00. MS $[\text{M}+\text{Na}]^+$: $\text{C}_{26}\text{H}_{35}\text{NNaO}_3$ requires: 432.2515, found: 432.2520

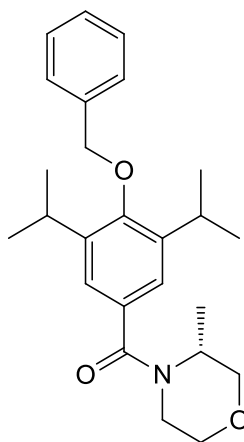
(S)-(4-(Benzyloxy)-3,5-diisopropylphenyl)(3-methylmorpholino)methanone



86c

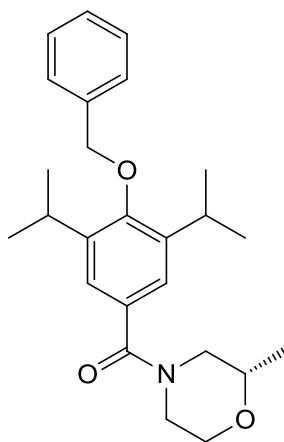
(S)-3-Methyl morpholine (0.12 mL, 1.2 mmol) was reacted with 4-(benzyloxy)-3,5-diisopropylbenzoyl chloride (264 mg, 0.8 mmol) according to **general procedure 3**. The crude product was purified by column chromatography (20:80 EtOAc/n-Hexane) to afford the product as an off white solid (164 mg, 52% yield). ^1H NMR (400 MHz, CDCl_3) δ 7.51 – 7.32 (m, 5H), 7.15 (s, 2H), 4.80 (s, 2H), 4.05 – 3.55 (m, 5H), 3.39 (hept, $J = 6.8$ Hz, 2H) 1.41 (d, 3H), 1.24 (d, $J = 6.8$ Hz, 12H). ^{13}C NMR (101 MHz, CDCl_3) δ 154.31, 142.42, 137.30, 132.01, 128.61, 128.08, 127.36, 122.88, 71.05, 67.18, 26.69, 24.00. MS $[\text{M}+\text{H}]^+$: $\text{C}_{25}\text{H}_{34}\text{NO}_3$ requires: 396.2533, found: 396.22546.

(R)-(4-(Benzyloxy)-3,5-diisopropylphenyl)(3-methylmorpholino)methanone

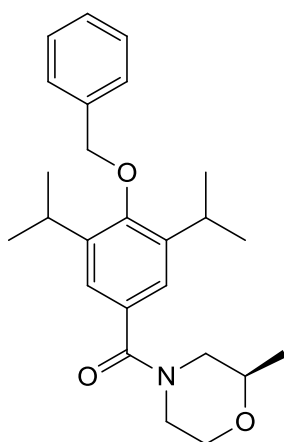


86d

(*R*)-3-Methyl morpholine (0.12 mL, 1.2 mmol) was reacted with 4-(benzyloxy)-3,5-diisopropylbenzoyl chloride (264 mg, 0.8 mmol) according to **general procedure 3**. The crude product was purified by column chromatography (20:80 EtOAc/*n*-Hexane) to afford the product as an off white solid (145 mg, 46% yield). ^1H NMR (400 MHz, CDCl_3) δ 7.52 – 7.31 (m, 5H), 7.15 (s, 2H), 4.80 (s, 2H), 3.92 – 3.66 (m, 6H), 3.38 (hept, $J = 6.8$ Hz, 2H), 1.41 (d, 3H), 1.24 (d, $J = 6.8$ Hz, 12H). ^{13}C NMR (101 MHz, CDCl_3) δ 154.31, 142.42, 137.30, 132.01, 128.62, 128.09, 127.36, 122.88, 71.05, 67.18, 26.69, 24.00. MS $[\text{M}+\text{H}]^+$: $\text{C}_{25}\text{H}_{34}\text{NO}_3$ requires: 396.2533, found: 396.22540.

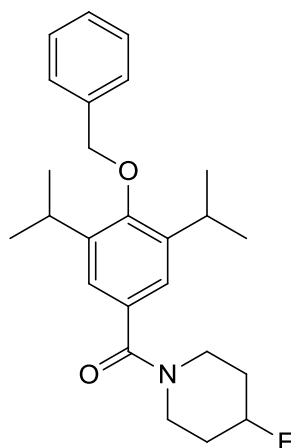
(S)-(4-(Benzyloxy)-3,5-diisopropylphenyl)(2-methylmorpholino)methanone**86f**

(S)-2-Methyl morpholine (0.12 mL, 1.2 mmol) was reacted with 4-(benzyloxy)-3,5-diisopropylbenzoyl chloride (264 mg, 0.8 mmol) according to **general procedure 3**. The crude product was purified by column chromatography (20:80 EtOAc/n-Hexane) to afford the product as an off white solid (132 mg, 42% yield). ^1H NMR (400 MHz, CDCl_3) δ 7.52 – 7.31 (m, 5H), 7.18 (s, 2H), 4.81 (s, 2H), 4.59 (s, 1H), 3.99 – 3.51 (m, 7H), 3.38 (hept, $J = 6.8$ Hz, 2H), (d, $J = 6.8$ Hz, 12H), 1.15 (s, 3H). ^{13}C NMR (101 MHz, CDCl_3) δ 170.82, 154.47, 142.36, 137.28, 128.62, 128.09, 127.37, 123.46, 72.14, 26.69, 23.99. MS $[\text{M}+\text{H}]^+$: $\text{C}_{25}\text{H}_{34}\text{NO}_3$ requires: 396.2533, found: 396.22547.

R)-(4-(Benzyloxy)-3,5-diisopropylphenyl)(2-methylmorpholino)methanone**86e**

(*R*)-2-Methyl morpholine (0.12 mL, 1.2 mmol) was reacted with 4-(benzyloxy)-3,5-diisopropylbenzoyl chloride (264 mg, 0.8 mmol) according to **general procedure 3**. The crude product was purified by column chromatography (20:80 EtOAc/*n*-Hexane) to afford the product as an off white solid (151 mg, 48% yield). ^1H NMR (400 MHz, CDCl_3) δ 7.52 – 7.34 (m, 5H), 7.18 (s, 2H), 4.81 (s, 2H), 4.59 (s, 1H), 4.13 – 3.31 (m, 7H), 3.15 (hept, $J = 6.8$ Hz, 2H), 1.24 (d, $J = 6.8$ Hz, 12H), 1.22 (d, 3H). ^{13}C NMR (101 MHz, CDCl_3) δ 170.84, 154.49, 142.37, 137.29, 128.63, 128.03, 127.38, 123.47, 76.46, 72.16, 66.57, 26.49, 24.01. MS $[\text{M}+\text{H}]^+$: $\text{C}_{25}\text{H}_{34}\text{NO}_3$ requires: 396.2533, found: 396.22539.

(4-(Benzyloxy)-3,5-diisopropylphenyl)(4-fluoropiperidin-1-yl)methanone

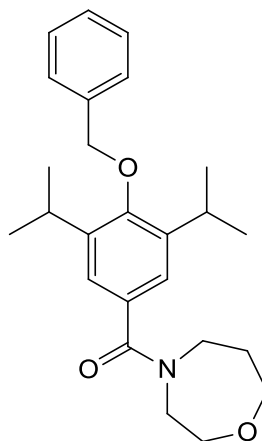


86g

4-Fluoropiperidine hydrochloride (167 mg, 1.2 mmol) was reacted with 4-(benzyloxy)-3,5-diisopropylbenzoyl chloride (264 mg, 0.8 mmol) according to **general procedure 3**. The crude product was purified by column chromatography (20:80 EtOAc/*n*-Hexane) to afford the product as an off white solid (158 mg, 50% yield). ^1H NMR (400 MHz, CDCl_3) δ 7.32-7.24 (m, 5H), 7.09 (s, 2H), 4.87 (d, $J = 48.4$ Hz, 1H) 4.72 (s, 2H), 3.88-3.56 (m, 4H), 3.30 (hept, $J = 6.8$ Hz, 2H), 1.80 (s, 4H), 1.15 (d, $J = 6.8$ Hz, 12H). ^{13}C NMR (101 MHz, CDCl_3) δ 171.44, 154.81, 142.70, 137.72,

132.35, 129.01, 128.48, 127.78, 123.55, 89.07, 87.36, 76.85, 27.11, 24.41. MS $[M+H]^+$: $C_{25}H_{33}FNO_3$ requires: 398.2490, found: 398.2490.

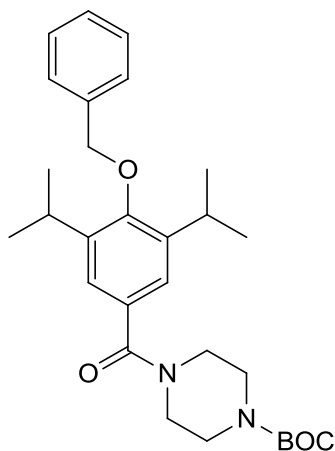
(4-(Benzyloxy)-3,5-diisopropylphenyl)(1,4-oxzepan-4-yl)methanone



86h

1,4-Oxazepane (121mg, 1.2 mmol) was reacted with 4-(benzyloxy)-3,5-diisopropylbenzoyl chloride (264 mg, 0.8 mmol) according to **general procedure 3**. The crude product was purified by column chromatography (20:80 EtOAc/n-Hexane) to afford the product as an off white solid (190mg, 78% yield). 1H NMR (400 MHz, $CDCl_3$) δ 7.51 – 7.34 (m, 5H), 7.17 (s, 2H), 4.80 (s, 2H), 3.84-3.53 (m, 8H), 3.39 (hept, J = 6.8 Hz, 2H), 2.07 (s, 2H), 1.23 (d, J = 6.8 Hz, 12H). ^{13}C NMR (101 MHz, $CDCl_3$) δ 154.12, 148.46, 142.32, 137.35, 132.79, 128.35, 127.38, 26.70, 24.03. MS $[M+H]^+$: $C_{25}H_{33}FNO_3$ requires: 396.2533, found: 396.2538.

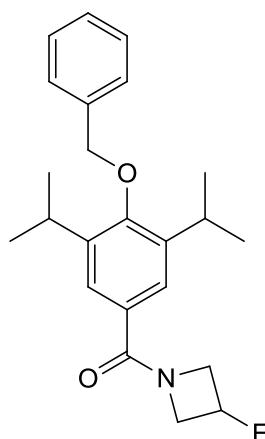
***tert*-Butyl 4-(4-(benzyloxy)-3,5-diisopropylbenzoyl)piperazine-1-carboxylate**



86j

tert-Butyl piperazine-1-carboxylate (418 mg, 2.25 mmol) was reacted with 4-(benzyloxy)-3,5-diisopropylbenzoyl chloride (500 mg, 1.5 mmol) according to **general procedure 3**. The crude product was purified by column chromatography (20:80 EtOAc/n-Hexane) to afford the product as a white solid. The product from this reaction was not isolated and was carried through crude.

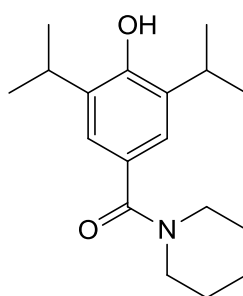
4-(benzyloxy)-3,5-diisopropylphenyl(3-fluoroazetidin-1-yl)methanone



86i

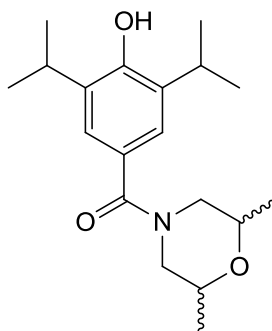
3-Fluoroazetidine hydrochloride (250 mg, 2.25 mmol) was reacted with 4-(benzyloxy)-3,5-diisopropylbenzoyl chloride (500 mg, 1.5 mmol) according to **general procedure 3**. The product from this reaction was not isolated and was carried through crude.

(4-hydroxy-3,5-diisopropylphenyl)(piperidine-1-yl)methanone

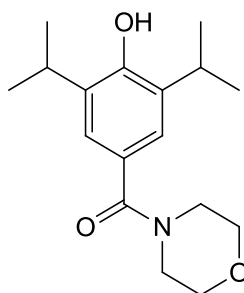


98

(4-hydroxy-3,5-diisopropylphenyl)(piperidine-1-yl)methanone (520 mg, 1.37 mmol) was reacted with Pd/C (32 mg, 0.27 mmol) **General procedure**. The crude product was purified by column chromatography (40:60 EtOAc/n-Hexane) to afford the product as an off white solid (111 mg, 96% yield). mp = 172-174°C: ^1H NMR (400 MHz, CDCl_3) δ . 7.13 (s, 2H), 5.17 (s, 1H), 3.74 (s, 4H), 3.15 (hept, $J = 6.8$ Hz, 2H), 2.74 (s, 6H), 1.26 (d, $J = 6.8$ Hz, 12H). ^{13}C NMR (101 MHz, CDCl_3) δ 171.43, 152.11, 134.14, 126.52, 123.21, 72.14, 66.68, 26.88, 22.68, 18.61. MS $[\text{M}+\text{Na}]^+$: $\text{C}_{18}\text{H}_{27}\text{NNaO}_3$ requires: 328.1899, found: 328.1889. CHN requires C: 70.79%, H: 8.91%, N: 4.59, found C: 70.56%, H: 8.55%, N: 4.61%

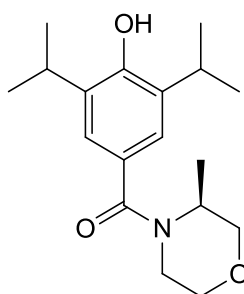
(2,6-Dimethylmorpholino)(4-hydroxy-3,5-diisopropyl)methanone**99**

(4-(Benzyloxy)-3,5-diisopropylphenyl)(2,6-dimethylmorpholino)methanone (520 mg, 1.27 mmol) was reacted with Pd/C (32 mg, 0.27 mmol) according to **General procedure**. The crude product was purified by column chromatography (40:60 EtOAc/n-Hexane) to afford the product as an off white solid (385 mg, 95% yield). mp = 168-170°C: ^1H NMR (400 MHz, CDCl_3) δ 7.12 (s, 2H), 5.24 (s, 1H), 3.62 (s, 4H), 3.16 (hept, $J = 6.8$ Hz, 2H), 2.59 (s, 2H), 1.24 (d, $J = 6.8$ Hz, 12H), 1.22 (s, 6H). ^{13}C NMR (101 MHz, CDCl_3) δ 170.97, 151.60, 133.67, 127.21, 123.27, 72.06, 65.88, 27.10, 22.63, 18.70, 15.28. MS $[\text{M}+\text{H}]^+$: $\text{C}_{19}\text{H}_{30}\text{NO}_3$ requires: 320.2220, found: 320.2230. CHN requires C: 71.44%, H: 9.15%, N: 4.38, found C: 70.98%, H: 8.87%, N: 5.11%

(4-(hydroxy)-3,5-diisopropylphenyl)(morpholino)methanone**77a**

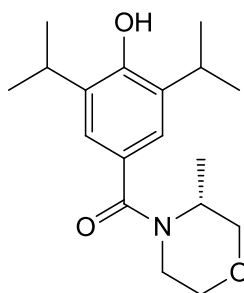
(4-Benzyloxy-3,5-diisopropylphenyl)(morpholino)methanone (470 mg, 1.3 mmol) was reacted with Pd/C (32 mg, 0.27 mmol) according to **General procedure** . The crude product was purified by column chromatography (40:60 EtOAc/n-Hexane) to afford the product as an off white solid (366 mg, 97% yield). Analysis consistent with 77.

(S)-(4-Hydroxy-3,5-diisopropylphenyl)(3-methylmorpholino)methanone

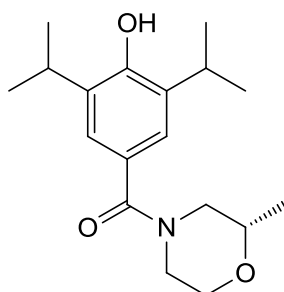


99

(S)-(4-(Benzyloxy)-3,5-diisopropylphenyl)(3-methylmorpholino)methanone (120 mg, 0.30 mmol) was reacted with Pd/C (35 mg, 0.03 mmol) according to **General procedure** . The crude product was purified by column chromatography (40:60 EtOAc/n-Hexane) to afford the product as an off white solid (84 mg, 90% yield). mp = 174-178°C: ^1H NMR (400 MHz, CDCl_3) δ 7.11 (s, 2H), 5.05 (s, 1H), 3.90 – 3.31 (m, 7H), 3.15 (hept, $J = 6.8$ Hz, 2H), 1.24 (d, 3H) 1.24 (d, $J = 6.8$ Hz, 12H). ^{13}C NMR (101 MHz, CDCl_3) δ 142.28, 128.51, 128.03, 127.38, 123.47, 72.16, 26.62, 23.80. MS $[\text{M}+\text{Na}]^+$: $\text{C}_{18}\text{H}_{27}\text{NNaO}_3$ requires: 328.1889, found: 328.1884. CHN requires C: 70.79%, H: 8.91%, N: 4.59, found C: 70.68%, H: 8.74%, N: 4.14%

(R)-(4-Hydroxy-3,5-diisopropylphenyl)(3-methylmorpholino)methanone**100**

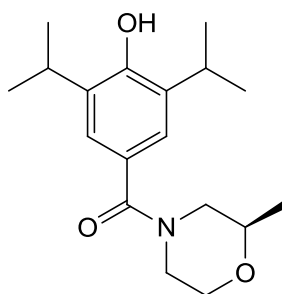
(R)-(4-(Benzyloxy)-3,5-diisopropylphenyl)(3-methylmorpholino)methanone (300 mg, 0.75 mmol) was reacted with Pd/C (89 mg, 0.075 mmol) according to **gGeneral procedure**. The crude product was purified by column chromatography (40:60 EtOAc/n-Hexane) to afford the product as an off white solid (227 mg, 98% yield). mp = 182-184°C: ^1H NMR (400 MHz, CDCl_3) δ 7.11 (s, 2H), 3.97 – 3.29 (m, 7H), 3.15 (hept, $J = 6.8$ Hz, 2H), 1.39 (d, 3H), 1.27 (d, $J = 6.8$ Hz, 12H). ^{13}C NMR (101 MHz, CDCl_3) δ 171.35, 151.42, 133.72, 127.70, 122.68, 71.07, 67.22, 27.15, 22.63, 15.48. MS $[\text{M}+\text{Na}]^+$: $\text{C}_{18}\text{H}_{27}\text{NNaO}_3$ requires: 328.1889, found: 328.1901. CHN requires C: 70.79%, H: 8.91%, N: 4.59, found C: 70.24%, H: 8.87%, N: 4.52%

(S)-(4-Hydroxy-3,5-diisopropylphenyl)(2-methylmorpholino)methanone**102**

(S)-(4-(Benzyloxy)-3,5-diisopropylphenyl)(2-methylmorpholino)methanone (100 mg, 0.25 mmol) was reacted with Pd/C (29 mg, 0.025 mmol) according to **General**

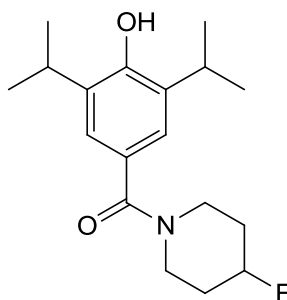
procedure . The crude product was purified by column chromatography (40:60 EtOAc/n-Hexane) to afford the product as an off white solid (74 mg, 96% yield). mp = 188-190°C: ^1H NMR (400 MHz, CDCl_3) δ 7.13 (s, 1H), 5.07 (s, 1H), 4.94 – 3.28 (m, 7H), 3.21 (hept, $J = 6.8$ Hz, 2H), 1.26 (d, $J = 6.8$ Hz, 12H), 1.18 (s, 3H). ^{13}C NMR (101 MHz, CDCl_3) δ 171.69, 152.26, 134.31, 127.24, 123.63, 72.54, 67.11, 27.41, 23.05, 19.03. MS $[\text{M}+\text{Na}]^+$: $\text{C}_{18}\text{H}_{27}\text{NNaO}_3$ requires: 328.1889, found: 328.1892. CHN requires C: 70.79%, H: 8.91%, N: 4.59, found C: 70.20%, H: 8.58%, N: 4.62%

(R)-(4-Hydroxy-3,5-diisopropylphenyl)(2-methylmorpholino)methanone

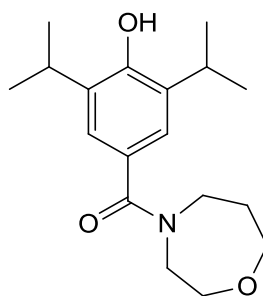


101

(R)-(4-(Benzyloxy)-3,5-diisopropylphenyl)(2-methylmorpholino)methanone (100 mg, 0.25 mmol) was reacted with Pd/C (29 mg, 0.025 mmol) according to **General procedure 5**. The crude product was purified by column chromatography (40:60 EtOAc/n-Hexane) to afford the product as an off white solid (75 mg, 97% yield). mp = 176-178°C: ^1H NMR (400 MHz, CDCl_3) δ 7.13 (s, 2H), 5.17 (s, 1H), 4.72 – 3.35 (m, 6H), 3.16 (hept, $J = 6.8$ Hz, 2H), 2.75 (s, 1H), 1.26 (d, $J = 6.8$ Hz, 12H), 1.18 (s, 3H). ^{13}C NMR (101 MHz, CDCl_3) δ 171.43, 152.11, 134.14, 126.52, 123.21, 77.29, 72.14, 66.68, 26.88, 22.68, 18.61. MS $[\text{M}+\text{Na}]^+$: $\text{C}_{18}\text{H}_{27}\text{NNaO}_3$ requires: 328.1889, found: 328.1899. CHN requires C: 70.79%, H: 8.91%, N: 4.59%, found C: 70.56%, H: 8.55%, N: 4.61%

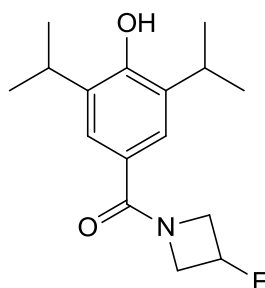
(4-Fluoropiperidin-1-yl)(4-hydroxy-3,5-diisopropyl)methanone**103**

(4-(Benzyloxy)-3,5-diisopropylphenyl)(4-fluoropiperidin-1-yl)methanone (278 mg, 0.70 mmol) was reacted with Pd/C (83 mg, 0.07 mmol according to **General procedure** . The crude product was purified by column chromatography (40:60 EtOAc/n-Hexane) to afford the product as an off white solid (197 mg, 92% yield). mp = 188-190°C: ^1H NMR (400 MHz, CDCl_3) δ 7.13 (s, 2H), 5.06 (s, 1H), 4.97 (d, J = 48.4 2H), 3.64 (s, 4H), 3.15 (hept, J = 6.8 Hz 2H), 1.88 (s, 4H), 1.26 (d, J = 6.8 Hz, 12H). ^{13}C NMR (101 MHz, CDCl_3) δ 171.44, 151.56, 133.67, 127.49, 122.95, 88.81, 87.11, 27.11, 22.64. MS $[\text{M}+\text{Na}]^+$: $\text{C}_{18}\text{H}_{26}\text{FNNaO}_2$ requires: 330.1845, found: 330.1842. CHN requires C: 70.33%, H: 8.53%, N: 4.56%, found C: 69.68%, H: 8.56%, N: 4.43%

(4-Hydroxy-3,5-diisopropylphenyl)(1,4-oxzepan-4-yl)methanone**104**

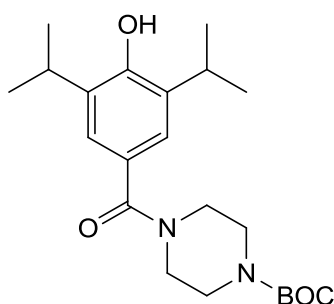
(4-(Benzyloxy)-3,5-diisopropylphenyl)(1,4-oxzepan-4-yl)methanone (150 mg, 0.38 mmol) was reacted with Pd/C (45 mg, 0.04 mmol) according to **General procedure** . The crude product was purified by column chromatography (40:60 EtOAc/n-Hexane) to afford the product as an off white solid (82 mg, 71% yield). mp = 184-186°C: ^1H NMR (400 MHz, CDCl_3) δ 7.12 (s, 2H), 3.83 – 3.80 (m, 8H), 3.15 (hept, $J =$, 6.8 Hz, 2H), 1.93 (s, 2H), 1.26 (d, $J = 6.8$ Hz, 12H). ^{13}C NMR (101 MHz, CDCl_3) δ 172.71, 151.33, 133.72, 128.33, 122.59, 69.81, 69.28, 52.68, 48.91, 48.57, 31.21, 27.08, 22.67. MS $[\text{M}+\text{Na}]^+$: $\text{C}_{18}\text{H}_{27}\text{NNaO}_3$ requires: 328.1889, found: 328.1886. CHN omitted due to inconsistent results.

(3-Fluoroazetidin-1-yl)(4-hydroxy-3,5-diisopropylphenyl)methanone

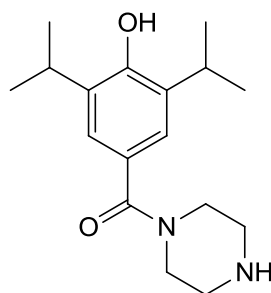


105

4-(benzyloxy)-3,5-diisopropylphenyl(3-fluoroazetidin-1-yl)methanone (387 mg, 1.05 mmol) was reacted with Pd/C (32 mg, 0.27 mmol) according to **general procedure 5**. The crude product was purified by column chromatography (40:60 EtOAc/n-Hexane) to afford the product as a white solid (223 mg, 76% yield). mp = 182-184°C: ^1H NMR (400 MHz, CDCl_3) δ 7.36 (s, 2H), 5.66 (s, 1H), 5.36 (m, 1H), 4.58 – 4.26(m, 4H), 3.19 (hept, $J = 6.8$ Hz, 2H), 1.25 (d, $J = 6.8$ Hz, 12H). ^{13}C NMR (101 MHz, CDCl_3) δ 154.52, 142.05, 130.80, 126.90, 124.57, 85.61, 62.68, 26.89, 24.39. MS $[\text{M}+\text{H}]^+$: $\text{C}_{16}\text{H}_{23}\text{FNO}_3$ requires: 280.1711, found: 280.1707 CHN requires C: 68.79%, H: 7.94%, N: 5.01, found C: 68.55%, H: 7.89%, N: 4.92%

***tert*-Butyl 4-(4-(hydroxy)-3,5-diisopropylbenzoyl)piperazine-1-carboxylate****111**

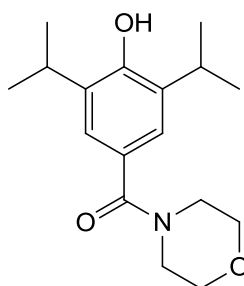
tert-Butyl 4-(4-(bezyloxy)-3,5-diisopropylbenzoyl)piperazine-1-carboxylate (200 mg, 0.42 mmol) was reacted with Pd/C (49 mg, 0.04 mmol) according to **general procedure 5**. The crude product was purified by column chromatography (20:80 EtOAc/n-Hexane) to afford the product as a white solid (159 mg, 98% yield). ¹H NMR (400 MHz, CDCl₃) δ 7.13 (s, 2H), 5.26 (s, 1H), 3.46 (s, 8H), 3.16 (hept, *J* = 6.8 Hz, 2H), 1.48 (s, 9H), 1.25 (d, *J* = 6.8 Hz, 12H). ¹³C NMR (101 MHz, CDCl₃) δ 171.50, 154.68, 151.70, 133.74, 127.14, 123.17, 28.39, 27.11, 22.63.

(4-(hydroxy)-3,5-diisopropylphenyl)piperazine-1-ylmethanone**106**

tert-Butyl 4-(4-(hydroxy)-3,5-diisopropylbenzoyl)piperazine-1-carboxylate (140 mg, 0.36 mmol) was added to a stirred solution of trifluoroacetic acid (0.41 mL, 5.4 mmol) in DCM (5 mL). The resulting reaction mixture was allowed to stir for 18 hours. The reaction was followed by TLC and upon completion the solvent was

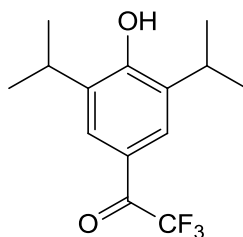
removed under vacuum. NaHCO₃ (10 mL) was added to the reaction mixture and the crude compound was extracted with EtOAc (3 x 20 mL) washed with H₂O (20 mL) and brine (20 mL). The combined organic extracts were dried over MgSO₄ and the solvent was removed under vacuum. The crude product was purified by trituration with EtO₂ to give the pure product as a white solid (62 mg, 60% yield) mp = 155-157°C: ¹H NMR (400 MHz, CDCl₃) δ 7.13 (s, 2H), 5.26 (s, 1H), 3.16 (hept, *J* = 6.8 Hz, 2H), 1.48 (s, 9H), 1.26 (d, *J* = 6.8 Hz, 12H). ³C NMR (101 MHz, CDCl₃) δ 171.29, 150.90, 133.57, 127.57, 122.98, 46.17, 34.37, 27.12, 22.35. MS [M+H]⁺:C₁₇H₂₇N₂O₂ requires: 291.2067, found: 291.2077. CHN omitted due to inconsistent results.

(4-Hydroxy-3-5-diisopropylphenyl)(morpholino)methanone (Microwave Reaction)

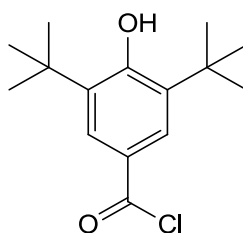


77b

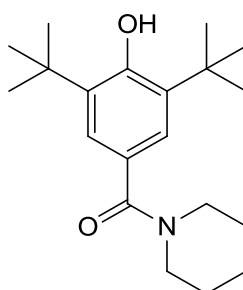
4-Bromopropofol (1 g, 3.9 mmol) was dissolved in 1,4-dioxane 20 added to a microwave vial (30 mL) along with morpholine (0.67 mL, 7.7 mmol), Na₂CO₃ (1.17 mg, 11.6 mmol), MO(CO)₆ (601 mg, 2.3 mmol) and *trans*-Bis(acetato)bis[o-(di-*o*-tolylphosphino)benzyl]dipalladium(II) (178 mg, 0.19 mmol). The reaction mixture was placed in a microwave reactor for 20 minutes at 165°C. Upon completion the mixture was diluted with H₂O (20 mL) and the crude product was extracted with EtOAc (3 x 30 mL). The combined organic extracts were washed with H₂O (20 mL) and brine (20 mL) before being dried over MgSO₄. The solvent was removed under vacuum and the crude product was purified by column chromatography (40:60 EtOAc/n-Hexane) to afford the product as a white solid (60% yield). The analysis was consistent with **77**.

2,2,2-Trifluoro-1-(4-(3,5-diisopropylphenyl)ethanone)⁹**108**

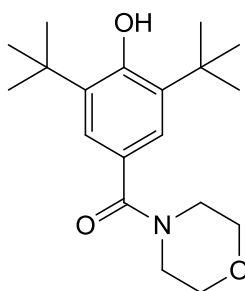
AlCl₃ (1.1 g, 8.4 mmol) was suspended in DCM and cooled to -48 °C. Trifluoroacetic anhydride (0.86 mL, 6.2 mmol in 2 mL DCM) was added drop wise and the resulting suspension was allowed to stir at -48°C for 30 mins. Propofol (1 g, 5.6 mmol in 2 mL DCM) was added drop wise and the reaction mixture was stirred at -48°C for 3 hours before being allowed to come to room temperature overnight. The reaction was monitored by TLC and upon completion the mixture was poured onto a mixture of ice and 2M HCl (150 mL of each) and stirred for 1 hour. The mixture was extracted with EtOAc (3x100 mL) and the combined organic extracts were washed with brine (100 mL) and dried over MgSO₄. The solvent was removed under vacuum. The crude product was purified by column chromatography (60:40 EtOAc/n-Hexane) to afford the product as a brown oil (2.7g, 45% yield). ¹H NMR (400 MHz, CDCl₃) δ 7.83 (s, 2H), 5.57 (s, 1H), 3.17 (hept, *J* = 6.8 Hz, 2H), 1.31 (d, *J* = 6.8 Hz, 12H). ¹³C NMR (101 MHz, CDCl₃) δ 179.91, 157.17, 134.58, 127.17, 123.12, 115.94, 27.45, 22.79. ¹⁹F NMR (376 MHz, CDCl₃) δ -70.48. MS [M+Na]⁺: C₁₄H₁₇F₃NaO₂ requires: 297.1078, found: 297.1079.

3,5-Di-*tert*-butyl-4-hydroxybenzoyl chloride**91**

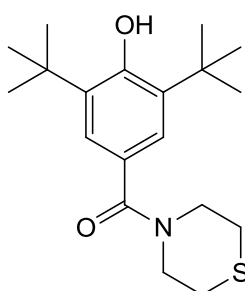
3,5-Di-*tert*-butyl-4-hydroxybenzoic acid (2 g, 8.5 mmol) was reacted with oxalyl chloride (1.4 mL, 17 mmol) according to **general procedure 2** to afford the product as a pale yellow oil. The product from this reaction was not isolated and was carried through crude.

(3,5-Di-*tert*-butyl-4-hydroxyphenyl)(piperidin-1-yl)methanone¹⁰**96**

3,5-Di-*tert*-butyl-4-hydroxybenzoyl chloride (1 g, 3.7 mmol) was reacted with piperazine (0.6 mL, 5.6 mmol) according to **general procedure 3**. The crude product was purified by column chromatography (40:60 EtOAc/n-Hexane) to afford the product as an off white solid (916 mg, 91% yield). mp = 147-149°C: ¹H NMR (400 MHz, CDCl₃) δ 7.23 (s, 2H), 5.37 (s, 1H), 3.75 – 3.29 (m, 4H), 1.73 – 1.54 (m, 6H), 1.43 (s, 18H). ¹³C NMR (101 MHz, CDCl₃) δ 171.79, 155.38, 135.99, 127.66, 124.73, 34.76, 30.58, 25.14. MS [M+H]⁺: C₂₀H₃₂NO₂ requires: 318.2433, found: 318.2431. CHN requires C: 75.67%, H: 9.84%, N: 4.41, found C: 75.48%, H: 9.88%, N: 4.44%

(3,5-Di-*tert*-butyl-4-hydroxyphenyl)(morpholino)methanone¹⁰**92**

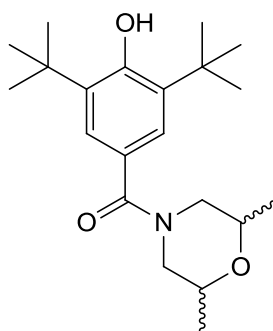
3,5-Di-*tert*-butyl-4-hydroxybenzoyl chloride (1 g, 3.7 mmol) was reacted with morpholine (0.5 mL, 5.6 mmol) according to **general procedure 3**. The crude product was purified by column chromatography (40:60 EtOAc/n-Hexane) to afford the product as an off white solid (957 mg, 81% yield). mp = 174-176°C: ¹H NMR (400 MHz, CDCl₃) δ 7.24 (s, 2H), 5.43 (s, 1H), 3.71 (s, 8H), 1.44 (s, 18H). ¹³C NMR (101 MHz, CDCl₃) δ 171.98, 155.70, 136.06, 126.20, 124.86, 67.30, 34.70, 30.38. MS [M+Na]⁺:C₁₉H₂₉NNaO₃ requires: 342.2045, found: 342.2056. CHN requires C: 71.44%, H: 9.15%, N: 4.38, found C: 71.03%, H: 9.13%, N: 4.28%

(3,5-Di-*tert*-butyl-4-hydroxyphenyl)(thiomorpholino)methanone¹⁰**93**

3,5-Di-*tert*-butyl-4-hydroxybenzoyl chloride (1 g, 3.7 mmol) was reacted with thiomorpholine (0.5 mL, 5.6 mmol) according to **general procedure 3**. The crude

product was purified by column chromatography (40:60 EtOAc/n-Hexane) to afford the product as an off white solid (1.04 g, 84% yield). mp = 182-184°C: ^1H NMR (400 MHz, CDCl_3) δ 7.21 (s, 2H), 5.42 (s, 1H), 3.88 (bs, 4H), 2.68 (bs, 4H), 1.44 (s, 18H). ^{13}C NMR (101 MHz, CDCl_3) δ 172.30, 155.68, 136.30, 126.72, 124.83, 34.71, 30.38, 28.27, 28.02. MS $[\text{M}+\text{Na}]^+$: $\text{C}_{19}\text{H}_{29}\text{NNaO}_2$ requires: 358.1817, found: 358.1825 CHN requires C: 71.44%, H: 9.15%, N: 4.38, found C: 71.25%, H: 9.09%, N: 4.19%

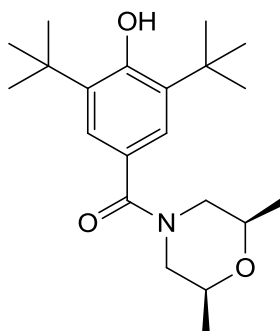
(3,5-Di-*tert*-butyl-4-hydroxyphenyl)(2,6-dimethylmorpholino)methanone



94

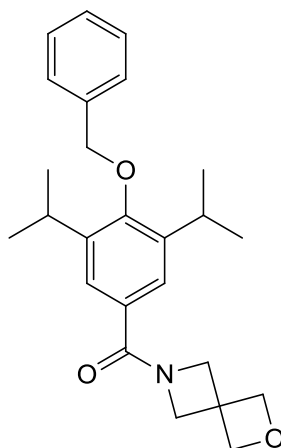
3,5-Di-*tert*-butyl-4-hydroxybenzoyl chloride (1 g, 3.7 mmol) was reacted with 2,6-dimethylmorpholine (0.7 mL, 5.6 mmol) according to **general procedure 3**. The crude product was purified by column chromatography (40:60 EtOAc/n-Hexane) to afford the product as an off white solid (820 mg, 68% yield). mp = 171-173°C: ^1H NMR (400 MHz, CDCl_3) δ 7.25 (s, 2H), 5.58 (s, 1H), 4.54-3.64 (m, 4H), 2.65 (s, 2H), 1.44 (s, 18H), 1.19 (d, 6H). ^{13}C NMR (101 MHz, CDCl_3) δ 135.85, 126.02, 64.17, 55.08, 34.46, 30.61, 28.26. MS $[\text{M}+\text{H}]^+$: $\text{C}_{21}\text{H}_{34}\text{NNaO}_3$ requires: 348.2539, found: 348.2526. CHN requires C: 71.44%, H: 9.15%, N: 4.38, found C: 71.78%, H: 9.58%, N: 3.88%

(3,5-Di-*tert*-butyl-4-hydroxyphenyl)((2S,6R)-2,6-dimethylmorpholino)methanone

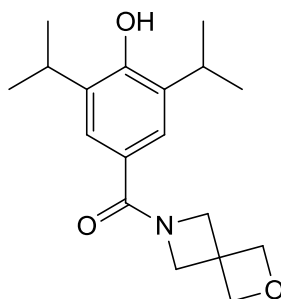


95

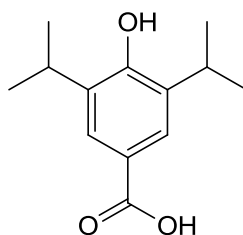
3,5-Di-*tert*-butyl-4-hydroxybenzoyl chloride (1 g, 3.7 mmol) was reacted with 2,6-dimethylmorpholine (0.7 mL, 5.6 mmol) according to **general procedure 3**. The crude product was purified by column chromatography (40:60 EtOAc/n-Hexane) to afford the product as an off white solid (820 mg, 68% yield). mp = 181-183°C: ^1H NMR (400 MHz, CDCl_3) δ 7.40 (s, 2H), 5.80 (s, 1H), 3.64 (bs, 4H), 2.68 (bs, 2H), 1.50 (s, 18H), 1.44 (bs, 6H). ^{13}C NMR (101 MHz, CDCl_3) δ 166.81, 158.67, 143.47, 136.02, 127.80, 71.97, 34.15, 31.43, 30.18. MS $[\text{M}+\text{H}]^+$: $\text{C}_{21}\text{H}_{34}\text{NO}_3$ requires: 348.2539, found: 348.2533. CHN requires C: 71.44%, H: 9.15%, N: 4.38, found C: 71.27%, H: 8.98%, N: 3.54%

(4-(Benzyloxy)-3,5-diisopropylphenyl)(2-oxa-6-azaspiro[3.3]heptan-6-yl)methanone**123**

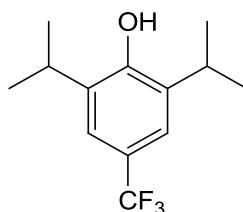
To a solution of 4-(benzyloxy)-3,5-diisopropylbenzoic acid (100 mg, 0.32 mmol) in DMF (5 mL) was added HATU (180, 0.48 mmol), K_2CO_3 (220 mg, 1.6 mmol) and 2-oxa-6-azaspiro[3.3]heptan-6-ium carboxyformate (101 mg, 0.35 mmol). The resulting solution was allowed to stir for 1 hour. Upon completion the reaction mixture was quenched with H_2O (20 mL) and extracted with EtOAc (3 x 30 mL). The combined organic extracts were washed with H_2O (3 x 30 mL), brine (20 mL), dried over $MgSO_4$ and the solvent was removed under vacuum. The crude product was purified by column chromatography (20:80 EtOAc/n-Hexane) to afford the product as a white solid (62 mg, 50% yield). 1H NMR (400 MHz, $CDCl_3$) δ 7.54 – 7.31 (m, 7H), 4.83 (d, $J = 11.7$ Hz, 6H), 4.40 (d, $J = 42.4$ Hz, 4H), 3.39 (hept, $J = 6.8$ Hz, 2H), 1.25 (d, $J = 6.8$ Hz, 12H). ^{13}C NMR (101 MHz, $CDCl_3$) δ 170.82, 157.83, 142.63, 128.66, 128.31, 127.37, 126.60, 125.44, 72.92, 60.89, 53.37, 26.39, 24.02. MS $[M+Na]^+$: $C_{25}H_{31}NNaO_3$ requires: 416.2202, found: 416.2186.

(4-Hydroxy-3,5-diisopropylphenyl)(2-oxa-6-azaspiro[3.3]heptan-6-yl)methanone**107**

(4-(Benzyloxy)-3,5-diisopropylphenyl)(2-oxa-6-azaspiro[3.3]heptan-6-yl)methanone (50 mg, 0.13 mmol) was reacted with Pd/C (15 mg, 0.12 mmol) according to **general procedure 5**. The crude product was purified by column chromatography (40:60 EtOAc/n-Hexane) to afford the product as a white solid (38 mg, 99% yield) ^1H NMR (400 MHz, CDCl_3) δ 7.35 (s, 2H), 5.43 (s, 1H), 4.82 (s, 4H), 4.39 (d, $J = 41.9$ Hz, 4H), 3.16 (hept, $J = 6.8$ Hz, 2H), 1.26 (d, $J = 6.8$ Hz, 12H). ^{13}C NMR (101 MHz, CDCl_3) δ 172.27, 154.00, 134.78, 125.74, 125.05, 82.10, 39.57, 28.22, 23.79. MS $[\text{M}+\text{H}]^+$: $\text{C}_{18}\text{H}_{26}\text{NO}_3$ requires: 304.1907, found: 304.1906. CHN requires C: 71.26%, H: 8.31%, N: 4.62, found C: 71.12%, H: 8.16%, N: 4.38%

4-Hydroxy-3,5-diisopropylbenzoic acid⁷**80**

NaClO₂ (1.3 g, 14.4 mmol) was added to a solution of (1.0 g, 4.8 mmol) NaH₂PO₄ (2.2 g, 14.4 mmol) and 2-methyl-2-butene (9.5 mL, 2M in THF) in BuOH/H₂O (1:1, 15 mL). The reaction was allowed to stir at room temperature for 16 hours. Upon completion the reaction mixture was diluted with Na₂CO₃ (50 mL) and was washed with EtOAc (50 mL). The aqueous layer was acidified to pH 1 (20 mL HCl, 1M) and extracted with EtOAc (3 x 30 mL). The organic extracts were collected and dried over MgSO₄ and concentrated under vacuum to afford the product. The product was purified column chromatography (80:20 EtOAc/n-Hexane) to give the product as a white solid (739 mg, 68% yield). ¹H NMR (400 MHz, CDCl₃) δ 7.85 (s, 2H), 5.30 (s, 1H), 3.21- 3.11 (m, 2H), 1.30 (d, *J* = 6.8 Hz, 12H). ¹³C NMR (101 MHz, CDCl₃) δ 172.25, 155.07, 133.42, 126.77, 121.39, 27.27, 22.45. MS: C₁₃H₂₂NO₃ [M+NH₄]⁺ requires 240.1595, found 240.1590.

2,6-Diisopropyl-4-(trifluoromethyl)phenol**109**

To an oven dried borosilicate vial (8 mL) was added Ir(Fppy)₃ (3.8 mg, 0.0056 mmol) and K₂HPO₄ (261 mg, 1.5 mmol). The vial was degassed by alternating vacuum evacuation and N₂ backfill (x3) before MeCN (4 mL) and propofol (0.89 mL, 0.5 mmol) were added. The resulting solution was again degassed by alternating vacuum evacuation at -78 °C and allowing the solution to come to room temperature under N₂ (x3). Trifluoromethanesulfonyl chloride (0.105 mL, 1.0 mmol) was added and the vial was placed 2 cm from a 26W compact fluorescent light bulb (daylight GE Energy Smart™ 1600 lumens). After 24 hours the reaction mixture was quenched with H₂O (10 mL) and the crude product was extracted with EtOAc (2 x 20 mL) washed with H₂O (20 mL), brine (20 mL). The combined organic extracts were dried over MgSO₄ and concentrated under vacuum to afford the product as a yellow oil (52 mg, 42% yield). ¹H NMR (400 MHz, CDCl₃) δ 7.30 (s, 2H), 5.16 (s, 1H), 3.17 (hept, *J* = 6.8 Hz, 2H), 1.28 (d, *J* = 6.8 Hz, 12H). ¹⁹F NMR (376 MHz, CDCl₃) δ -61.26 (s). ¹³C NMR (101 MHz, CDCl₃) δ 152.65, 126.16, 120.71, 120.51, 27.11, 22.36. MS [M+H]⁺: C₁₃H₁₈FO₃ requires: 247.1305, found: 247.1302. CHN requires C: 63.40%, H: 6.96 found C: 63.94%, H: 6.98%.

6.1 References

1. Eckle, V.S., *et al.* 4-bromopropofol decreases action potential generation in spinal neurons by inducing a glycine receptor-mediated tonic conductance. *British Journal of Pharmacology* **171**, 5790-5801 (2014).
2. Ahmed, S., Shahid, I., Dhanani, S. & Owen, C. P. Synthesis and biochemical evaluation of a range of sulfonated derivatives of 4-hydroxybenzyl imidazole as highly potent inhibitors of rat testicular 17 α -hydroxylase/17,20-lyase (P-45017 α). *Bioorganic & Medicinal Chemistry Letters* **19**, 4698-4701, (2009).
3. Vandoorn, J.A. & Meijboom, N. synthesis of some functionalized phosphinocarboxylic acids. *Phosphorus Sulfur and Silicon and the Related Elements* **42**, 211-222 (1989).
4. Irlapati, N.R., Baldwin, J.E., Adlington, R.M., Pritchard, G.J. & Cowley, A.R. Studies towards the biomimetic synthesis of pyridomacrolidin. *Tetrahedron* **62**, 4603-4614 (2006).
5. Cooke, A., Anderson, A., Buchanan, K., *et al.* Water-soluble propofol analogues with intravenous anaesthetic activity. *Bioorganic & Medicinal Chemistry Letters* **11**, 927-930, (2001).
6. Volod'kin, A.A. & Ershov, V.V. Sterically hindered phenols. *Russian Chemical Bulletin* **11**, 1213-1215 (1962).
7. Pramanik, C., Kotharkar, S., Pradipet, P., *et al.* Commercial Manufacturing of Propofol: Simplifying the Isolation Process and Control on Related Substances. *Organic Process Research & Development* **18**, 152-156 (2014).
8. Roth, B. Baccanari, D. P., Sigel, C. W., Hubbell, J. P., Eaddy, J., Kao, J. C., Grace, M. E., Rauckman, B. S.. 2,4-diamino-5-benzylpyrimidines and analogs as antibacterial agents .9. lipophilic trimethoprim analogs as antigonococcal agents. *Journal of Medicinal Chemistry* **31**, 122-129, (1988).
9. Stewart, D. S. Savechenkov, P.Y., Dostalova, Z., Chiara, D.C., Ge, R., Raines, D E., Cohen, J.B., Forman, S. A., Bruzik, K.S., Miller, K.W. p-(4-Azipentyl)propofol: A Potent Photoreactive General Anesthetic Derivative of Propofol. *Journal of Medicinal Chemistry* **54**, 8124-8135, (2011).
10. Wolf, E., Rossmannith, E., Bartlett, R. & Schleyerbach, R. Preparation of 3,5-di-tert-butyl-4-hydroxybenzamides as antiinflammatories. 20 pp. (Hoechst A.-G., Fed. Rep. Ger. . 1988).